Cranfield University

Paul Comley

Grinding Processes and their Effects on Surface Integrity

School of Industrial & Manufacturing Science

PhD Thesis

Cranfield University

School of Industrial & Manufacturing Science

PhD Thesis

2005

Paul Comley

Grinding Processes and their Effects on Surface Integrity

Supervisors: **Prof. J. Corbett**
Prof. D. J. Stephenson

March 2005

This thesis is submitted in partial fulfillment of the requirements for the degree of Doctor of Philosophy

Abstract

The introduction of high performance grinding machines in combination with the latest superabrasive technology has the potential to impact significantly on existing process chains. The aim of the research was to look at both the high and low rate removal grinding processes and their effects on the surface integrity, as a means to exploit the above technologies.

A major objective was to determine the feasibility of High Efficiency Deep Grinding (*HEDG*) in cylindrical plunge grinding. *HEDG* is a high speed removal process which differs from conventional forms of grinding in that it uses large depths of cut together with high feedrates. Together, these changes affect the thermal energy partitioning within the work zone. Through this work an understanding of the process conditions enabled the development of this process, such that prevention of thermal damage to the finished workpiece surface is achievable. At the opposite extreme to the high material removal rates of *HEDG*, work was carried out in the high precision finish grinding regime. Developments were undertaken to look at the implementation of a modified path into the normal cylindrical plunge grinding action, in a process referred to as *Superfinish Grinding*. The aim of this process being to demonstrate an improvement to the surface texture primarily through a reduction in grinding directionality.

Surface integrity is an important consideration in the development of any grinding process. Damage as a result of grinding is predominately of a thermal nature and results in changes to the material properties in the near surface region. One such change is the residual stress, which was measured using Barkhausen Noise intensity instrumentation, which provided a reliable early indication to a build up in thermal energy. Developments in thermal modelling supported by temperature measurements provided a better understanding of the HEDG regime. The model employed new energy partitioning theories together with circular arc modelling of conditions along the contact length. A model was derived to predict the surface finish produced with the *Superfinish Grinding* approach, this again provided an increased understanding of the grinding process.

Industrial trials have shown how *HEDG* can be implemented on standard production machine tools for the cylindrical plunge grinding of crankshaft components. The process demonstrated the potential for improved surface integrity, whilst maintaining surface finish and form accuracy. The same grinding machine was also used to generate high quality surfaces using a *Superfinish Grinding* process. Roughness values of the order of $0.1\mu m$ R_a were routinely obtained exhibiting reduced levels of grinding directionality. Thus, using a single machine tool and a single set-up, exceptionally high stock removal rates are achievable in a roughing cycle followed by superfinishing to generate the required surface characteristics and profile.

Acknowledgements

I wish to acknowledge the support from the following groups and individuals throughout this project:

The *School of Industrial and Manufacturing Science (SIMS)* at *Cranfield University*, specially for the guidance from Professors D.J Stephenson and J. Corbett, and assistance from Andrew Baldwin.

The generous support of my sponsor Cranfield Precision, and its parent company Landis Lund, who allowed me to undertake this work as part of the following contracts:

- Development of Innovative Manufacturing Technologies for Reducing Process Chain (FP5 – Growth Project "Ultraflex", Contract No. G1RD – CT2000 – 00370)
- A New Grinding Regime - Thermal Limitation to Material Removal by Grinding (EPSRC Grant No. GR/R68795)

Finally, thanks to my wife Amanda and son Samuel who both provided a great deal of encouragement and support throughout this work.

Publications:

Towards a More Efficient Grinding Process

P. Comley, D. J. Stephenson and J. Corbett

5th International Conference on Behaviour of Materials in Machining, 12-13 November 2002, pg 303-306, ISBN: 1-86125-156-4

High Efficiency Deep Grinding and the Effect on Surface Integrity

P. Comley, D. J. Stephenson, J. Corbett

Advances in Abrasive Technology VI, Key Engineering Material Vols. 257-258 2004, pg 207-212, ISBN: 0-87849-933-4

Table of Contents:

Figures:

Tables:

Notation:

a	-	Depth of cut
A	-	Constant
Al_2O_3	-	Aluminium Oxide
b_s	-	Grinding Wheel Width
B	-	Constant
BN	-	Barkhausen Noise
C	-	Specific Heat Capacity
CBN	-	Cubic Boron Nitride
C_{factor}	-	C-factor
CP	-	Cranfield Precision
D_e	-	Effective Wheel Diameter
d_g	-	Grinding Wheel Grit Size
d_{max}	-	Depth limit of PVD coatings
e_c	-	Specific Grinding Energy
e_{ch}		Chip Energy
d	-	Depth of cut
f	-	Signal Frequency
F_r	-	Temperature Ratio
$HEDG$	-	High Efficiency Deep Grinding
HRC	-	Hardness Rockwell C
h_f	-	Fluid Convention Coefficient
h_o	-	Constant
k	-	Thermal Conductivity
K^*	-	Characteristic Grinding Value
l_c	-	Contact Length
LL	-	Landis Lund
n_c	-	Number of Active Grits per unit surface area
P	-	Peclet Number
PVD	-	Physical Vapour Deposition
q_f	-	Fluid Heat Flux
q_{ch}	-	Chip Heat Flux
q_t	-	Total Heat Flux
q_s	-	Wheel Heat Flux
q_w	-	Workpiece Heat Flux
Q'_w	-	Specific Material Removal Rate
r	-	Average Width-Depth Ratio of groove produced on Surface
R_a	-	Surface Roughness – Centre line average
R_{ch}	-	Partition Ration of Chip
R_f	-	Partition Ration of Fluid
R_{sw}	-	Partition Ration of Workpiece-Wheel
R_w	-	Partition Ration of Workpiece
R_t	-	Surface Roughness – Peak to valley
R_q	-	Surface Roughness – RMS
R_z	-	Surface Roughness – Ten Point Height
SEM	-	Scanning Electron Microscope

SGE	-	Specific Grinding Energy
SiC	-	Silicon Carbide
s_p	-	Peripheral Speed of Workpiece
s_t	-	Crossfeed
t	-	Constant
T_b	-	Mineral Oil Film Boiling Temperature
T_{ch}	-	Chip Temperature
T_b	-	Mineral Oil Film Boiling Temperature
T_{con}	-	Contact Surface Temperature
T_{fin}	-	Finished Surface Temperature
u	-	Specific Grinding Energy
u_{ch}	-	Chip Energy
u_{pl}	-	Ploughing Energy
u_{sl}	-	Sliding Grinding Energy
v_f	-	Axis Infeed Velocity
v_s	-	Grinding Wheel Velocity
v_w	-	Workpiece Velocity
W	-	Wheel Width
x	-	Transverse Rate
y	-	Constant dependant on Grit Size
z	-	Constant
α	-	Thermal Diffusivity
β_w	-	Constant
δ	-	Electromagnetic Skin Depth
λ	-	X-Ray wavelength
μ_o	-	Relative Permeability of Vacuum
μ_r	-	Relative Permeability of Material
ρ	-	Density
σ	-	Conductivity of Material
θ	-	Diffraction Angle
θ_m	-	Temperature
π	-	Pi

1 Introduction

Cranfield Precision (CP) specialises in the development of special purpose machine tools typically in the 'state of the art' sector. The combination of their own proprietary *CNC* control system, process development capability, design and production facilities make CP a unique company. Acquired by Landis Lund for *R&D* activities in 1995, it is still situated on the University campus with which it maintains a close working relationship. Landis Lund (LL) are manufacturers of cam and crankshaft grinding machines for the automotive industry. LL has maintained prominence in this sector by developments including the first *CNC* camshaft-grinding machine using an electronic gearbox. Such developments were done in conjunction with CP, hence the intent and ability to introduce new technology within the production machine tool sector is well established.

The research objective for Cranfield Precision and its parent Landis Lund was to develop a better understanding and hence enhance the application of grinding processes within their field of machine tool expertise. An integral part of this development was the requirement to monitor surface integrity. This in itself is becoming increasingly recognised as being important to the production of components with the required surface quality. The findings from this research will ensure that LL remain competitive in the Machine Tool industry with their grinding products. Grinding regimes at both extremes of the material removal rate were selected for investigation and the current surface integrity techniques assessed.

Work undertaken for this research has contributed to two Government funded projects. The first Ultraflex was intended to develop innovative manufacturing technologies for reduction of the process chain in the automotive industry. The objective was to minimise the number of process steps to both rough and finish grind automotive components, producing finished surfaces of an optical quality. Two components were selected, the first a transmission shaft, the second an engine crankshaft. The second project was titled 'Thermal Limitations to Metal Removal by Grinding (High Efficiency Deep Grinding)' and its objective was to study grinding zone temperatures and coolant efficiency in order to optimise material removal rates whilst reducing surface and sub-surface damage. There are a number of collaborators within both these projects including Universities, machine tool and tool manufacturers, together with automotive producers. Further detail are given in the appendix.

1.1 Grinding

Grinding is traditionally a finishing process employed to apply high quality surfaces to a workpiece. This was possible due to the increased number of cutting edges present on a grinding wheel over that of conventional single point cutting tools. Better control of grinding wheel topography through wheel production and following that with dressing techniques have produced progressively better finish grinding capabilities.

Today finish grinding is constantly being pushed to the limits in order to achieve the high levels of surface quality required by the advancing technical and precision aspects of modern products. Typical of these products are automotive engines where developments such as higher power outputs and lower environmental emissions have

placed increasing tighter tolerances and quality demands on engine components. The increasing demands mean that the use of post-grind processes such as lapping, honing and belt/stick finishing have been introduced to achieve surface texture specifications. The use of such additional manufacturing processes adds cost to the process chain with additional machines and cycle times. As a result there is additional pressure to reduce the cost of preceding operations in order to maintain the overall cost levels.

At the other extreme of material removal rate further developments in grinding technology together with the machine tools has resulted in grinding being increasingly competitive as a roughing process. Here large quantities of material typically in the region of *1kg* on a crankshaft forging are removed before subsequent hardening, tempering, straightening and finish grinding. Over recent years grinding and milling have competed in this field, and small advances swing the balance periodically between the two technologies.

The aspect of automotive engine production important to LL and facing increasing competition is the grinding of crankshafts, this will form the focus of the research. Materials utilised for crankshafts are either a cast iron or low alloy steel. Steel has been selected for this research, as it provides the greatest challenges to the production process because of the greater difficulty in grinding this material. A typical process chain for the steel components would be machining of centres and end diameters of a forging, followed by drilling, machining of pins and mains, hardening, straightening, finish grinding of all bearing faces and finally superfinishing. There are a number of operations within the process chain for the crankshaft in which grinding can be employed, those of interest here are the cylindrical plunge grinding operations. The two operations suitable for this mode of grinding within the cycle are:

1) Rough grinding of the main and the pin features both with journal and web faces
2) Finish grinding of main and pin journals

The crankshaft features are illustrated in Figure 1.1

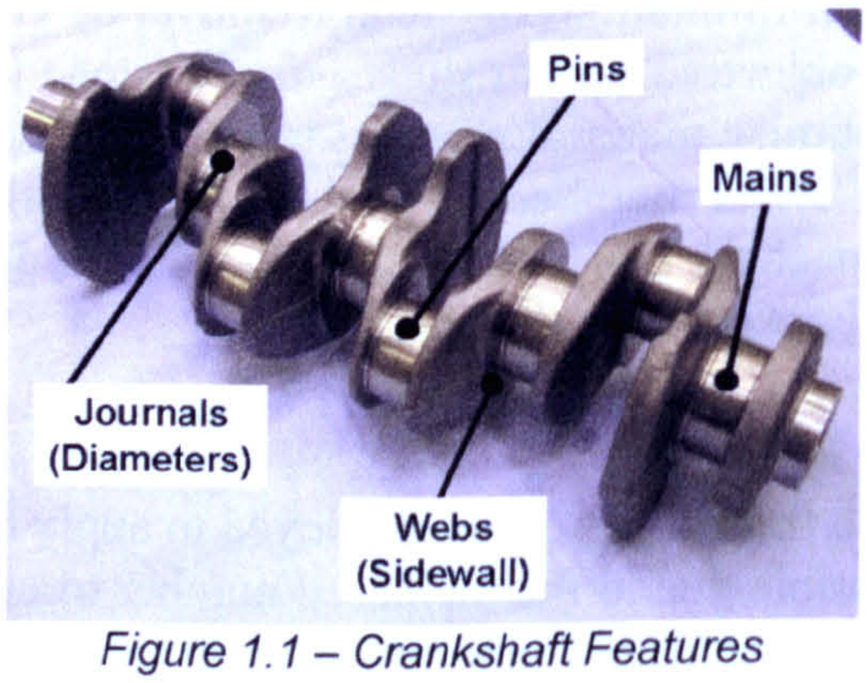

Figure 1.1 – Crankshaft Features

Currently as stated the rough grinding operation is in direct competition with turn milling. Turn milling currently has a higher removal rate but a reduced tolerance control, hence increased material removal is required with the finish grind process. Whereas rough grinding although with a reduced material removal rate has an improved accuracy and hence leaves a reduced amount of material for removal in the finish grind stage. This is illustrated in Figure 1.2. The finish grinding operation is followed by post-process operations to achieve the higher quality surfaces required. This is commonly

carried out using specialist superfinishing machines, which produce roughness figures down to $0.1\mu m$ R_a. The process is similar to honing but requires an additional investment in machines and time.

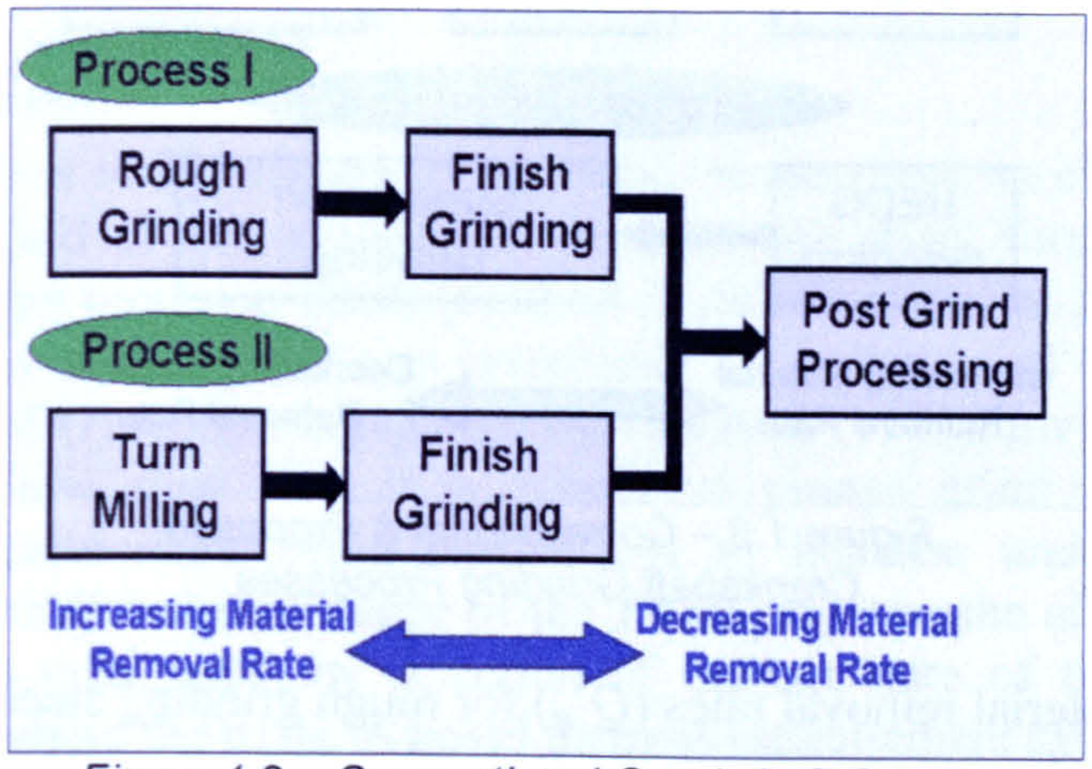

Figure 1.2 – Conventional Crankshaft Grinding Processes

Developments in rough grinding have led to higher removal rates. These improvements are dependent on high grinding wheel and workpiece speeds coupled with large depths of cut. This permits extremely high stock removal rates without thermal damage to the component surface, and is referred to *as High Efficiency Deep Grinding (HEDG).* The material removal rates for *HEDG* can compete with conventional cutting processes such as turn milling. To date this regime of grinding has only been applied in surface and peel grinding modes and, in these cases, to a limited extent. It is proposed to investigate the application of the *HEDG* regime in a cylindrical plunge-grinding mode and to validate the thermal characteristics. An important aspect of this investigation will be the surface integrity of the component.

Current plunge grind finishing operations involve a straight feed into the component, followed by a sparkout operation and then retraction. Superfinishing machine tools utilise belt or stone abrasive together with a transverse oscillating motion under force control. It is proposed to use the CNC system of an existing cylindrical production-grinding machine to translate the grinding wheel in a transverse oscillatory motion. This will further improve the surface roughness by reducing the magnitude of the grinding lay produced by conventional plunge grinding. Although oscillation has been applied to grinding machines in the past this has been done mechanically and with much greater levels of amplitude than that proposed within this research.

Figure 1.3 shows where the *HEDG* and *Superfinish* grinding processes would align with the current production processes for the manufacture of automotive crankshafts. It is expected that *HEDG* will increase the attainable material removal rate to the current or even higher level than that of turn milling. The aim of *Superfinish* grinding is to produce higher quality surfaces compared to those currently achieved with finish grinding. The result of this would be to remove the need for additional machinery and, reduce the process chain still further.

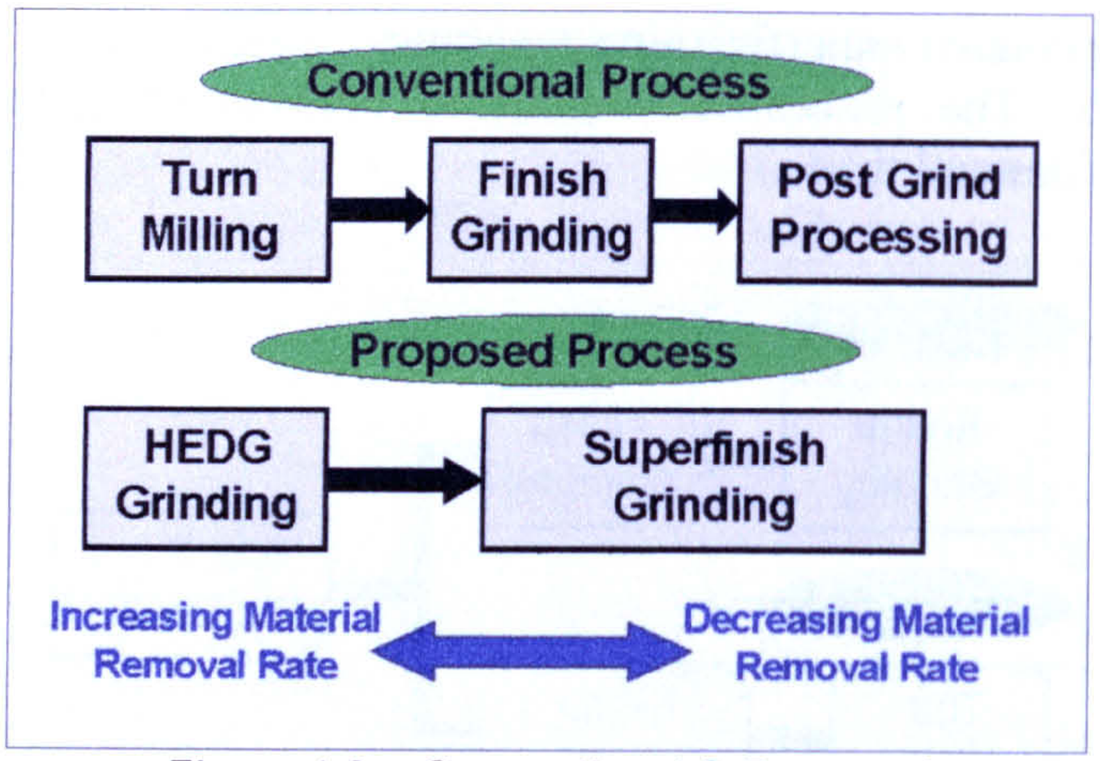

Figure 1.3 – Conventional & Proposed Crankshaft Grinding Processes

Current specific material removal rates (Q'_w) for rough grinding steel crankshafts with electroplated *CBN* wheel together with the research target are given in

.

Customer	Feature	Q'_w (mm³/mm.s)	
		Sidewall	Diameter
A	Mains & Pins	200	50
B	Mains & Pins	500	140
Ultraflex (^{t} - Target)	Mains & Pins	1000^t	200^t

Table 1.1 – Current Commercial Grinding Q'_w Rates

1.2 Surface Integrity

The *HEDG* and *Superfinish* regimes of grinding have different requirements with regard to the surface integrity. In *HEDG* it is the near surface region that is of most importance. Here the material characteristics and residual stresses in the near-surface region may cause problems both in the heat treatment process and finishing operation. Dependent on the depth of such effects there is the possibility that the finishing operation may not fully remove the affected zone, thus adversely affecting the final component performance. The surface finish is of secondary importance, as this will have a minimum effect on the subsequent processes of hardening and finish grinding. With the finish and Superfinishing process it is the surface finish that is of primary importance, as these are low removal rate process and as such would not normally introduce damage in the near surface region. Therefore in this case it is the surface roughness that is of interest, which in conventional plunge grind finishing operations is dominated by the grinding lay.

This work investigated the methods of evaluation for surface integrity applicable to the requirements for *HEDG* and *Superfinish Grinding*. These in turn were used to evaluate

and form a better understanding of the grinding regimes. As such a thorough understanding of the methods for quantifying the surface properties such as profile, stress, hardness, and burn, produced from the grinding tests were required.

1.3 Research Scope

The research aim was to investigate the grinding process and its effect on the surface integrity. With regard to the grinding there were two main thrusts, one for rough grinding and the other precision finish grinding. With rough grinding where the material removal is high it was the intention to investigate the existence of the High Efficiency Deep Grinding (*HEDG*) regime as reported by Tawakoli (1993). Investigations involved the grinding of a low alloy steel in a cylindrical plunge grind mode with thermal modelling and measurement being carried out to increase understanding. As the objective was to establish the existence of the *HEDG* regime, the effect of coolant type or application was minimised, by selection of current state of the art systems and commonality throughout the trials. A novel thermal measurement system was developed for use in cylindrical grinding as an aid to process understanding and the assessment of thermal loading. The results were tested against data from a thermal model developed in parallel with this work at Cranfield University. The second thrust of the grinding investigations was in the precision finish grind region, a low material removal rate process and in this instance referred to as *Superfinish Grinding*. Here the investigations looked at the surface finish and implemented a modified grind path to address grinding directionality issues commonly referred to as lay. Techniques for the assessment of the surface integrity were studied and the most relevant for each application selected for use in the analysis of surface produced from both grinding regimes.

The scope of the research was defined as:

> *The research will look at the grinding process and the effects this has on the component surface. Both 'High Efficiency Deep grinding with its high stock removal, and Superfinishing with micron level removal rates will be studied. The surface and subsurface investigation of components produced will enable characterisation and interrelationship analysis to be carried out. The aim is to increase the understanding and performance of the grinding process primarily through the study of the surface properties produced*

1.4 Workplan and Objectives

Initially a review of current developments in the relevant fields was undertaken, this is fully covered in Chapter 2 – Literature Review. This began with the field of grinding covering both the extremes of the material removal scale, namely *HEDG* and *Superfinishing*. Then abrasives and the structure of grinding wheels are introduced together with issues concerning and the 'state of the art' for coolant application. Following this the grinding wheel considerations themselves were covered, initially looking at the abrasive grit and the introduction of superabrasives. Then finally progress made with wheel structures. With the issues relating to grinding covered, the next step concerned the surface integrity. Here the first step was to consider the importance of the

surface integrity and how grinding affects it. The mechanical interaction changes the surface texture, and the injection of thermal energy cause metallurgical changes to the near surface zone. Analysis techniques to measure both aspects were identified.

The next step was to establish suitable machine tools, analysis techniques and layout the program of trials and analysis, this is covered in *Chapter 3*. The work was carried out on a number of machine tools, initially one located in the School of Industrial and Manufacturing Science at the Cranfield University. These tests were aimed at establishing the boundaries of both the *HEDG* and S*uperfinish* grinding regimes. Two machines located at Landis Lund were used for the full trials, one for HEDG and the other for Superfinish, the split was primarily for software and wheel issues. Details are given on the techniques for surface and sub surface characterisation, namely surface finish, visual, microstructural and residual stress and where they were employed. Also covered are the novel thermal measurement technique developed for cylindrical grinding and the assessment procedures carried out on the HEDG grinding wheels to determine wear. Finally test programs are described both for the *HEDG* and *Superfinish Grinding* trials; in both cases initial tests were carried out in a surface grind mode following by a cylindrical plunge grind mode. Surface grind work aimed to establish the effect of grinding without further process interaction resulting from sparkout, as the latter cannot be easily eliminated from cylindrical plunge grinding operations. Whilst cylindrical plunge grind work established the existence of the *HEDG* regime and effectiveness of the modified path grind theory for precision finish grinding.

The grinding investigations began with the *HEDG* work. Surface grinding tests looked at the effect of the grinding action on the surface integrity of the component using a setup representative of a production environment. The surface grinding mode ensured that there was no further surface to wheel interaction post *HEDG* grind, that may affect the surface integrity produced. The objectives for this series of tests were to establish the burn threshold of the material, test different grit size grinding wheels and develop the analysis techniques for the detection of thermal damage. This in turn enabled the existence of the *HEDG* regime to be determined. Cylindrical Grinding with analogous samples progressed the investigation into the *HEDG* regime utilising a grinding mode suitable for the production of automotive crankshaft components, using a set-up representative of a production environment. There were a number of objectives for this portion of the investigations. These were to initially establish the Specific Material Removal Rate (Q'_w $mm^3/mm.s$) attainable with cylindrical grinding and test different types of grinding wheel type structures, and then to develop the proposed method for thermal measurement of the finished surface and apply a thermal model and determine correlation. Finally it was necessary to determine the existence of *HEDG* in cylindrical grinding. The production cylindrical grinding trials carried out on production machinery with real crankshaft components concluded the investigations into *HEDG*. The objective was to apply Specific Material Removal Rate (Q'_w $mm^3/mm.s$) attained in previous work to a production environment and validate the process application by measurements of residual stress, geometry, grinding wheel wear.

Superfinish Regime grinding investigations were carried out together with modelling of the surface finish performance. The aim of the surface grinding trials was to determine the type of grinding wheel together with truing and dressing techniques required for the

full program of work. Results provided benchmark performance data for subsequent trials. The initial cylindrical plunge-grinding tests were carried out to provide surface finish data in both the conventional straight plunge grind and modified path plunge grind modes. The final phase of the cylindrical plunge grinding trials was carried out on a production machine tool to demonstrate that implementation of the modified grind path enhanced the surface finish values. Results were correlated with modelling predictions. The grinding investigations are described in two sections, the *HEDG* in *Chapter 4* and *Superfinish Grinding* in *Chapter 5*.

A discussion of the findings is contained in *Chapter 6*, followed by the conclusions and recommendations for further work in *Chapter 7*.

2 Literature Review

This chapter introduces the background and current understanding of grinding together with its effect on the surface integrity. The first section looks at grinding technology in general and then goes on to discuss *HEDG* and *Superfinish Grinding* regimes. Following this the issue of surface integrity is reviewed with special attention being paid to the techniques utilised in surface and near-surface assessment.

2.1 Grinding

Grinding has been with us from earliest times when it was used to grind stones to the required shape for cooking and eating utensils (Malkin, 1989). It can be described as a machining process that utilises hard abrasive particles as the cutting medium, Whitehouse (1994) categorizes this into three main types of processes, namely:

Grinding: *Fixed grain, high speed.*

Honing: *Grains held rigidly, but speeds are low and reciprocating movement often used. Superfinishing is similar except that a slight axial vibration is used.*

Lapping: *Grains are loose, contained in a fluid and therefore free to move*

A forecast for the future of production engineering carried out by Merchant (1971), predicted that grinding would play an increasingly important part of the machining processes with new developments being made. This has proved to be the case with subsequent developments such as superabrasives, High Speed Grinding and High Efficiency Deep Grinding (*HEDG*) having been made. Today grinding is an important operation employed in manufacturing, once used primarily as a finishing process it now has established a place in high material removal processes. Issues important in the continuing development of grinding are correct macro and micro surface profile for the intended purpose, compressive residual stresses, minimum quantity lubrication and high productivity.

2.1.1 Grinding Regimes

Developments made in grinding regimes include Creep feed, High speed and *HEDG* with high material removal rates, and high precision grinding with low removal rates. Creep feed, high speed and *HEDG* are used for rough grinding processes where removal rate rather than surface finish is an issue. Whereas high precision grinding is used as a finishing operation for which surface finish is the overriding concern. Abrasive developments together with improvements in machine stiffness have played a major role in the development of these processes (Kuang & Jen-Sheuan, 1994 & Inasaki et al, 1993).

2.1.1.1 Creep Feed Grinding

Creep feed grinding is characterised by the use of slow workpiece velocity coupled with large depths of cut (Malkin, 1989). The increased depth of cut results in an increased wheel-workpiece contact length show by the relationship in Equation 2.1. As a result higher specific grinding energies are present than those associated with regular surface grinding, and there is the potential for even greater increases as process conditions deteriorate over a period of time. The effect of greater specific grinding energies

coupled with longer contact zones required additional steps to be taken to avoid thermal damage to the workpiece.

$$l_c = \sqrt{(a \cdot D_e)}$$ *Equation 2.1 – Contact Length*

Where:

l_c	-	*Contact length*	*(mm)*
a	-	*Depth of cut*	*(mm)*
D_e	-	*Effective Wheel Diameter*	*(mm)*

Brinksmeier & Minke (1993) reported on the influence of coolant systems and concluded this was a major area of importance and that improvement in these had a significant impact on the grinding performance. Liverton (Shaw, 1996) demonstrated the application of creep feed grinding in a cylindrical plunge-grinding mode. The process used a 2mm incremental depth of cut, 1rpm workpiece and 30m/s wheel speed with an Al_2O_3 wheel. Data reported by Shaw (1996, pg.398), shown in Table 1.1, provides a comparison between creep feed and conventional grinding processes.

Parameter	*Creep Feed*	*Conventional*
Wheel	*38 A 60 I V*	*19 A 60 K/L V*
Wheel Diameter (mm)	*600*	*600*
Wheel Speed (m/s)	*60*	*35*
Wheel Depth of Cut (mm)	*5*	*0.0172*
Work	*AISI 1045*	*AISI 1045*
Work Diameter (mm)	*155*	*115*
Work Speed (mm/min)	*122*	*34,350*
Width of Cut (mm)	*30*	*50*
Specific Grinding Energy (J/mm^3)	*50*	*31*
Grinding Ratio	*113*	*24*
Effective Wheel Diameter (mm)	*123*	*97*
Wheel – Work Contact length (mm)	*24.8*	*1.29*
Mean Undeformed Chip Thickness (μm)	*0.55*	*3.1*

Table 2.1 – Comparison of Creep Feed & Conventional Cylindrical Grinding Operations

For the creep feed process the depth of cut is increased from 0.0172mm up to 5mm whilst the workpiece velocity is reduced form 34,350mm/min down to 122 mm/min. This effectively increases the specific material removal figures and reduces the mean undeformed chip thickness. The result is improved wheel wear and surface finish, without thermal damage to the component's surface.

There are many applications for which Creep Feed Grinding is used in today's manufacturing environment. Current applications include:

- Profile grinding of aerospace turbine blade root forms in a single pass
- Flute grinding of drills and milling cutters from solid bar
- Form grinding of gear teeth in single pass
- Camshaft lobe grinding in single revolution of workpiece

The increased power requirement and forces associated with Creep feed grinding however mean that the machine tools and grinding wheels have a higher cost than those utilised with conventional machines.

Work on thermal modelling described by Rowe (2001b & 2001c) investigated the effect when larger depths of cut are used. He concluded that the increased contact length, a result of the increased cut, meant that temperatures in the contact and finished zones were unlikely to be uniform, see Figure 2.1. Therefore he proposed that a triangular heat flux distribution be used for modelling.

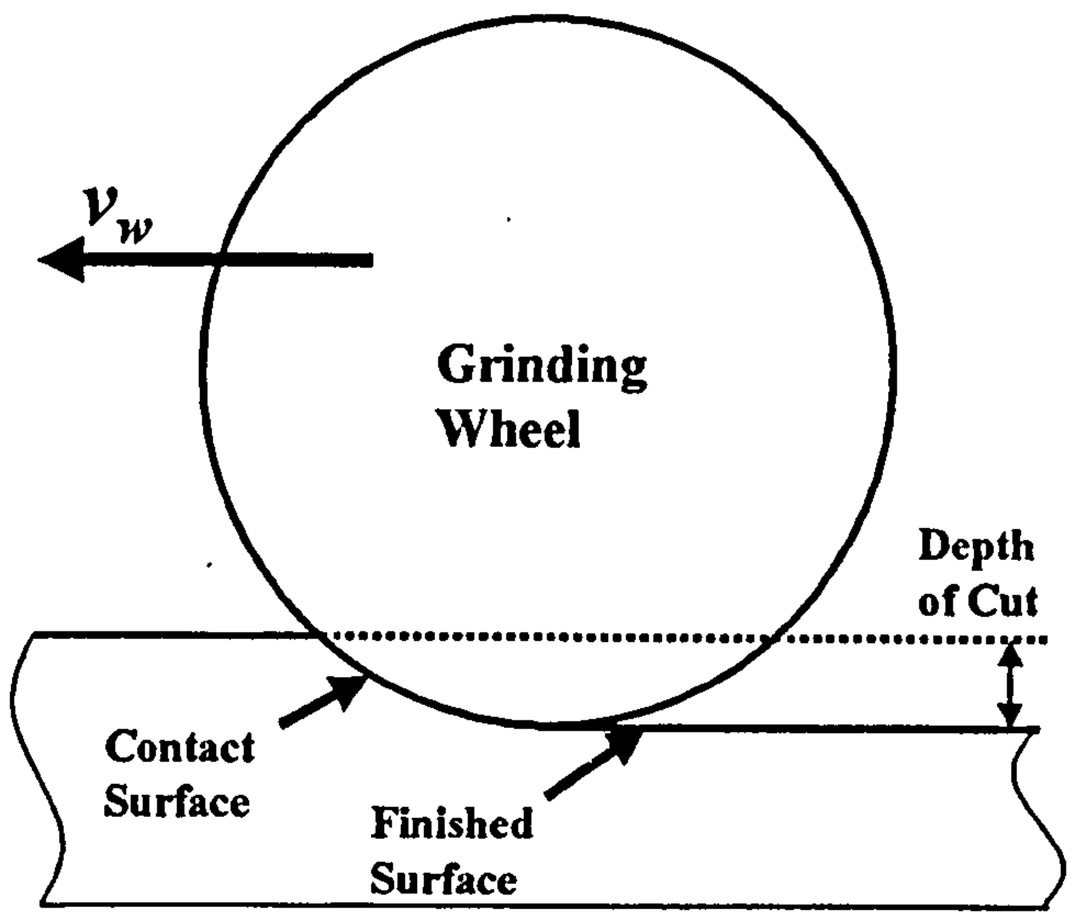

Figure 2.1 – Grinding Contact Surfaces

Therefore the proportion of heat energy reaching the finished surface would be less than that found by conventional modelling. Subsequent grinding trials carried out provided good correlation in support of this approach.

2.1.1.2 High speed Grinding

With the increasing progress in grinding wheel construction technology came the capability to attain higher peripheral wheel speeds, up to *200m/s* with electroplated wheels in some cases. A development stemming from this high speed grinding utilises extremely high feedrates together with small depths of cut. One application employing this technology today is in the manufacture of aerospace turbine blades. The profile grinding mode process produces turbine blade root forms by multiple passes with continuous dressing and in one such application is known commercially as *Viper Grinding* (Gibbons, 2005). As in the case with creep feed grinding, the machinery for this grinding regime is more expensive than conventional units.

2.1.1.3 High Efficiency Deep Grinding

Advances in superabrasive technology, wheel design and machinery enabled the development of a new regime of grinding referred to as High efficiency Deep Grinding

(*HEDG*). This utilises higher wheel and workpiece speeds coupled with a larger depth of cut, thus *HEDG* is in fact a hybrid of creep-feed and high speed grinding.

The process as described by Tawakoli (1993) permits extremely high stock removals Table 2.2 provides a comparison of typical machining parameters together with the specific material removal rates for conventional, Creep feed and *HEDG* surface grinding regimes.

Machine Settings	Grinding Approach		
	Conventional	Creep-feed	HEDG
Depth of Cut a (mm)	Low 0.001-0.05	High 0.1-30	High 0.1-30
Workpiece Speed v_w (m/min)	High 1-30	Low 0.05-0.5	High 0.5-10
Wheel Speed v_s (m/s)	low 20-60	low 20-60	High 80-200
Specific Material Removal Rate Q'_w ($mm^3/mm.s$)	Low 0.1-10	Low 0.1-10	High 50-2000

Table 2.2 – Process Variables & Q'_w rates for Different Grinding Modes

Investigations reported on by Brinksmeier & Minke (1993) stated that there were a number of machine tool issues that required addressing to successfully implement the *HEDG* process. These comprised high machine stiffness, high spindle powers coupled with high wheel speeds and the use of superabrasive wheel technology. Tawakoli (1993) applied the *HEDG* regime during a set of laboratory grinding trials on a machine tool with a specification that met these criteria. A specific material removal rate (Q'_w) of $1000mm^3/mm.s$ was achieved on thin samples. The total net power was seen to increase with the higher wheel speed, however the component related to material removal remained approximately constant. This meant that the energy seen by the workpiece did not increase in proportion to the increase in material removal, therefore suggesting that the thermal energy input may not have risen. The increase in the no load state was attributed to the increased braking effect caused by the higher-pressure coolant application. Tawakoli suggested that with the increased depth of cut and specific stock removal there would be an associated increase in the contact zone temperature. He reasoned this would not result in higher surface zone temperatures if the transfer of heat from the contact to surface zone was not too great, therefore concluding that the threshold for *HEDG* was governed by control of heat transfer to the surface zone temperature. Tawakoli proposed this would be the case, as with the increased work speed there was less time for the transfer of heat from contact to surface zone. Therefore he reasoned that the trend for the surface zone temperature versus Q'_w was as shown in Figure 2.2.

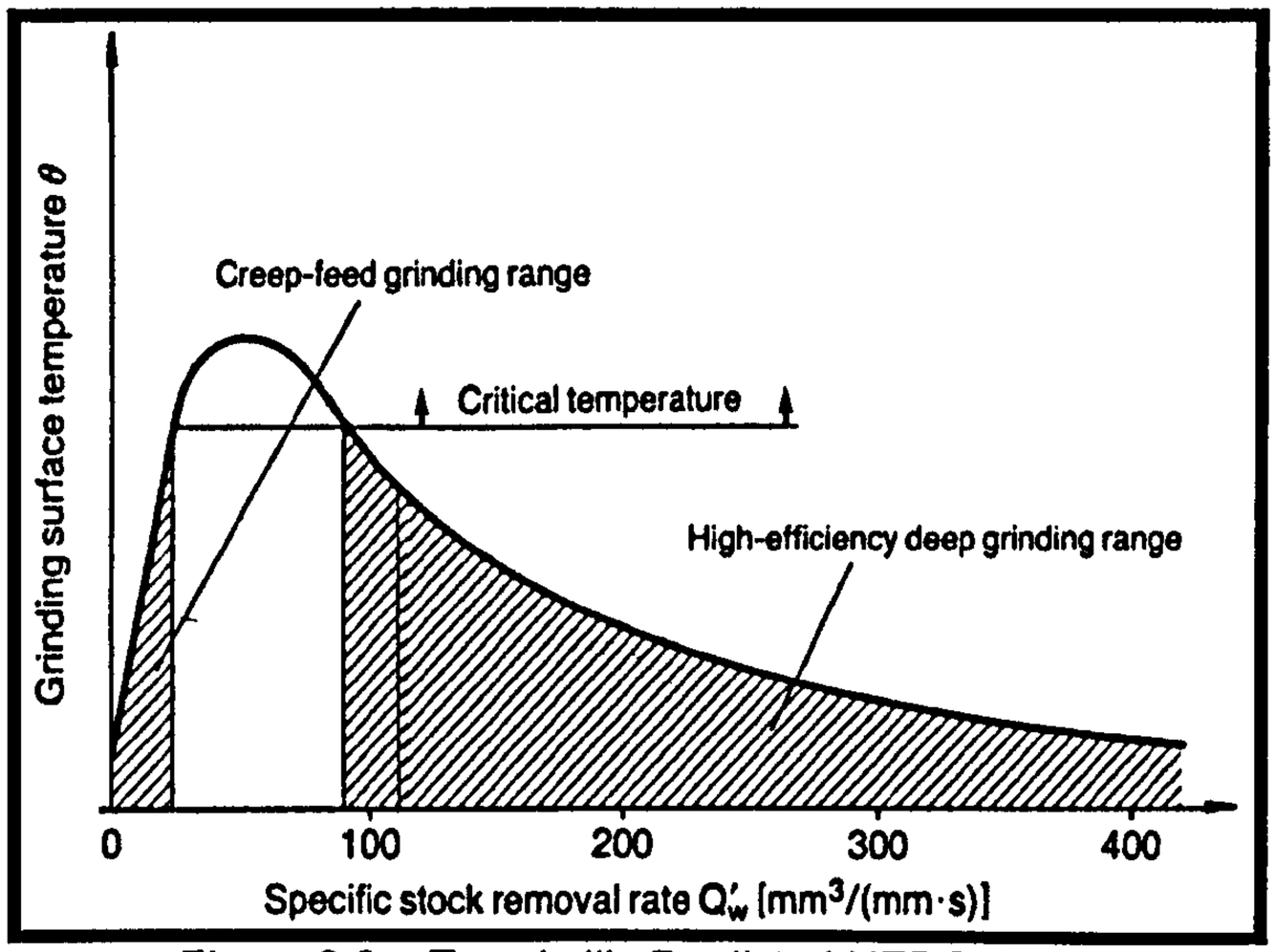

Figure 2.2 – Tawakoli's Predicted HEDG Curve

Further investigations were carried out by Rowe (2001a & 2000c) which addressed the thermal aspects of the *HEDG* regime, both thermal modelling and grinding trials were carried out. Temperatures for the contact surface were found to be in excess of that which would result in thermal damage. However the work concluded that a combination of the increased contact length and high wheel speed resulted in lower temperatures at the finished surface and therefore prevented thermal damage at this point. Grinding trials carried out on *IN718* (Stephenson et al, 2001) found that in the high Q'_w region of *HEDG* only around *10%* of the heat entered the workpiece. This finding was supported by thermal modelling carried out, and correlated with the previous findings by Rowe. Stephenson et al (2002) describes some investigations carried out on a low alloy steel in the *HEDG* regime where trials were undertaken in both the surface grind and cylindrical peel grind modes. Q'_w rates in excess of $400mm^3/mm.s$ were achieved in the latter mode without any thermal damage to the component's surface. Finally Stephenson (2003) states that in the *HEDG* regime significant reductions in the finished workpiece temperature are possible. The thermal properties of both the workpiece material and abrasive are important considerations as they have a direct input on the partitioning of the heat energy between the workpiece, wheel, coolant and grinding chips. A thermal model was presented which took all these factors into account and allowed their effects to be interpreted.

The research carried out into the *HEDG* regime to date has concentrated on the surface grind mode, with some more recent investigations going on to look at the cylindrical peel grind mode. No published work has been found, to date, on the existence of *HEDG* in the cylindrical plunge grind mode.

2.1.1.4 High Precision Grinding

Typically today's ultra precision grinding can produce surfaces of an optical grade on certain materials, namely brittle materials such as glasses, Shore (1995). In these cases the grinding mode commonly utilised has the wheel and workpiece rotation in perpendicular orientations, as illustrated in Figure 2.3. This reduces surface roughness grinding directionality in the form of grinding lay. With hardened alloy steel

components, such as crankshafts in the automotive industry, the cylindrical plunge grinding mode, has workpiece and wheel motions in a common plane. Figure 2.4 demonstrates the relative motions.

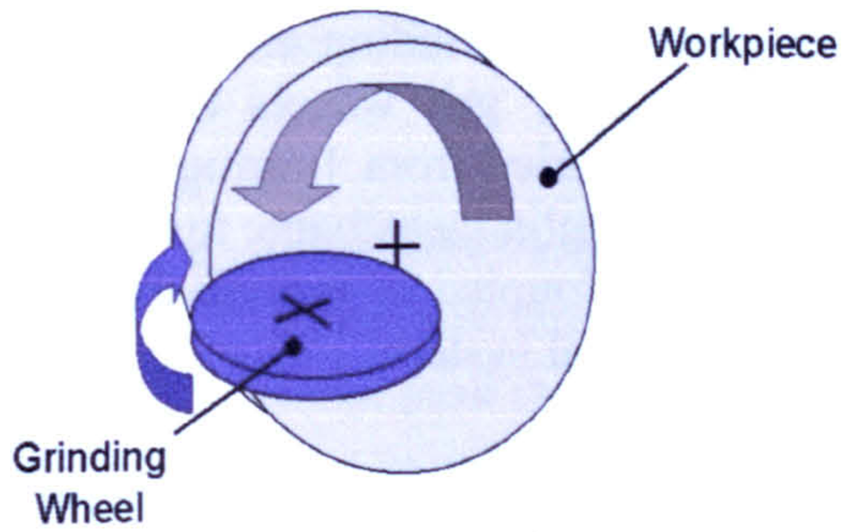

Figure 2.3 – Face Grinding Configuration

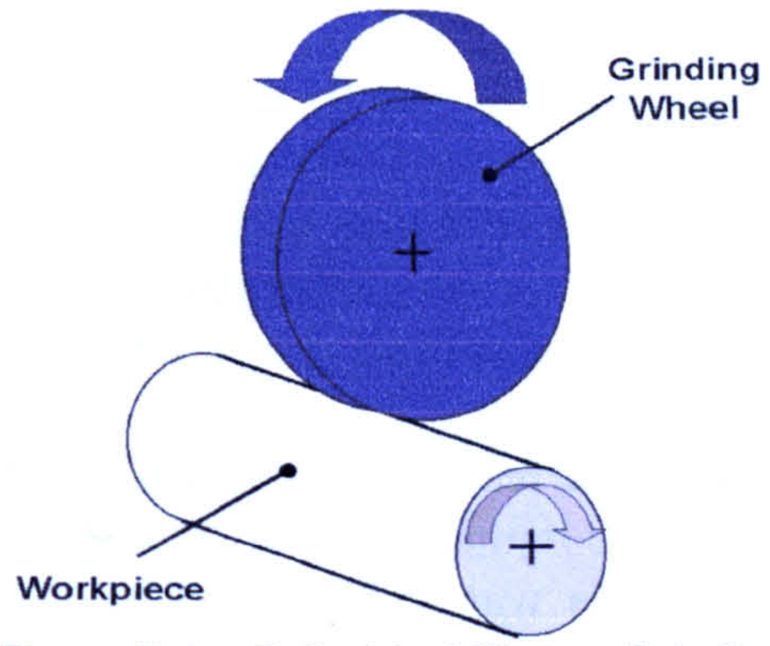

Figure 2.4 – Cylindrical Plunge Grinding Configuration

The result is a greater degree of directionality produced on the finished component surface. To reduce directionality the final high quality surface finish is commonly applied using Superfinishing machines, a process first researched in the 1930's (Shaw, 1996) for automotive bearings to improve the fatigue life. The Superfinishing process applied on these types of machines is similar to that of honing using shaped abrasive sticks or abrasive coated belts. The basic differences to honing lie in the reduced oscillating stroke and pressures employed. The oscillation coupled with the rotation of the part, both at low speeds, produce a randomly overlaid zigzag effect, which reduces any grinding directionality present. The process is used to refine the surface finish rather than for size control. Marinescu (1997) describes the superfinishing of *M50* steel with this technique. Today, machines such as the Supfina manufactured by Supfina Grieshaber GmbH & Co claim roughness figures of down to $0.1\mu m$ R_a. The process is illustrated in Figure 2.5. A novel application used by Loladze et al (1982) for high precision grinding utilises an oscillatory motion orientated perpendicularly superimposed onto the grinding motion. The work was carried out in a face-grinding configuration as illustrated in Figure 2.6.

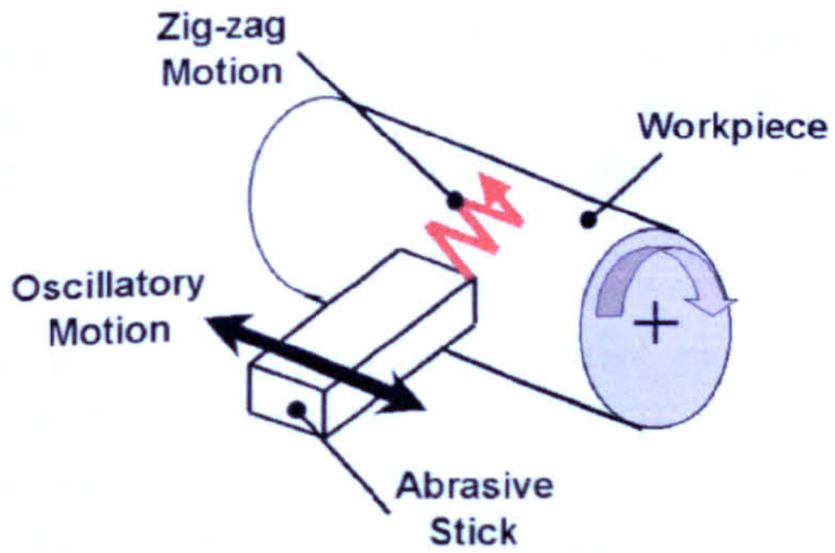

Figure 2.5 – Superfinishing Process Configuration

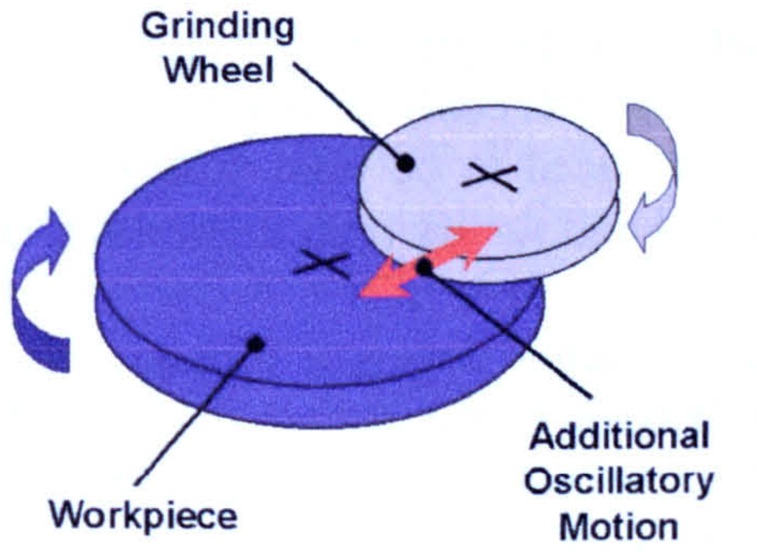

Figure 2.6 – High Precision Oscillatory Lapping Configuration

This produced enhanced surface roughness due to the modified grind path employed. The process configuration and cutting action were similar to that of lapping, the main

difference being in the use of a bonded grinding wheel as opposed to a lapping plate and abrasive slurry. Maksoud & Dean (1988) reported experimental investigations into camshaft grinding using an additional oscillatory motion. The oscillation was effected using a mechanical drive linked directly to the workpiece drive. It concluded that oscillation during either the infeed or sparkout in cylindrical grinding are effective in reducing surface finish, and can allow the use of coarser grit wheels than would normally be required. The amplitudes of oscillation used varied from 1mm up to 4mm. The limitation of this approach was that the mechanical coupling was liable to vibration, which would have a detrimental effect on surface finish. Coupled to this the frequency of oscillation was limited by the bandwidth of the mechanical system.

No published research was found for the use of high Speed CNC controlled oscillatory motion in conjunction with modern linear axis drive technology to improve surface quality. This was investigated in this research in the cylindrical plunge grinding of crankshafts to improve surface quality by the elimination of grinding directionality. Grinding directionality is described in the section covering surface finish.

2.1.2 Grinding Wheels

Grinding wheels consist of a combination of abrasive grits held in a bond structure with filler/pores. These are either formed into a wheel or fixed to a base material such as steel or aluminum to form a wheel. The grinding action of a wheel is dependent of the type and ratios of these three components. A keynote paper by Webster & Tricard (2004) summarizes the current innovations in abrasive products.

The two grinding regimes under investigation for this research are at opposite ends of the material removal scale, *HEDG* at the high end and *Superfinish Grinding* at the low end. Hence both investigations place different requirements on the grinding wheels. The remainder of this section will look in greater depth at the abrasives and wheel structure (bond and wheel type) with regard to the intended applications.

2.1.2.1 Abrasives

There are two main classifications of abrasive, conventional with materials such as aluminum oxide (Al_2O_3) and silicon carbide (SiC) and superabrasives which are either diamond or cubic boron nitride (CBN). The Al_2O_3 and SiC abrasives are still widely used in conventional grinding processes where cycle time is not critical and both machine tool and wheel costs need to be kept low. Superabrasives have a higher performance and therefore need to be used with higher specification machine tools to fully utilise this potential and justify their higher unit cost.

Fused alumina covers a number of mineral products which increase in performance from bauxite brown based alumina (BFA), through alumina-based white fused alumina (WFA), to Sol-Gel types. The manufacturing process for these abrasive material are described by Malkin (1989). Regular or brown aluminum oxide can be produced by fusing calcined bauxite with a small amount of coke and iron in an electric arc furnace at around 2,500°C. The material has a lower hardness and friability (higher toughness) relative to the purer white variety. White aluminum oxides are produced by the fusion of pre-purified Bayer process alumina in the Hall-Heroult electric arc furnace. The white grades are nearly *100%* Al_2O_3 and have sharp fracture facets. The more recently

developed Sol-Gels are produced by converting a colloidal dispersion of hydrosol ("sol") consisting of geoethite ($Al_2O3\ H_2O$) to a semi-solid gel. The gel is dried to a glassy state, crushed to produce grains of the correct size, and finally fired at *1300°C*. An abrasive property generally used to gauge performance is the Knoop Hardness, figures quoted by Harris (2000) for the abrasive types discussed above are given in Table 2.3.

Abrasive Substance	***Knoop Hardness (kg/mm²)***
Aluminum Oxide (brown)	*1,850*
Aluminum Oxide (white)	*1,950*
Aluminum Oxide (Sol-Gel)	*2,100*

Table 2.3 – Relative Knoop hardness of Al_2O_3 Abrasive Materials

Silicon carbide abrasive offers higher Knoop hardness than the various types of Aluminum oxide, and figures quoted by Malkin (1989) and Harris (2000) are between *2,480* and *2830 kg.mm²*. Silicon carbide is made by the reduction of sand with excess amounts of coke at temperatures above *2000°C* in an electric furnace. Silicon carbide offers an enhanced performance for non-ferrous materials. However because of its chemical composition it reacts with iron and steel alloys and as such is not generally suitable for these materials.

Superabrasive materials consist of diamond and cubic boron nitride (*CBN*). Diamond comes in both natural and synthetic forms, whereas *CBN* is solely a synthetic material. Diamond is the hardest known material and *CBN* is the next hardest and Hayden (2003) describes the emergence of these substances. Investigations to produce a synthetic diamond began at *GE* around *1951* with the first product introduced *1957*. The technique basically involved taking a graphite structure up to pressures in excess of 68kbar and temperatures of *3,500 °C*, with the addition of a molten iron nickel or cobalt catalyst to trigger the reaction. *CBN* was first produced in 1957 whilst *GE* were conducting further experiments to produce a substance harder than diamond, in this instance the base material was a hexagonal boron nitride. This was again taken to high temperatures (1500-2000°C) and pressures (50-90kbar), in this case with a catalyst of alkali metals and nitrides of lithium, calcium and magnesium to produce synthetic *CBN*. Initially because of its reduced hardness, compared to that of diamond, the full extent of the material's potential was not realised. Subsequent work revealed that *CBN* was suitable for the grinding of carbon steels for which diamond was not suitable.

GE commercially introduced *CBN* in 1969 as Borazon *CBN*, an abrasive intended for grinding hardened steel. The intrinsic strength and structure can be altered by variations in the process conditions, it can be produced either as monocrystaline, blocky-shaped large crystals or as strongly bonded microcrystalline grits that are irregular in shape. Malkin (1989) gives the crystal structure, density, melting point and knoop hardness for these materials. These together with values for other grinding abrasive materials are produced in Table 2.4. It is clearly apparent that the superabrasives *CBN* and diamond out perform the conventional abrasives in regard to both knoop hardness and melt

temperature. In comparison to *CBN,* diamond offers enhanced properties, but diamond as with *SiC* is not suitable for use on ferrous alloys because of its chemical composition.

Parameter	Aluminum Oxide (Al_2O_3)	Silicon Carbide (SiC)	Cubic Boron Nitride (CBN)	Diamond (C)
Crystal Structure	Hexagonal	Hexagonal	Cubic	Cubic
Density (g/cm^3)	3.98	3.22	3.48	3.52
Melting Point (°C)	2040	~2830	~3200 at 105kbar	~3700 at 130kbar
Knoop Hardness† (kg/mm^2)	2100	2400	4700	8000

† Approximate value – depends on crystal orientation and purity

Table 2.4 – Properties of Abrasive Materials

Grit hardness although an important parameter is not the only one that is significant to the abrasive medium's grinding performance. A proportion of the heat energy from the grinding process will be conducted away by the abrasive, the magnitude of which is dependent on the thermal conductivity of the abrasive itself. Morgan et al (1998) investigated the effective thermal conductivity of alumina and *CBN* in order to increase the accuracy of current partition heat ratio calculations and hence thermal modelling of the grinding process. He determined values of *35 W/mK* for alumina and *240 W/mK* for CBN. Therefore it is clear that *CBN* should offer an advantage over that of alumina in that an increased ratio of heat energy can be removed from the grinding zone. Rowe & Chen (2000) undertook an investigation into the performance of *CBN* wheels and concluded that the high thermal conductivity of the *CBN* allowed cooler grinding and as a result reduces the occurrence of undesirable tensile residual stresses.

CBN because of the advantages described is currently extensively utlised in the automotive industry for both rough and finish grinding in the production of crankshafts and camshafts. Hence this abrasive was chosen to conduct the grinding research described in this thesis.

The morphology of *CBN* is very complex, with its eight octahedral crystal faces being of two different types, four are terminated with nitrogen and four with boron. This is unlike diamond where all the faces are identical. Growth rates of the two types of face govern the final structural shape of the *CBN*. If growth rates of the different faces are equal then an octahedron will result, however if one type grows to the exclusion of the other the result will be a tetrahedron. The result of this is that the structure of the *CBN* can vary between a cubic and octahedral (as with diamond) and also between an octahedral and tetrahedral, see Figure 2.7. To aid designation of the structural properties Bailey & Juchem (1998) describes a series of numbers that are used, the first number describes the degree of cube to octahedral and the second the degree of tetrahedral to octahedral morphology. For example a cubic would be 0/8, and a tetrahedron 8/0.

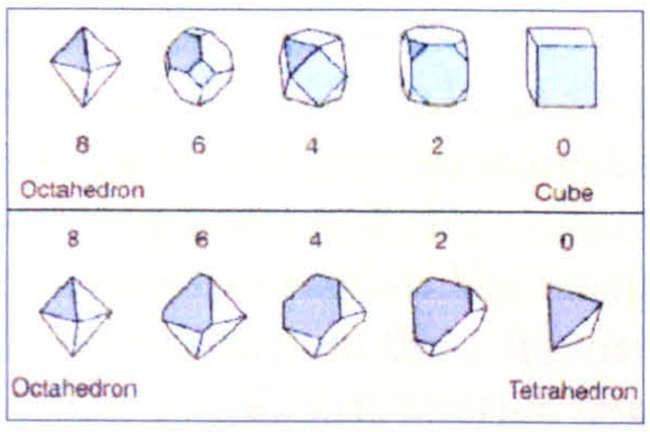

Figure 2.7 – Model System for CBN Structure

There are a number of producers of *CBN* grit, and these supply the grinding wheel manufacturers. A supplier's abrasive grit manufacturing process data and properties are commercially sensitive therefore data is not generally available. Grinding wheel manufacturers select these abrasive grit types and match them to a selection of bond materials and manufacturing techniques. The result is a product, which they believe will give an enhanced performance to that of their competitors. Bailey & Juchem (1998) covers a range of *CBN* abrasive grit currently available from one manufacturer Element Six (formally *DeBeer's)*, designated *ABN*. There are a number of types, which are named *ABN200, ABN 300, ABN 600* and *ABN800* these are illustrated in Figure 2.8. The structure of the *CBN* affects its physical properties such as strength, thermal stability and fracture behavior, Figure 2.9 shows the characterisation of the four *ABN* grades.

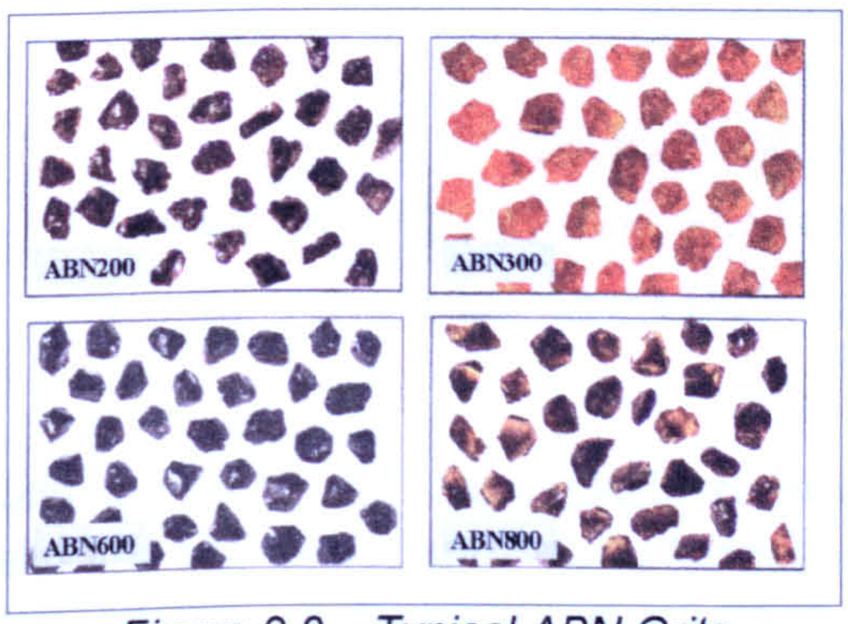

Figure 2.8 – Typical ABN Grits

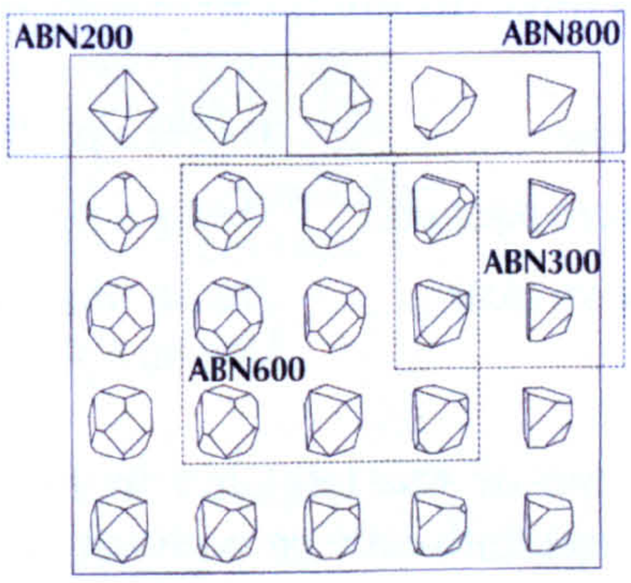

Figure 2.9 – CBN ABN Grades

ABN200 consists of black, friable irregular shaped particles. Its strength, thermal stability and sharpness make it particularly suitable for a wide range of standard vitrified bond applications. The fracture characteristics of the grit ensure that, on impact, small fragments break away from each particle. This contributes to free cutting characteristics combined with good wheel life. *ABN300* comprises clear amber coloured, irregular shaped, friable crystals. It is of a similar strength to *ANB200*, with a different crystal morphology, and hence, different fracture characteristics. The fragments are larger than with *ABN200*. In addition, its surface characteristics make it ideally suited for use in a wide range of electroplated tools. Its friability makes it ideal for use in metal bond tools that require a high degree of free cutting. *ABN600* is a black, blocky shaped, high strength abrasive with good thermal stability. It is used primarily in sintered and electroplated metal bonds, where the impact loads on the abrasive particles are high, and also in certain other application where a strong, blocky particle with relatively negative rake angle is required. Fractures with small breakaways and associated cracking in the crystal surface leading to additional controlled fracture.

ABN800 abrasive is a dark brown coloured, strong and very thermally stable. The particle shapes are sharp and angular, with a predominately truncated tetrahedral morphology. This unique combination of desirable crystal characteristics makes it highly suited for used in demanding vitrified bond applications. The thermal stability of the material ensures no significant reduction in strength after conventional firing. It is a high strength material similar to *ABN600* but more thermally stable. Fractures are sharp and angular with little associated surface cracking

The properties of *ABN600* or *ABN800* in an electroplated wheel would appear to be suitable for *HEDG* trials, with the *ABN800* having increased thermal stability. However one other aspect is the grit size available in each of these types in the case of *ABN 800, is* its exceptional thermal stability which is not as evident with sizes coarser than *B181*. Therefore the most suitable grit type would be the *ABN600* which is available in sizes up to *B427*. Work by Werner & Tawakoli (1988) on grinding deep slots at high speed reported the successful application of *ABN600* in high removal regimes. Similar products are available from other manufacturers such as *GE*, namely Borazon *CBN 500* which is very similar in performance to *ABN600*. Type *ABN200* would appear to be more suitable for the superfinish investigation either in a raw form for vitrified bond or metal clad for resin bond.

With use the abrasive grit is subject to wear. The wear can be assessed by dividing the grit into three different categories, namely:

New:	*This is a particle that has no visible damage*
Micro fractured:	*This is a particle that exhibits some clear damage to the particle.*
Deep Hole:	*This is where a particle is lost from the surface of the wheel leaving a cavity in the bond.*

The image of the left side in Figure 2.10 shows a photograph of a grinding wheel surface exhibiting these types of grit conditions. Whilst on the right hand side is a basis for the interpretation of such results in the form of a hypothetical particle wear progression for single layer electroplated wheels.

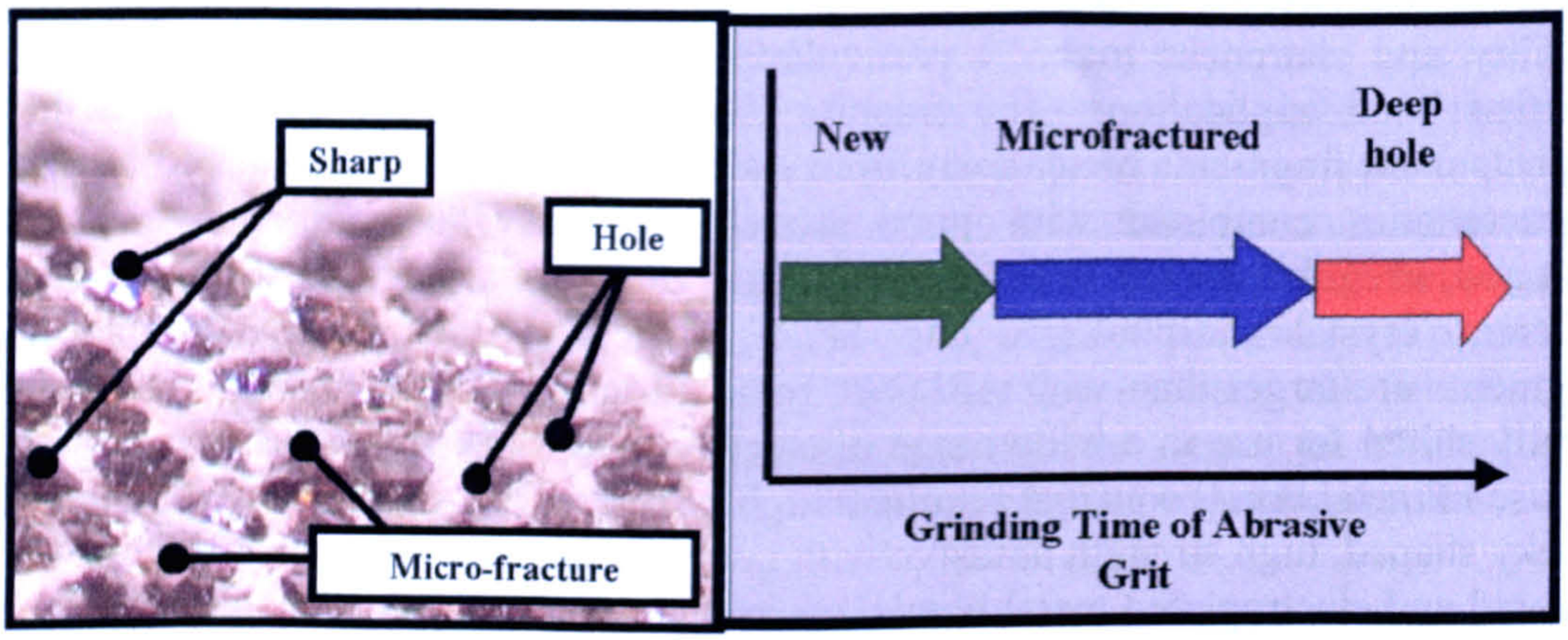

Figure 2.10 – Hypothetical Grit Wear Classification & Progression

In a new tool, all grit particles start off as *'New'* grit particles. After performing some work, they begin to wear by microfracture, and would be categorised as *'Microfractured'*. Finally, the grit particle is lost from the surface, leaving a *'Deep Hole'*. The distribution of particles visible on the wheel surface will follow some progression similar to that depicted in Figure 2.11 where material removed and wheel life are related to the progression along the bottom axes. Thus measurement of the particle type ratios enables an assessment of the wheel life to be made. Shi & Malkin (2003) stated that wheel failure tended to occur by stripping of the abrasive layer when the radial wear reached about 70%-80% of the grain dimension"

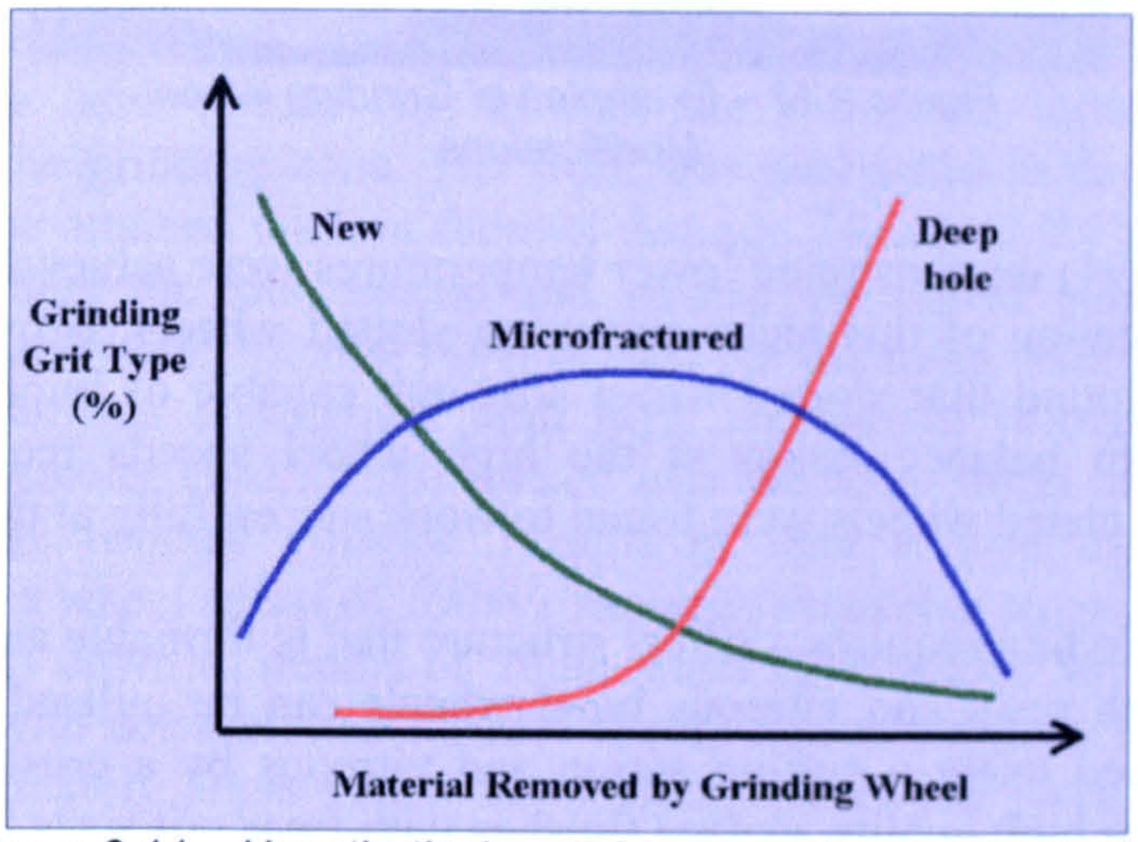

Figure 2.11 – Hypothetical particle wear category distribution progression for grit on a single layer electroplated tool

2.1.2.2 Structure

With superabrasive wheels the abrasive in held in a bond which in turn is applied to a disc of base material. The base material used is dependant on the intended wheel application, two typical materials are aluminum and steel, the later offering increased wheel strength and hence higher operating speeds. Methods of bonding these grits to the wheel include resin, metallic, vitrified bonding and electroplated types, all except the latter are capable of post manufacture forming. With resin, vitrified or metal bonds the abrasive is mixed with a binder and filler before final processing, and it is the filler that ultimately provides the porosity. Electroplated types differ in that the grit is placed onto the wheel surface and a plating applied over the top to hold the grits in place. In this case there is no filler to provide porosity hence the surface form is an important consideration to achieve an acceptable level of coolant retention and swarf removal.

Previous *HEDG* research carried out by Tawakoli (1993) showed that electroplated CBN wheels were the most successful as these wheels were able to run at speeds in excess of *120m/s* and stand the higher forces involved in grinding. With electroplated wheels the application of the grinding fluid is more difficult due to the lack of porosity within the wheel design, there is no porous bond structure in this instance. One approach to this problem is to improve the coolant application, which will be discussed subsequently. Another approach is to modify the shape of the wheel periphery, and this can be achieved by slotting or partial plating of the wheel surface. Work on creep feed

grinding reported by Suto et al (1990) describes a slotted wheel with the coolant feed from an internal channel through holes to the wheel periphery. Figure 2.12 shows how such modifications are made.

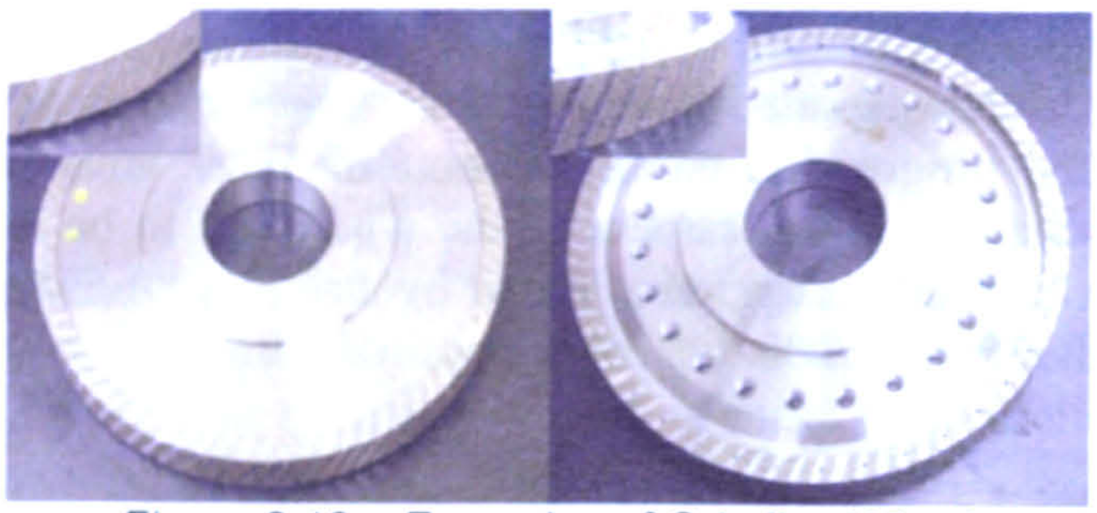

Figure 2.12 – Examples of Grinding Wheel Modifications

Zheng & Gao (1994) demonstrated lower temperatures were achievable in the grinding zone by the application of this technique using slotted wheels. However the work by Tawakoli (1993) found that slotted wheel although capable of improving the coolant flow suffered from balance issues at the high wheel speeds required for *HEDG*. However partially plated wheels were found to work successfully at the higher speeds.

Precision finish grinding requires a wheel structure that is formable and can therefore be trued in-situe. Both resin and vitreous bond wheels can be utilised, resin wheels are conventionally trued using a cutting action and vitreous by a crushing action. Resin wheels can produce high quality surface finishes with finer grit sizes but the softer bond means that bond breakdown/wear can occur with higher loads produced by increased removal rates. Conversely the vitreous bond wheels produce coarser surface finishes but the stronger bond structure enable higher forces to be taken by the wheel allowing higher removal rates. Coupled to this the nature of the vitreous bond provides a more open and therefore porous structure leading to improved coolant application.

2.1.3 Coolant

Grinding processes employ liquids as coolants which are used to reduce friction in the wheel-workpiece contact zone by lubrication, flush out grinding swarf and remove thermal energy from the contact zone. There are two basic types of coolant oil and water based. The oil-based normally consist of *80-95%* basic oil and can be divided into four groups, namely basic oil without additives, basic oil with chemically active additives, basic oil with surface active additives and basic oil with chemically active additives and *EP* additives (additives that form stable adsorption layers). Water based coolants can be divided into two groups. The first water-based solutions made up of inorganic and/or organic substances together with water. Second water-based emulsions containing *20-70%* oil, used in concentrations between 2 & 15%. Today's increasingly strict legislation targeted at the control of health hazards and environmental pollution mean that the real cost of the fluids used for the grinding process is rising substantially (Howes et al, 1991). Hence there is a sound economic basis for fluid minimisation or elimination strategies. Work that was reported by Howes (1990) showed that a critical limitation to the effectiveness of a coolant was film boiling of the fluid. Film boiling

was found to occur at 130^oC for water based fluids and about 300^oC for oil fluids. Later work by Stephenson (2002) also found the value for modern oils to be around 300^oC.

Brinksmeier (1999) brought together current thinking and discussed the role of the fluid in grinding. This covered friction in grinding, coolant types and compositions, coolant application, and the impact of cooling, friction and lubrication in the contact zone. Brinksmeier went on to conclude that: " No entirely uniform statements can be made as to the comparisons of oils, emulsions and solutions concerning workpiece roughness and residual stresses. Only a reduction of tool wear by the use of oil due to increased lubrication is clear". An approach to the coolant application described by Yokogawa & Yokogawa (1993) proposes for cylindrical grinding that in addition to a nozzle directed into the workpiece wheel gap, another is directed onto the rear side of the workpiece. The object of the latter nozzle was to cool the workpiece independently to what happened within the grinding zone. The work was successful in that it enabled higher removal rates to be attained without thermal damage. However the technique involved using different fluids for each nozzle and so had the added complication of fluid separation to contend with. Mineral oil was used for the main nozzle and the potential for flash explosion was highlighted with high application velocities. Further work reported by Brinksmeier et al (2000) looked into the application of shoe nozzles and their effect on the residual stresses. Results of tests carried out at Q'_w rates of $10mm^3/mm.s$ with a wheel speed of $100m/s$ showed favourable stress profiles, with little or no tensile stress down to depths of $70\mu m$ when shoe nozzle were used. Under the same conditions with conventional nozzles tensile stresses approaching 600MPa were witnessed approximately $10\mu m$ below the surface. Hence the work demonstrated that shoes nozzles were an effective method to increase compressive residual stresses whilst using relatively low coolant flow rates. Webster et al (1995) also carried out work investigating nozzle design. In this case the thrust of the work was to construct nozzles that produced a coherent jet of coolant and match the coolant exit speed with that of the grinding wheel periphery. The nozzles performed well, successfully allowing coolant to be targeted into the grinding zone from a distance up to 300mm away, the distance in itself allowed more scope for the design of the coolant application and well as better alignment. Matching of the coolant and wheel speed addressed issues with boundary layer around the wheel, hence this technique offered positive benefits when at running higher wheel speeds. Ebberll et al (2000) also reported on the importance of addressing the wheel boundary layer issue. In many cases the pressure and flow of coolant are increased in an attempt to reduce the onset of thermal damage. Klocke et al (2000) points out that this, without specific attention to nozzle design, may have the effect of increasing the hydrodynamic forces between the wheel and workpiece, resulting in higher grinding loads to overcome and thus geometric inaccuracies.

Investigations by Tawakoli (1993) into the HEDG regime demonstrated the effectiveness of the different coolant types by means of the observed surface temperatures. The findings showed that mineral oils produced the lowest temperatures followed by water based emulsion then dry grinding. Today most automotive manufactures utilise mineral oils for high removal rough grinding operations.

2.1.4 Workpiece Materials

The material is an important aspect to be considered in the overall grinding process if a successful outcome is to be achieved. Stephenson & Jin (2003) states that the thermal characteristics of the material are important in determining the temperature of the component's surface during grinding. Properties relating to thermal performance namely specific heat capacity, thermal conductivity and diffusivity vary considerably between different materials, see examples given by Stephenson (2003) in Table 2.5.

Material		Density (kg/m^3)	Specific Heat Capacity (J/kgK)	Thermal Conductivity (W/mK)	Thermal Diffusivity ($x10^{-6}$ m/s^2)
Steel	51CrV4	7770	460	42	11.7
	M50	7870	437	25.7	7.47
IN718		8220	424	11.45	2.72

Table 2.5 – Thermal Properties of Materials

The effect of these thermal properties on the heat transfer process within the grinding zone can be considered in terms of the peclet number. The peclet number is a dimensionless parameter and is dependant on the workpiece speed which is representative of the sliding speed of the heat source together with the contact length and thermal diffusivity of the material. The precise relationship is given in Equation 2.2.

$$P = \frac{v_w \cdot l_c}{4\alpha}$$

Equation 2.2 – Peclet Number

Where:

v_w	-	*Work Speed*	*(m/s)*
l_c	-	*Contact Length*	*(m)*
α	-	*Thermal Diffusivity*	*(m^2/s)*

Figure 2.13 illustrates the variation in peclet number versus Q'_w (surface grinding) for a number of different materials that often require grinding; the thermal properties are given in Table 2.5. There are large differences in the peclet number, which in turn would be expected to result in similar variations in the workpiece temperature. For example *In718* is commonly used in the aerospace industry for jet turbine engines, where the materials low thermal conductivity makes it resistant to creep in the high temperatures experienced within the engine. This material property however has the opposite effect in grinding resulting in high thermal gradients that in turn can lead to microstructural damage. *51CrV4* currently in use for transmission components in the automotive industry has a low peclet number and hence lower thermal gradients and potentially less microstructural damage. *M50,* a material used in the bearing industry, lies between the other materials.

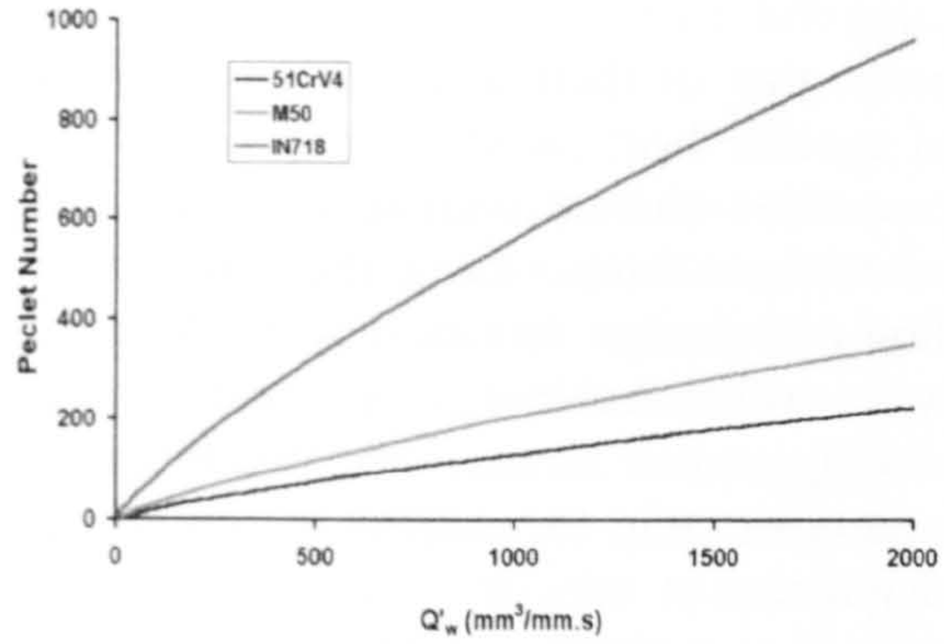

Figure 2.13 – Peclet Number versus Q'_w

There are a number of different types of materials commonly used in the automotive industry for the manufacture of crankshaft components which can be classified in three main groups, namely chilled cast-iron, soft cast-iron and low alloy steel. Typically cast iron materials are the less demanding to grind, requiring lower levels of spindle power. Whereas the low alloy steels require higher power and hence commonly require high power spindle drives to be integrated on the machine tool. The material selected for this research work is a low alloy steel, whose material designation is *38MnSiVS6*, the chemical composition is given in Table 2.6.

Element		Composition (%)	Element		Composition (%)
Carbon	C	0.35 - 0.4	Vanadium	V	0.08 - 0.13
Silicon	Si	0.5 - 0.8	Aluminum	Al	0 - 0.1
Manganese	Mn	1.2 - 1.5	Copper	Cu	0 - 0.3
Phosphorus	P	0 - 0.035	Tungsten	W	0 - 0.1
Sulphur	S	0.03 - 0.065	Titanium	Ti	0 - 0.05
Chromium	Cr	0 - 0.3	Cobalt	Co	0 - 0.1
Molybdenum	Mo	0 - 0.15	Lead	Pb	0 - 0.15
Nickel	Ni	0 - 0.4			

Table 2.6 – Chemical Composition of 38MNSiVS6

The low alloy steel can be described as a precipitation hardening ferritic - pearlitic steel with vanadium for regulated cooling from the temperature of hot forming. It has a density of $7820\ kg/m^3$ and a melting temperature of 1490^oC. The thermal properties of the *38MnSiVS6* steel are given in Table 2.7, namely values for specific heat capacity and thermal conductivity over the temperature range of 20^oC to 600^oC.

Temp (°C)	Specific Heat Capacity C (J/kg.K)	Thermal Conductivity K (J/kg.K)	Temp (°C)	Specific Heat Capacity C (J/kg.K)	Thermal Conductivity K (J/kg.K)
20	461	46.7	400	536	41.1
100	479	47.8	500	558	38.2
200	499	46.7	600	587	35.3
300	517	44.1			

Table 2.7 – Thermal Properties of 38MNSiVS6

Another important property, that of thermal diffusivity, can be derived from thermal conductivity, density and specific heat capacity as specified by Equation 2.3. It can be seen that the thermal properties change with temperature. Therefore if the material surface has been elevated to these temperatures the material's response to the thermal input as a result of grinding will change. In turn this may lead to a change in the thermal energy distribution between wheel, coolant, chips, and workpiece and can affect the final condition of the resulting ground surface. The distribution of the thermal energy is commonly defined by a partition ratio for each of the components, this is described in more detail later in the chapter.

$$\alpha = \frac{k}{\rho \, . C}$$

Equation 2.3 – Thermal Diffusivity

Where:

k	-	*Thermal Conductivity*	*(W/(m.K)*
ρ	-	*Density*	*(kg/m^3)*
C	-	*Specific Heat Capacity*	*(J/kg.K)*

Figure 2.14 shows the Peclet number versus Q'_w, both for the steel selected and two others for which previous *HEDG* surface grinding investigations have been carried out (Stephenson et al 2003, Stephenson & Jin 2002, Johnstone 2002). The selected steel has the lowest peclet numbers of the group of steels and as such has the highest thermal conductivity and therefore lowest material contact and finished surface temperatures. This property makes the selected *38MnSiVS6* steel a suitable candidate for the sucessful implementation of the *HEDG* regime.

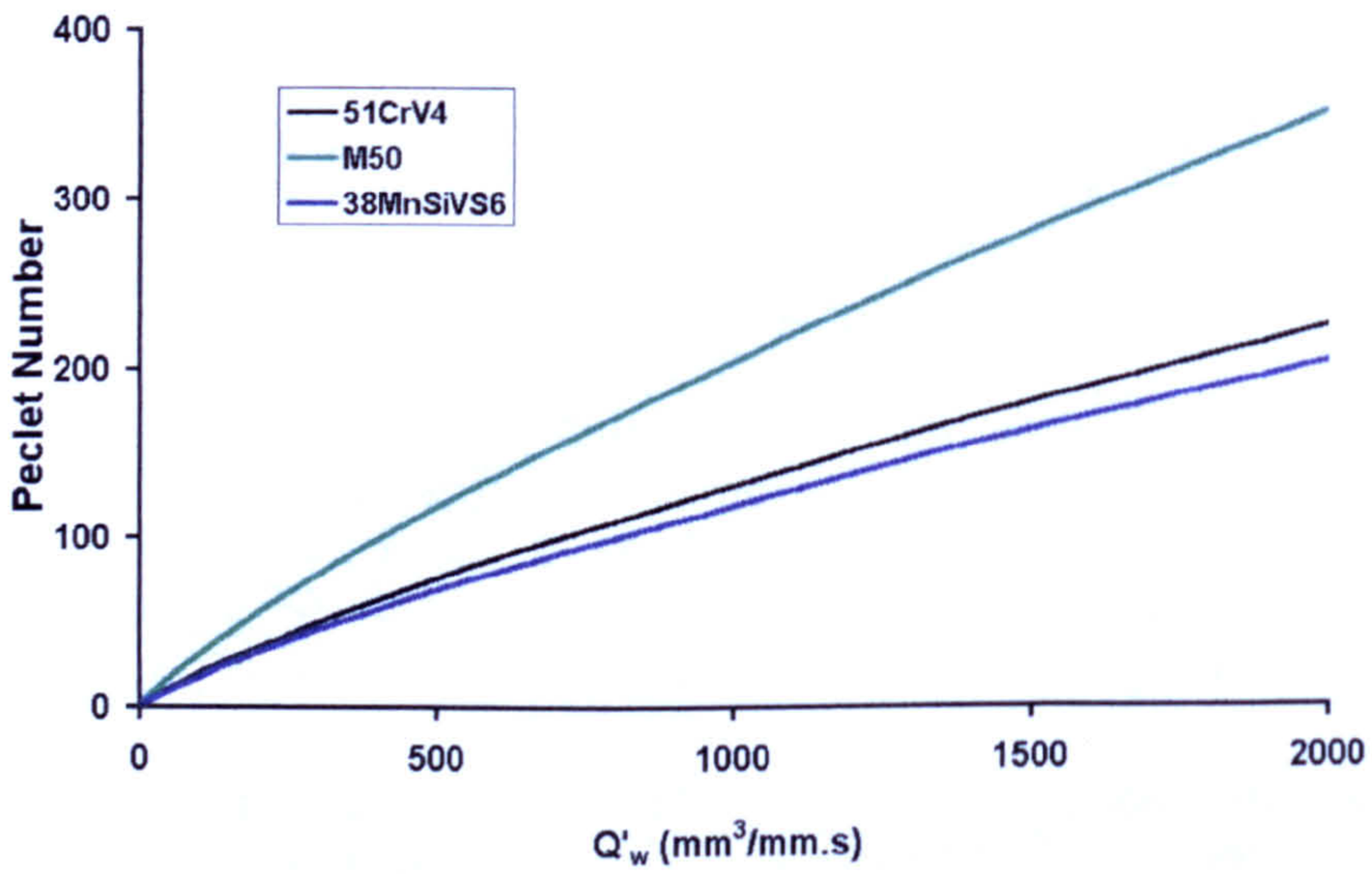

Figure 2.14 – Peclet Number versus Q'_w for Steels

2.2 Surface Integrity

The surface integrity resulting from the grinding process is recognised as having a significant impact on the component's performance. Shaw (1996) and Brinksmeier

(1999) describe the three areas that relate to surface integrity, namely surface finish, metallurgical damage, and residual stress.

Whitehouse (1994) defines surface finish as the deviations of a work-piece from its intended shape and includes such features as deviations from roundness, straightness, flatness, and importantly relevant to surface integrity - surface texture. There are instruments and techniques to measure these features and mathematical modelling to predict resultant ground surface characteristics; these will be discussed later. Malkin (1989) and Shaw (1996) discuss the importance of metallurgical damage with regard to the grinding process. They report the previous research in this area, of which an important conclusion is that most grinding damage is thermal in origin and can be detected by changes in the surface metallurgy. The methods utilised for metallurgical examination will be discussed. Grinding induces residual stresses in to the surface region of the product, and this affects the mechanical properties of the product. A compressive residual stress in the surface region is desirable for engineering components, however thermal gradients can induce tensile residual stresses. Techniques for the measurement of residual stress will be investigated.

With thermal effects being acknowledged as the cause of grinding damage, measurement and/or prediction are important aspects with regard to surface integrity. There have been a number of approaches to the measurement issue ranging from thermocouples to infrared radiation sensors utilising fibre optics (Malkin 1989). There has also been extensive associated work in thermal modelling of the grinding process.

2.2.1 Surface Finish

As discussed Whitehouse (1994) defines surface finish as the deviations of a work-piece from its intended shape and includes such features as deviations from roundness, straightness, flatness, and importantly relevant to surface integrity - surface texture. He goes on state that measurement of surface texture provides a link between the manufacturing and use of a component. Manufacturing data includes parameters such as machine performance, tool wear and vibration, whereas examples of functional data are bearing/lubrication, friction.

Surface geometry is made up of three components, namely form, waviness and roughness. The combination of the two latter of these is accepted to be the surface texture. Figure 2.15 shows a diagrammatic representation. Separation of these components for quantitative analysis is achieved by filtering of the surface profile measured (i.e. roughness – high frequency, form – low frequency). The surface texture is representative of the grinding processes performance, the two main aspects of interest are the surface roughness and grinding lay. The latter is commonly referred to as directionality. Standardisation enables accepted surface roughness terms to be used to qualify surfaces and correlate them with accepted production techniques. Table 2.8 from Booker (1984) shows published values for R_a – Centre line Average used as a guide to production capabilities.

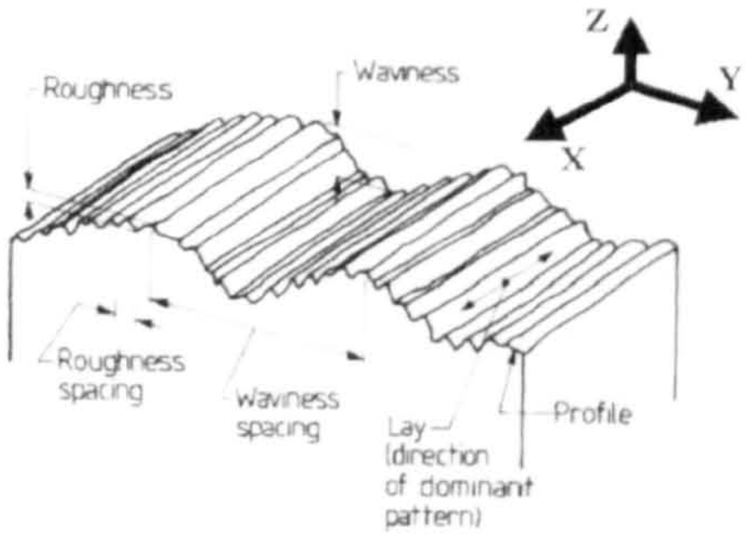

Figure 2.15 – Diagrammatic of Surface Texture

Process	Roughness – R_a (μm)	
	Average	Special
Grinding	0.1 – 1.6	0.025 – 6.3
Honing	0.1 – 0.8	0.025 – 1.6
Polishing	0.1 – 0.4	0.0125 – 0.8
Lapping	0.05 – 0.4	0.0125 – 0.8
Superfinishing	0.05 – 0.2	0.0125 – 0.8

Table 2.8 – Process Capabilities for Surface Roughness

The UK and USA commonly utilise R_a for surface roughness whereas Europe and Japan commonly use R_t – peak-to-valley roughness. These parameters have no defined relationship, for a ground surface the ratio is approximately 5 (R_t/R_a) but for a honed surface the ratio is nearer to 10. There are a variety of instruments described by Whitehouse (1994) available to measure the surface texture, which include both contact and non-contact devices. The former are normally profilerometers equipped with a fine stylus, which take a single trace across the surface – a 2D measurement. Recent developments in software for these types of instruments have enabled multiple traces to be combined, thus producing a 3D contour map of the surface, however traces can still only be taken one at a time. Most instruments have a range of styli available with radii from *50μm* down to *2μm*, and for surface texture where roughness is of primarily interest a small tip radius is necessary. The non-contact instruments generally employ optical techniques such as digital phase shifting interferrometry. These instruments can produce a 3D surface map in one measurement and with the sub-nanometre resolution possible with interferrometry can attain R_a values as low as *1-2nm*. This is typically a factor of 10 better than stylus instruments.

In surface grinding the lay of the surface texture, as illustrated in Figure 2.16, is in the direction of the wheel rotation and workpiece motion. Hence the magnetude of a 2D-profile trace perpendicular to the lay (as shown by the 'Y' axis in Figure 2.15) will include the effect of the lay. Thus this measurement orientation is the most representative of the interaction between the wheel and workpiece surface, namely the grinding process and can be referred to as the macro-roughness. Profile measurements taken along the lay (as shown by the 'X' axis in Figure 2.15) provide information relating to the abrasive grit to workpiece interaction excluding the effects of the wheel, and can be referred to as the micro-roughness. Hence this measurement provides information on the process limit resulting from the abrasive grit and material selection. Roughness data for a 3D surface map will be a combination of these two measurements. In most instances software functions within the surface mapping instruments allow the XY orientation to be selected enabling 2D roughness measurements to be obtained.

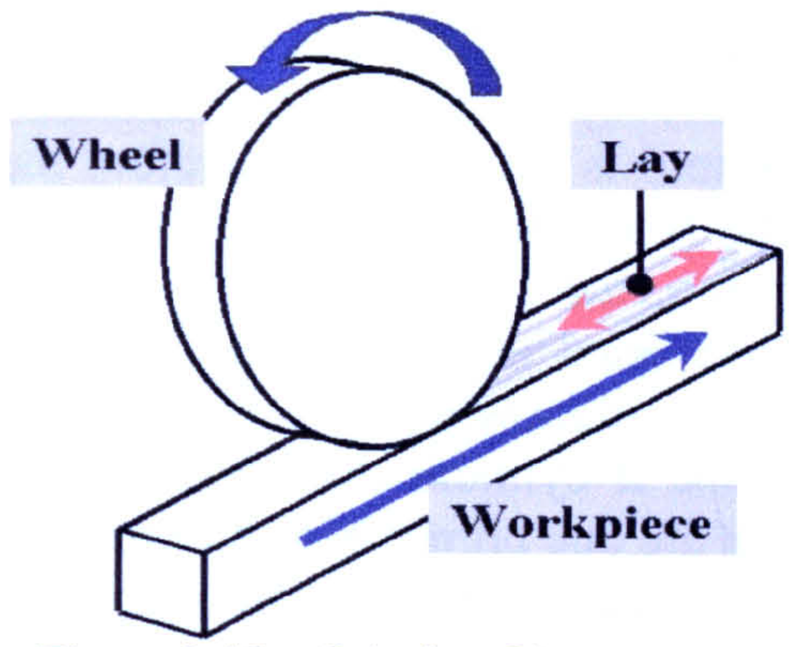

Figure 2.16 – Grinding Directionality

With rough grinding such as *HEDG* all the surface finish components are important as both form and surface texture need to be held within the production limits. However as previously discussed it is the surface texture which provides information on the grinding process itself and so is of interest in this work. Therefore the macro-roughness data will be the primary measurement taken to demonstrate the process capability.

With finish grinding again it is the macro-roughness that is of paramount importance as it includes the grinding directionality (lay). However the micro-roughness measurements provide a valuable indication of the grit material interface and thus the ultimate capability of the grinding process. Crooks & Parker (1996) talks about the importance of the grinding directionality for crankshaft components and states that reductions in this feature led to improvements in the component's performance. DeVries & Colwell (1982) investigated the effect of grinding then lapping in the same direction against grinding then lapping perpendicularly. In the former case roughness magnitudes were decreased by the lapping operation. However in the latter case both the roughness magnitude and lay were reduced resulting in a better overall surface. These findings are in keeping with the current post finish grinding operations carried out in selected instances in the automotive industry on the bearing surfaces. The operation is referred to as superfinishing and is carried out with specialist machines as described by Wickman (2001). These machines use either a belt or stone abrasive oscillated side to side whilst the workpiece rotates, the rate and magnitude of oscillation together with the workpiece rotational speed are all controllable. Surface roughness figures of below 0.1umRa are achievable on these machines, and also importantly the grinding directionality is reduced.

For both rough and finish grinding in the cylindrical plunge-grinding mode the sparkout operation is an important contributor to improvements in the surface finish. Chen & Rowe (1999) undertook research into modelling of the surface roughness for plunge grinding and showed that sparkout was a vital tool in improving the macro-roughness. To obtain the best improvement it was necessary to use longer sparkout periods than that used conventionally for solely size and roundness control.

A grinding wheel is made up of a large number of abrasive grits randomly distributed within the bond structure. This makes the grinding process very difficult to analysis in the same way as is possible with deterministic cutting processes such as turning. It is

reasonable however to accept that the envelope of the highest grains on the grinding wheel will be transferred directly to the ground surface and seen as a negative, providing that the machine tool is very rigid. Therefore the features of the grinding wheel which may affect the resultant surface roughness are the density of grits, the distribution of their protrusion, the elasticity of the grit and bond structure and the fracture characteristics of the bond and grit. Associated parameters, which have an effect, will be dressing of the grinding wheel and sparkout. Shaw (1996) goes on to state that each grinding method, be it cylindrical or surface, has its own set of grinding surface characteristics, which are due primarily to differences in work speeds and length of cut. There are two main approaches in determining the predicted surface roughness that is generated during the grinding process. One is purely by theoretical modelling where all the different wheel conditions are analysed. The other is by a simplified modelling approach where empirical constants determined by previous work are used. The main thrust of the research covered by this thesis concerns the performance of cylindrical grinding, and with this in mind the modelling work reviewed was purely concerned with this aspect. For cylindrical plunge grinding Whitehouse (1994) states that the most significant parameter affecting surface roughness is the speed ratio. The speed ratio is the quotient of the infeed axis feedrate divided by the peripheral speed of the workpiece. Where the magnitude of the axis infeed per revolution of the workpiece is greater than the expected roughness then Equation 2.4 provides an approximation for the surface roughness R_z.

$$R_z = K^* \cdot \left| \frac{v_f}{v_w} \right|^{-2/3}$$

Equation 2.4 – Surface Roughness (1)

Where:

K^*	-	*Characteristic Grinding Value*	-
v_f	-	*Axis infeed*	*(m/s)*
v_w	-	*Peripheral workpiece speed*	*(m/s)*

When the magnitude of the axis infeed per revolution of the workpiece is less than the expected roughness as would be the case if sparkout is being used then the relationship changes to that given by Equation 2.5.

$$R_z = K^* \cdot \left(1 + \left| \frac{v_w}{v_f} \right| \right)^{-2/3}$$

Equation 2.5 – Surface Roughness (2)

The Characteristic Grinding Value is influenced by the factors associated with the grinding conditions such as contact length and can be determined empirically. Whitehouse (1994) goes on to describe work carried out by Nakayama K & Shaw which takes the effect of sparkout on the surface roughness another stage. It assumed that each pass of sparkout multiplies the effective number of cutting grits in proportion. They went on to produce a relationship between R_t and the grinding parameters as shown in Equation 2.6 for a given wheel dressing.

$$\mathbf{R_t} = \frac{h_0}{2}\left[1+\left(\frac{2v}{VAh_0^{\,2}\sqrt{2\rho D}}\right)\right]$$

Equation 2.6 – Surface Roughness (3)

Where:

A	-	*Constant*	-
h_0	-	*Constant*	-
v	-	*Workpiece speed*	*(m/s)*
V	-	*Wheel Speed*	*(m/s)*
ρ	-	*Grain Radius*	*(m)*
D	-	*Wheel Diameter*	*(m)*

Work carried out by Yossifon & Rubenstein (1982) on aluminum wheels attempted to link grinding parameters to surface roughness, and from this work they produced the relationship shown in Equation 2.7.

$$\mathbf{R_a} = \left(\frac{v}{V}\cdot\frac{x}{W}\cdot\frac{1}{r\cdot n_c}\cdot\frac{d}{D_e}\right)^{3/2}\phi(a)$$

Equation 2.7 – Surface Roughness (4)

Where:

W	-	*Wheel Width*
d	-	*Depth of Cut*
v	-	*Workpiece speed*
V	-	*Wheel Speed*
x	-	*Transverse Rate*
D	-	*Wheel Diameter*
n_c	-	*No of Active Grinding Grits per unit surface area*
r	-	*Average Width-Depth ratio of groove produced on the surface*

Both Equation 2.6 and Equation 2.7 are dependant on constants based on the number of active wheel grits and the grit radius. These parameters are difficult to determine even in electroplated wheel applications where the wheel surface is not constantly being eroded. Once resin or vitrified wheels are considered then the approach becomes even more complex. Malkin (1989) addresses the issue of predicting the ground surface roughness in both the approaches, initially referring to the 'ideal surface roughness' and then proceeding to the 'empirical roughness behavior'. Previous empirical roughness behavior investigations discussed by Malkin states that for conventional cylindrical plunge grinding the relationship given by Equation 2.8 holds:

$$R_a \propto d_g^{\,y}$$

Equation 2.8 – Surface Roughness (5)

Where:

d_g	-	*Grinding Wheel grit size*
y	-	*constant dependant on grit size*

For transverse grinding the relationship is defined as shown in Equation 2.9:

$$R_a \propto \left(\frac{b_s}{s_t}\right)^{-z}$$ *Equation 2.9 – Surface Roughness (6)*

Where:
b_s - Grinding Wheel width
s_t - Crossfeed
z - Constant

These latter two empirical relationships offer a relatively simplified means to predict surface roughness values for both cylindrical plunge and transverse grinding and will be used within the superfinish grinding investigations. The proposed trials involving grinding in a modified path (a sideways oscillation superimposed on conventional infeed) should produce roughness values that lay between the two predictions. Thus it is proposed to investigate a vector based combination of the two formulae as part of this research.

2.2.2 Metallurgical

Malkin (1989) reports on a visual method used for the identification of grinding burn. Identification is effected by the presence of a bluish temper colour on the ground surface that is a result of oxide layer formation. This technique is however rather subjective to interpretation especially as the use of some kinds of coolant may themselves result in a degree of discolouration. Another factor to be considered is that any surface discolouration will be removed by subsequent spark-out operations without the removal of the associated damage. This is especially relevant to cylindrical plunge grinding where some degree of sparkout naturally occurs.

Metallurgical damage can also be observed by changes in the microstructure and mircohardness, by micro-cracks and changes to fracture and fatigue strength. Other changes include stress corrosion and wear properties. A common approach to detection of thermal damage in grinding involves the use of the first two cases, microstructural and microhardness. The first microscopically examines samples for damage, identifying alterations to the surface structure as outlined by Shaw (1996). This process involves sectioning the sample in the area of interest, mounting this to enable polishing of the surface whilst preserving the exposed surface edge. The polished edge is etched to reveal the microstructure, at which point it can be optically inspected. For steels, dark areas represent overtempered martensite, and light areas untempered martensite, grey areas represent the unaffected material. Shaw & Vyas (1994) describes these effects in greater detail and demonstrates how the surface temperature can be calculated from the known depth penetration of any untempered martensite layers using elementary heat transfer texts. Malkin (1989) discusses the relationship of microhardness at the surface to burn. Burn causing reaustenitization and hence rehardening of the surface layer, the latter is commonly referred to as 'white layer' and is measurable with mircohardness testers.

2.2.3 Residual Stress

The grinding process is accepted as inducing residual stresses in to the surface region of the product and, as already stated, can significantly affect the mechanical properties of

the product. A compressive residual stress in the surface region is desirable for engineering components. The stresses in a body (with no external influences applied) are elastic and so produce a balanced internal system of forces. Hence for a body with compressive stresses in the surface there will be an equal integrated tensile stress within the core (Shaw, 1996). Malkin (1989) states "that residual stresses are induced by non-uniform plastic deformation near the work-piece surface". He suggests that the mechanical interaction of the abrasive grits and the surface produces a result akin to shot peening. Shot peening impacts the surface with hard spherical balls resulting in small impressions which is recognised as forming a thin plastic zone, which stretches the surface relative to the bulk of material. Since the system is a balanced body with both surface and bulk having the same length, the stresses in the surface become compressive and the bulk tensile. Therefore the surface would be expected to have predominantly compressive residual stress due to localised plastic flow, similar along and across the grinding lay. He goes on further to say "tensile residual stresses are caused mainly by the thermally induced stresses and deformation that are associated with the grinding temperature and its gradient from the surface into the workpiece". In the grinding zone there is constraint of the hotter surface material by the cooler bulk material. This constraint of the hotter material can lead to plastic flow, thus resulting in higher contraction on cooling than the bulk, hence a tensile skin. To balance this tensile residual stress there would be a corresponding compressive residual stress in the material bulk. This suggests therefore that if the thermal effect, which causes tensile residual stresses in the grinding process can be reduced sufficiently or removed, then ground surfaces with a compressive residual stress would be possible.

There are a number of possible methods to investigate residual stress in the surface region of components. Fields & Kahles (1971) and Fields et al (972) outlines a number as listed in Table 2.9. *XRD* is the most widely used whether in the nondestructive or destructive applications. The former nondestructive method can only be used to examine the near surface region because of x-ray penetration limitations, whereas the destructive method with material layer removal between successive measurements allows a greater penetration.

Non-Destructive Techniques			***Destructive Techniques***
Commonly Employed	***Specialised***	***Possible with further Developments***	
X-Ray Diffraction	*Ultrasonic Velocity*	*Eddy Current* *Electrochemical Potential* *Ultrasonic Attenuation* *Micro-Magnetic*	*X-Ray Diffraction (Layer Removal)*

Table 2.9 – Residual Stress Measurement Techniques

More recently studies (Brinksmeier et al 1982, Coyle 1984, Borland 1994, Lucca et al 1998) have revisited the area and investigated how instrument developments have advanced the field of residual stress measurement. One technique that has now come to the forefront is in the use of micro-magnetic techniques based on Barkhausen Noise (BN) intensity. Webster et al (2002) demonstrated that the residual stress approach to the assessment of thermal damage is far more sensitive than the other methods of

detection, namely visual burn, nital etch, power surge and hardness change. He went on to state that the micromagnetic method to monitor residual stress compared well with conventional methods.

Currently *XRD* is a widely used and accepted method, with the emergence of the micro-magnetic techniques offering a true alternative with an in-process capability. Thus these methods will be used to determine residual stress levels in this investigation.

2.2.3.1 XRD

Stresses in the surface region of the material can be determined by measurement of the changes in crystallographic structure. X-Ray Diffraction (*XRD*) determines the change in spacing of crystal lattice planes by diffraction of x-rays of a given wavelength. By applying Bragg's Law as given in Equation 2.10 an estimate of the corresponding residual stress can be calculated.

$$\lambda = 2d \sin \theta$$ *Equation 2.10 – Bragg's Law*

Where:

- λ - *X-Ray wavelength*
- d - *Lattice spacing*
- θ - *Diffraction angle*

There are many texts that cover the theory in great depth, such as Cullity (1967). He states that with *XRD* measurements of residual stress, the strain of the grains is not parallel to the surface and hence this must be obtained taking measurements at an angle referred to as Ψ. The strain parallel to the surface is then determined by interpolation, the lattice strains and $\sin^2\Psi$ value have been shown to have a linear relationship. To establish this relationship it is necessary to know the values for the Modulus of Elasticity and Poisson Ratio of the material at a micro level as opposed to the bulk state. Measurements are made over a range of Ψ angles. Because of this requirement to measure at an angle Ψ the surface roughness will affect readings especially when higher values of Ψ are used, therefore care must be taken in comparisons between samples with differing levels of grinding finish. The depth of penetration of the method varies with different materials, for steel it is normally nominally 5-10μm. To achieve higher levels of penetration it is necessary to employ a layer removal technique such as electro-polishing in conjunction with successive measurements, which therefore becomes an expensive time consuming and destructive procedure. Coyle (1984) goes on to outline the different types of instrument available which include non-portable laboratory and portable industrial units. Because of the large size of the X-Ray tube and detector system a large clear area is required around the region. There is also an issue of the radiation hazard to be considered. However XRD measurement does provide an absolute value of stress, as opposed to many other techniques investigated. However in this program of research it is intended to only use the tool to provide a reference for residual stress data collected using the BN instrument.

2.2.3.2 Barkhausen Noise Intensity

Borland (1994) discusses the emergence of the micro-magnetic technique that is based on Barkhausen Noise intensity, originally discovered in 1919 by Professor Barkhausen.

Simply, if a ferromagnetic material is placed in an oscillating magnetic field, each magnetic domain in the surface of the material produces an electronic pulse which collectively produce a noise-like signal called Barkhausen noise.

There are two material characteristics described by Fix (1990) which affect the intensity of the Barkhausen noise signal in the surface region, namely the presence and distribution of elastic stress and the metallurgical state. Elastic Stress affects the stability of the domain structure and the introduction of a magnetic field results in a signal being produced which is representative of movement in the domain structures. The higher the compressive stress then the lower the level of movement, hence a lower BN intensity. Conversely higher levels of tensile stress result is greater domain structure movements and therefore higher BN intensity values. Shaw (1998) shows how these two factors interact and affect BN intensity levels, see Figure 2.17.

Therefore the final result is that the desirable compressive stress results in low BN intensity reading. However any hardening of the microstructure as a result of thermal damage has a similar effect in that it too reduces the BN intensity readings. Therefore it is fortunate that the changes in residual stress occur before the onset of changes in the microstructural hardness as a result of thermal damage. Moorthy et al (2002) discusses the depth penetration of the technique and quotes the relationship given in Equation 2.11 where it can be seen that this is dependent on both the measurement frequency and material properties.

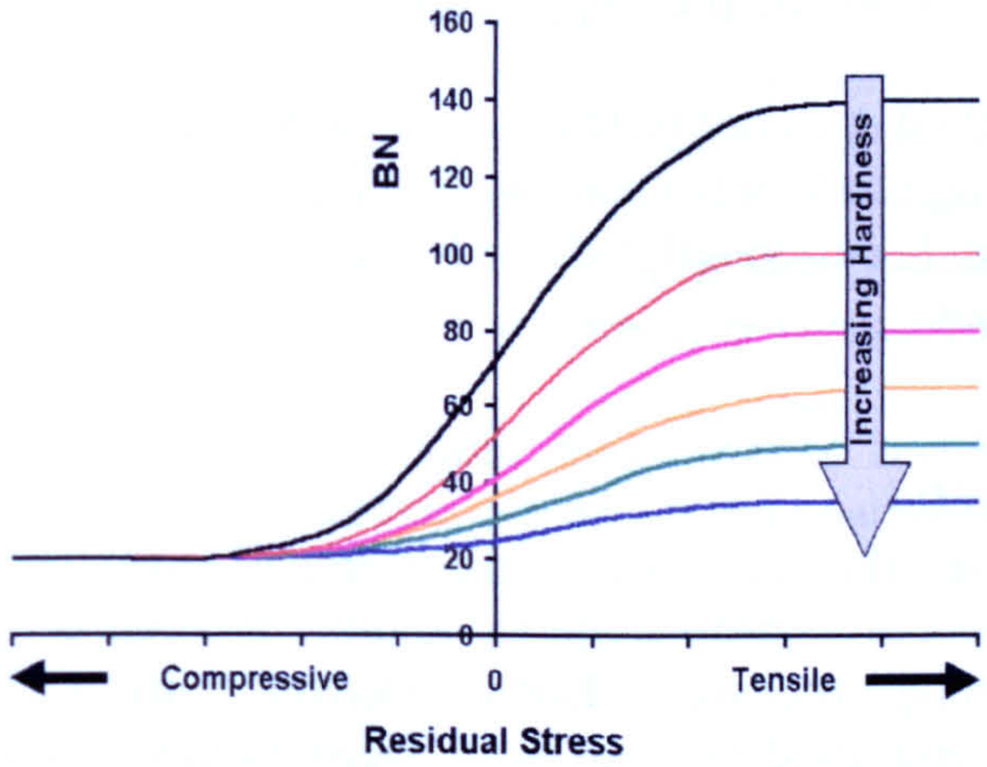

Figure 2.17 – Variation in BN Reading with Stress & Hardness

Equation 2.11 – Depth Penetration of BN Signal

$$\delta = \frac{1}{\sqrt{\pi \cdot f \cdot \sigma \cdot \mu_0 \cdot \mu_r}}$$

Where:

δ	-	*Electromagnetic Skin Depth*
f	-	*Signal Frequency*
σ		*Conductivity of Material*
μ_0		*Relative Permeability of Vacuum*
μ_r		*Relative Permeability of Material*

Moorthy (2002) reports that in the case of case-carburised EN36 steel where the conductivity is $3.15 \times 10^6\ \Omega^{-1}m^{-1}$, and the relative permeability can be taken as 200, the magnitude of penetration in regard to frequency is given by the values in Table 2.10

Signal Frequency (Khz)	*Penetration (μm)*
1-2	*600-475*
2-3	*475-375*
3-4	*375-325*
4-5	*325-275*
5-8	*275-225*
10-20	*200-150*
20-1000	*150-20*

Table 2.10 – BN Penetration versus Frequency

Rollscan a type of BN intensity instrumentation reported by Wojtas et al (1998) and produced by the company Stresstech, works at a frequency of 125Hz in standard settings. Therefore this would have a penetration in the same order as that of the XRD instrumentation. Hillmann (1998) demonstrated the use of BN to detect grinding burn in camshafts, with the identification of changes in the level of residual stress. Others such as Fix (2000) have also demonstrated the use of Barkhausen noise for residual stress identification in a number of different applications in grinding.

In conclusion the method does not produce absolute values of residual stress, but in fact produces a relative magnitude dependant on the change in the material characteristics in the near surface zone. If calibrated and used in a controlled way, changes in residual stress can be monitored.

2.2.4 Thermal Effects

As previously discussed thermal effects have been acknowledged as the cause of most grinding damage, and its measurement and/or prediction is important to the development of grinding processes. Thermal measurement of the grinding process is difficult and the techniques developed have been primarily employed in laboratory environments. Thermal modelling offers the advantage of predicting the workpiece temperature through the use of process measurables, and as such is more suited for production environments.

2.2.4.1 Measurement

There have been a number of approaches to the measurement issue ranging from thermocouples to infrared radiation sensors utilising fibre optics (Malkin 1989). Others include photoelectric cells, thermal resistors and heat sensitive paints. Two more recent novel methods are PVD coatings and thermocouples embedded within a diamond fibre contained within a grinding wheel. Work on the former approach will be discussed in greater depth. The latter method was part of work carried out into the manufacture and

use of diamond fibres in a grinding wheel (Smith et al 1999). Tawakoli (1993) also describes single and two wire thermocouples as those most commonly used methods for measuring grinding temperature.

Snoeys et al (1978) discusses the use of thermocouples and concludes that because of the large temperature gradients in the vicinity of the grinding zone it is necessary to reduce the dimensions of the thermocouples to a microscale. Tawakoli (1993) recognised this requirement for a reduced size. He introduced sheathed thermocouples with a diameter of 0.05mm, these were K-type made of CrNi/Cr. A number of these were placed at set depths below the surface and measurements taken from all the sensors during a single run. The combination of all the traces allowed a picture of the temperature distribution to be built up and enabled differences in process parameters to be studied. Rowe (1995 & 1996) went further with the development of a single pole foil thermocouple. This approach allowed the thickness of the measuring junction to be reduced down to as low as 25μm with the workpiece acting as the second pole. The thermocouple was positioned at the sample surface with the connection being made during the grinding process by the wheel itself. Signals collected during a single pass of the wheel showed a temperature profile across the grinding zone with spikes resulting from individual abrasive grains. It was concluded that the single pole method attenuates the spikes whilst preserving the temperature profile. Guo et al (1999) describes an embedded K chromel-alumel thermocouple initially positioned 2mm beneath the sample surface in a similar fashion to Tawakoli, but in this case went on to expose the thermocouple. Dependant on grinding parameters between 5 to 45 passes were required to achieve exposure, and readings were taken during each pass to build a picture of the temperature distribution. Rowe (2001a) went on to demonstrate that a development of the single pole foil thermocouple device was able to measure the grinding temperatures associated with *HEDG*. Results showed there was good correlation between these and an inclined heat source model. Further development (Rowe, 2001b) describes the use of a J-type thermocouple constructed with a 25um diameter constantan wire.

Kato (1997) reported a novel temperature measurement technique, developed for surface grinding applications. The technique used a PVD coating applied as a sandwich between two sections of a testpiece, the coating was a minimal 0.2μm thickness so as not to influence the bulk material. The testpiece was then ground across the coating interface, the heat generated by the grind melted the coating by an amount proportional to the surface temperature. Post grind the testpiece was separated and the melt depth of the coating from the ground surface measured. This data was plotted as illustrated in Figure 2.18, T_{C1} represents the coatings melt temperature and d_{C1} the melt depth of coating from the ground surface. Kato used a number of coatings with a range of melting points over a series of test grinds using the same grinding parameters to produce a number of datasets. These were then added to the chart as illustrated in Figure 2.18, $T_{C1} - T_{C3}$ represent three coatings melt temperatures and d_{C1}-d_{C3} the associated melt depths of the coatings. He saw that the temperature in the workpiece decreased exponentially as a function of the depth within the near surface zone. Hence by extrapolation it was possible to obtain a temperature for the ground surface. The coatings that Kato found to produce reliable results together with their melt temperatures, are given in Table 2.11.

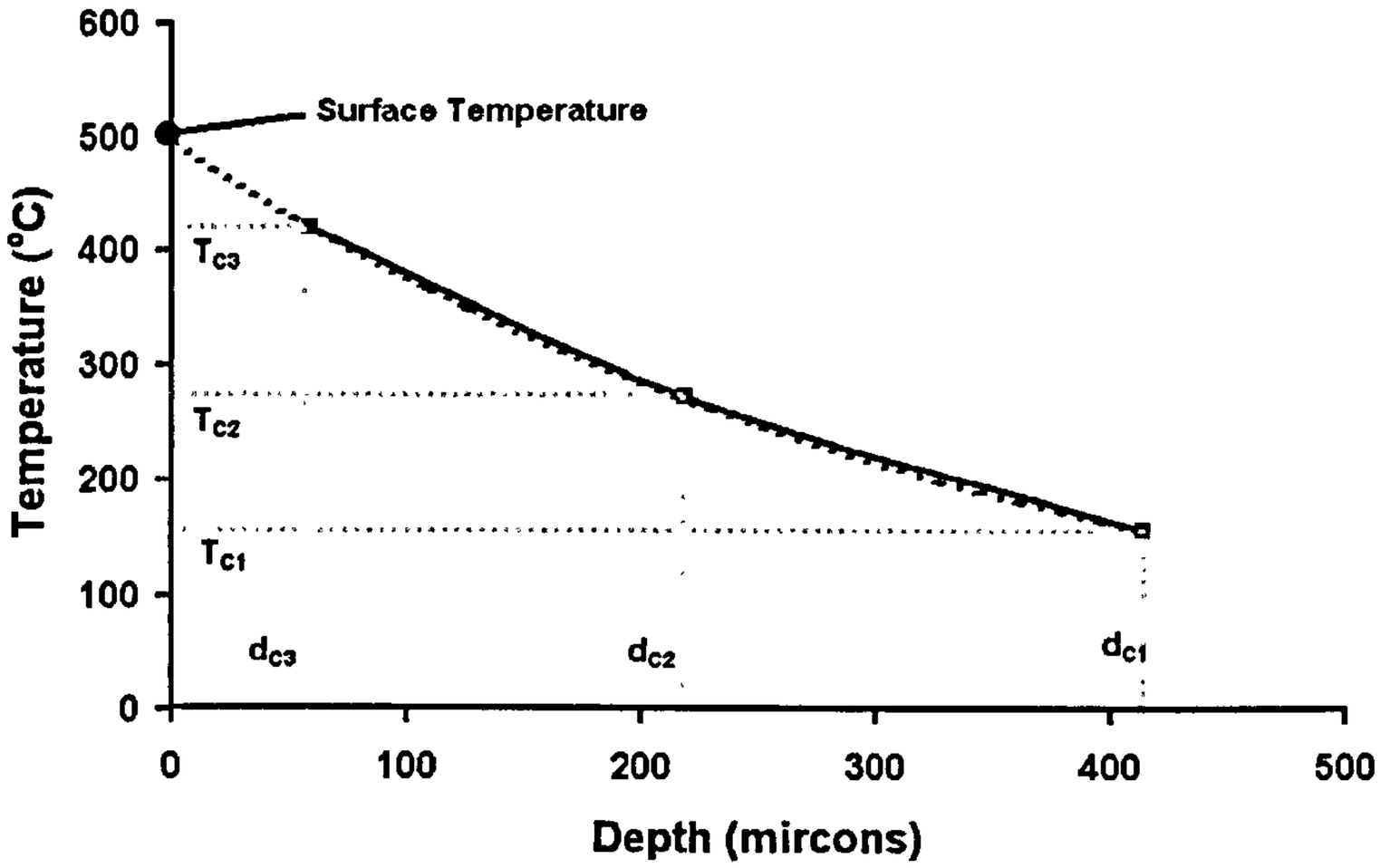

Figure 2.18 – PVD Temperature Chart

Material	***Melting Pt (K)***
Lithium fluroride	*115*
Antimony	*904*
Tellurium	*723*
Lead	*601*
Bismuth	*545*
Indium	*429*
Bi-Pb Alloys	*399*
Roses Alloy	*370*
Anatomical Alloy	*334*

Table 2.11 – PVD Coating Materials

Further work by Kato (2000) refined the procedure and concluded that the maximum working depth for the coating was that given by Equation 2.12. At greater depth the exponential relationship was found to no longer be applicable.

$$d_{max} = \frac{8 \cdot \alpha}{v_w}$$

Equation 2.12 – Depth Limit of PVD Coatings

Where:

v_w	-	*Workpiece speed*	*(m/s)*
α	-	*Thermal Diffusivity*	*(K^{-1})*

The use of log plots was also introduced which simplified the determination of the surface temperature as data points now lay on a straight line, see Figure 2.19. The current status for both thermocouples and PVD coatings has been researched. In conclusion it was found that both methods provide the ability to measure the temperatures of the grinding zone for surface grinding applications. The transfer of this

technology to cylindrical grinding for the planned research work here poses problems in transferring the signals from a rotating component without degradation. It will be seen that in the PVD approach there is more scope for transference to the cylindrical mode

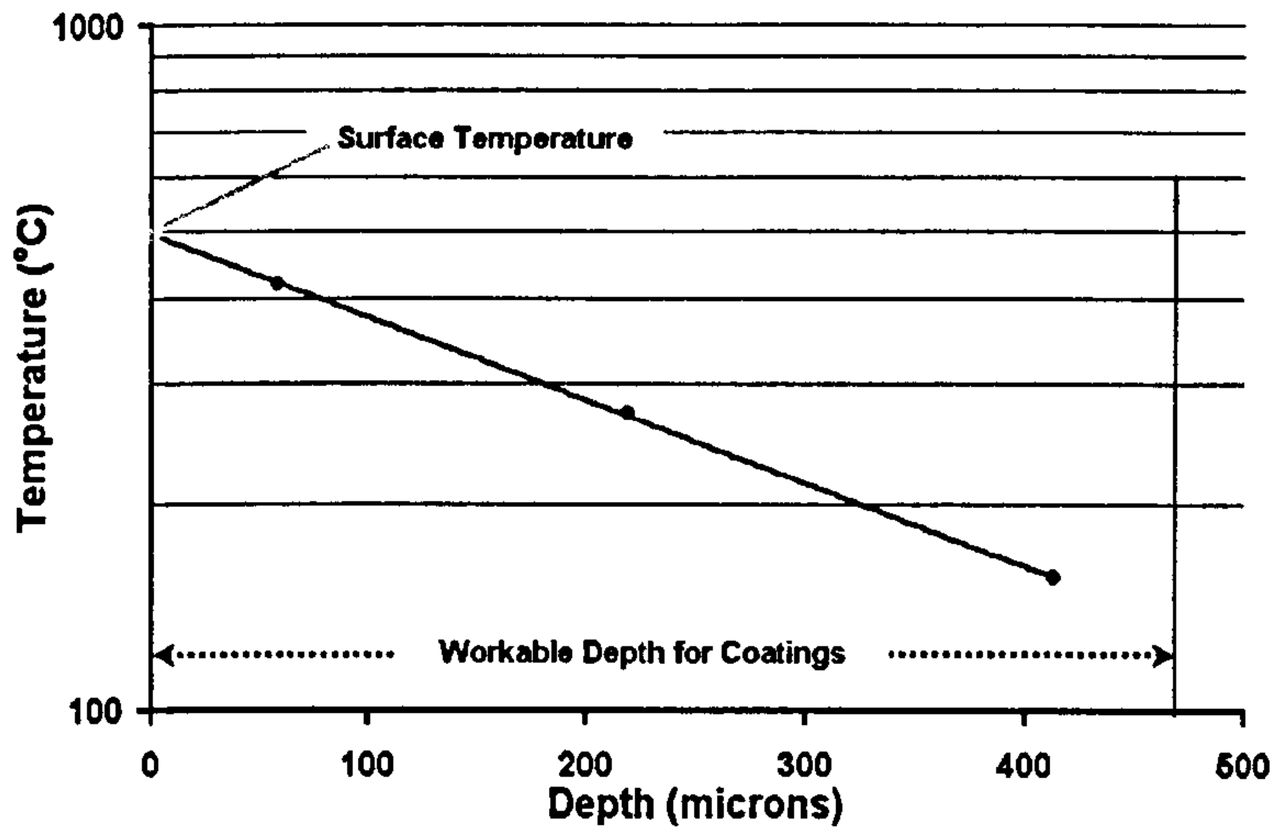

Figure 2.19 – PVD Temperature Log Chart

2.2.4.2 Modelling

There has also been extensive work carried out on the thermal modelling of the grinding process. Jaeger carried out some of the earliest work which is described by Shaw (1996) and Malkin (1989). He initially stated that the total grinding energy is made up of components for chip, ploughing and sliding actions, as shown by Equation 2.13.

$$u = u_{ch} + u_{pl} + u_{sl}$$ *Equation 2.13 – Grinding Energy Components*

Where:

- u_{ch} - *Chip Energy*
- u_{pl} - *Ploughing Energy*
- u_{sl} *Sliding Energy*

He developed a sliding heat source model based on a heat flux uniformly distributed across the grinding contact length. He also concluded that virtually all the sliding and ploughing energy together with approximately 55% of the chip formation energy is transferred in to the ground surface. The work was based on studies of shallow cut grinding for which Jeager developed his theory to give the relationship shown in Equation 2.14

$$u = u_0 + B \cdot d_e^{1/4} \cdot a^{-3/4} \cdot v_w^{-1/2}$$ *Equation 2.14 – Jaegers Equation*

Where:

- u - *Specific Grinding Energy*
- u_0 - *0.45u_{ch} (Energy to Chip)*
- B - *Constant*
- v_w - *Grinding Wheel Surface Speed*

a - *Depth of Cut*
d_e - *Effective Grinding Wheel Diameter*
note: d_e is the actual grinding wheel diameter for surface grinding

The next step was to plot the data in the format given by this relationship, namely specific Grinding Energy versus the function $f(d_e^{1/4}, a^{-3/4}, v_w^{-1/2})$, then to visually classify all the surface ground as burnt or unburnt. This enabled a burn threshold line to be drawn along the boundary of burnt/unburnt data points. A typical example is illustrated in Figure 2.20, and in this case there are a number of boundary lines which show increasing temperature of burn threshold as an example. The chart enables a prediction of the Specific Grinding Energy to be made for specified grinding parameters, namely depth of cut, work-piece velocity and effective grinding wheel diameter. Hence once a burn threshold chart has been experimentally derived for a specific material the onset of burn can theoretically be determined and thus avoided.

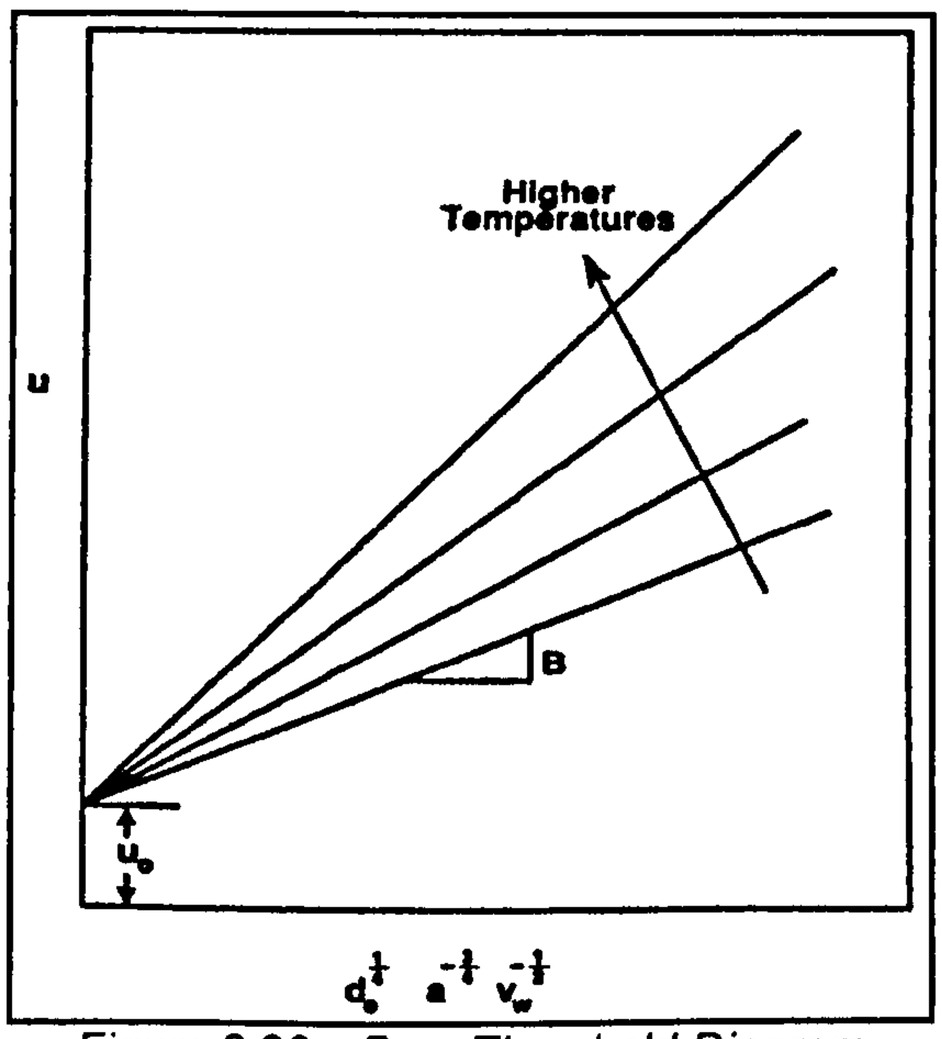

Figure 2.20 – Burn Threshold Diagram

Jaegers went on to predict the workpiece burn temperature from the gradient of the burn threshold line in conjunction with Equation 2.15

$$B = k\theta_m / 1.13\,\alpha^{1/2}$$ *Equation 2.15 – Jaegers Temperature Equation*

Where:
k - *Material thermal conductivity*
α - *Thermal diffusivity*
θ_m *Temperature rise*

Tönshoff et al (1992) discussed the different approaches to both physical and empirical modelling. He explained that although empirical models could produce reasonably accurate predictions, the range that such models could successfully cover was limited,

as they did not contain all the grinding variables. Physical modelling offered a more comprehensive approach but needed more development to improve its accuracy. Investigations made by Guo & Malkin (1994) identified that coolant fluid film burn out was a limiting factor in creep feed as once this occurred the component surface became burnt. Kuang & Jen-Sheuan (1994) reported on the improved performance given by wheels made with CBN grit to that of Al_2O_3 in the avoidance of grinding burn. Rowe (1996a & 1996b) investigated this in further depth and found the use of *CBN* decreased the amount of heat into the workpiece because of the high conductivity of *CBN* itself . Measurements suggested that the thermal conductivity of *CBN* was not however as high as in the raw state (1200W/mK) and was in fact closer to 240 W/mK, but this was still significantly higher than values of 35 W/mK for Al_2O_3. Rowe (1997) goes on to discuss the grinding energy being partitioned between conduction into the workpiece, conduction into the grinding abrasive, convection into the chips and finally convection to the grinding fluid. This approach coupled with the improved *CBN* data was shown to improve model predictions. Later work described by Rowe (2001b & 2001c) investigated what happens where larger depths of cut than those considered by Jaegers model are used. He concluded that the increased contact length, resulting from the greater depth of cut, meant that temperatures in the contact and finished zones were unlikely to be uniform, see Figure 2.1. Therefore he proposed that a triangular heat flux distribution be used for modelling. The result of this development was that the proportion of heat energy reaching the finished surface was predicted to be less than that found by Jaeger and hence temperatures were lower. Results from grinding trials provided good correlation thus supporting this theory. Guo et al (1999) went on to suggest that the heat energy should be partitioned between the abrasive grains and fluid separately. Burn threshold studies reported by Stephenson (2001) show a burn threshold chart for *IN718*, which is typical of that illustrated in Figure 2.20. Trials were carried out predominately in the high material removal region associated with the *HEDG* regime, and there was a clear boundary between burnt and unburnt surfaces. Using Jeager's approach as given in Equation 2.15 the temperature of the boundary region was estimated to be greater than 2000°C, which clearly was not the case. Further analysis using the inclined heat source method with the triangular heat flux distribution (Rowe, 2001a) predicted values of between 400 °C and 750 °C, which correlated more closely with the analysis of surfaces. Jin (2002) reported on a similar study but in this case using high carbon steel in the *HEDG* regime. He concluded that the burn threshold is determined by factors such as contact length, Q'_w, wheel speed and that it is necessary to consider energy partitioning in the modelling. Modelling and analysis from ground specimens found workpiece damage was thought to occur around 400°C. Rowe (2001b) carried out further modelling and experimental work in high removal grinding and from his finding proposed the concept of a circular arc heat flux distribution.

Stephenson & Jin (2003) and Rowe (2003) bring together the developments to date. Stephenson goes on to discuss the importance both of the abrasive and the workpiece thermal properties and how these affect the heat partitioning. The total heat flux generated during grinding is distributed between the different areas around the grinding zone, namely the fluid, grinding chips, wheel and workpiece as illustrated by the flowchart in Figure 2.21.

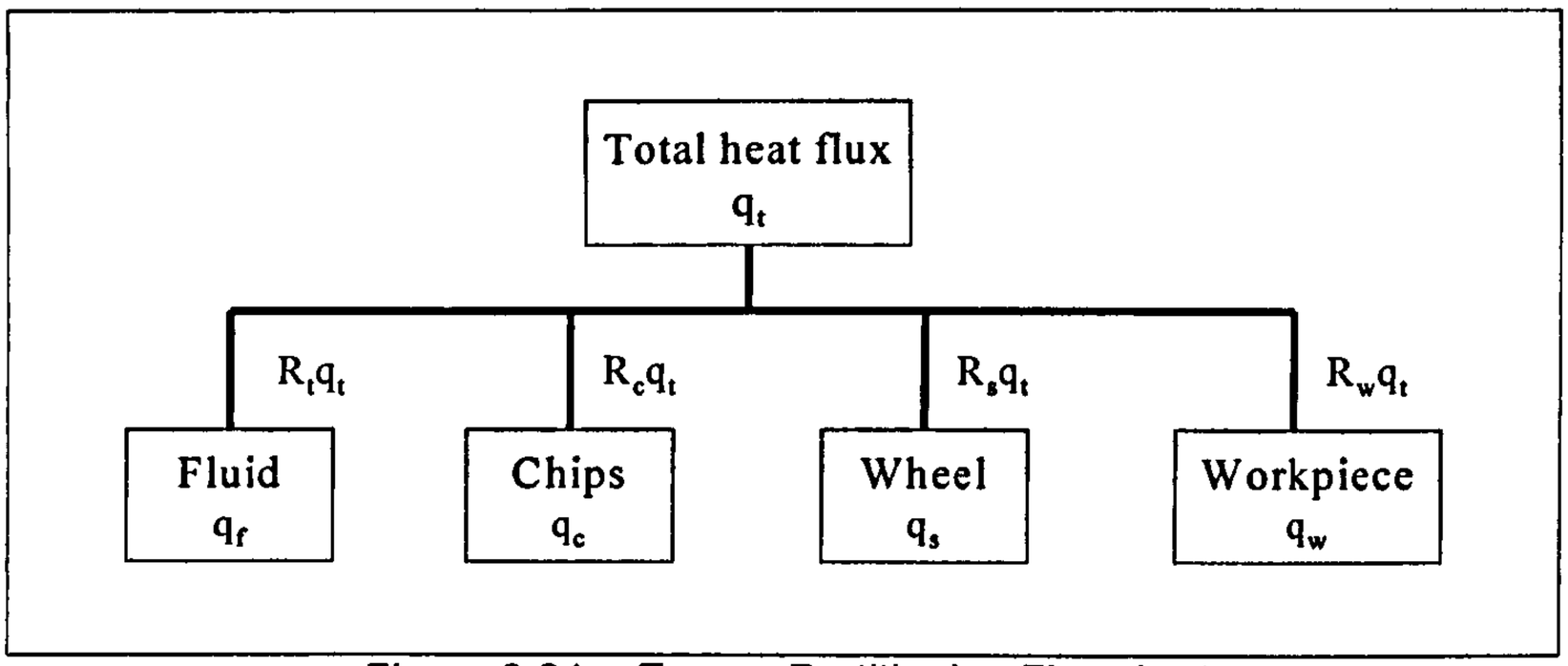

Figure 2.21 – Energy Partitioning Flowchart

The total heat flux can be estimated from Equation 2.16.

$$q_t = \frac{e_c \cdot a_e \cdot v_w}{l_c}$$

Equation 2.16 – Total Heat Flux

Where:

q_t	-	*Total heat flux*
e_c	-	*Specific Grinding Energy*
α_e	-	*Depth of cut*
v_w	-	*Feed rate*
l_c	-	*Contact length*

The specific grinding energy can either be measured during the grinding process or modeled using the exponential relationship given in Equation 2.17

$$e_c = A \cdot Q'_w{}^{-t}$$

Equation 2.17 – Specific Grinding Energy

Where:

e_c	-	*Specific Grinding Energy*
A	-	*Constant*
Q'_w	-	*Specific Material Removal Rate*
t	-	*Constant*

Stephenson quotes typical values of A and t for a number of different materials as given in Table 2.12

Workpiece/Abrasive	***A***	***t***	***v_s (m/s)***
Steel/CBN	*70*	*0.25-0.4*	*100-150*
Steel/Al_2O_3	*140*	*0.45*	*60*
IN718/CBN	*150*	*0.28*	*150*
MAR M002/CBN	*400*	*0.7*	*150*
Ti-6-4/ Al_2O_3 (shallow Cut)	*106*	*0.56*	*30*
Ti-6-4/ Diamond (shallow Cut)	*53.1*	*0.0619*	*30*

Table 2.12 – SGE Constants for Various Materials

The chip energy is given by Equation 2.18. The maximum energy that can be removed by the grinding chip occurs when the chips approach the material's melting temperature, which is thought to be the case within the *HEDG* regime.

$$e_{ch} = \rho \cdot C \cdot T_{ch}$$

Equation 2.18 – Grinding Chip Energy

Where:

e_{ch}	-	*Chip Energy*
ρ	-	*Density of Material*
C	-	*Specific Heat Capacity of Material*
T_{ch}	-	*Chip Temperature*

Thus the heat flux convected away by the grinding chips is given by Equation 2.19

$$q_{ch} = \frac{e_{ch} \cdot a_e \cdot v_w}{l_c}$$

Equation 2.19 – Heat Flux of Grinding Chips

Where:

q_{ch}	-	*Heat Flux of Grinding Chips*
e_{ch}	-	*Specific Grinding Energy*
a_e	-	*Depth of cut*
v_w	-	*Feed rate*
l_c	-	*Contact length*

For the fluid Stephenson states that the maximum heat can be estimated by Equation 2.20. For mineral oil the film boiling temperature is around 350°C.

$$q_f = (T_b - T_0) \cdot h_f$$

Equation 2.20 – Heat Flux of Grinding Fluid

Where:

q_f	-	*Heat Flux of Grinding Fluid*
T_b	-	*Mineral Oil Film Boiling Temperature*
T_0	-	*Ambient Temperature*
h_f	-	*Fluid Convection Coefficient*

Thus the partition ratio for the grinding fluid is given by Equation 2.21

$$R_f = \frac{q_f}{q_t} = \frac{(T_b - T_0) \cdot h_f \cdot l_c}{e_c \cdot a_e \cdot v_w}$$

Equation 2.21 – Partition Ration for Grinding Fluid

Whilst for the grinding chips the energy partition ratio can be estimated by Equation 2.22

$$R_{ch} = \frac{q_{ch}}{q_t} = \frac{e_{ch}}{e_c}$$

Equation 2.22 – Partition Ration for Grinding Chips

Stephenson goes on to look at the energy partitions for the wheel and workpiece. The first stage uses the model developed by Hahn which looks at a workpiece-wheel partition ratio, see Equation 2.23

$$R_{ws} = \frac{R_w}{R_w + R_s} = \left(1 + \frac{0.97 \cdot k_g}{\beta_w \sqrt{r_0 \cdot v_s}}\right)^{-1}$$

Equation 2.23 – Hahn's Workpiece-Wheel Partition Ratio

Where:

R_{ws}	-	*Partition Ratio of Workpiece-Wheel*
R_w	-	*Partition Ratio of Workpiece*
R_s	-	*Partition Ratio of Wheel*
k_g	-	*Thermal conductivity of Abrasive*
β_w	-	*Material Constant √(kρC)*
r_0	-	*Radius of Abrasive Grit*
v_s	-	*Peripheral Wheel Speed*

The Partition ratio relationship can also be considered as in Equation 2.24

$$R_s + R_w = 1 - R_{ch} - R_f$$

Equation 2.24 – Workpiece-Wheel Partition Ratio Relationship

Thus the energy partition coefficients for the grinding wheel and workpiece can be expressed in the form given in Equation 2.25 and Equation 2.26.

$$R_w = R_{ws}\left(1 - R_{ch} - R_f\right)$$

Equation 2.25 – Workpiece Partition Ratio

$$R_s = R_w\left(\frac{1}{R_{ws}} - 1\right)$$

Equation 2.26 – Wheel Partition Ratio

The grinding temperatures for the contact and finished workpiece surface can then be calculated using these energy partition relationships, see Equation 2.27 and Equation 2.28. Values for the *C-Factor* and temperature ratio can be derived from the circular arc thermal model proposed by Rowe (2001b) discussed earlier. In Rowe's model the magnitude for the *C-Factor* and temperature ratio are seen to reduce with increases in the depth of cut and feedrate. Hence predicted temperatures for grinding in the *HEDG* regime will be lower than that for shallow cut.

$$\left(T_{con}\right)_{Max} = C_{factor} \cdot \frac{R_w \cdot q_t}{\beta_w} \cdot \sqrt{\frac{l_c}{v_w}}$$

Equation 2.27 – Contact Surface Temperature

$$\left(T_{fin}\right)_{Max} = F_r \cdot \left(T_{con}\right)_{\max}$$

Equation 2.28 –Finished Surface Temperature

Where:

C_{factor}	-	*C-Factor*
F_r	-	*Temperature Ratio*

By using the derived partition ratio coefficients Stephenson compares the dissipation of the heat energy in both shallow cut and *HEDG* regimes for steel over a range of Q'_w. In the shallow cut instance calculation shows that a significant proportion of the heat energy goes to the workpiece. Energy removed by the coolant is high at the lower

removal rates but climbs steady as the removal rates increase whereas the opposite is true with regard to the grinding chips. In the *HEDG* regime it is shown the ratio of energy entering the coolant (at low Q'_w rates) and grinding chips (at high Q'_w rates) is far greater than for shallow cut. Therefore, in proportion, far-reduced levels of energy reach the workpiece surface. Comparisons of results for conventional (Al_2O_3) and superabrasive (*CBN*) show that the latter significantly increases the energy removed by the wheel thereby reducing the ratio entering the workpiece. Moving onto the temperature, Stephenson demonstrates that in the case of *HEDG* the finished surface temperature for steel rises to a peak as the *Q'w* rate increases then begins to drop for further increases in *Q'w* as shown in Figure 2.2. This typifies the *HEDG* temperature hump first demonstrated by Tawakoli (1993). Finally the effect of thermal characteristics of the material are illustrated, with high thermal diffusivity materials such as the steel resulting in lower finished surface temperatures. Whereas low thermal diffusivity materials such as *IN718* result in higher temperatures.

Jin & Stephenson (2004) carried out *FEA* thermal modelling of the *HEDG* regime, and the results were found to correlate well with experimental data. Importantly comparisons with current 2D analytical thermal modelling using current energy partitioning theory, showed good alignment under steady state conditions and where complex geometry was not involved.

In conclusion, current thermal modelling techniques as described above and summerised by Stephenson (2003) and Rowe (2003) can provide a reliable means with which to predict surface temperatures in both conventional and *HEDG* regimes. They show that in conventional shallow grinding the majority of the heat is removed by the coolant for steels exhibiting high thermal diffusivity. However with newer materials with low thermal diffusivity, such as those being used in the aerospace industry, the selection of abrasive plays a more important role. In this case superabrasives such as CBN with high conductivity conduct a far higher proportion of the energy away from the workpiece material. In the *HEDG* regime the material plays a vital role, with material of high diffusivity allowing a greater proportion of the heat energy to be removed as a result of the high wheel speed through the grinding chips. This together with the implementation of superabrasives ensures that a far lower proportion of energy reaches the workpiece.

3 Experimental Procedures & Equipment

The experimental procedures described here were selected to enable the study of both *High Efficiency Deep Grinding (HEDG)* and *Superfinish* Grinding together with their effect on the surface integrity of the component. This chapter is divided into three sections covering the machine tools, techniques employed for both grinding modes, and finally the surface integrity analysis tools utilised.

Three machine tools were selected, the Edgetek five axis *CNC* superabrasive grinding unit, the LL *CNC* twin wheel orbital grinding unit, and the LL *CNC* LT1 Grinding unit.

A common approach was used for the study of both *HEDG* and *Superfinish* modes, this being initially to carry out trials in a surface grinding configuration, then to proceed onto the more complex cylindrical plunge grinding configuration. The latter process simulates that utilised within the automotive industry for the production of crankshaft components. The aim of the former trials was to study the implications to surface integrity with a simplified grinding action and one that had no possible additional interaction between the grinding wheel and component. Such interactions generally take place, one instance being that of *'sparkout'* where a continuing grinding action occurs in the dwell between infeed and retraction of the grinding wheel axis. This generally occurs with high stock removal grinding, which has high grinding forces that can result in some limited deflection of the machine structure. This deflection reduces as the grinding forces drop at the end of the infeed and results in some addition material removal. The action of *sparkout* improves the surface quality but also may remove some effects of the *HEDG* process on the surface integrity.

A number of different approaches were used to investigate the surface integrity as described later, these included methods for both assessing the surface profile and near surface structure. The former measurements were aimed at the surface finishes produced and were utilised primarily in the analysis of the *Superfinish Grinding* trials. The latter were used to investigate levels of damage introduced by the grinding in the near surface zone.

3.1 Machine Descriptions

A brief overview of the machines is given herein, all are production machines without any special modification and currently in use within industry today. The Edgetek SAM machine is produced by *Jones & Shipman* a subsidiary of *Renold Machine tools*. Such machines are currently used in the automotive industry for the production of transmission components and also in the aerospace industry for the grinding of jet engine turbine blades root forms. The *CNC Twin Wheel Orbital Grinder* is produced by *Landis Lund* a division of *Unova* as is the LT1. This machine is used within the automotive industry for the grinding of crankshafts. All three machines are currently built within the UK and for these trials those used for the rough grinding trials have been equipped with fire suppression systems. The Edgetek using an argonite gas with an automatic trigger and the Twin Wheel machine CO_2 gas with a manual trigger system.

The Edgetek has previously been used to carry out *HEDG* research on aerospace turbine components Nickel based Superalloys and *M50* bearing steel, both in a surface grinding

mode (Johnstone, 2002). Prior to this work no investigations had been carried out in a cylindrical plunge-grinding configuration. This machine was used for the initial grinding trials.

The *CNC Twin Wheel Orbital Grinder* and *LT1* are designed for use in a cylindrical plunge grind mode and can be used for both rough and finish grinding within conventional parameters, which in the case of rough grinding is up to specific material removal rates (Q'_w) of 250mm^3/mm.s. Some initial rough grinding trials up to Q'_w values of 500mm^3/mm.s had been carried out prior to this research. The aim was to use this machine to validate the advances made as a result of the *HEDG* process development at Cranfield.

Cylindrical plunge mode grinding have been carried out both on the Edgetek and the production LL grinding machines, for the former it was necessary to use an analogous component to represent the crankshaft, due to both workspace and *CNC* limitations.

3.1.1 Edgetek

The Edgetek located in the School of Industrial and Manufacturing Science (*SIMS*) at Cranfield University is a versatile machine suitable for research and development applications. Being located at the University its close locality enabled longer programs of work to be undertaken. The main limitations of this machine with regard to this study were the relatively low spindle power (*27kW*), and size of component – a full crankshaft would not fit into the workspace envelope. The initial grinding investigations were carried out on this machine. It is a five axes CNC grinding machine designed to utilise superabrasive CBN grinding technology to achieve high stock removal working in a creep feed or high speed surface grinding mode. Table 3.1 shows a typical specification provided by the manufacturer for the machine.

X Axis Travel	*18.6" (472 mm)*
Y Axis Travel	*12.8" (325 mm)*
Z Axis Travel	*12.0" (305 mm)*
B Axis Rotary	*12.59" (317.5mm) Diameter*
5th Axis	*A or rotary tilt versions*
Spindle HP	*35 HP (27KW)*
Spindle RPM	*14,000 RPM, higher RPMs available*
Way System	*Schneeberger Hi-precision Linear Roller Bearing Ways*
Position Feedback	*Heidenhain Linear Scales on X,Y, Z*
Feed Rate	*to 157 IPM (66 mm/sec)*
Rapid Traverse	*0 to 300 IPM (126 mm/sec)*
Voltage	*200-230 volts, 3 Phase 60 Cycle*

Table 3.1– Edgetek Machine Specification

The machine was equipped with the optional B axis rotary table onto which the optional 5th rotary axis could be mounted for the cylindrical grinding tests. The 5th axis selected for these tests was a rotary spindle with an operating range of 100 to 1000rpm.

3.1.2 CNC Twin-Wheel Orbital Grinding Machine

The LL twin wheel machine located at the machine tool manufacture's site was a production grinding machine designed specifically for the grinding of crankshafts. However the machine being less versatile was only suitable for tests on crankshaft components, this together with the location and a limited period of availability meant

that only the final grinding trials were programmed for this machine. The main machine features are:

- A Landis Lund CNC control system
- Hydrostatic slideways and wheel spindles
- CBN grinding wheel technology
- Wheel dressing spindles
- Variable speed work drive
- Linear motor technology

The maximum available grinding wheel spindle power of *80kW* on this machine offers an enhanced capability for the high material removal rate - *HEDG* - research. The machines high stiffness achieved by the use of hydrostatics bearings together with a high spindle speed and power capability mean that the machine is also highly suitable to fully utilize the advantages of superabrasive grinding wheel technology. Figure 3.1 below shows a photograph of the machine used for the trials.

Figure 3.1– Photograph of Orbital Twin-Wheel Crank Grinding Machine

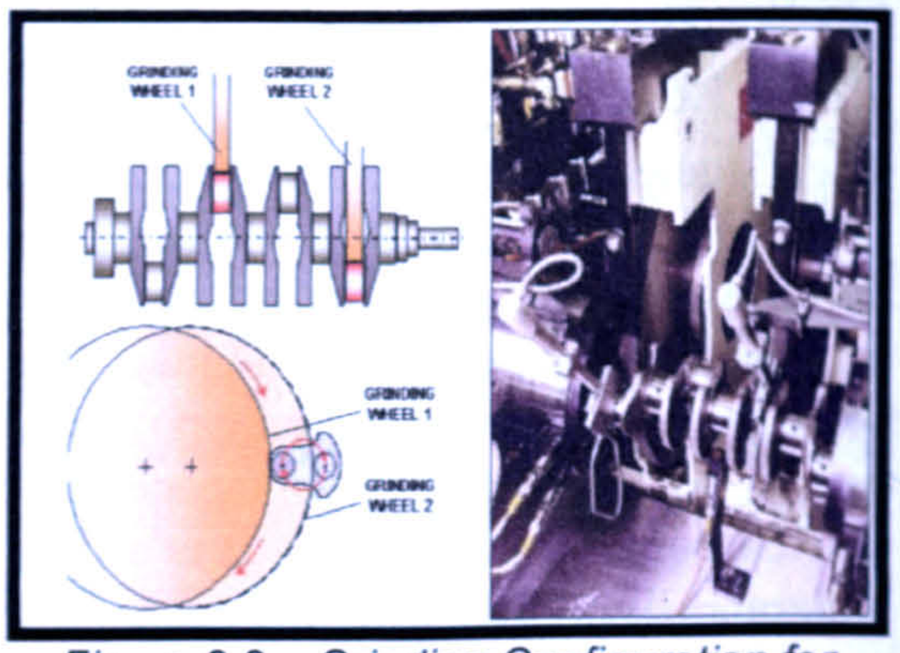

Figure 3.2 – Grinding Configuration for Orbital Twin-Wheel Crank Machine

The machine has dual spindle work heads, which subject to suitable component geometry enables the grinding of features simultaneously. This facility reduces the total grind cycle time and therefore makes the unit more competitive as a production machine tool. All grinding operations on the crankshaft component are carried out in one setting this increases the geometric accuracy of pieces and by eliminating component re-positioning maintains a reduced cycle time. The single setting grind is made possible by the implementation of an orbital grinding wheel path as illustrated in Figure 3.2. The grinding wheel infeed axis is slaved to the workpiece spindle and moves in and out to maintain the correct position relative to the crankshaft pin journals and pin webs centres. The maximum speed achievable for the workpiece spindle whilst utilising this technique is 100rpm. Crankshaft main journals and main webs are concentric to the spindle rotation and therefore are ground in a conventional cylindrical plunge grind operation. The machine has the facility to log all linear and rotary axes position and power data throughout the grinding cycle, this was utilised primarily to determine the net grinding power.

A development crankshaft provided by an automotive manufacturer was used for the trials, the material was the same as that used in bar stock form for the initial tests. Fixtures and coolant application systems were manufactured specifically for these trials.

3.1.3 LT1 – Production CNC Cam & Crankshaft Grinding Machine

The LT1 machine was also located at the machine tool manufacture's site again a production-grinding machine in this case designed for both the grinding of camshaft and crankshafts. The main machine features are:

- Landis system CNC control
- Hydrostatic wheel head ways, cross-slide and spindle
- Variable speed work drive
- Linear motor technology
- CBN grinding wheel technology
- Wheel dressing spindles
- Totally enclosed grinding area
- Suitable for cam, crank and transmission components

The machine has a high stiffness achieved by the use of hydrostatic bearing slideways and spindle. High Stiffness and a high speed spindle enable this machine to fully utilize the advantages of superabrasive grinding wheel technology. The machine used for the trials is shown in Figure 3.3.

Figure 3.3 – LT1 Production Cam & Crankshaft Grinding Machine Tool

Figure 3.4 shows the inside of the machine in both cam and crankshafts configurations. The machine used for the trials was fitted with a truing/dressing spindle intended for use with a vitrified finishing wheel. Grinding wheels used as standard for finishing operations would have an abrasive grit size in the region of 150-200μm.

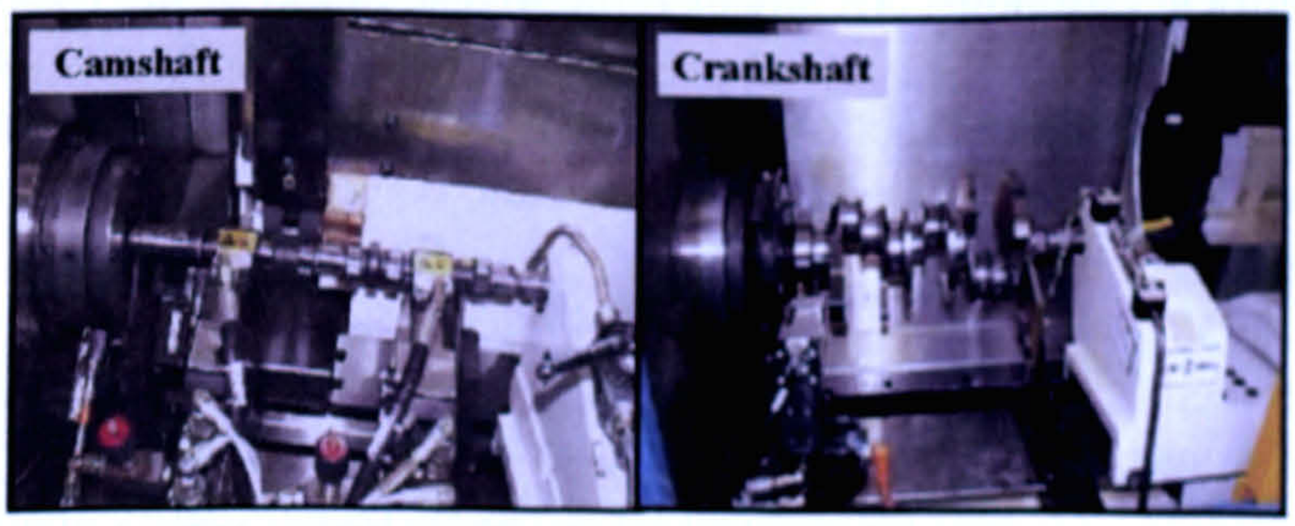

Figure 3.4 – Photograph of LT1 with Cam & Crankshaft Components

The machine has the facility to log all linear and rotary axes positions and power data throughout the grinding cycle, this was utilised primarily to determine performance of the modified path oscillatory motion.

3.2 Test Procedures

This section details the grinding techniques, parameters and measurements made for both *HEDG* and *Superfinish* grinding regimes trials. Work spindle power measurements were taken with the objective of studying the specific grinding energy and estimating the grinding temperatures of the workpiece using thermal modelling. The thermal modelling techniques utilised are currently under development at Cranfield University (Stephenson, 2003), details of which are discussed within the literature review. To validate the modelling developed for cylindrical plunge grinding a thermal measurement technique was developed as part of this research program to determine the grinding temperature. This has been used in the HEDG cylindrical tests.

3.2.1 HEDG Regime

The work carried out on the Crankshaft components has been split into three stages:

- Surface Grinding of Samples
- Cylindrical Grinding of Samples
- Cylindrical Grinding of Crankshaft Components

An automotive company supplied all the material *38MnSiVS6*, in barstock form for the samples and the crankshafts as forgings. All the material was in an unhardened state. Hardness measurements were taken to confirm a typical hardness between 26 and 30HRC. Trials were carried out with the material in this state.

Stage 1 – Surface Grinding. To investigate surface integrity resulting from the grinding action on analogous components. The surface grind mode ensured that there was no further surface to wheel interaction post *HEDG* grind, that may affect the surface integrity produced. The key areas were:

- Establish the burn threshold of the material
- Apply best current coolant practice. Scrubbers and nozzle technology
- Develop the analysis techniques to be used for detecting thermal damage
- Investigate the existence of the *HEDG* regime
- Test different grinding wheel grit sizes

Stage 2 – Cylindrical Grinding. To advance the investigation of the *HEDG* grinding in a grinding mode suitable for the production of automotive crankshaft components, using a set-up representative of a production environment. For this the key areas were:

- Establish the Specific Material Removal Rate (Q'_w $mm^3/mm.s$) attainable with cylindrical grinding
- Determine the existence of *HEDG* in cylindrical grinding
- Develop method for thermal measurement of finished surface
- Test different types of grinding wheel type normal and segmented
- Assess grinding process using residual stress surface integrity analysis
- Apply recent developments in thermal modelling

Stage 3 – Production Cylindrical Grinding. Validate the grinding investigations to date on production machinery with real crankshaft components. Key areas were:

- Apply Specific Material Removal Rate (Q'_w $mm^3/mm.s$) attained in previous work to production environment with a target improvement of 30% to the crankshaft production cycle
- Validate process application residual stress geometry wheel life etc

3.2.1.1 Surface Grinding

The first series of trials were carried out in the surface grinding mode, this was done to ensure no further grinding wheel / sample interaction after the designated cut had been carried out. This allowed a visual inspection of the sample surface to be carried out and visual grinding burn to be recorded. Grinding power was monitored for all tests by means of a Hall Effect sensor connected to the machine's grinding spindle.

Two sets of tests were carried out. The initial set of tests was conducted over the range of 1 to 180 $mm^3/mm.s$ Q'_w, the aim being to establish the basic process conditions. These tests covered the conventional creep feed grinding regime and the lower range of *HEDG*. The grinding parameters used are given in Table 3.2

Parameter		Value
Specific Removal Rate	Q'_w	1-180mm^3 /mm.s
Depth of Cut	A	0.1-4mm
Feedrate	V_w	2-90mm/s
Grinding Wheel Speed	V_s	100-200m/s
Grinding Wheel Grit Size	-	213μm

Table 3.2 - Parameters for 1st Set of HEDG Grinding Trials

The second set were carried out over a higher range of 5 to 1000 $mm^3/mm.s$, the upper level of these tests were accepted to be well into the *HEDG* regime (Tawakoli 1993). Grinding parameters are given in Table 3.3.

Parameter		Value
Specific Removal Rate	Q'_w	5-1000mm^3 /mm.s
Depth of Cut	A	1-10mm
Feedrate	V_w	5-100mm/s
Grinding Wheel Speed	V_s	100-200m/s
Grinding Wheel Grit Size	-	213 & 151μm

Table 3.3 - Parameters for 2nd Set of HEDG Grinding Trials

The grinding arrangement utilised is illustrated in Figure 3.5. For these tests steel-bodied electroplate grinding wheels with CBN grit sizes of 151 μm and 213 μm were used. The coolant supply configuration comprised a 6.5mm diameter nozzle with at 10bar with 75 litres/*min* flow, coupled with 3 scrubber nozzles 1mm diameter at 50 bar with 5 *litres/min* flow. Previous research reported by Webster et al (1995) indicated this to be a potential improvement over that currently employed. The 6.5 mm diameter nozzle had a specially formed internal section to ensure a laminar fluid flow of the coolant. Samples were located in a machine vice bolted to the machine axis. Prior to the

test a light surface cut was taken to establish touch, followed by a sparkout grind during which the power level was monitored.

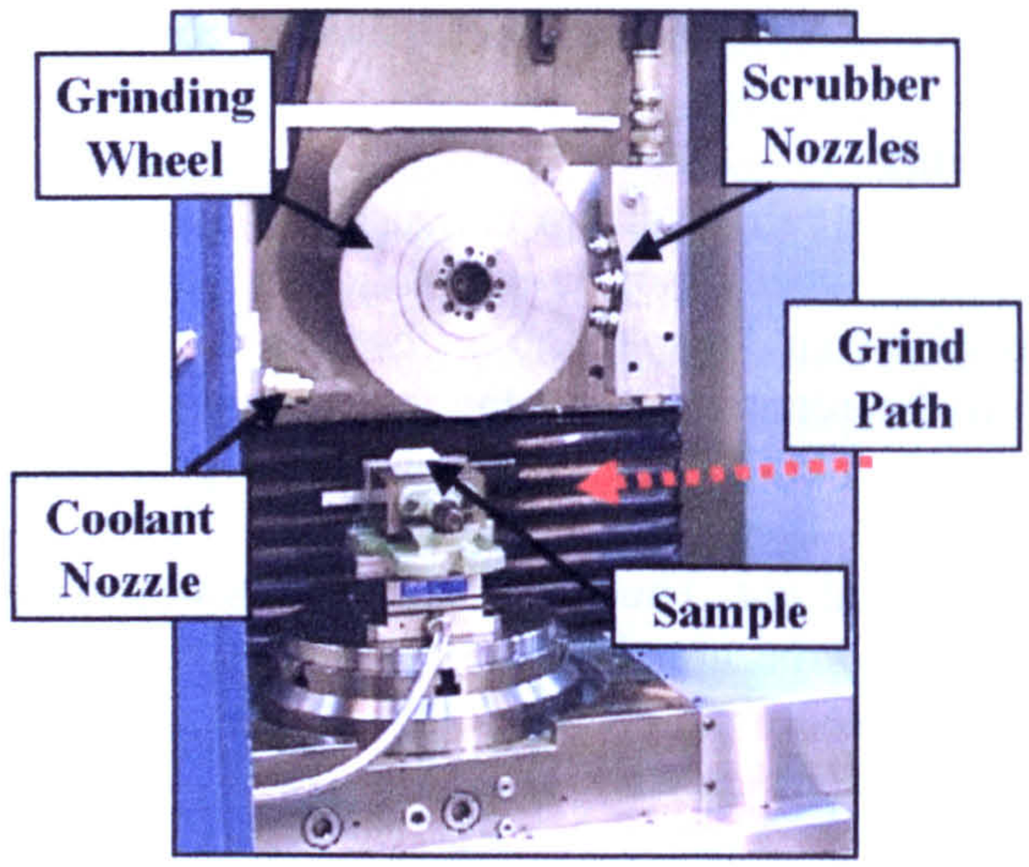

Figure 3.5 – HEDG Set-up

3.2.1.2 Cylindrical Grinding

For the cylindrical grinding trials a spindle was added onto the rotary B-axis of the Edgetek, as shown in Figure 3.6. Note that sample features were representative of the web and journal of a crankshaft. Table 3.4 gives the grinding parameters for this series of tests.

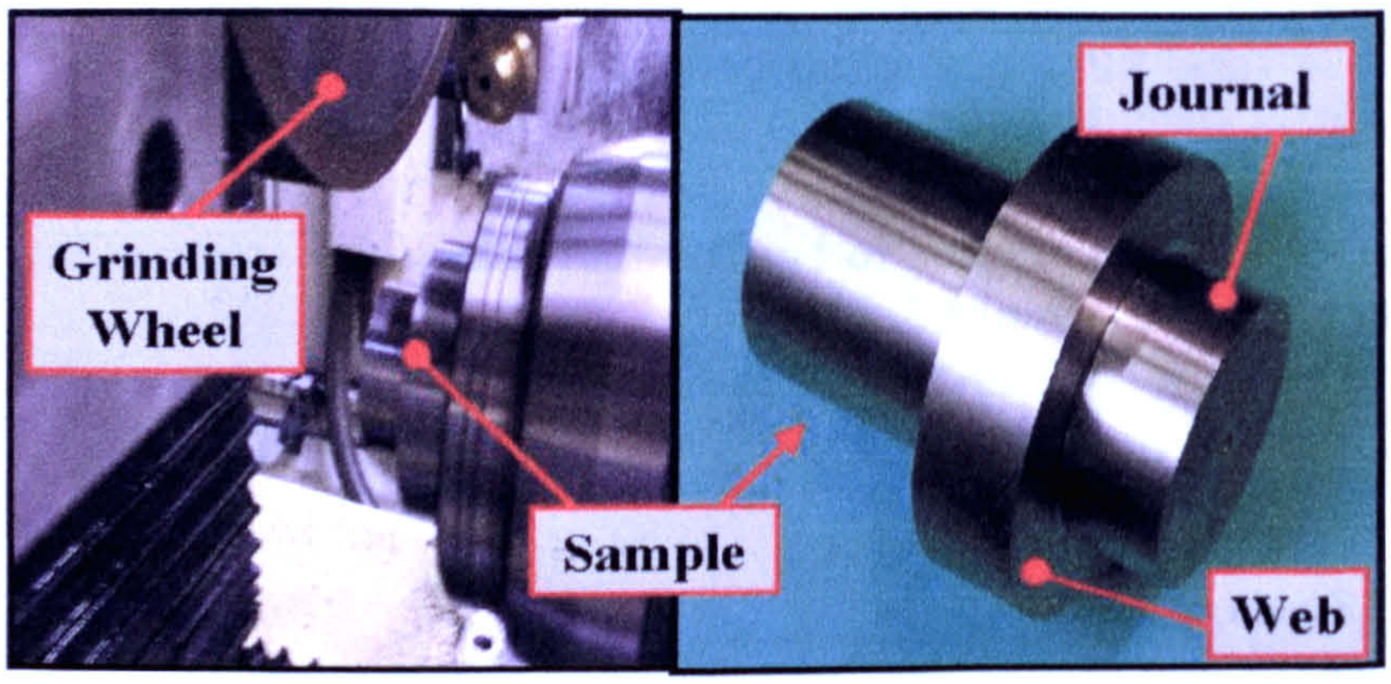

Figure 3.6 – Cylindrical Grinding Set-up

Parameter		Value
Specific Removal Rate	Q'_w	Up to 3000mm^3 /mm.s
Grinding Wheel Speed	V_s	100 &200m/s
Grinding Wheel Grit Size	-	427, 252 & 213 µm

Table 3.4 - Parameters for Cylindrical HEDG Trials

As part of the development for coolant application both a segmented grinding wheel and a specially modified segmented wheel with internal coolant channels were tested. The basis for the segmented wheel was to allow better swarf removal from the grinding zone and increase the coolant penetration, a technique utilised in creep feed grinding

applications. See Figure 3.7. The modified wheel with internal coolant channels was intended to allow a reduced coolant quantity to be utilised, with the coolant being fed directly into the grinding zone by centrifugal force. This approach is commonly used in precision grinding as a means to reduce the level of sub surface damage introduced to glass components through the thermal shock associated with grinding. See Figure 3.8.

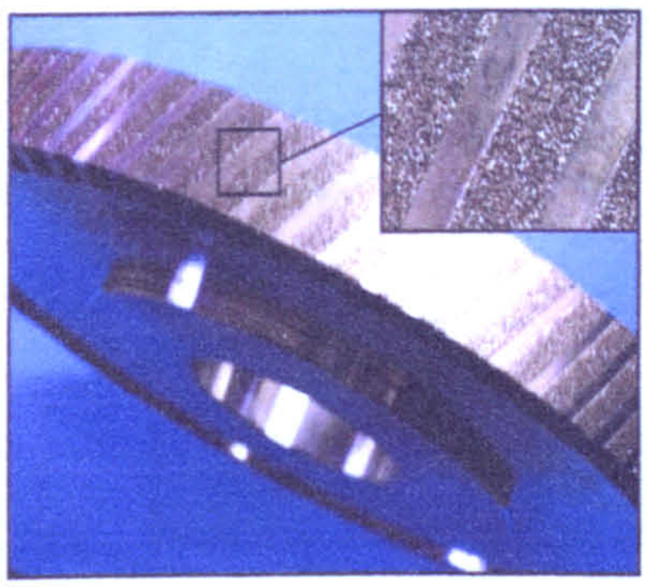

Figure 3.7 – Segmented Grinding Wheel

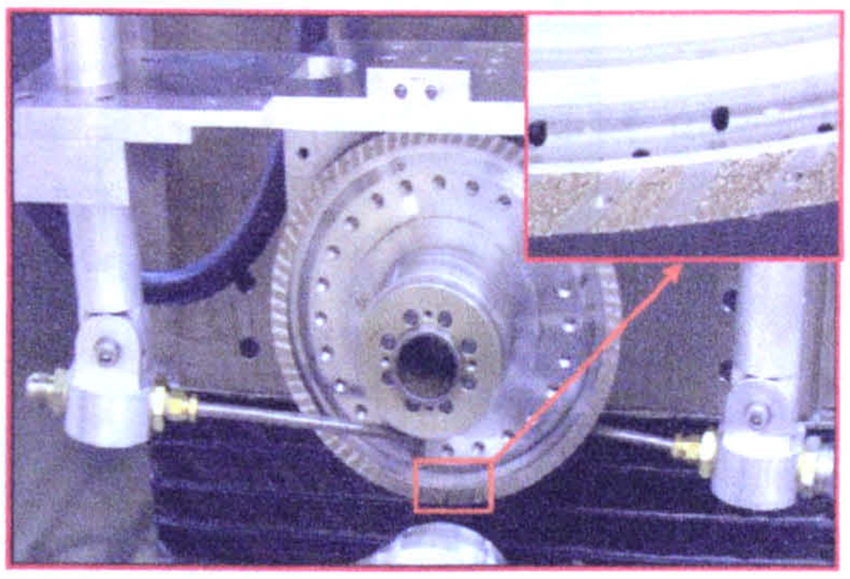

Figure 3.8 – Set-up for Modified Segmented Grinding Wheel

As previously discussed thermal damage caused by grinding was a major issue and therefore both thermal modelling work and thermal measurements were required. Thus the final objective for this stage was to implement the thermal modelling proposed by Stephenson (2003) and carry out temperature measurement to validate the findings. The grinding power data was applied to the thermal model produced for cylindrical grinding thus producing a prediction of the temperatures at the grinding zone. Next the temperature measurement was carried the utilising the development described herein.

Kato (1997) developed a novel temperature measurement technique for use with surface grinding. Kato's technique has been developed in this research for application to cylindrical plunge grinding. To do this a split testpiece has been manufactured from barstock in the material of interest, as illustrated in Figure 3.9. A PVD coating was applied (by the Nanotechnology department at Cranfield University) to one of the mating surfaces and the testpiece assembled for grinding. The grinding takes place across the mating interface, and hence the coating is melted by an amount proportional to the temperature.

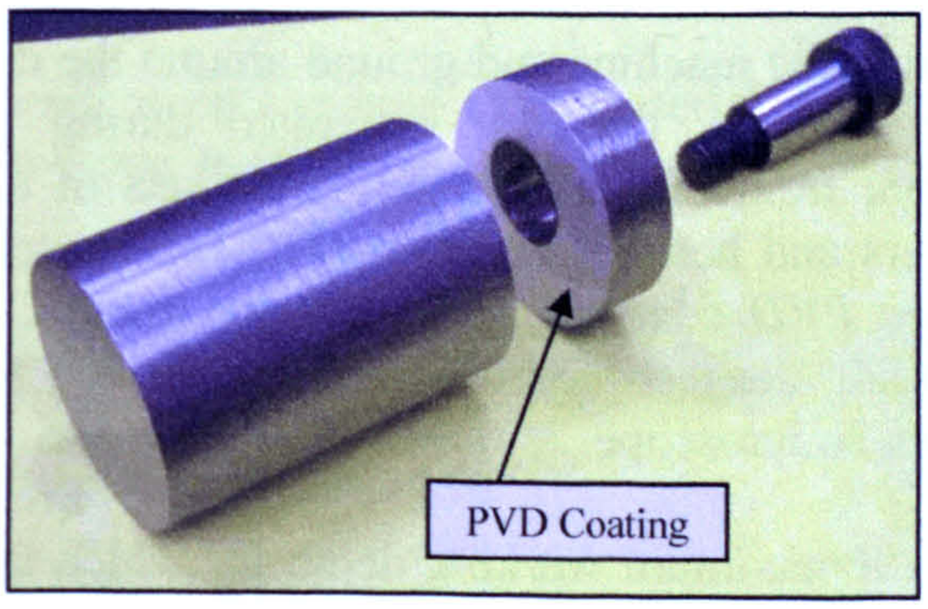

Figure 3.9 – Thermal Measurement Assembly

The applied coatings were approximately 0.2μm thick hence preparation of the mating surface was critical to the success of this method. Initially the mating surfaces were

precision ground to ensure they were both flat and parallel, subsequently they were then lapped to produce a polished high quality surface finish. The lapping was carried out progressively beginning with 25μm then 8μm and finally 3μm diamond grit. The set-up used is shown below in Figure 3.10.

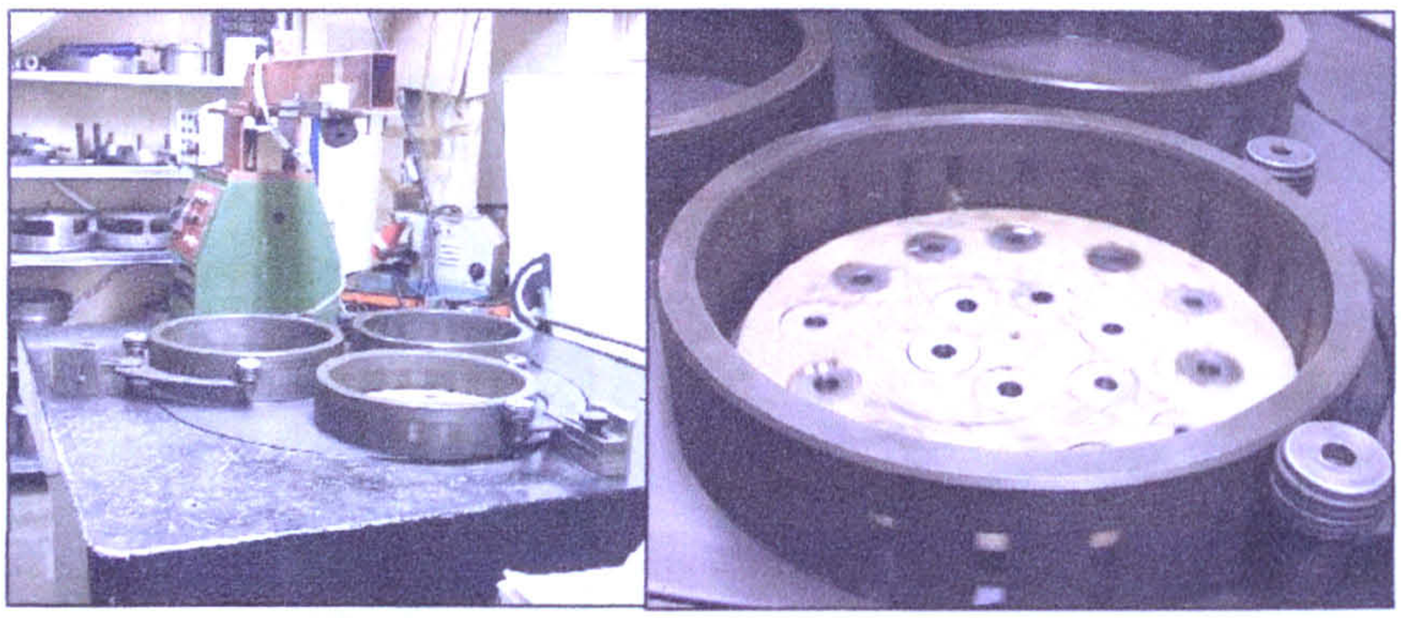

Figure 3.10 – Lapping Set-up for Thermal Samples

The resulting quality of the mating surface was checked using both a form interferometer and surface roughness instrument. The flatness was approximately *0.4μm*, and the *s*urface roughness was *30nm* R_a. Figure 3.11 Shows the interferometric fringe pattern on the left and a visual image of the surface on the right. The result of the preparation was that the surfaces were a close fit.

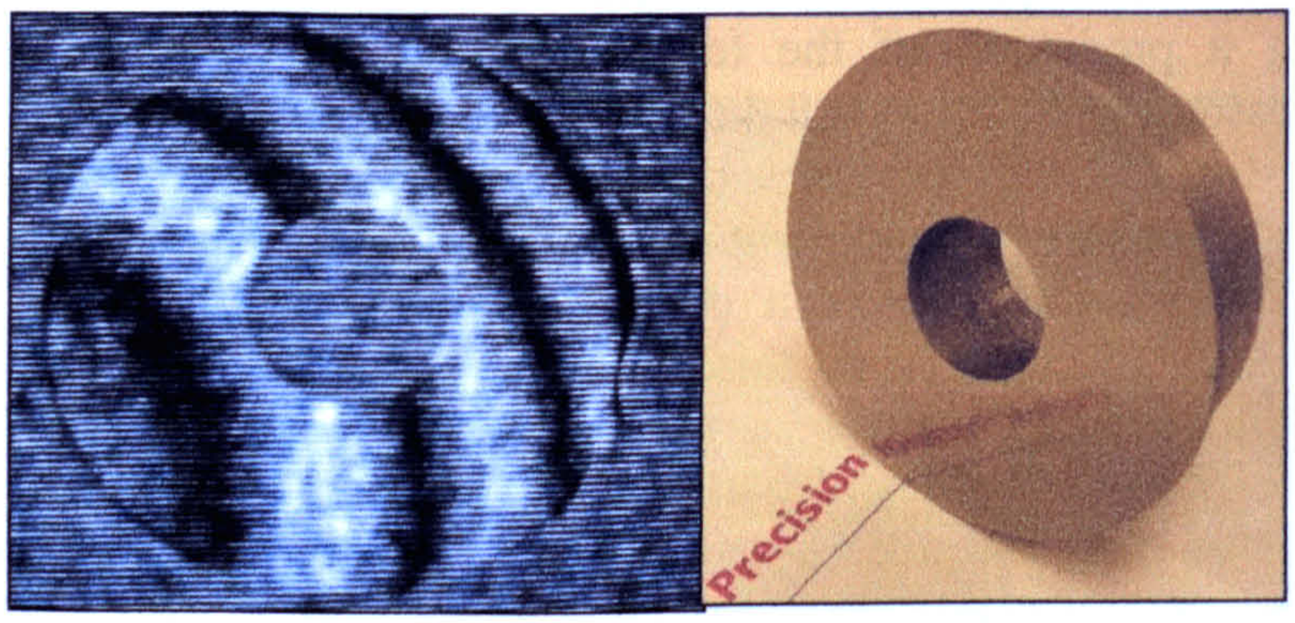

Figure 3.11 – Lapped Thermal Sample

Testpieces were located in the machine and ground around the circumference across the interface between the surfaces, the heat generated during the grind melting the sandwiched coating back from the outer edge. Three sets of test-pieces were ground with identical parameters and hence a constant Q'_w, each testpiece having a different *PVD* coating. The three *PVD* coatings selected were indium, bismuth and zinc. On completion of the grinding the test-pieces were disassembled for measurement of the melt depth with an optical microscope.

Kato states that there is a maximum working depth for which the relationship between the melt depth and temperature can be considered as consistent, this is given by Equation 3.1

$$d_{max} = \frac{8.\alpha}{v_w}$$

Equation 3.1– Kato's Equation for Maximum Coating Working Depth

Where:

v_w	-	*Workpiece Speed*	*(mm)*
α	-	*Thermal Diffusivity*	*(K^1)*

For application with cylindrical plunge grinding the workpiece speed is given by Equation 3.2

$$v_w = \frac{\pi . D . v_r}{60}$$

Equation 3.2 – Workpiece Speed in Cylindrical Plunge Grinding

Where:

v_w	-	*Workpiece periphery Speed*	*(m/s)*
v_r	-	*Workpiece rotational speed*	*(rpm)*
D	-	*Workpiece Diameter*	*(mm)*
α	-	*Thermal Diffusivity*	*(K^1)*

Thus Kato's equation may be rearranged the form given by Equation 3.3

$$d_{max} = \left(\frac{480}{\pi.D}\right).\left(\frac{\alpha}{v_r}\right)$$

Equation 3.3 – Derived Equation for Maximum Coating Working Depth

Where:

v_r	-	*Workpiece rotational speed*	*(rpm)*
D	-	*Workpiece Diameter*	*(mm)*
α	-	*Thermal Diffusivity*	*(K^1)*

and

$$\alpha = \frac{k}{\rho . C}$$

Where:

k	-	*Thermal Conductivity*	*(W/(m.K)*
ρ	-	*Density*	*(kg/m^3)*
C	-	*Specific Heat Capacity*	*(J/kg.K)*

The relationship is dependent on the host steel material's thermal properties, namely thermal diffusivity. This value itself changes as the materials temperature increases as specified in Table 3.5

Temp	*C*	*k*
20	*461*	*46.7*
100	*479*	*47.8*
200	*499*	*46.7*
300	*517*	*44.1*
400	*536*	*41.1*
500	*558*	*38.2*
600	*587*	*35.3*

Table 3.5 – Thermal Properties of Steel (38MnSiVS6)

Using Equation 3.3 together with the thermal data from Table 3.5 and the material density of *7820kg/m*^{3} a profile for the workable coating depth was established. Figure 3.12 shows the profile together with the melting temperatures of the three PVD coatings selected.

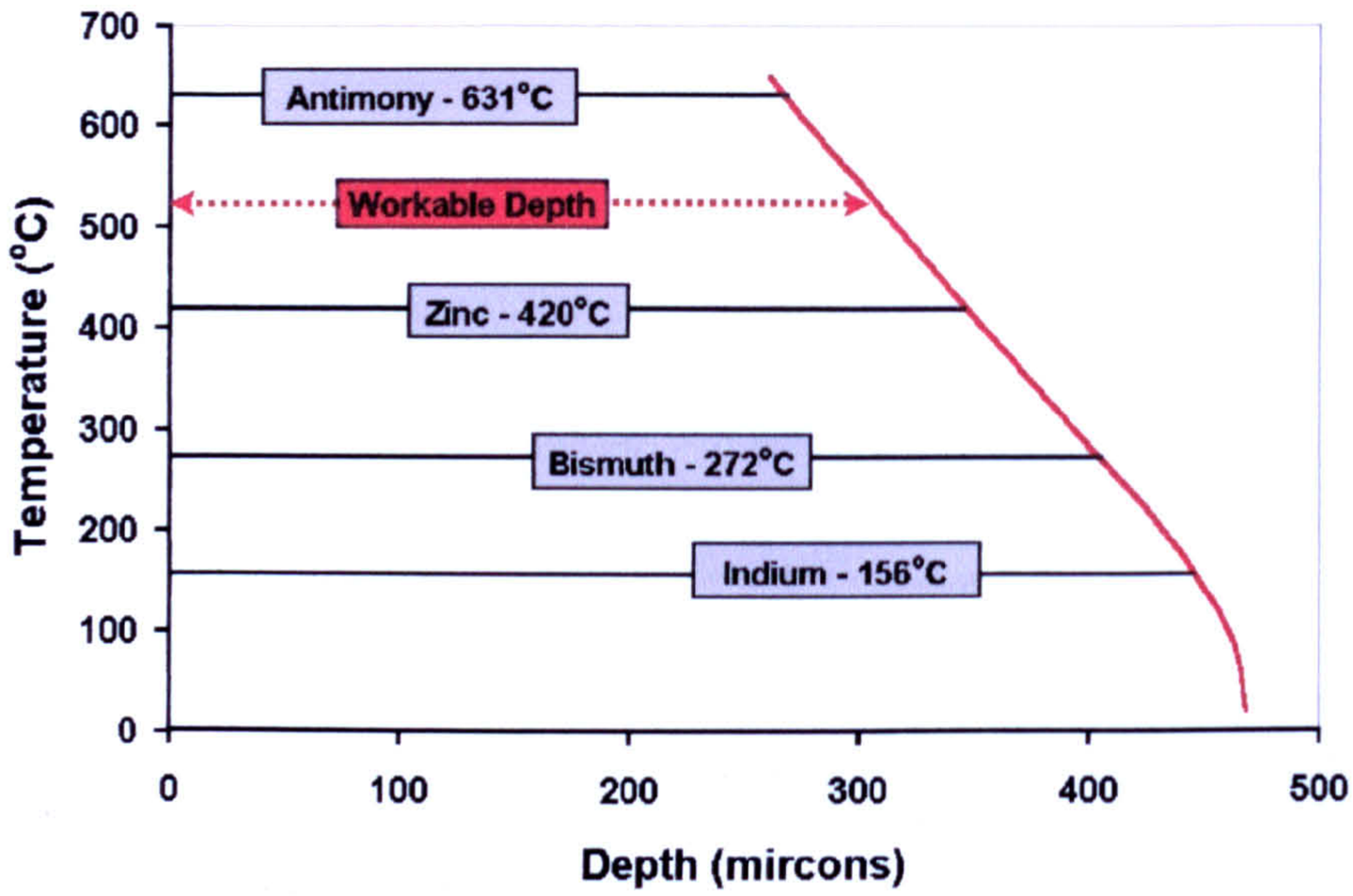

Figure 3.12 – Workable depth for PVD Coatings

Figure 3.13 shows images of typical coated surfaces after grinding trials to verify the experimental procedures. The melt depths of the different coatings in this case indium, bismuth and zinc are designated *X*, *Y* and *Z* respectively.

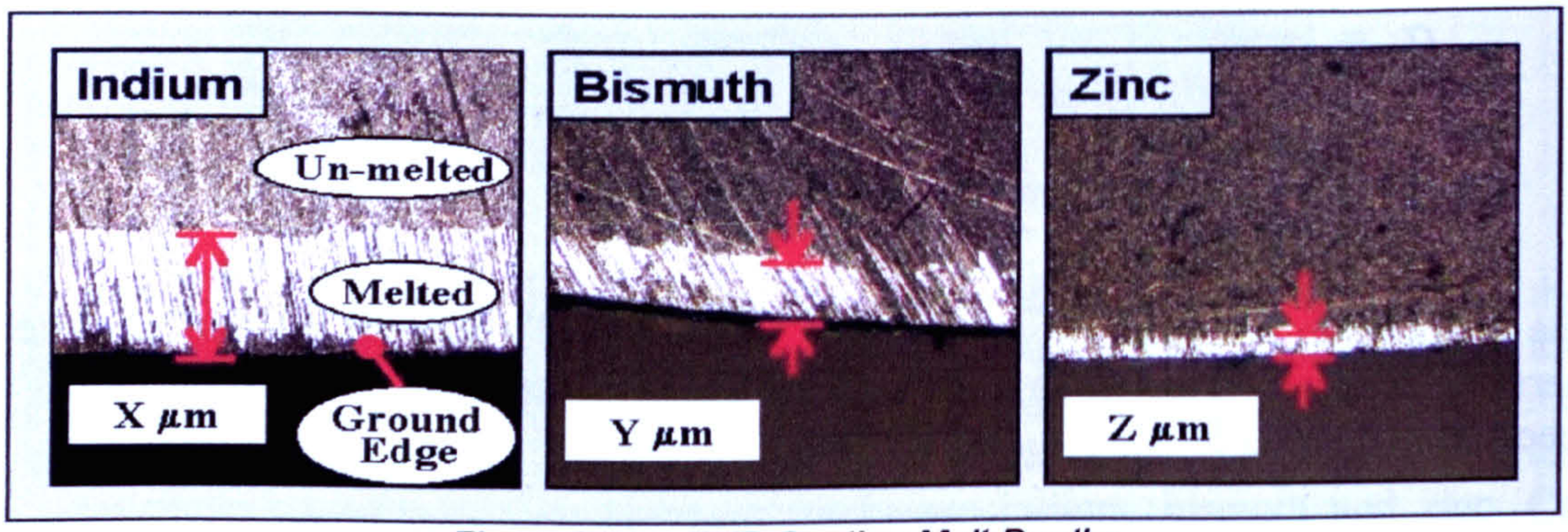

Figure 3.13 – PVD Coating Melt Depths

The final stage of the technique was to plot the PVD melt depth data (*X*, *Y* and *Z)* with the PVD coating melt temperatures, 420°C for zinc, 272 °C for bismuth and 156 °C for indium. A representative plot is shown in Figure 3.14 with the maximum coating depth profile included. It can be seen that if the line joining the data points is extended back to the temperature axes then the surface temperature of the ground surface can be obtained.

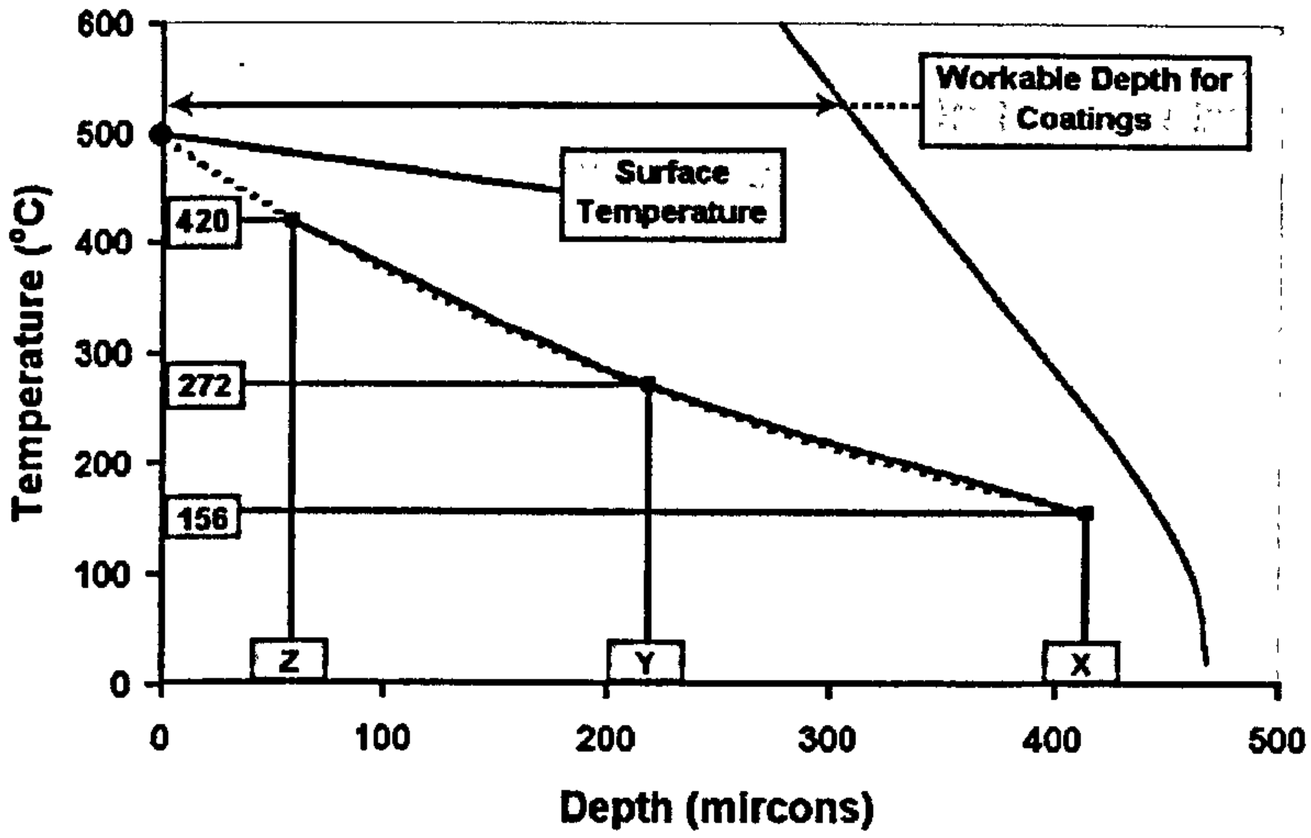

Figure 3.14 – PVD Coating Plot of Depth versus Temperature

Further investigations by Kato (2000) refined the technique. Kato established that the trend of the PVD temperature versus depth profile within the workable region defined by the maximum depth calculation was exponential. Thus if a Log plot was used as illustrated by Figure 3.15 then the line joining the data points becomes linear and determination of the axis intersection is both simpler and more reliable

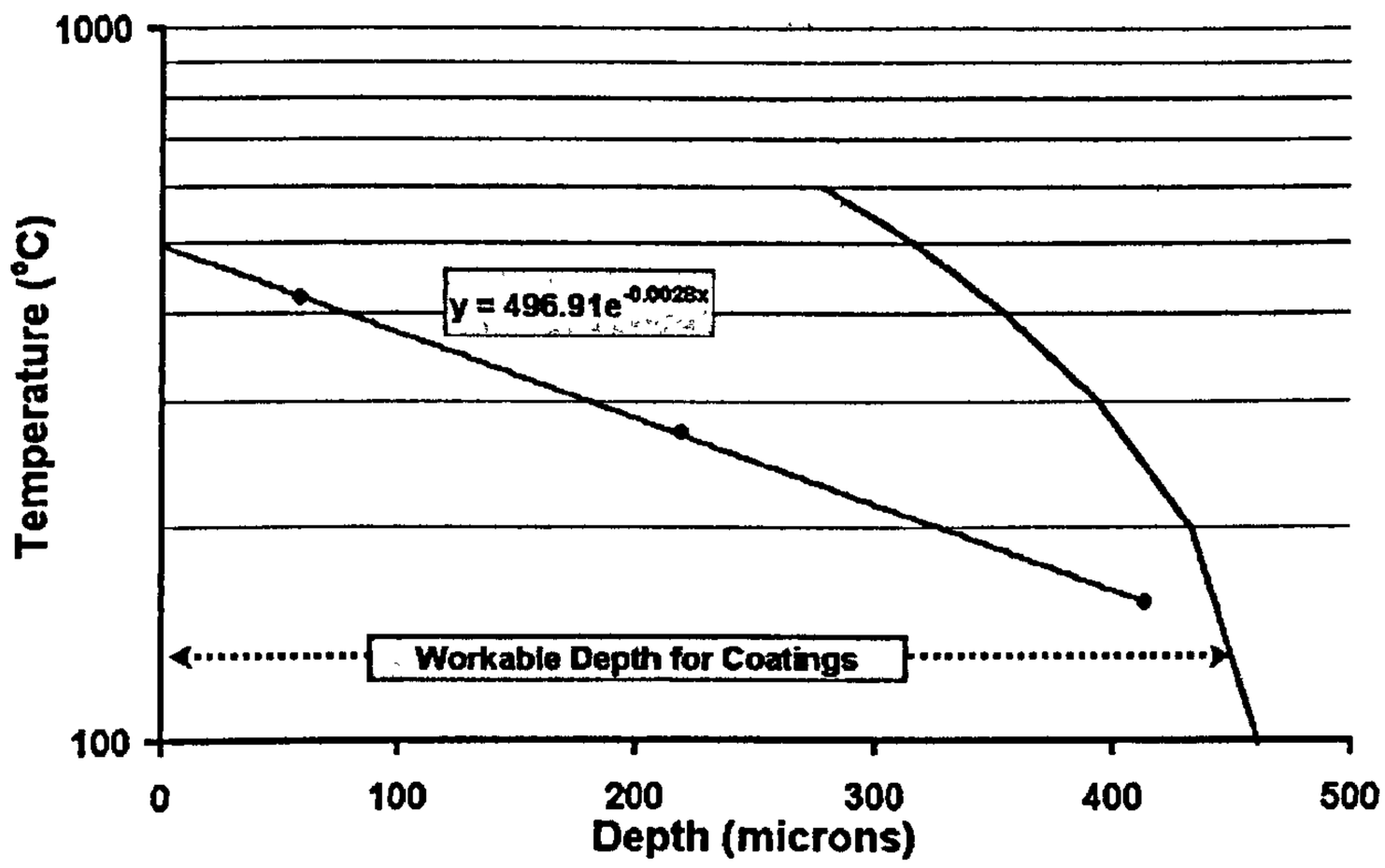

Figure 3.15 – PVD Coating Log Plot of Depth versus Temperature

The final part of this work was to examine the wheel surface using optical microscopy for evidence of abrasive grit failure.

3.2.1.3 Production Cylindrical Grinding

The components used for these trials were two different prototype crankshafts supplied by an automotive company. The crankshafts were for diesel units and manufactured

from a precipitation hardening ferritic/pearlitic steel whose designation is given as 38MnSiVS6. Photographs of the two crankshaft components are shown in Figure 3.16.

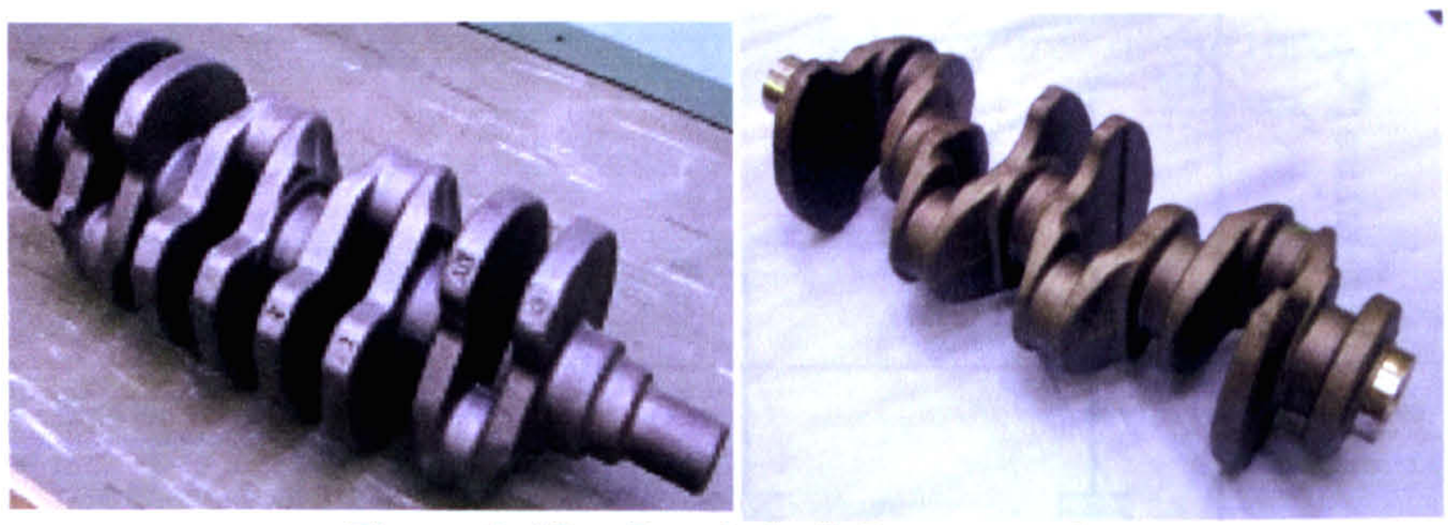

Figure 3.16 – Crankshaft Components

Metallurgical examinations were carried out on the forged crankshaft material in order to determine whether there would be difference resulting from the components forged skin. Figure 3.17 shows a pair of cross sectional microstructural images prepared as described by Higgins (1973). The left-hand image shows the microstructure found from the edge down to approximately 150μm below the surface. There is no significant difference in the structure to that of the right-hand image, which was taken from the centre portion of the component.

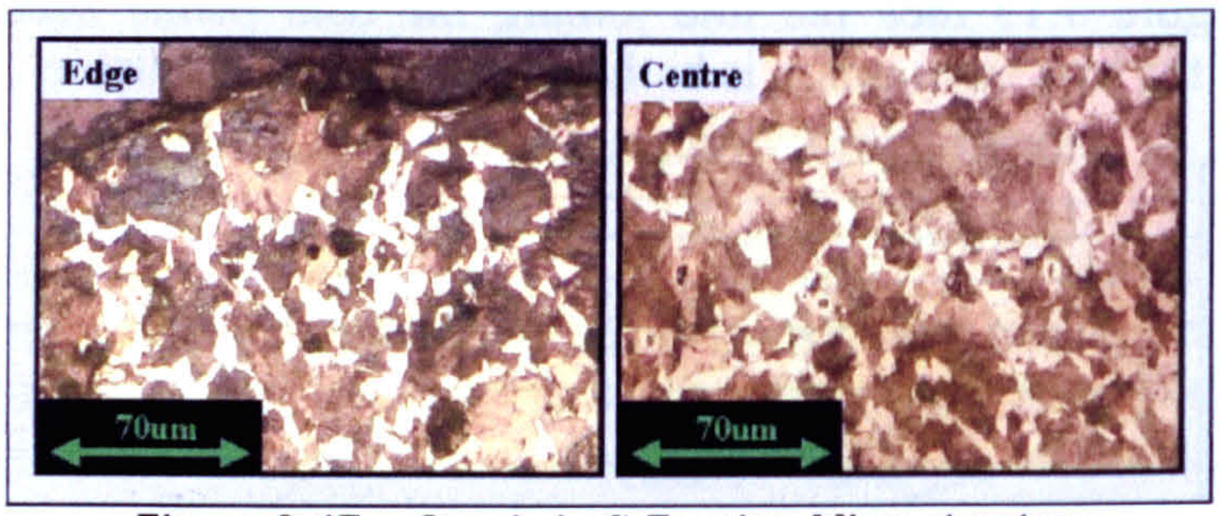

Figure 3.17 – Crankshaft Forging Microstructure

Microharness tests were carried out on both samples with a 200g load. The results are shown in Table 3.6. It can be seen that the microhardness values are similar once a depth of 70μm is reached. With grinding depths of in excess of 1mm it was concluded from the metallurgical examination that there was no significant component 'skin effect' that would in turn have an impact on the grinding trials.

Micro-hardness (H_v)		
Centre Region	Edge	Depth from Edge (μm)
282	335	50
286	371	55
285	298	60
265	305	65
267	261	70

Table 3.6 – Micro-hardness Data for Crankshaft Forging

There were two stages to the grinding trials for which the aim was to establish the viability of *HEDG* as a process for the production of rough-machined crankshafts. All the tests were conducted on the LL twin wheelhead *CNC* production-grinding machine

at the manufacturer's site in Yorkshire. The grinding set-up used with the LL machine is shown in Figure 3.18. The left-hand image the crankshaft located in the machine, the twin grinding wheels each mounted on their own axes, and the emergency CO_2 fire extinguisher nozzle. The right-hand image shows the coolant arrangement with main (upper) and spark arrestor (lower) nozzles used with pressures of 9bar and the scrubber unit nozzle maintained at 75bar.

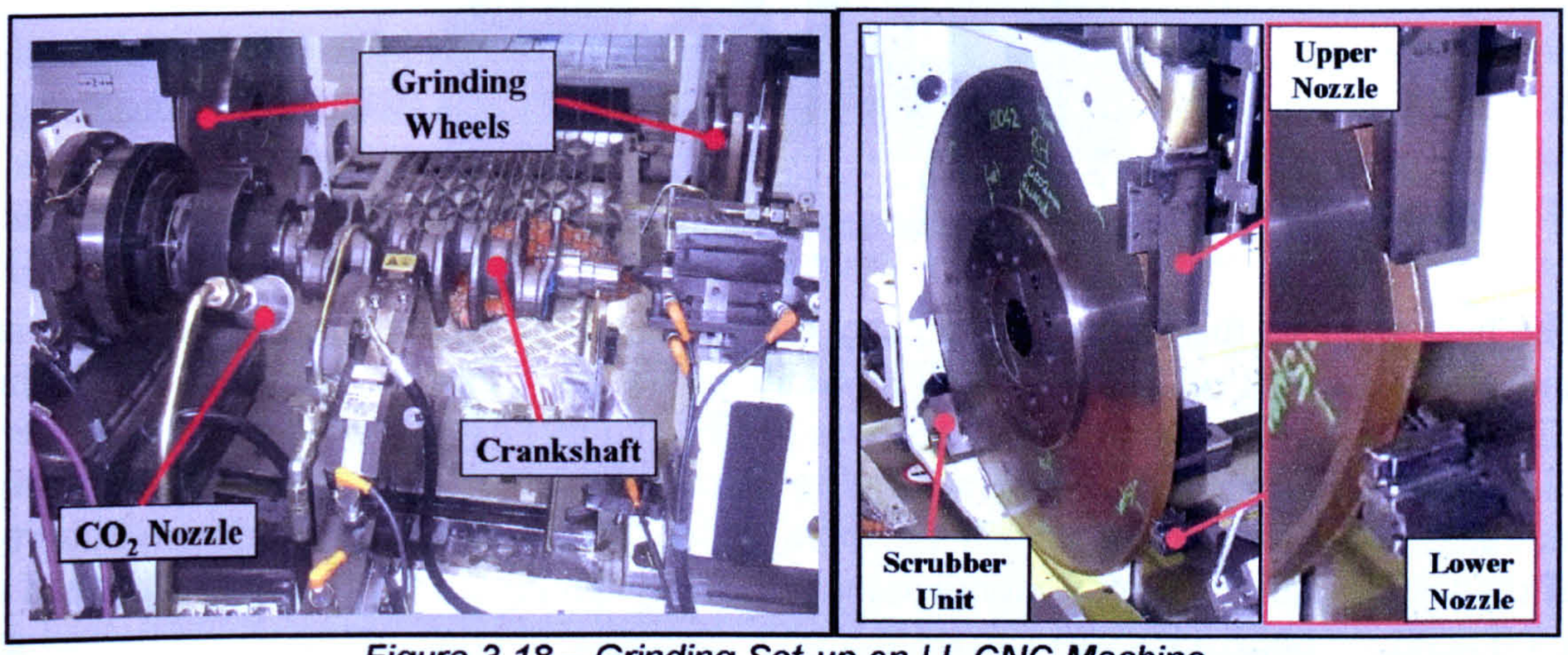

Figure 3.18 – Grinding Set-up on LL CNC Machine

The first stage of work was carried out with rectangular section peripheral grinding wheels, the corners of which had a 1mm radius. A cross-sectional profile is shown in Figure 3.20. Tests were carried out on sections of the component to represent the machining of web faces and journal diameters. A range of Q'_w from *80* up to *2000mm³/mm.s* were used and in conjunction a number of different grinding wheels tested at cutting speeds from 120 up to 180m/s. The range of grinding parameters are given in Table 3.7. This provided an opportunity to transfer the previous research to a production environment and validate *HEDG* on a production machine. At this stage the full form of the crankshafts was not ground to full geometrical production specifications, but rather surfaces to represent web face and journal diameters. A total of 100 crankshafts were ground whilst monitoring spindle power data.

Web Face		
Specific Removal Rate	Q'_w	*Up to 2000mm³ /mm.s*
Journal		
Specific Removal Rate	Q'_w	*Up to 250mm³ /mm.s*
Grinding Wheels		
Speed	V_s	*120-180m/s*
Grit Size	-	*252 & 356µm*
Type	-	*Normal & Segmented*

Table 3.7 - LL HEDG Cylindrical Grinding Trials

Analysis was carried out on the ground components over the full range of Q'_w values for evidence of thermal damage. This was achieved by sectioning the crankshafts as

illustrated in Figure 3.19 and then measuring web faces and journal diameters with the BN equipment for an indication of the level of residual stress present.

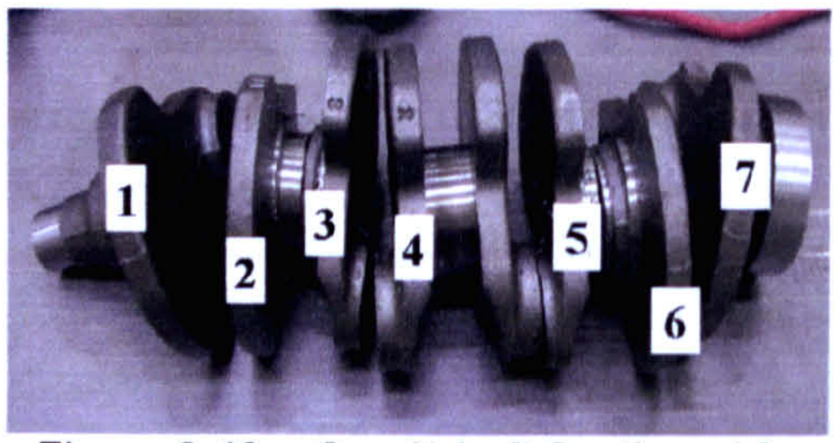

Figure 3.19 – Crankshaft Sectioned for Residual Stress Measurement

The next stage of this work was to carry out examinations of grinding wheel for wear and possible signs of breakdown as a result of the high loading associated with the HEDG regime. The examination itself was carried out by an abrasive grit manufacturer, Element 6. Optical microscopy was used to inspect the wheel surface, the wheels being mounted under a microscope with a camera system attached. To increase the reliability of the visual interpretation a montage technique was employed to ensure images had a good depth of field. This was carried out on both edges and the centre of each wheel as illustrated in Figure 3.20. The wheel edges related to the grinding of the crankshaft web feature – high Q'_w long path grind, whereas the wheel centre corresponded to the journal feature – lower Q'_w short path.

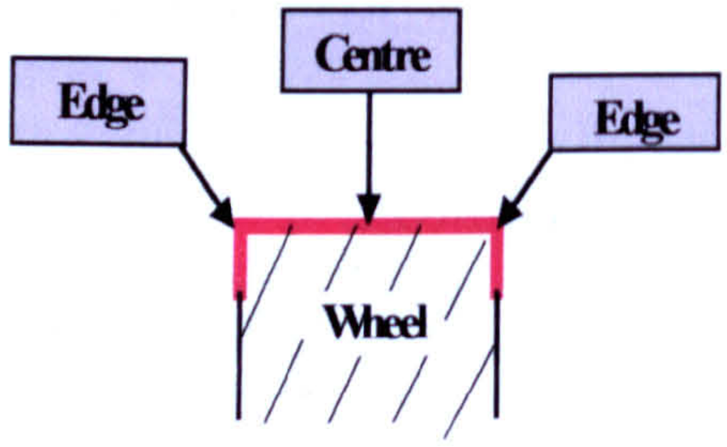

Figure 3.20 – Positions for Grit Wear Analysis

The degree of wear was divided into three different categories, new (sharp), micro-fracture or hole. In a new tool all grit particles start off as sharp grits, after performing some work they begin to wear by microfracture. Finally the grit particle is lost from the surface leaving a hole. This provided a defined level of wear for each abrasive grit, and cumulatively for each wheel and its features. Figure 2.10 shows examples of this classification on the left side together with the hypothetical wear progression versus grinding time for these definitions on the right side.

Every particle in the visible field of view was classified into one of the 3 categories, then the wheel was rotated and the process repeated until a total distance of 2cm had been covered. The wheel was then rotated 90 degrees and the technique repeated. Once this had been done for the three wheel locations the results were tabulated in order to formulate an assessment of the wheel condition.

Finally using the grinding rates established above estimations were made for the grinding times achievable with the HEDG process, these were compared against current values.

The second stage of these grinding trials took the research the final step to the production of full form crankshaft components. This provided an opportunity to fully validate the *HEDG* process in a production environment with real components. The photograph on the left-hand side in Figure 3.21 shows a fully ground crankshaft, and the right-hand image shows an enlargement of the main bearing diameter. As can be seen in the case of a fully ground component there are typically undercuts at the interface between the diameter and side face features. The function of these undercuts is to eliminate stress concentration that would be caused by a sharp corner.

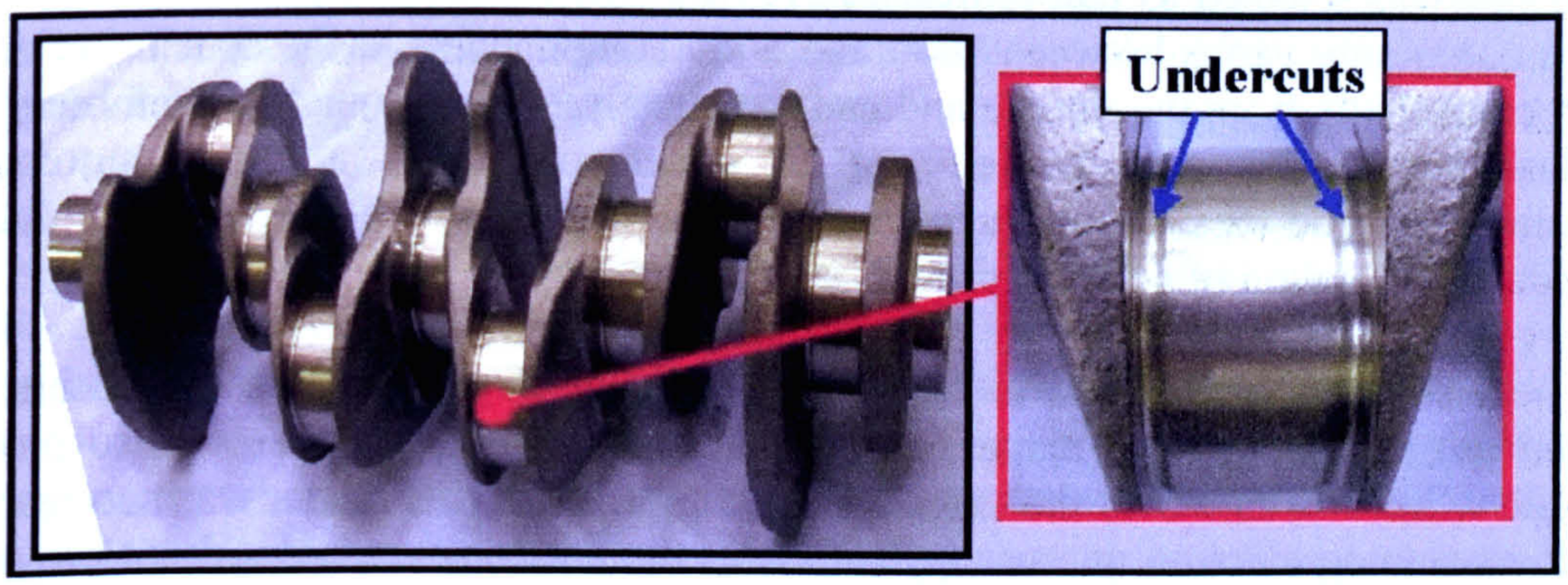

Figure 3.21 – Fully Ground Crankshaft

These undercuts require the addition of a lip feature on the edge of the grinding wheel as can be seen in Figure 3.22. The addition of this feature can lead to coolant application issues resulting in additional thermal loading in the component surface, which can in turn introduce tensile residual stresses. Another consideration is that wheel wear may well be affected with increased wear levels around the lip area.

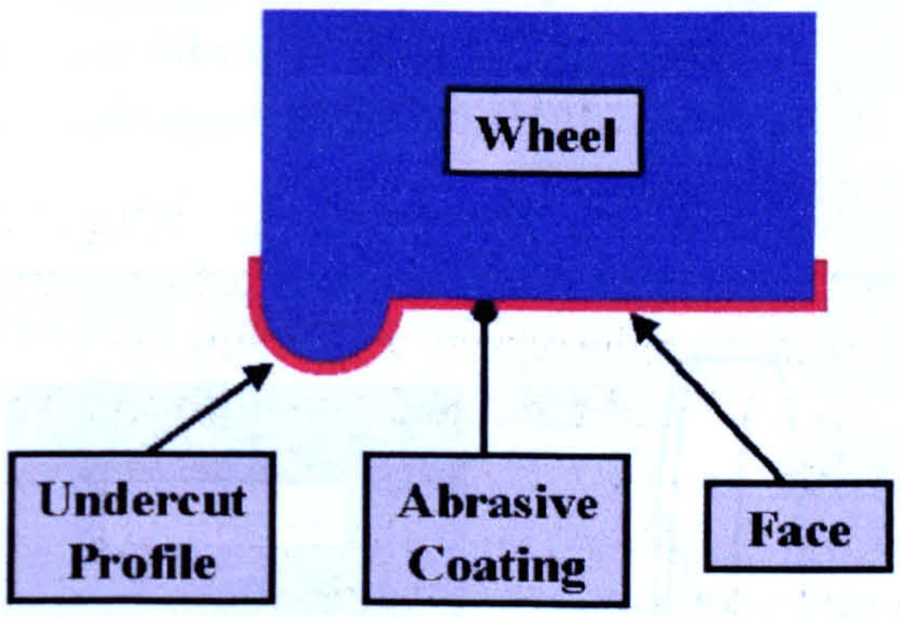

Figure 3.22 – Grinding Wheel Profile

There were two series of trials carried out. In the initial set 70 components were ground the initial 45 at Q'_w rates of $1000mm^3/mm.s$ for the web feature and $250mm^3/mm.s$ for the main and journals. Two smaller batches were ground at slightly reduced rates. All the rates used are given in Table 3.8. Power data was monitored and residual stress measurements carried out on a crankshaft from each batch.

Crankshaft No.	Q'_w ($mm^3/mm.s$)	
	Web	Journal
1-45	1000	200
46-55	500	200
56-65	250	200

Table 3.8 - Table of Removal Rates used for Crankshafts

The second set, a batch of approximately 950 crankshafts were ground at Q'_w rates of $250mm^3/mm.s$ for the web feature and $200mm^3/mm.s$ for the main and journals. The batch size was selected as that representative of a typical wheel life for rough grinding which commonly varies between 1000 and 2000 components. At the conclusion of the batch crankshafts from the middle and end were analysed for geometric conformity and residual stress, this was carried out in conjunction with a major automotive manufacturer. The mean power trend was compiled from spindle power cycle data to provide an indication of both the process stability and wheel wear.

The next stage as before was to carry out a full wheel grit analysis, again this was carried out by the abrasive manufacturer Element Six. The objective was to provide realistic wheel life data over the extended grinding trial. In this case it was necessary to employ scanning electron microscopy (*SEM*) as the previous method did not provide a sufficient depth of field, required for the lip form on the grinding wheel. Sample size constraints, placed by the use of a *SEM* to carry out the measurements, required removing sections from the periphery of the grinding wheel. It was planned to take two sections from each the left and right-hand grinding wheels. Before the sectioning of the wheels dimensional measurements of each wheel were carried out using a co-ordinate measuring machine (*CMM*), the aim to establish the magnitude of concentricity for the wheel periphery to the location bore. This is turn would enable an informed choice of sample position for the grit analysis. The segments taken were approximately 50mm long and 16mm wide. Each segment was divided into two areas for analysis, the middle and the lip as illustrated in Figure 3.23. Using a *x50* magnification 16 *SEM* images were taken along the length of each segment.

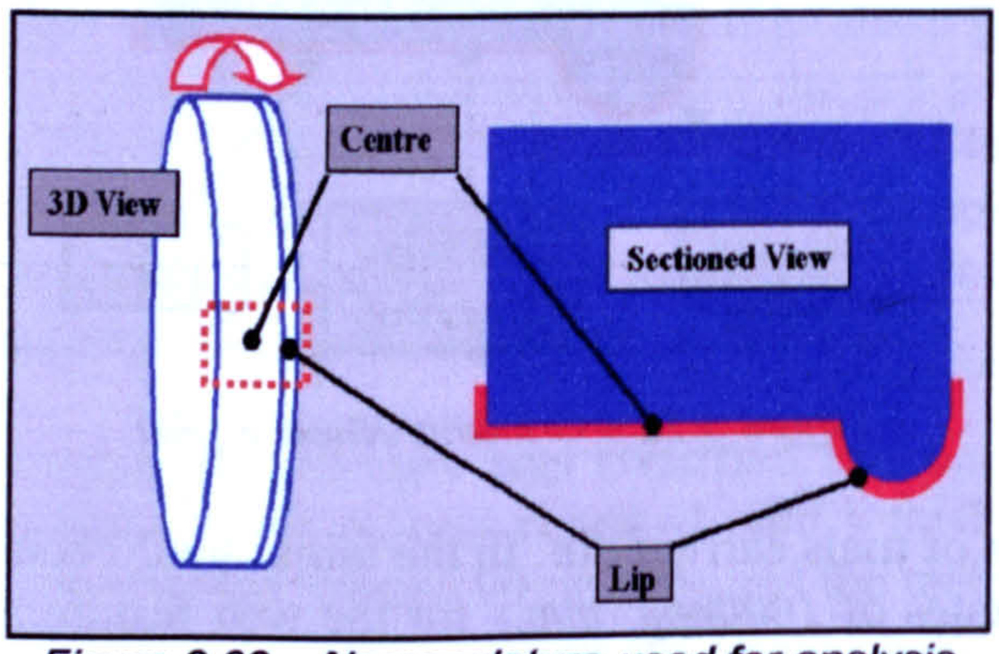

Figure 3.23 – Nomenclature used for analysis of grinding wheel segments

The *CBN* abrasive grit was classified into three types as before – new (sharp), working (microfractured) or hole and the data tabulated for consideration.

Finally cycle times for the *HEDG* process were compared with those being used currently on production machinery for the rough grinding of automotive crankshafts.

3.2.2 Superfinish Regime

As with the *HEDG* trials the initial tests were carried out in a surface grind mode with subsequent work using a cylindrical plunge-grinding mode. Prior to the full program of trials benchmark tests were carried out on the *LT1* production machine with a vitreous wheel, the same as that selected for the program of work. The surface and first cylindrical grinding trials were carried out on the Edgetek machine tool at *CU* and following that the final cylindrical trials on a production camshaft grinding machine tool, the *LT1* at Landis Lund in Yorkshire.

3.2.2.1 Benchmark Trials

The benchmark trials were carried out in a cylindrical plunge grind mode. The aim was to effectively gauge the performance of subsequent grinding trials with the improved truing techniques and modified path motions. A number of tests were carried out in a standard setup using the selected wheel. The wheel was a 46µm grit *CBN* grit vitreous bond grinding wheel with the same specification as that intended for use in the full trials. The standard dresser wheel and spindle are shown on the left and right in Figure 3.24, the dresser was a B&T unit onto which a single layer dresser wheel is mounted. The grinding parameters are given in Table 3.9.

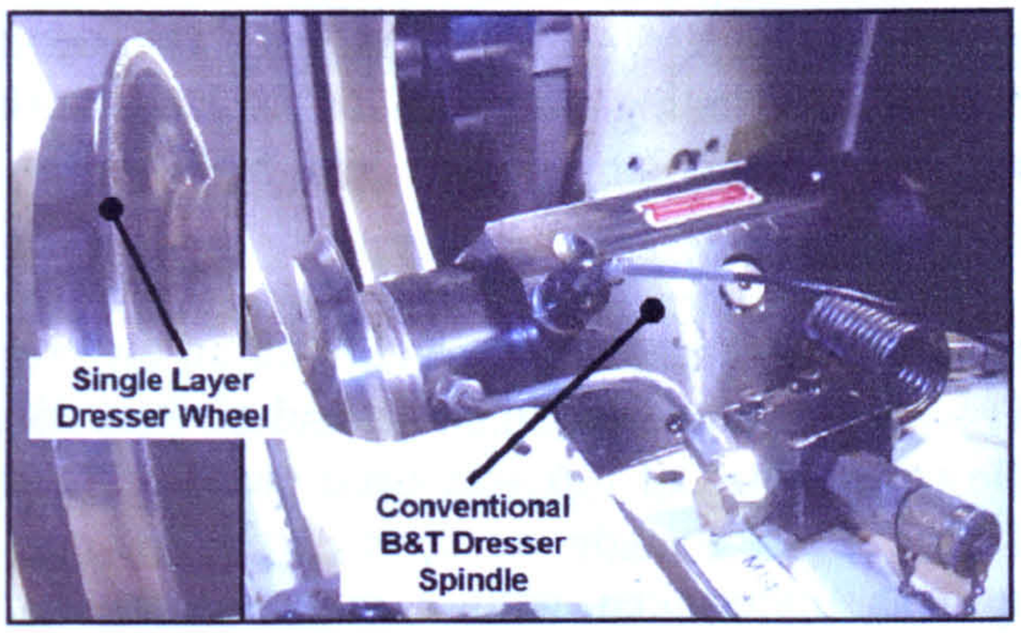

Figure 3.24 – Conventional LT1 Dresser Wheel & Spindle

Parameters		Values
Oscillation	Rate	0,1,2,5 Hz
	Amplitude	0, 0.04mm
Depth of Cut		10 µm
Feedrate		0.002mm/s
Workpiece Speed		2rpm
Grinding Wheel Speed		60m/s

Table 3.9 - Parameters for Benchmark Cylindrical Plunge Grinding Trials

3.2.2.2 Surface Grinding

The grinding arrangement utilised was the same as that for the surface grinding *HEDG* trials, and is shown below in Figure 3.25. Samples were held in a machine vice bolted onto the Kistler dynamometer, which in turn was bolted to the machine.

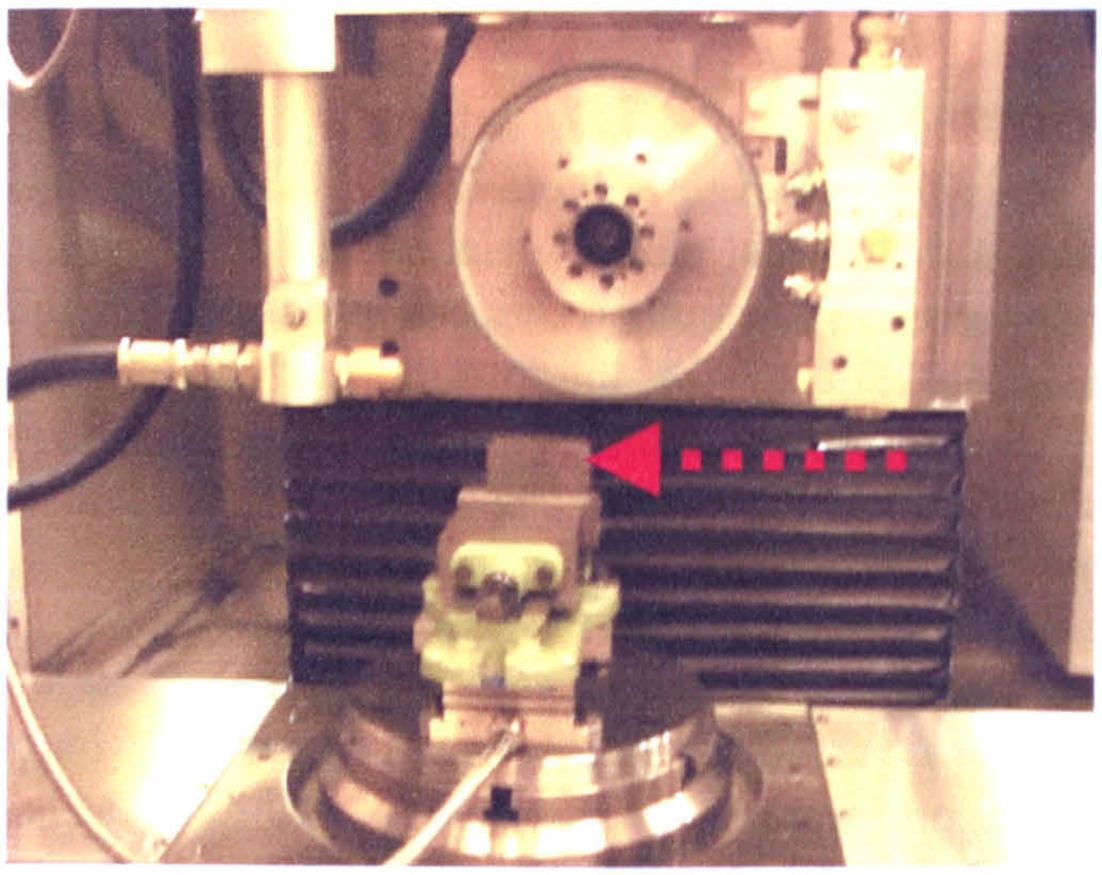

Figure 3.25 – Superfinish Surface Grinding Set-up

The target for the surface finish was $0.1\mu m$ R_a and therefore a $46\mu m$ CBN grit wheel was selected based on manufacturer's recommendations. Two different CBN wheel bond types were evaluated, vitreous and resin - the wheels were designated WS1 & WS2 respectively. Both wheels required in-situ truing on the spindle to achieve the level of wheel runout required for high precision grinding. The demands on the coolant configuration for this type of grinding over that of *HEDG* is greatly reduced and so flow-rates of 45 *l/min* for the coolant nozzle and 5 *l/min* for the grinding wheel scrubbers were used.

The vitreous bond grinding wheel was crush trued with an electroplated *D301 N 200G* ($300\mu m$ diamond grit) wheel mounted on an additional air bearing spindle, as shown in Figure 3.26. A spindle speed ratio of *0.6* was used (with both surface running in the same direction) and five passes made at $5\mu m$ depth of cut with a feedrate of *200mm/min.* Dressing was undertaken with a conventional stick. Both truing and dressing operations were carried out with coolant applied.

The resin bonded grinding wheel was trued and dressed by a brake dresser fitted with a silicon carbide wheel without coolant. The set-up is shown in Figure 3.27. Ten passes with a $10\mu m$ depth of cut at *150mm/min* were taken. Dressing was undertaken with a conventional stick.

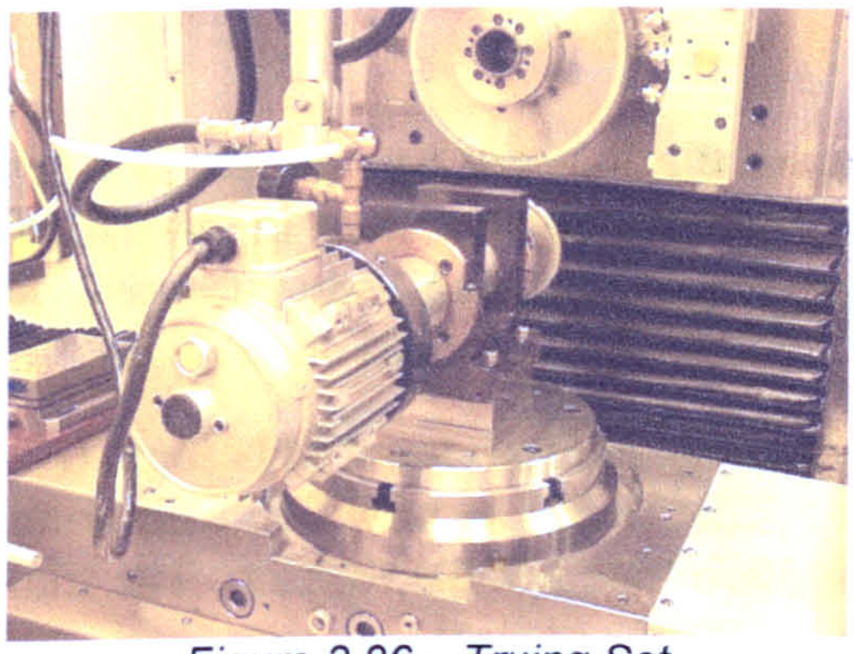

Figure 3.26 – Truing Set up for Vitrified Wheel

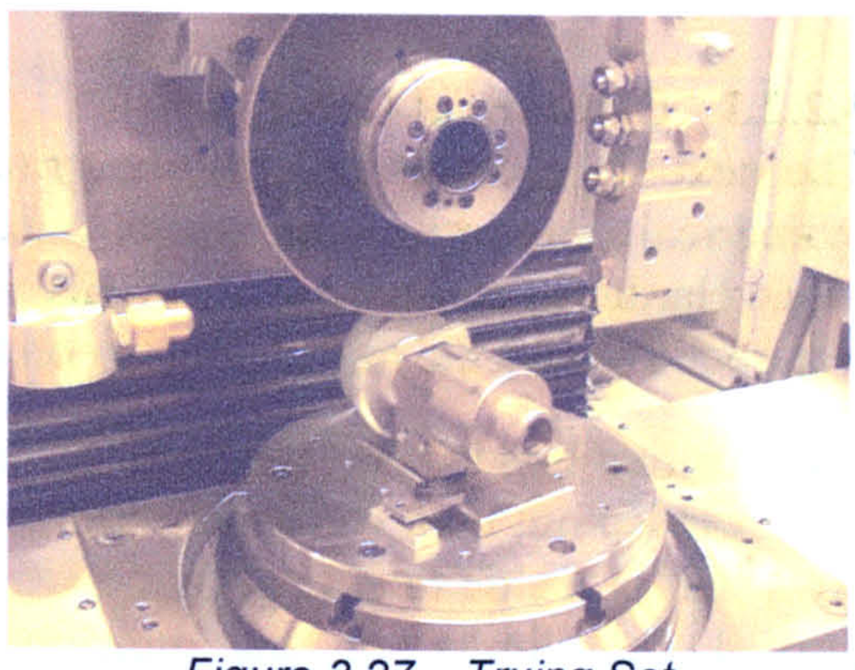

Figure 3.27 – Truing Set up for Resin Wheel

Prior to the required grinding test a light surface cut was taken to establish touch, followed by a sparkout grind during which power and force levels were monitored. The grinding test parameters are detailed in Table 3.10

Parameters		**Values**
Specific Removal Rate	Q'_w	*0.025-2mm^3 /mm.s*
Depth of Cut	*A*	*5-20 µm*
Feedrate	V_w	*5-100mm/s*
Grit Size	-	*46µm*
Vitreous Wheel Speed	V_s	*60-120m/s*
Resin Wheel Speed	V_s	*42-60m/s*

Table 3.10 - Parameters for Surface Grind Superfinish Trials

As previously discussed an improvement in grinding performance should be possible by the application of an oscillatory motion to the grinding path. At this stage the full requirements to achieve this on the machine are not yet in place. However as a test to demonstrate the principle in part the sample was turned through 90 degrees and the grind path modified to that shown in Figure 3.28. This reproduced the effect of an oscillatory pass without the forward path motion and it also acted as a demonstration of the machine's grinding performance.

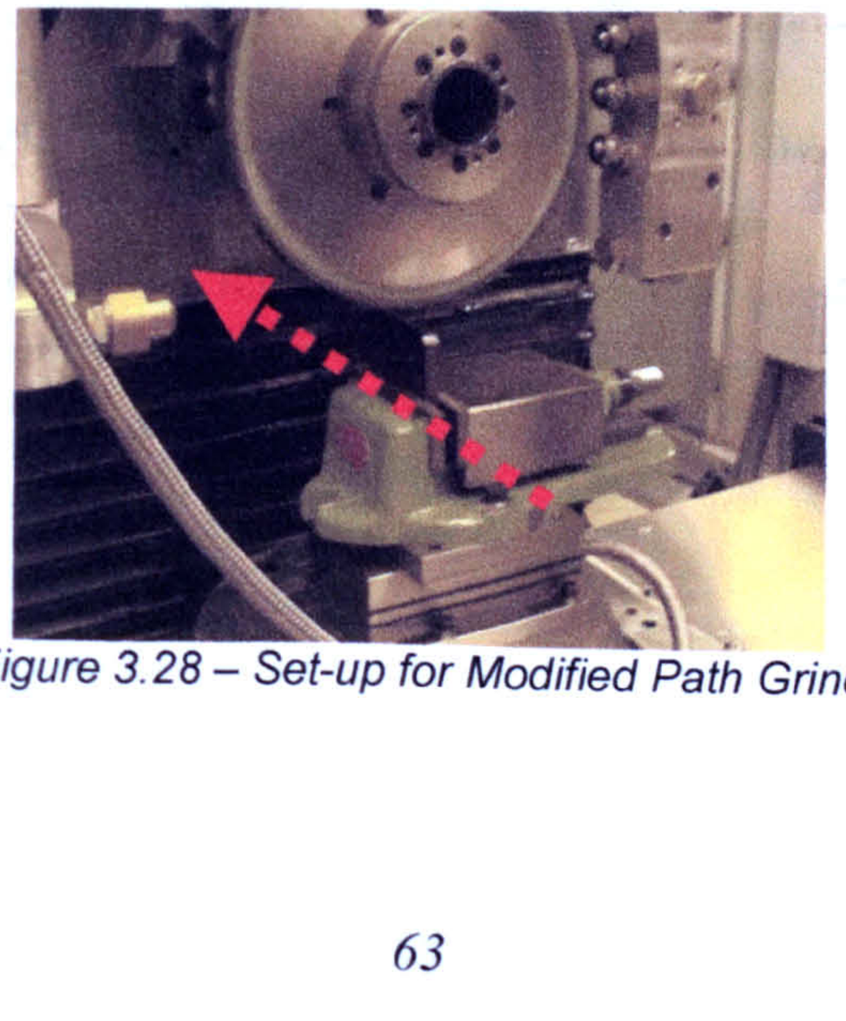

Figure 3.28 – Set-up for Modified Path Grind

3.2.2.3 Cylindrical Grinding

The next stage of the Superfinish grinding trials on the Edgetek was carried out in a cylindrical grinding mode, which once again was similar to that used in the *HEDG* trials. Hardened components – 48HRC - representative of crankshaft features were used. Figure 3.6 shows the machine setup on the left and the component used on the right.

The vitrified bonded B46 grinding wheel was used, this was crush trued as before. Tests were carried out both with and without a modified path grind. The modified path grinds consisted of a side to side grinding wheel motion during the spindle rotation. The trials pushed the limits of the machines standard CNC control system with the implementation of the oscillatory motion. The maximum rate of oscillation proved to be 720 cycles/revolution, which equates to a 0.5° revolution of the workpiece for each oscillation. This would not be a limitation on the Landis Lund production machine intended for the application of this development. The grinding parameters used for the tests are given below in Table 3.11

Parameters	***Values***
Amplitude of Oscillation	*0.5 mm*
Depth of Cut	*10-20 µm*
Feedrate	*64-240mm/min*
Grinding Wheel	*CBN Vitrified Bond*
Grit Size	*46µm*

Table 3.11 - Parameters for Cylindrical Superfinish Grinding Trials

3.2.2.4 LT1 Production Cylindrical Grinding

The final phase of the trials was carried out on a modified LT1 cam and crankshaft grinding machine tool, a typical machine is shown in Figure 3.3. Modifications made to the machine tool included the introduction of prototype axis control software to enable the modified path oscillatory motion, and the wheel truing/dressing system.

The axis oscillation software was implemented into the machines system program. The software output produced a square position demand superimposed on the existing axis demand. Both the frequency and magnitude of the square wave were selectable. The modified path input was selectable from within the machine part program. This was set to introduce the function during the final finish grind step of 10µm.

For the truing and dressing operations a Wendt Boart dresser spindle designed specifically such operations was fitted together with a peripheral metal bonded truing wheel. A photograph of the spindle and wheel together with their specifications are produced in Figure 3.29.

Figure 3.29 – Wendt Boart Dresser Spindle and Table of Wheel Specifications

Initial tests established that the standard machine touch sensor unit did not offer sufficient sensitivity to pick up touch for the truing operation. The probable reason for this being a combination of two factors. The first relating to the use of a small grit size grinding wheel resulting in lower touch forces. Secondly the unit was located on the grinding wheel spindle unit and therefore with the higher inertia of this wheel to that of the truing wheel the system became less sensitive. Therefore a sensing setup was attached to the dresser spindle and wired into the machine. The setup was as shown in Figure 3.30, and comprises an accelerometer attached to a HP analyser. This system was successful in detecting touch of the truing wheel and was used through the trials to control the grinding wheel truing process. Steel bar material (specification 38MnSiVS6) hardened to 48HRC was used for all the trials, a typical setup for the machine is shown in Figure 3.31

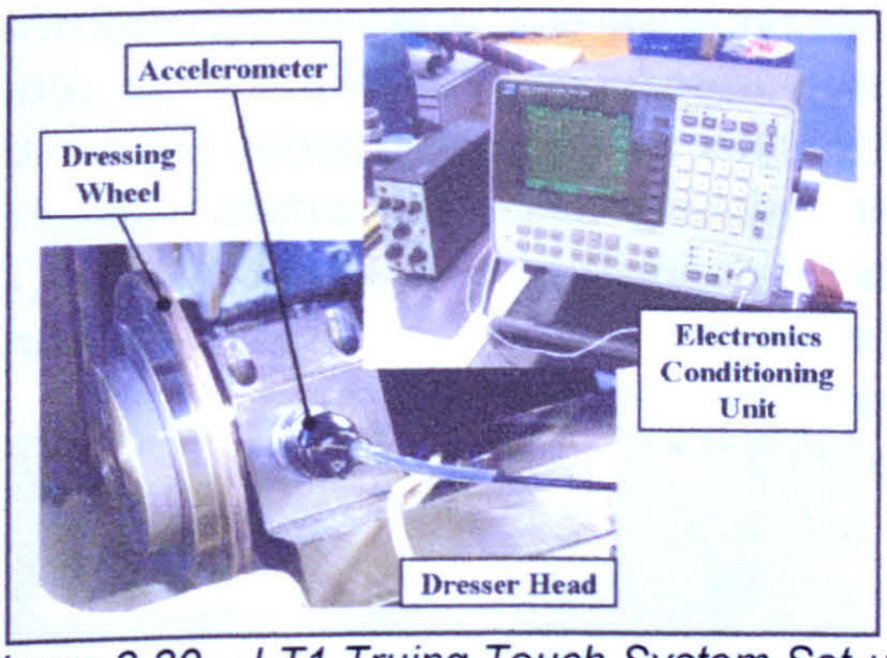

Figure 3.30 – LT1 Truing Touch System Set-up

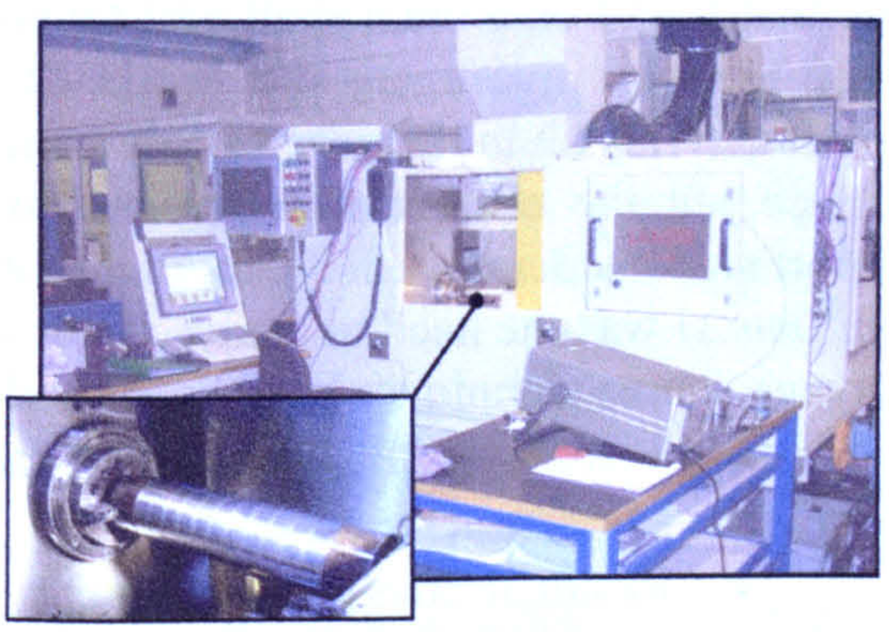

Figure 3.31 – Component located in LT1 for Grinding Trials

With the dresser modifications made two sets of trials were carried out. In the first set tests were first carried out in a standard cylindrical plunge mode with increasing values of feedrate, these covered a Q'_w range from *1* to *12mm³/mm.s*. Grinding parameters are given in Table 3.12. A 0.6 ratio crush operation was used.

Parameters	Values
Depth of Cut	50 µm
Feedrate	0.005 – 0.048mm/s
Workpiece Speed	2rpm
Grinding Wheel Speed	60m/s

Table 3.12 - Parameters for Standard Cylindrical Plunge Grinding Trials

The next stage was to introduce an oscillatory side to side motion of the grinding wheel axis during the plunge operation. Frequencies used were 1,2 and 5Hz with magnitudes of 0.08, 0.25 and 0.5mm. As before a 0.6 ratio crush operation was used, and the quality of the surface finish was monitored. A summary of the grinding parameters employed in these trials is given below in Table 3.13

Parameters	***Values***
Oscillation Rate	*0,1,2,5 Hz*
Amplitude	*0, 0.04, 0.25, 0.5mm*
Depth of Cut	*10 µm*
Feedrate	*0.002mm/s*
Workpiece Speed	*2rpm*
Grinding Wheel Speed	*60m/s*

Table 3.13 - Parameters for Modified Path Oscillatory Grinding Trials

3.3 Methods of Surface & Sub Surface Characterization

A number of different approaches were used to investigate the surface integrity; these included methods for both the surface profile and near surface structure. The surface profile measurements were aimed at assessing the surface finishes produced and were utilised primarily in the analysis of the *Superfinish* grinding trials. In finishing operations the surface texture is important to the component's functionality and such effects as grinding lay will have an influence on the performance as a bearing surface like that found on a crankshaft and camshaft. The near surface structure measurements were used to investigate the levels of damage introduced primarily by the rough grinding (*HEDG*) in the near surface zone. As it is not a finishing operation it is not the surface but the near surface region left after finishing that is important. Hence an important consideration in attempting to increase the specific material removal rate *(Q'_w $mm^3/mm.s$)* was the need to analyse both the surface and near surface region for thermal damage. Three techniques have been used to carry out this function namely:

- Visual inspection of ground surface
- Microstructural examination
- Residual Stress Measurement

3.3.1 Surface Finish

Surface finish measurements of samples were carried out initially using a *RTH Form Talysurf* and subsequently for the higher quality surface with a *Wyko Topo-3D Surface Profiler* and *Wyko RST,* the latter two instruments having a similar level of performance. All instruments were located on site at Cranfield Precision on the Cranfield University Campus

The *RTH Form Talysurf* is a profile contact displacement instrument capable of form, waviness and roughness measurements. The instrument consists of

- A traverse unit used to trace the stylus across the sample surface. It houses a laser interferometric transducer together with motor and gearbox. A straightness datum is incorporated into the unit enabling measurements of up to *120mm* long to be made without reference to any external datum.
- A contact stylus, there are a number of different lengths and tip radii available

- A granite base onto which a support arm is mounted with a ballscrew to position the traverse unit vertically ready for measurements
- An electronic interface unit with joystick. The joystick carries out the vertical positioning of the traverse unit and horizontal positioning of the stylus
- A PC with software to drive the instrument and analyze data produced

The measurement range is dependent on the stylus length; a *60mm* stylus gives a range of *6mm* whereas a *120mm* stylus gives a *12mm* range. The application of the skidless pickup technology is what enables the instrument to carry out form measurements in addition to purely surface finish. For the work carried out in this project the instrument was used to quantify the surface finish of samples. The instruments measurement capability and error level is dependent on the stylus tip radius used. There are a number of different styli available with radii from *50μm* down to *2μm*. For surface finish measurements a small tip radius is advantageous, a *5μm* tip radius used to measure an R_a of *0.5μm* could be expected to have errors of only *2%* error (Dagnall, 1997). Whereas a *2μm* radius tip at measurements of *40nm* R_a could have errors up to *30%*. For this reason use of the Talysurf was limited to values down to the region of *40nm* R_a below this point measurements were made with the other instruments described. As measurements made were used on a comparative basis actual errors were in fact far smaller than the figures quoted. Figure 3.32 shows a photograph of the instrument.

Readings are taken by simply placing the component onto the granite table with the measurement orientation required in line with the travel of the transverse unit. The stylus is then positioned and measurement parameters selected from dropdown menus on the PC. The measurement parameters were length, sample length, number of samples. Surface roughness output parameters selected for these trials were R_a, R_q, and R_t. Results were displayed via the PC, a typical output profile from the instrument is shown in Figure 3.33

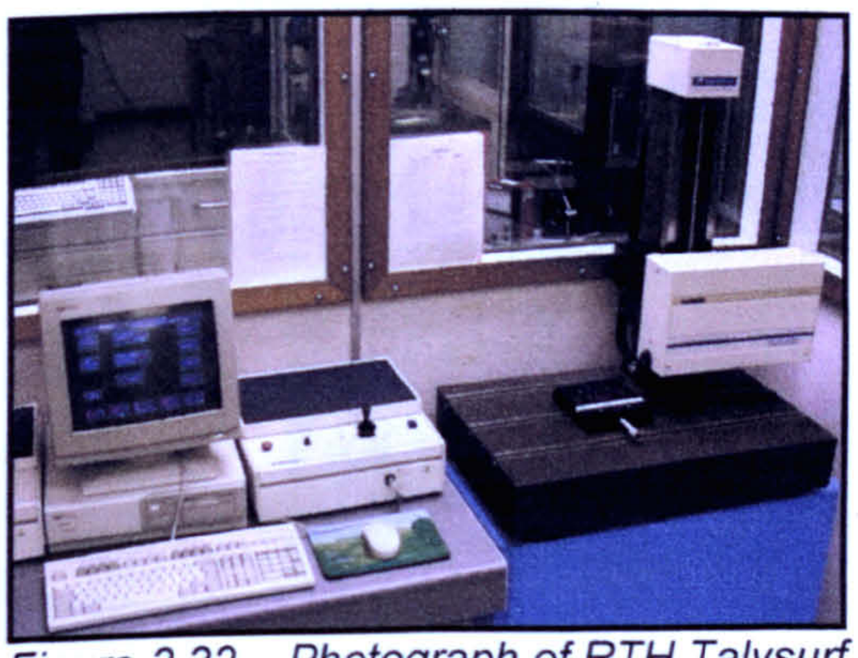

Figure 3.32 – Photograph of RTH Talysurf

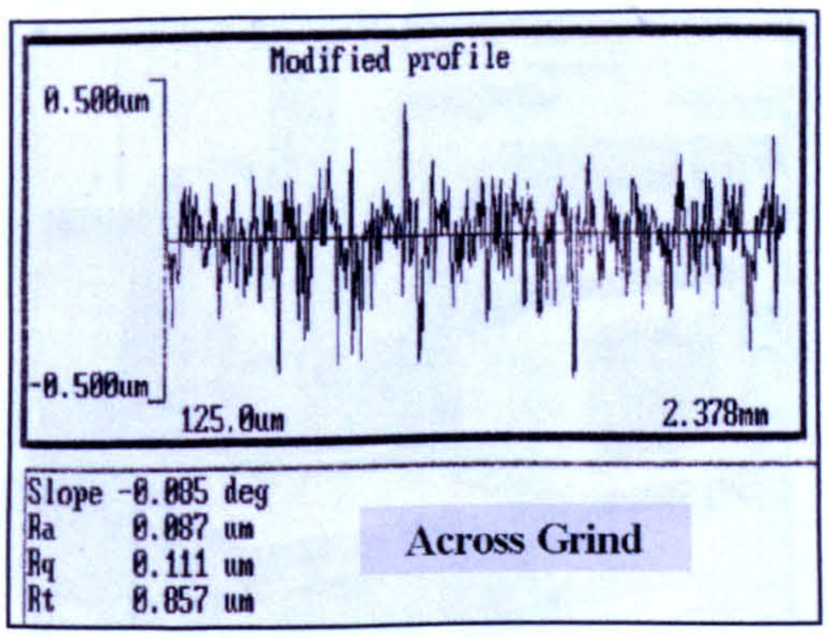

Figure 3.33 – Typical output from RTH Form Talysurf

The *RTH Form Talysurf* was used to measure surface finish on the *HEDG* samples to monitor the grinding wheel performance under the extreme conditions in which there is a probability of grit breakdown due to thermal shock. With the Superfinish work the instrument was used to initially measure the surface finishes produced.

The *Wyko Topo-3D Surface Profiler* determines surface profile by digital phase shifting interferrometry. The interferometer is located in the magnification head and produces

fringes by combining a beam of light reflected off the sample with a beam of light reflected off an internal reference surface. Multiple frames (5 sets) of data are created by translation of the reference mirror within the head using piezo actuators. This precisely alters the optical path through a complete wavelength enabling the instrument to resolve the data between the initial fringe pattern lines. The magnification head is fitted with a Linnik optic that allows measurements to be made at a long working distance. The magnification of this unit is *x40* which equates to a measurement area of *250μm by 250μm.* The interferometer has sub-nanometre resolution, which enables the instrument to reach R_a values down to *1-2nm.* The remainder of the instrument comprises…

- A microscope stand for supporting the various parts of the instrument
- A support arm for holding the magnification head together with trinocular head and illuminator
- Motorized Z axis stage to raise and lower the support arm operated by a joystick
- A tilt/tip stage for adjusting the sample tilt
- A white light illuminator
- A trinocular head with eyepiece and camera for viewing and analyzing fringes
- High voltage driver for piezo actuators
- A PC with piezo driver and fringe analysis software

A photograph of the instrument is shown in Figure 3.34. To take readings the sample is placed on the tilt/tip table below the microscope objective. This is then positioned to provide a minimum of three fringes Measurement options are selected using the software menus, the measurement is then carried automatically and the results displayed on the PC screen. The *Wyko Topo-3D Surface Profiler* was used solely for the Superfinish samples produced, with the plane surface measurement capability the instrument could accurately monitor grinding directionality primarily in the form of grinding lay as demonstrated in Figure 3.35

Figure 3.34 – Photograph of Wyko Topo-3D Surface Profiler

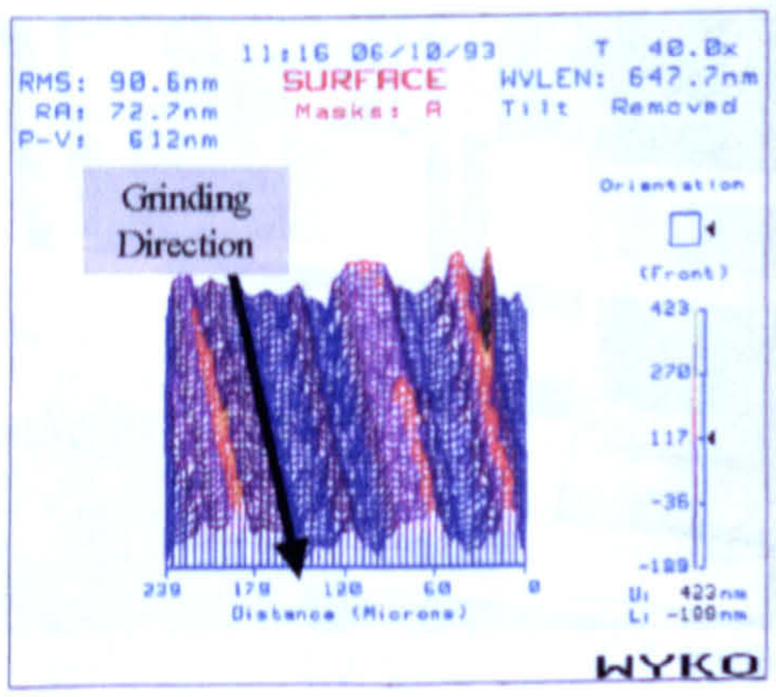

Figure 3.35 – Wyko Topo Profile Demonstrating Instrument Capability

The *Wyko RST* is similar in construction and performance to the *Wyko Topo 3D* instrument. It is a highly sensitive interferrometric microscope with the interferometer built into the objective. The objective is mounted onto a flexure, which is in turn translated by a piezo actuator. This motion enables the instrument to resolve across the

fringes. The difference to the previous instrument being that the reference mirror as opposed to the optic is translated. The flexure enables an enhanced range of measurement of up to $10\mu m$. The remainder of the instrument comprises…

- A microscope stand for supporting the various parts of the instrument
- A support arm for holding the objective/flexure assembly and the illuminator
- Manuel Z axis stage to raise and lower the support arm to focus instrument
- A tilt/tip stage for adjusting the sample tilt
- A white light illuminator
- A camera for viewing and analyzing fringes
- High voltage driver for piezo actuator
- A PC with piezo driver and fringe analysis software

A photograph of the instrument is shown below in Figure 3.36. To take readings the sample is placed on the tilt/tip table and the microscope object brought into focus and a fringe pattern obtained. As with the previous instrument the measurement and output options are selected on the software and readings taken automatically. The *Wyko RST Surface Profiler* was again used for the Superfinish samples produced, and as stated had a similar capability making it interchangeable with the Topo 3D for the initial flat surface ground sample surfaces produced. Where the RST differed is with an enhanced range of measurement – up to $10\mu m$ – it was suitable for the measurement of curved surfaces such as those produced by cylindrical grinding where it was able to maintain focus across the whole field of view for the sample. A typical instrument output is shown in Figure 3.37

Figure 3.36 – Photograph of Wyko RST Surface Profiler

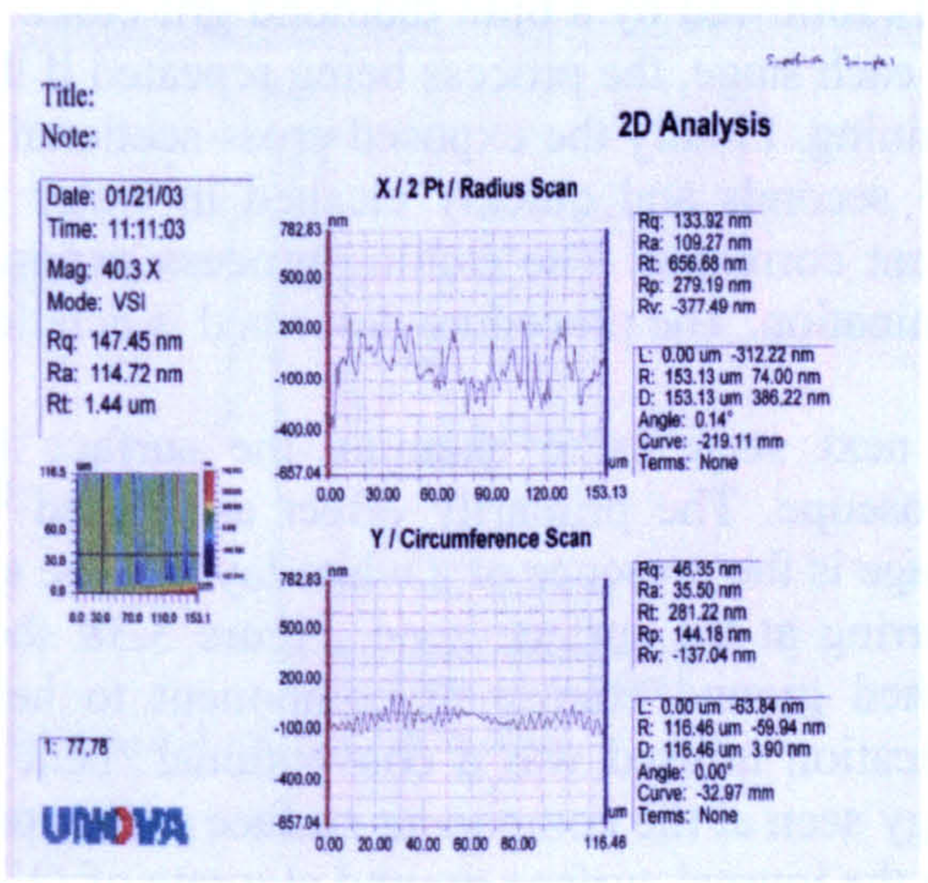

Figure 3.37 – Wyko RST Profile Demonstrating Instrument Capability

3.3.2 Visual

Thermal damage as a result of grinding is traditionally identified by the presence of grinding burn which appears as a bluish temper colour on the ground surface: a result of oxidation. This can be visually identified and categorized according to the degree of discolouration. The degree of colouration can be difficult to interpret at the initial stages of damage and in some cases may instead be a result of coolant burn out on the

component surface. Also evidence of discolouration can be removed by the following process interactions such as spark-out, but without the removal of the associated damage.

Surface ground samples were carefully inspected for signs of discolouration, where this was evident follow up analysis techniques were employed to confirm or disprove the interpretation.

3.3.3 Microstructural

The micro-structural approach used two techniques. The first was to microscopically examine a cross-section of the ground sample for damage, seen in the form of visual alterations to the near surface material microstructure. The second was to carry out a micro-hardness profile of the cross-section, which would identify the level, and depth of structural changes

Preparation of the sample was the same for both techniques. The first task was to produce a cross-section of the area of interest. In the case of the rough ground samples which were unhardened this was simply a case of sawing and filing, however for the superfinished samples which had been hardened to 48HRC it was necessary to section by wire EDM. The samples were then mounted ready for polishing, this was carried out by potting the samples in a filled phenolic resin agent using a heated press tool. Samples were then mounted in a plate fixture for polishing; a force of 5lbs/sample was applied for a period of 3mins. This was carried out with 120, 220 and 1200 silicon carbide papers followed by a 6μm diamond grit cloth. The samples were cleaned and inspected after each stage, the process being repeated if there was any evidence of deep scratching remaining. Finally the exposed cross-sectional surface was etched with a 3% nital acid for 5 seconds and quickly cleaned in water to remove the acid and then alcohol to prevent corrosion. The etching process exposes the grain boundaries ready for visual examination. The procedure described is detailed by Higgins (1973).

The next stage is to examine the surface for signs of structural change using a microscope. The primarily effect associated with high temperature thermal grinding damage is the presence of a white layer at the surface. This is a result of the rehardening occurring at the surface zone. Figure 3.38 shows two cross-sectional samples from a finished ground crankshaft component to help illustrate the technique. The coolant application utilised was a conventional 'bent pipe' coolant nozzle, hence the thermal energy seen at the component surface was expected to be high. The image on the left is from the journal surface ground at a rate of $Q'_w - 100mm^3/mm.s$, there is no evidence of microstructure change. The right-hand image is from the web face, here the removal rate was higher at $Q'_w - 250mm^3/mm.s$, it can be clearly seen that there is a white layer $65\mu m$ deep on the web feature, This made the component unacceptable to the customer.

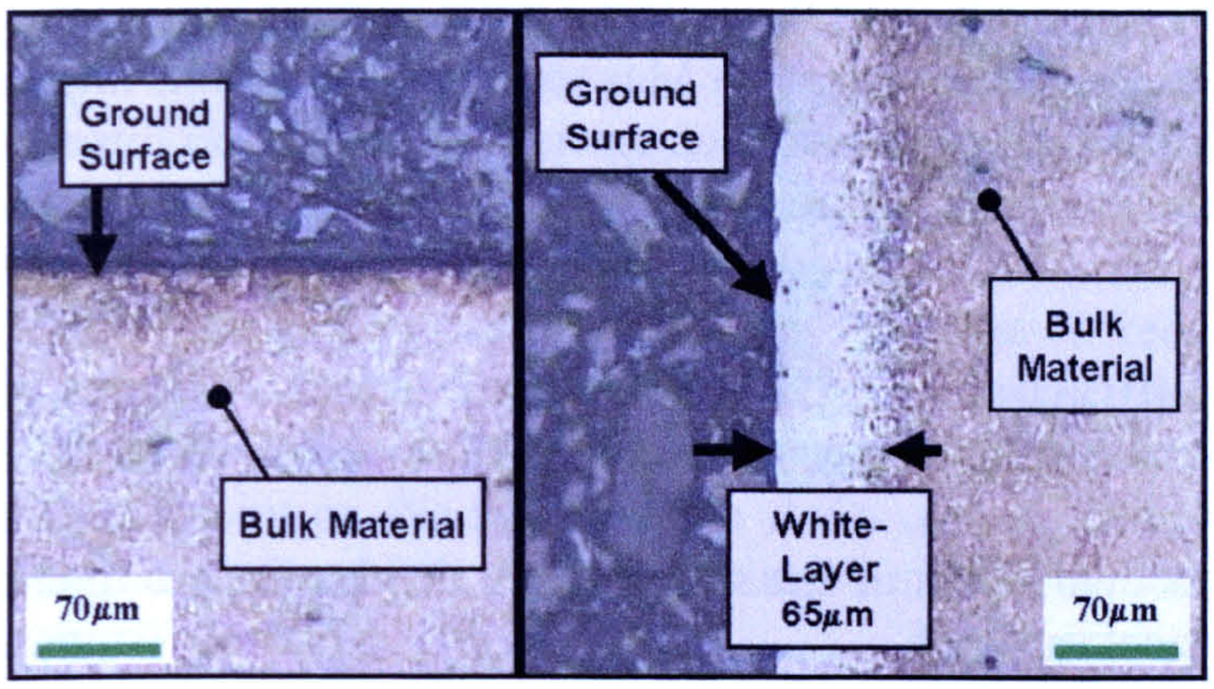

Figure 3.38 – Microstructural Images of the Cross-section of Damaged & Undamaged Crankshafts

The mounting and polishing preparation used for the microstructural analysis was the same as that required for the micro-hardness analysis. Therefore it was possible to directly transfer the samples over for this analysis once the microstructural observations had been completed. The micro-hardness analysis involved building a hardness profile for the near surface region generally down to depth of *300μm,* an example of which can be seen on the right in Figure 3.39. In this case a re-hardening peak has been illustrated such as would be typical for the right-hand microstructural image in Figure 3.38. Data points are built up from a number of micro-hardness readings taken at increasing distances down from the ground surface as illustrated by the sketch on the left-hand side in Figure 3.39.

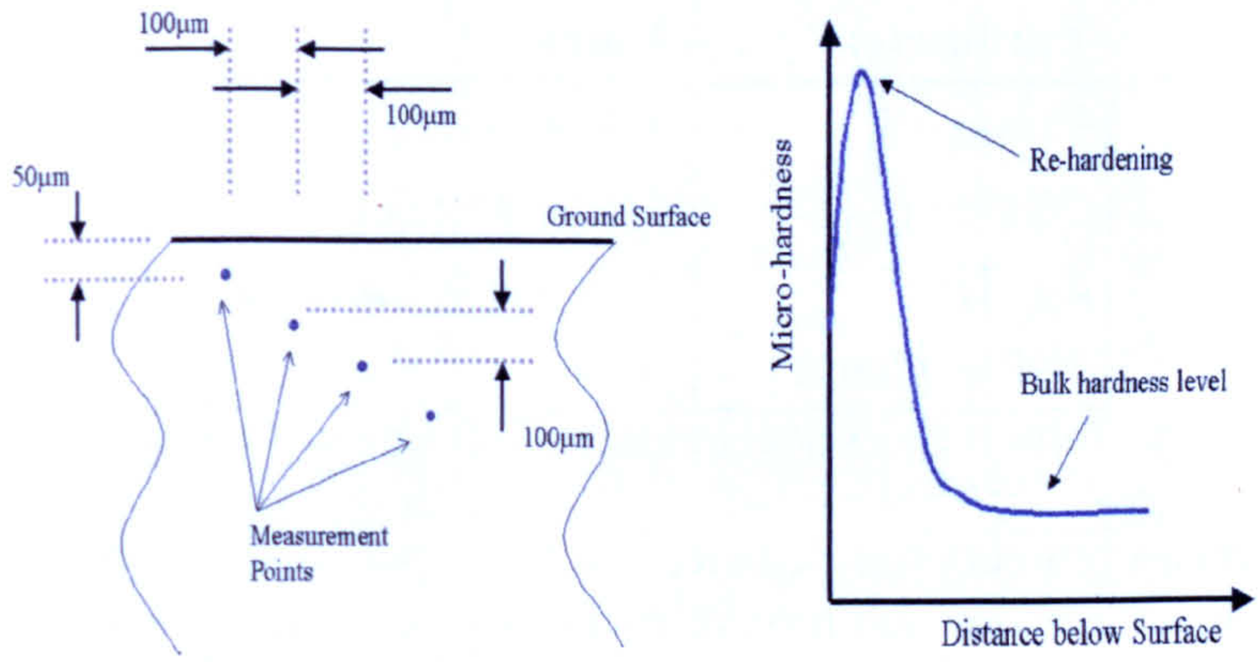

Figure 3.39 – Micro-hardness Analysis Technique

3.3.4 Residual Stress

The grinding process is accepted as inducing residual stresses into the surface region of the product, and as already stated can significantly affect the mechanical properties of the product. A compressive residual stress in the surface region is desirable for engineering components, however the effect of high thermal loading as a result of aggressive grinding can result in tensile residual stresses as discussed in Chapter 2.

There are a number of possible methods to investigate residual stress in the surface region of components, Table 2.9 show those listed by Fields et al (1972). For this work

two methods have been selected, the first the most well known and accepted is the X-Ray Diffraction method. The other is a Magneto-Absorption technique, which offers an in-process capability, less work has been carried out to date on this method, and so less is currently known about this technique.

3.3.4.1 X-Ray Diffraction

The *XRD* measurement technique gives an absolute value of stress. With XRD it is possible to determine:

- The residual stress of the surface, to a depth of approximately 10μm for the alloy steel samples.
- The stress gradient of the surface to a predetermined depth by successive analysis and layer removal stages.

The aim of using this technique was to establish a better understanding of the Barkhausen Noise intensity approach to enable further residual stress measurement work to be carried out primarily with this instrument and help with its introduction into the sponsoring Company - Landis Lund.

A few early measurements on surface HEDG samples were carried out on a instrument in the SIMS at Cranfield University in order to validate residual stress measurement obtained with the Barkhausen Noise intensity instrument. The *XRD* equipment had been modified for the measurement of residual stress as part of previous research programs. Parameters used for the analysis of the HEDG ground samples are given below in Table 3.14.

Parameter	**Values**
Power	30KW & 20mA
2θ	149 to 159 deg
Psi Tilt	10deg at 0.1 interval
X-Ray Count	6000

Table 3.14 - Parameters for XRD Measurements

All subsequent measurements were carried out by a specialist team who were located in the R&D division of a major automotive manufacturer. These measurement were used to validate residual stress findings in the crankshafts produced in the production environment.

Due to the size constraints of both the XRD unit it was not feasible to measure complete components, hence small samples were sectioned from the workpiece. Care was taken to ensure the size was sufficient to avoid any relaxation of the stresses in the near surface region by this operation. The working space constraint of the instrument meant that this technique was a destructive test.

3.3.4.2 Barkhausen Noise Intensity

The instrument works as a comparator and therefore requires calibration before use. The calibration is carried out by taking readings from both ground samples that are

undamaged and thermally damaged. There are two modes of operation *Rollscan* and *μscan*, the former uses fixed frequencies and filters providing measurements to a consistent depth commonly *20μm*. It allows a surface to be scanned over and a reading produced for the sample length. This enables ground surfaces to be inspected along the length of a grind, thus identifying changes such as the onset of grinding burn. The *μscan* allows a higher level of interaction with control over the range of frequencies and filters to be applied, the result is control over the depth of measurement penetration allowing surface gradients to be determined. It is aimed more as a research tool with readings being taken at a single point on the surface. The *Rollscan* mode has been selected for this work, this being the most widely selected for introduction into industrial application at this point in time.

A photograph of the instrument in a configuration suitable for measurements on camshaft lobes is shown below in Figure 3.40. The main system components are the signal generation and processing unit (*BN* Unit) this provides the magnetic signal to the sensor head which is in contact with the sample, the unit processes the return signal which is detected by sensitive coils in the sensor head. The strength of the return signal is displayed in units of magnetic power (*MP*). A fixture may be used as in the case illustrated here to hold and rotate the sample, additionally a computer with Stresstech's *Viewscan* software may be linked to the *BN* unit to improve data processing.

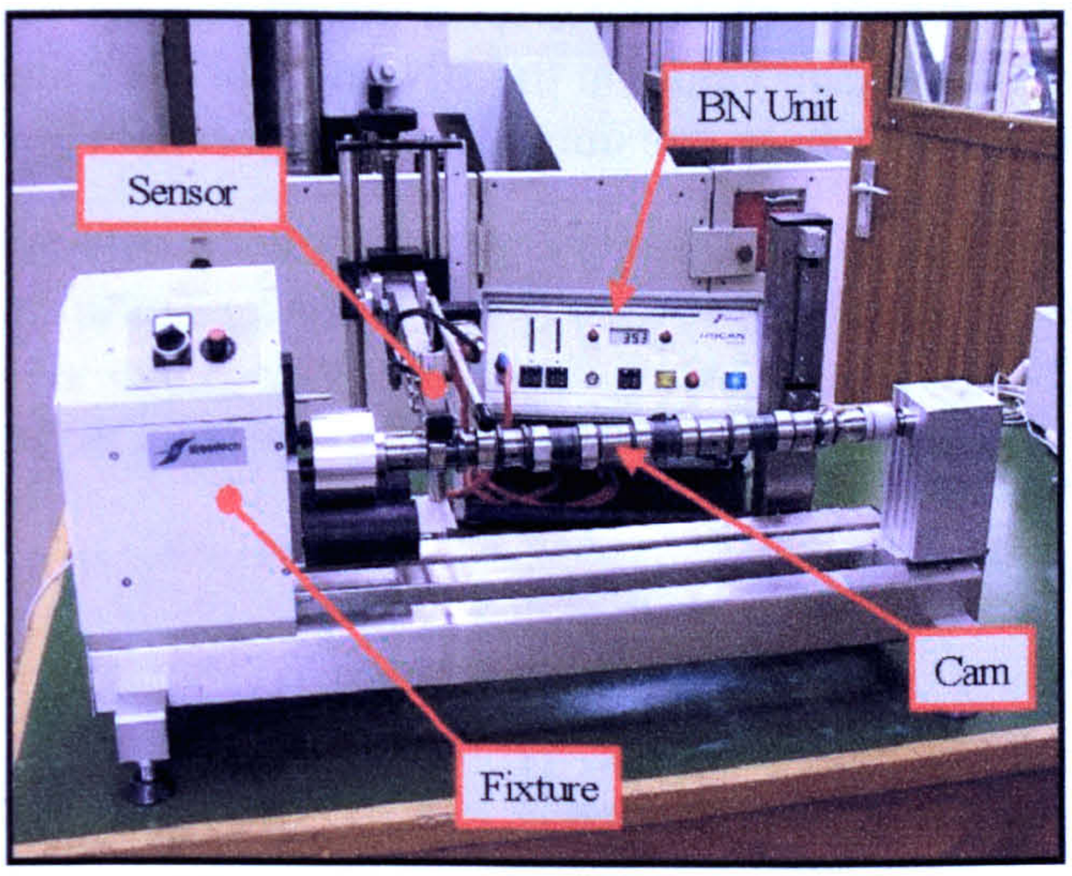

Figure 3.40 – Photograph of Stresstech Barkhausen Noise Intensity Gauge

There are a number of different sensor types available which give a greater flexibility to the instrument and these allow bearing, camshaft and crankshafts amongst others to be analysed. For the work carried out here a flat sensor for surface ground samples and a cylindrical sensor for the curved surfaces associated with the crankshaft samples were used. In addition some preliminary work has been done as a familiarization exercise, this was carried out on camshafts for which a camshaft sensor was used. Both the cylindrical and camshaft sensors are shown in Figure 3.41.

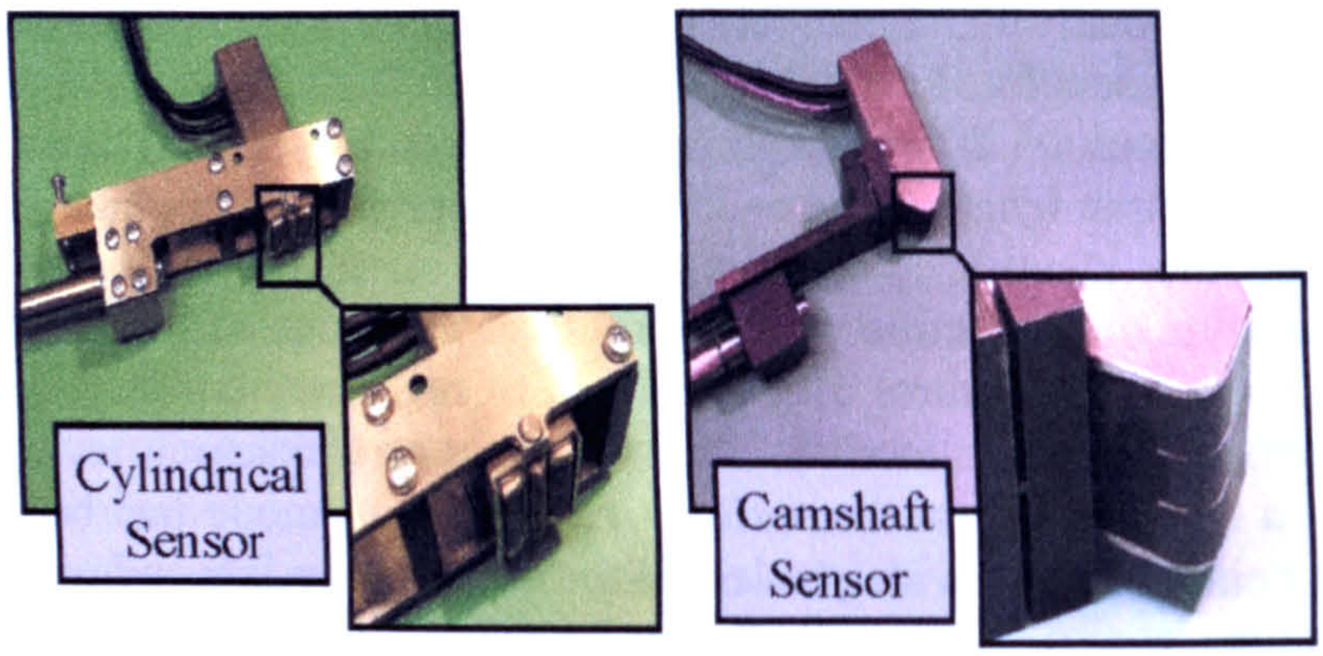

Figure 3.41 – Photograph of Stresstech BN Sensors

The instrument calibration was carried out using a thermally damaged component and a good component. Each was subject to a series of measurements with the sensor held static against the component. The procedure involved increasing the level of input signal (*Magn*) from 10 to 100 insteps of 10 whilst monitoring the sensor output in units of magnetic power (*MP*). The result is produced below on the left in Figure 3.42. In order to obtain the optimum sensitivity the input level relative to the maximum difference in output for the two components was required, this was found by plotting the difference as in the right of Figure 3.42. In this instance a value of *40Magn* was selected. The final step was to set the base level output reading which was carried out by adjustment of the sensor gain value on the BN unit, for the camshaft data illustrated here the gain was set to give a base line output reading of *40MP*.

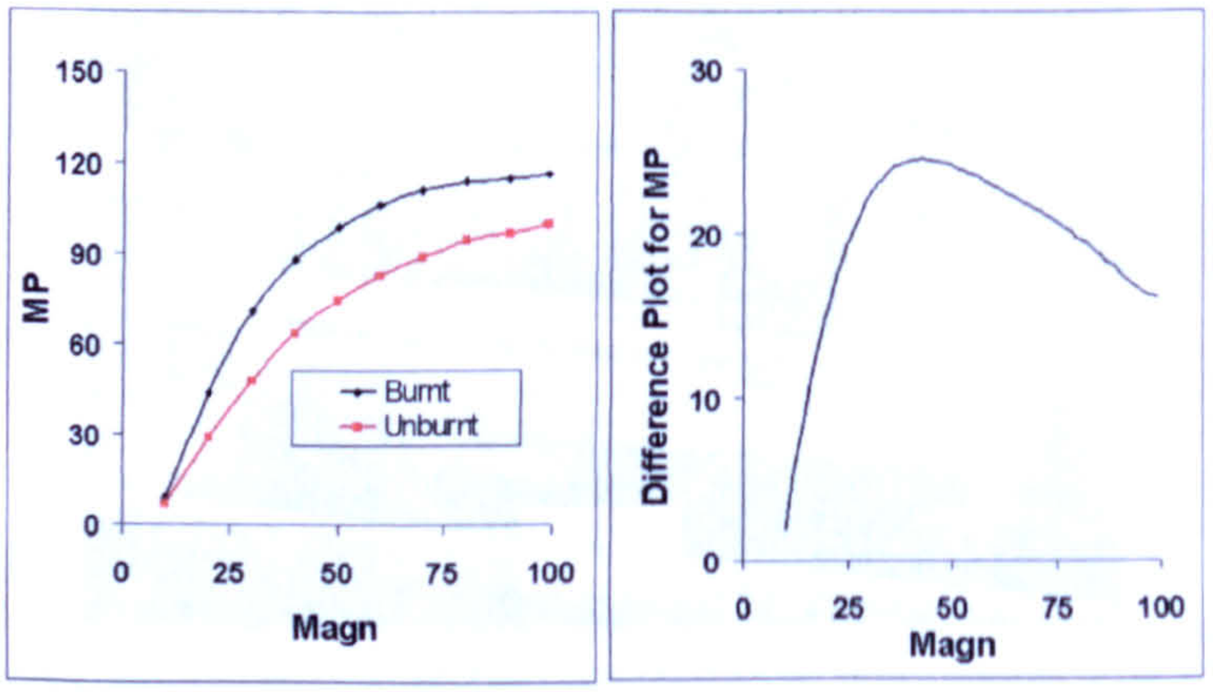

Figure 3.42 – Calibration Charts for BN Sensors

Following the calibration a number of measurement tasks were undertaken in order to fully assess the instrument, one of which was carried out on a series of camshafts produced by a machine tool manufacturer during the commissioning phase and for which the results are detailed below.

Figure 3.43 shows the profile trace for a full rotation (360°) of two lobes. The output remains level about the base figure of *40MP*, which indicates that no thermal damage has resulted from the grinding process. The grinding parameters used to produce the camshaft were well below those normally expected to produce damage in components, there was no evidence of grinding burn on the ground surface.

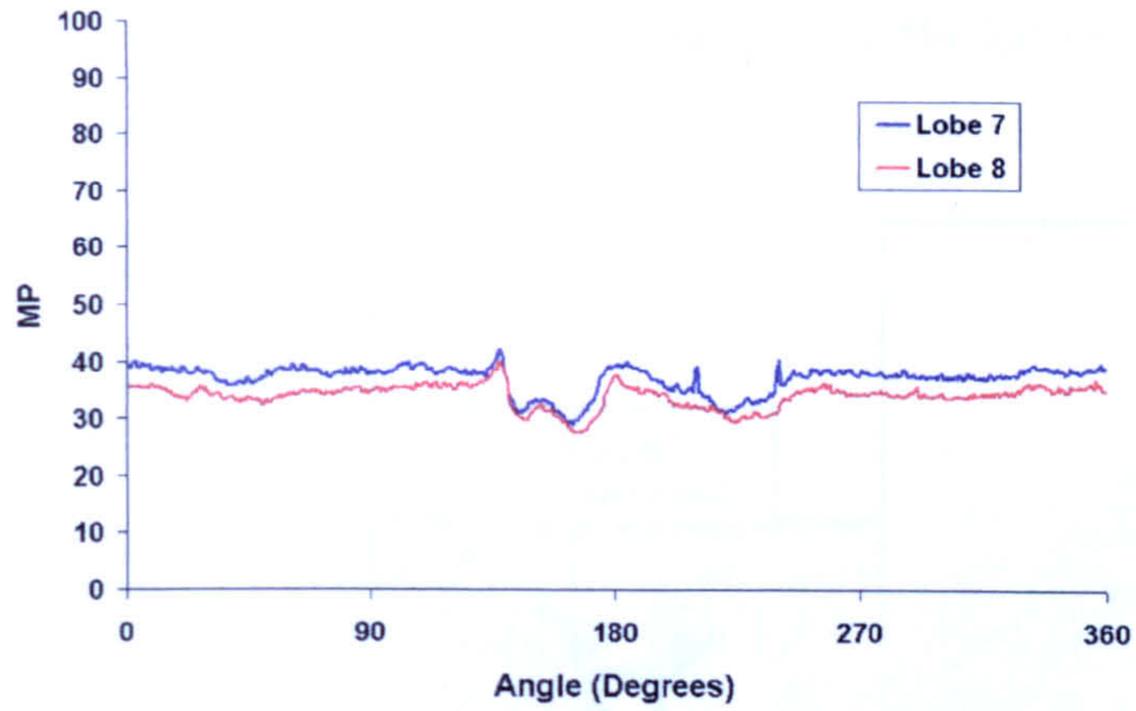

Figure 3.43 – Measurement Trace for Undamaged Camshaft Lobes

The next profile trace in Figure 3.44 is again for a full rotation of two lobes, the camshaft in this instance was produced with grinding parameters normally associated with thermal damage to the component. For a large proportion of the rotation the output again remains at the base level of *40MP*, but for the areas relating to the nose and re-entrant portion of the camshaft lobe high outputs were seen. These indicated the presence of thermal damage in the form of high tensile residual stress. As stated in Chapter 2, desirable compressive residual stress in a component produces low output values of *MP* whilst the presence of undesirable tensile residual stress results in high values. Visual examination of the lobes showed signs of the oxide layer indicating burn.

The identification of visual burn can be very subjective and the evidence can be removed by further surface/grinding wheel interaction such as that occurring with sparkout. The latter is commonly employed at the final stage of the grind feed in production environments to improve the surface finish and form of components.

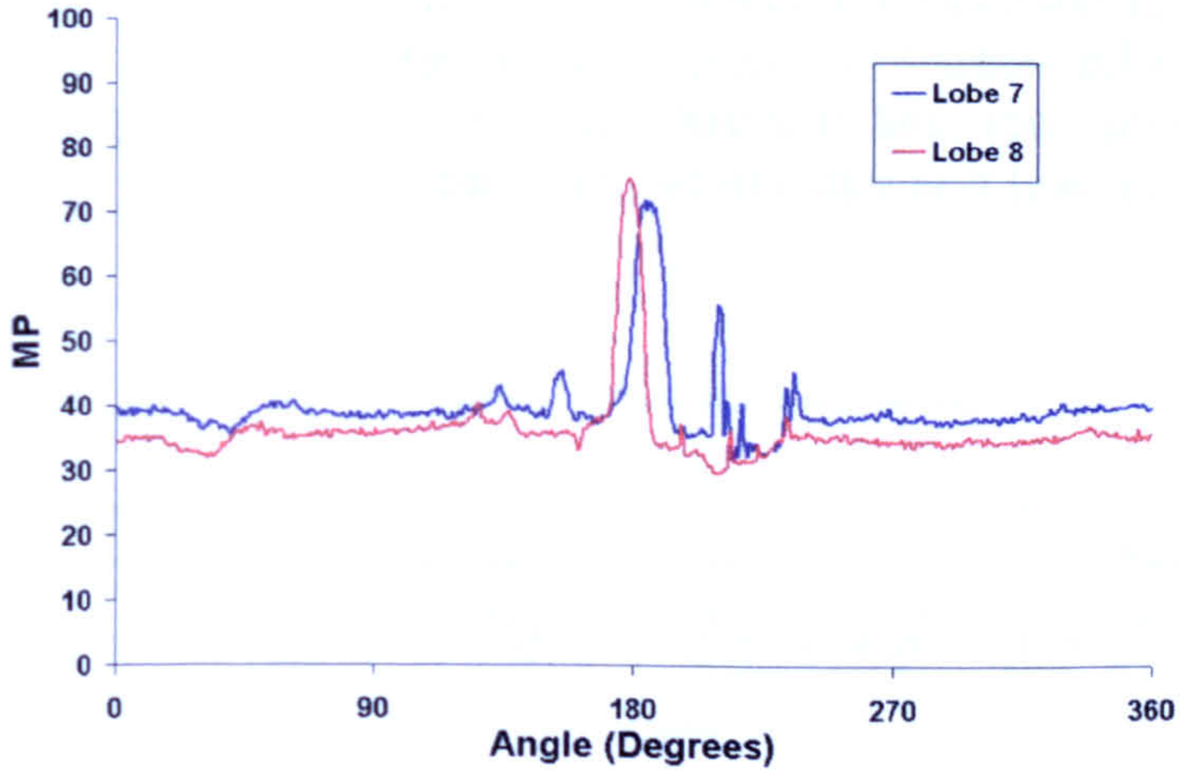

Figure 3.44 – Measurement Trace for Damaged Camshaft Lobes

To fully validate the findings a microstructural analysis was carried out on one of the damaged lobes. The lobe was sliced perpendicular to its axis of rotation, then sectioned as shown in Figure 3.45, each section was then polished and etched to reveal any evidence of thermal damage. The microstructural images of the nose (top left) and re-

entrant (top right) sections of the camshaft lobe clearly show the formation of a white layer caused by the thermal effect of grinding. The results clearly support those of the BN analysis.

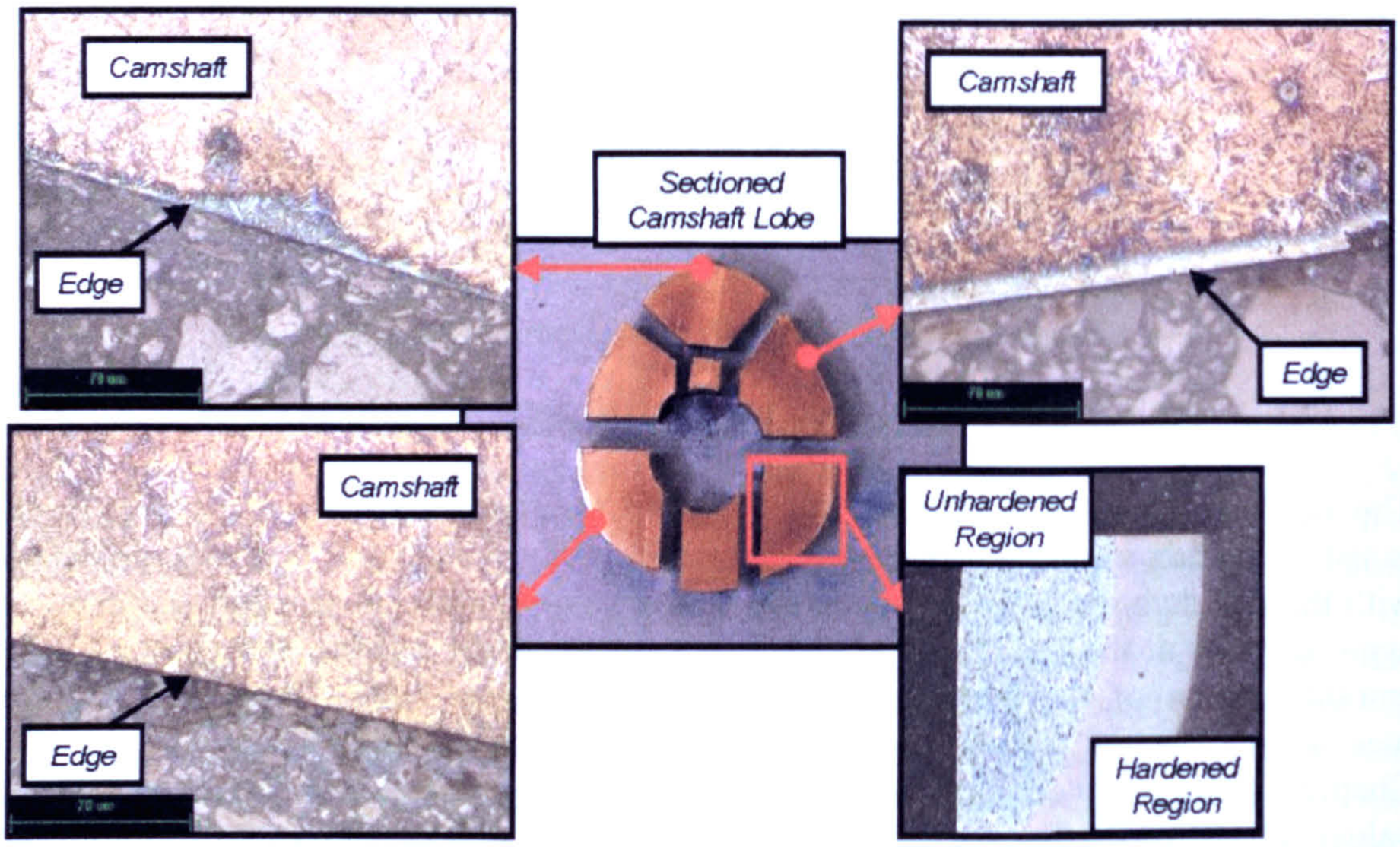

Figure 3.45– Microstructural Analysis for Damaged Camshaft Lobes

Analysis of grinding samples was carried out with this instrument using a flat sensor for surface ground samples, in either a static mode for single readings or drawn across the grind path by hand for profile readings.

Moorthy et al (2002) discusses the depth penetration of the technique and quotes the relationship given in Equation 2.11 where it can be seen that this is dependant on both the measurement frequency and material properties. The depth penetration for the rollscan instrument on steel was stated to be in the order of 30μm.

4 HEDG Regime Grinding Investigations

The HEDG grinding investigations carried out are fully detailed in this chapter, both the grinding and analysis works are presented. There were three stages of trials namely, surface grinding, cylindrical grinding and finally production cylindrical grinding. The objectives of these three stages were as defined in section 3.2.1.

4.1 Surface Grinding

The grinding investigations covered a broad range of specific material removal rates Q'_w, beginning at 1 and reaching up 1000 $mm^3/mm.s$, the higher level being governed by machine spindle power limitations. The work was carried out in two series of trials, the setup configuration together with full details for the machining parameters are given in *Chapter 3 – Experimental Procedures and Equipment*. To summarize the initial set of tests were conducted within a Q'_w range of *1* to *180*$mm^3/mm.s$ to establish the basic process conditions. The range of these tests covered both that of conventional creep feed grinding regime and the lower range of *HEDG*. The second set were over the higher range of *5* to *1000*$mm^3/mm.s$, the upper level of these tests were accepted to be well within the range of the *HEDG* regime (Tawakoli 1993).

The grinding spindle power was measured with a *Hall Effect* sensor. Figure 4.1 shows a typical power measurement for a grind cycle from these trials. The spindle startup was used to calibrate the sensor as this used the full spindle power available (*27kW*). The grind peak shown represents total grind power, and the base level was the power required to run the spindle, accelerate and push the coolant through the gap. The power required for material removal referred to as the grind power is the difference between the grind and base power values.

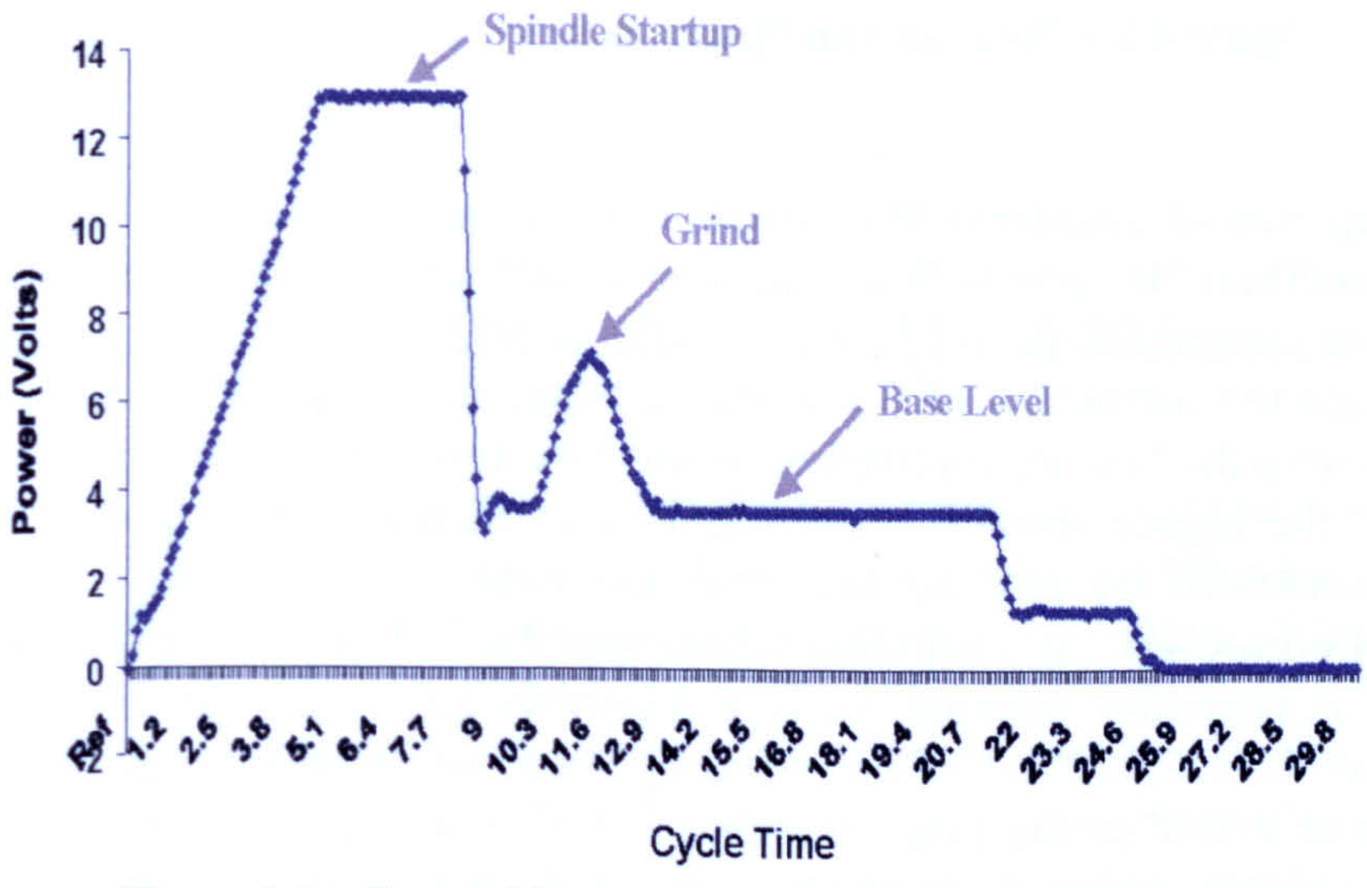

Figure 4.1 – Power Measurement for Typical Grind Cycle

Figure 4.2 shows the total spindle power versus the specific material removal rate (Q'_w) for the tests carried out with the initial 10mm grind width. The power trends for the different spindle speeds of 100m/s and 200m/s are clearly evident, the latter requiring far higher power levels. Tawakoli (1993) states that the higher wheel speeds are a major

contribution to the successful implementation of the *HEDG* regime Both lines approach the maximum spindle power limit at moderate values of Q'_w. This demonstrates the envelope of grinding with the setup utilised and it was concluded that to increase the range of $1000mm^3/mm.s$ Q'_w then a reduced width of cut would need to be used. Consequently some of the following tests used a reduced width below that of 10mm, one implication of this action was the inability to analyse such samples for near surface stress with the *BN* residual stress instrument.

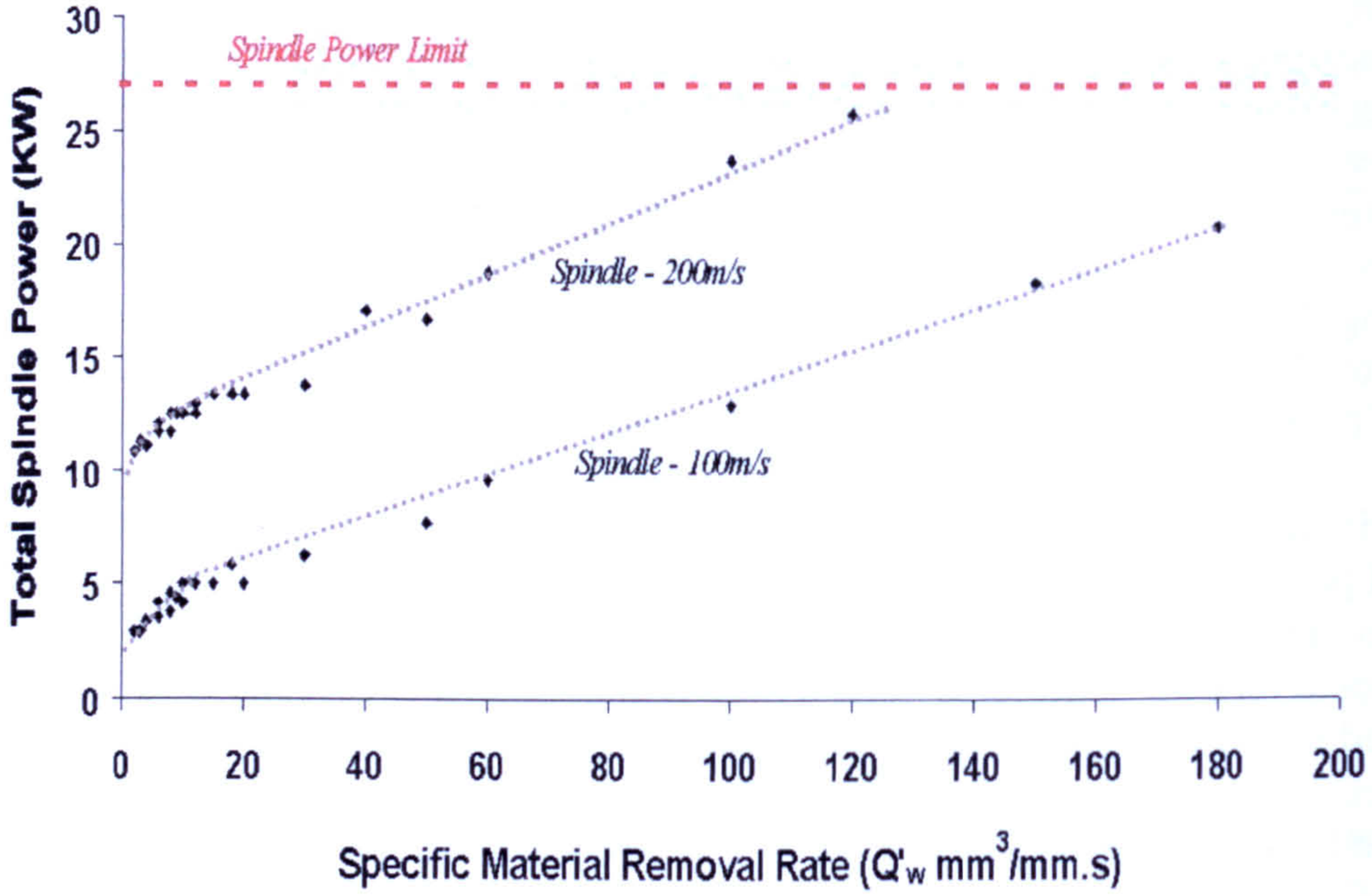

Figure 4.2 – Total Spindle Power versus Q'_w (10mm Grind width)

The next step was to determine the distribution of the process spindle power used and from this ascertain the proportion that was attributable to the grinding action. The spindle power comprises, power to run spindle, accelerate coolant to wheel speed, push coolant though the restriction of the grinding zone, and finally to remove material. All components save the last are referred to as the base level or sparkout power. The results indicate that the higher spindle speed requires an increased base power level. This is clearly demonstrated by plotting the total and base power readings for both spindle speeds, as in Figure 4.3. At a grinding wheel speed of *100m/s* the base level or sparkout power as it is normally referred to, is a relatively small proportion (*2.5kW*) of total spindle power (*27kW*). At the higher grinding speed of *200m/s* this proportion however is far higher at *9.8kW* of the total available *27kW*. It was concluded from this step that the higher spindle power consumption for the increased grinding wheel speed – Identified by Tawakoli for successful implementation the *HEDG* regime - does not in fact subject the material removal component of the process to an equivalent increase in power and hence thermal input. This highlights the added benefit that would be possible by improvements to the coolant delivery which would in turn reduce the base power level.

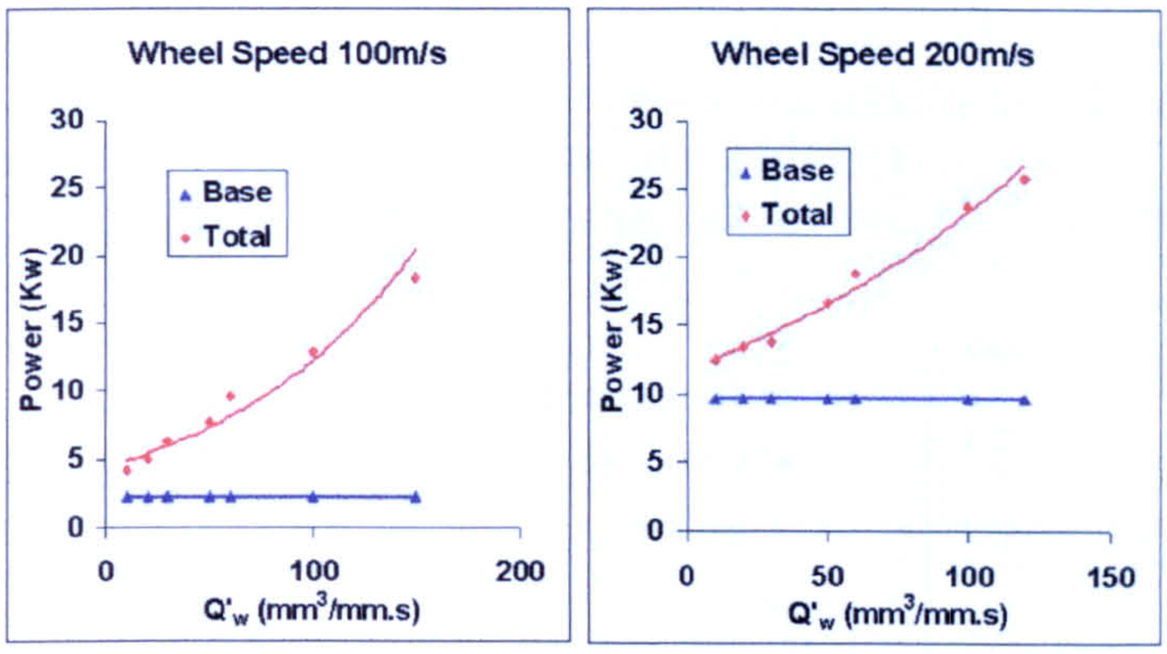

Figure 4.3 – Q'_w against Spindle Power

The final step of the initial trials was to understand the implication of the grinding wheel grit size. To determine the upper limit of each wheel, samples were classified visually as burn or unburnt. The charts in Figure 4.4 plot Specific Material Removal Rate against grinding wheel speed and show at which stage burn occurs for both the *213μm* and *151μm* grinding wheels. It was concluded from these that at the lower wheel speeds there was not a significant advantage in using the larger grit wheel, however at the higher speed of *200m/s* higher levels of Q'_w were attainable without burn. Therefore subsequent surface grinding trials were carried out with the larger grit wheel. For later work carried out in the cylindrical mode grit sizes of *213μm* and above were selected.

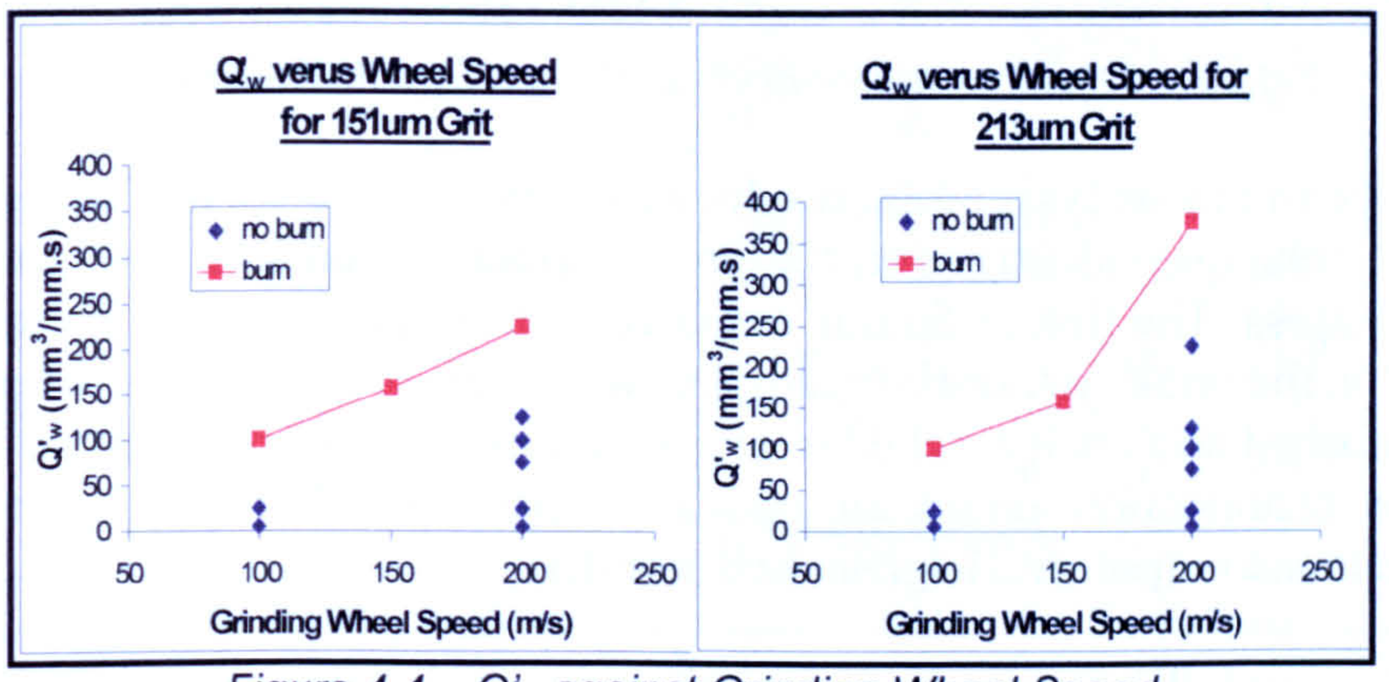

Figure 4.4 – Q'_w against Grinding Wheel Speed

The second series of trials over the range of *5* to *1000mm^3/mm.s* were carried out and together with the initial trial results the base level power figures subtracted and Specific Grinding Energy (*SGE*) figures calculated, as described in *Chapter 3*. At this stage surface integrity assessment was carried out solely by visual inspection of the sample surfaces classifying them as burnt or unburnt. In order to interpret the results, the data was put into the form of a burn threshold diagram as proposed by Jaeger (Malkin, 1989). The diagram is essentially a plot of *SGE* against the function $f(d_e^{1/4}, a^{-3/4}, v_w^{-1/2})$, where d is the effective grinding wheel diameter, a is the depth of cut, and v_w is the surface speed of the grinding wheel. The function is derived from the Jaeger thermal model, which predicts the thermal effect of the above parameters on the workpiece for conventional surface grinding. Once the data has been plotted a transition line can be placed separating the burn and unburnt sample points. Figure 4.5 shows the burn threshold chart produced with the threshold line. The threshold line allows both the

grinding limitation to be established in relation to spindle power, and surface temperature values to be calculated. However at this stage placement of the boundary line was deemed to be rather subjective as there were no burnt points in the *f(dav)* region of *1.0* or above so no further assessment could be undertaken.

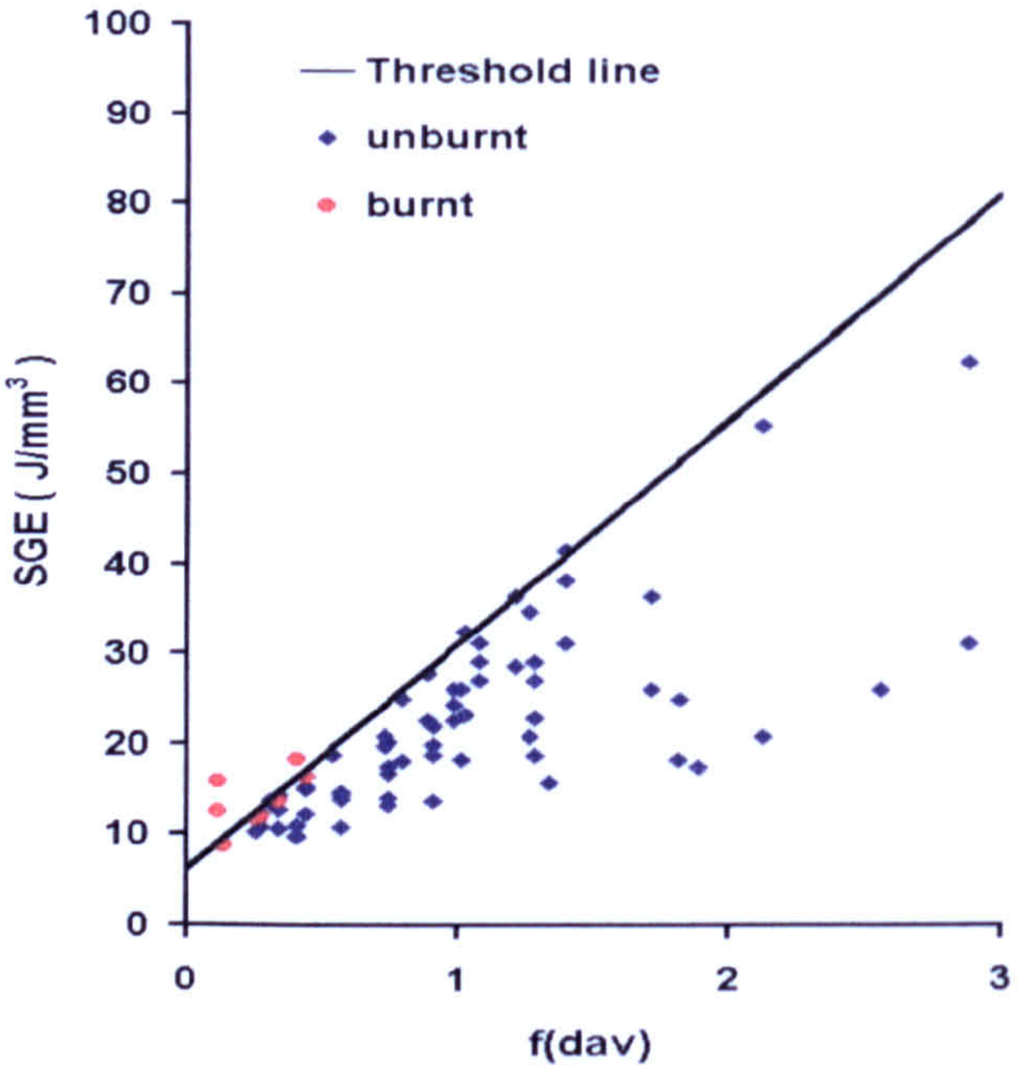

Figure 4.5 – Burn Threshold Chart (Visual Sample Assessment)

The next stage to the analysis of the results was to investigate the surface integrity fully utilising the techniques identified in *Chapter 3*, namely microstructural, microhardness and residual stress. The first technique employed was microstructural, a limited number of potentially the most interesting samples were selected. Samples were sectioned, mounted, polished and finally etched to expose the cross-sectional microstructure of the material for examination under an optical microscope. The results together with machine input and output data is given in Table 4.1.

Samples *W1-1* and *W2-1* were both ground at low Q'_w rates of $5mm^3/mm.s$ with the *213μm* and *151μm* grinding wheels respectively. Neither of these samples had any visible surface discolouration and thus it had been concluded so far that there was no thermal damage. Microstructural analysis supported this conclusion is that there was no evidence of structural changes in the near-surface region. It was a similar situation with samples *W1-6* and *W1-8* both ground with the *213μm* grit wheel at a Q'_w rate of $100\ mm^3/mm.s$. There was neither surface discolouration nor changes in the microstructure of the specimens. The next set of samples to be examined were those for *W2-6* and *W2-8*, these had again been ground at a Q'_w of $100\ mm^3/mm.s$ but in this case with the *151μm* grit wheel. In both cases the *SGE* was of a higher magnitude than that of the previous samples ground at the same rate. *W2-6* produced with the lower wheel speed of *100m/s* had surface discolouration and had therefore been classified as burnt. Whereas W2-8 ground with the higher wheel speed of *200m/s* had had no surface discolouration and had been designated unburnt. Both surfaces together with images of their microstructure can be seen in Figure 4.6 and Figure 4.7 respectively. It is clear in the

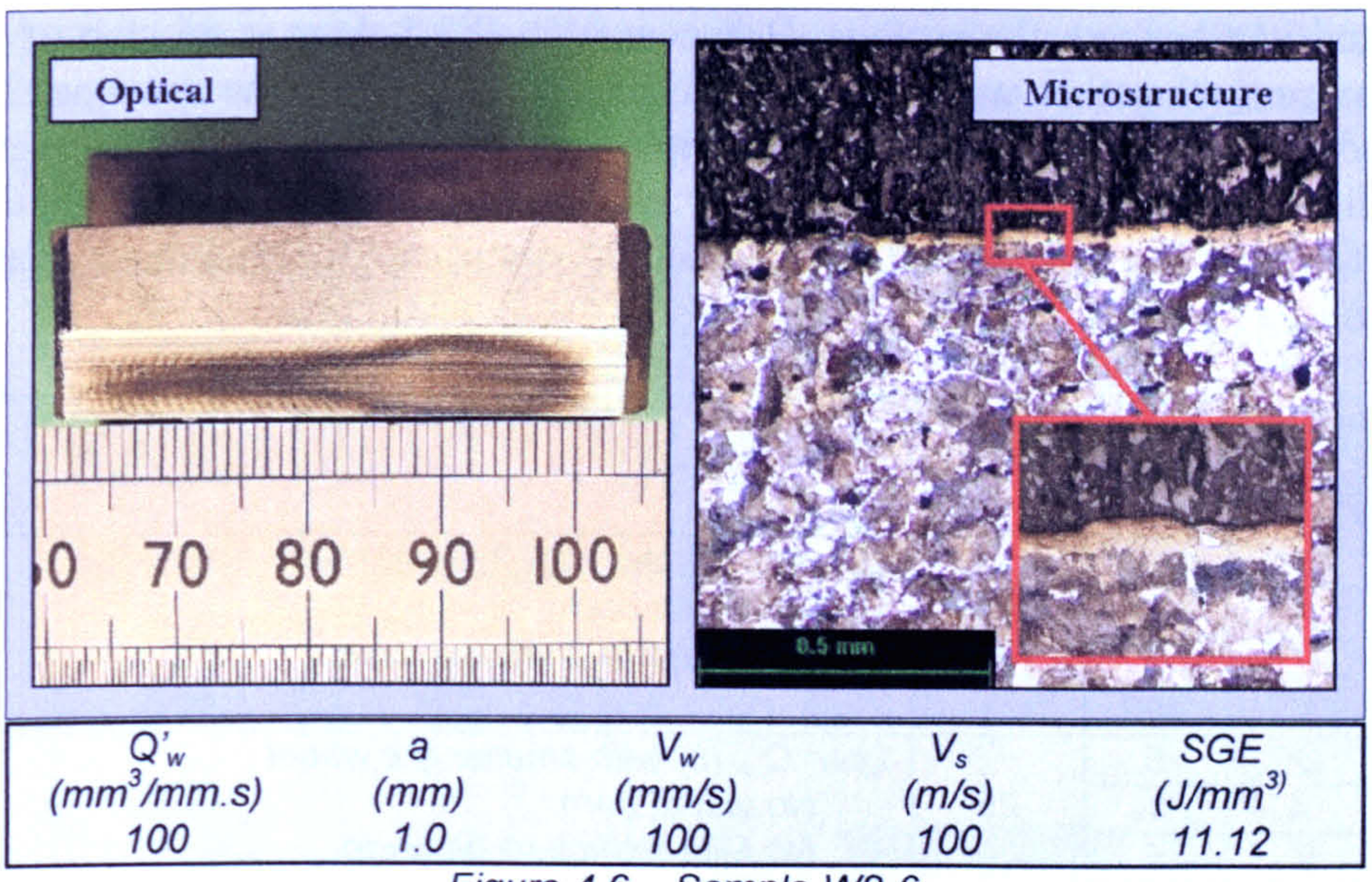

Q'_w ($mm^3/mm.s$)	a (mm)	V_w (mm/s)	V_s (m/s)	SGE (J/mm^3)
100	1.0	100	100	11.12

Figure 4.6 – Sample W2-6

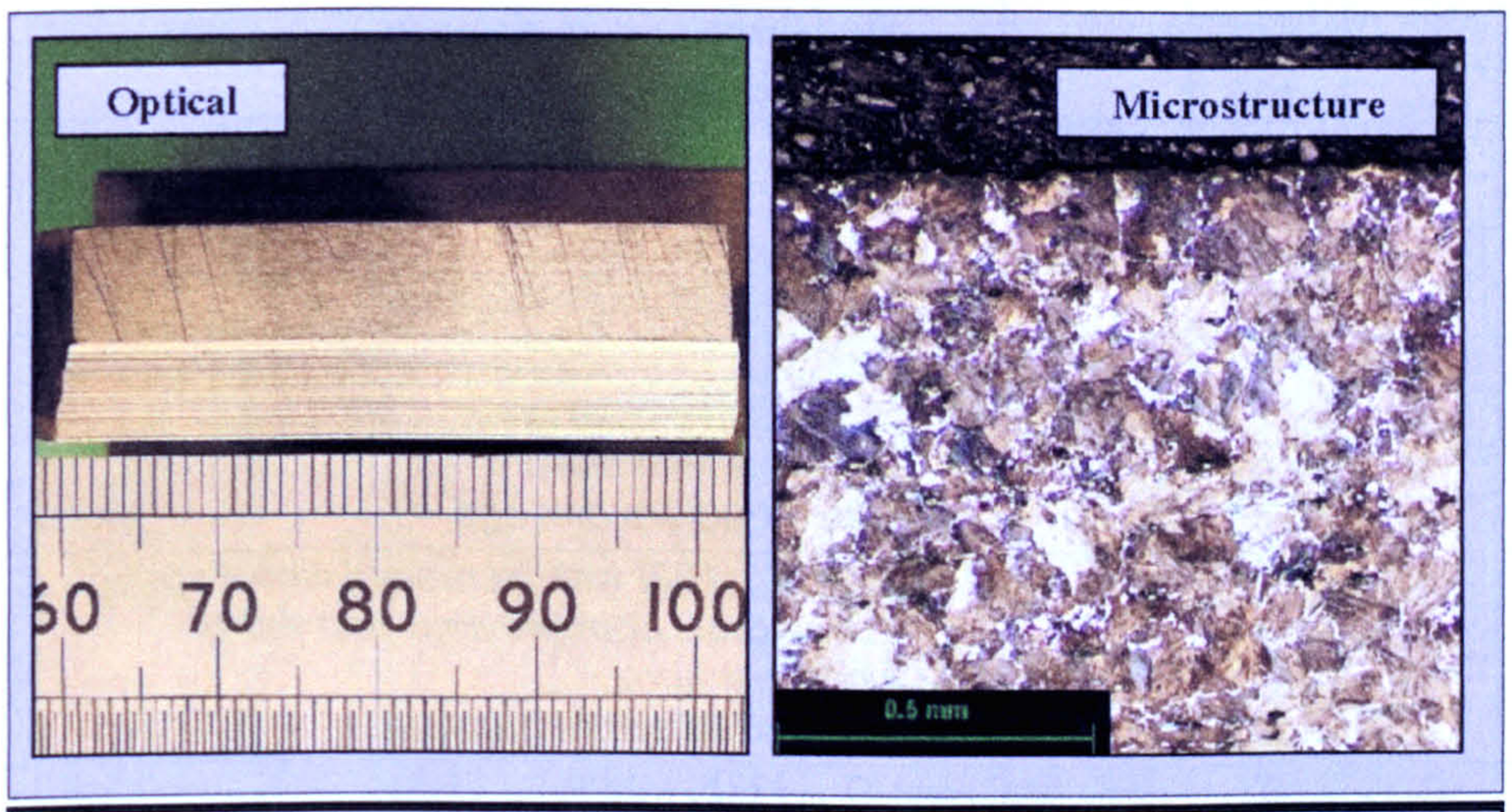

Q'_w ($mm^3/mm.s$)	a (mm)	V_w (mm/s)	V_s (m/s)	SGE (J/mm^3)
100	1.0	100	200	10.91

Figure 4.7 – Sample W2-8

Moving on to samples *W1-12* and *W2-12*, both ground at a Q'_w rate of $375mm^3/mm.s$ with the $213\mu m$ and $151\mu m$ grit wheels respectively. The *SGE* values were extremely close suggesting a similar condition for both samples. Visually both had evidence of surface dis-colouration which in the case of the sample produced with the larger grit wheel was marginally less. Neither sample showed any sign of microstructural changes.

Finally for samples *W1-14* and *W1-15* both ground with the $213\mu m$ grit wheel at a Q'_w rate of $500mm^3/mm.s$. The first with a grinding wheel speed of *100m/s* and the second *200m/s*. Both had showed surface disc-colouration and been classified as burnt, although the dis-colouration was far greater for that of the sample produced with the lower wheel speed. Images of the surface and microstructure are shown in Figure 4.8

case of *W2-6* that there is evidence of microstructural damage in the form of a white layer at and just beneath the surface. However with *W2-8* there is no sign of any such damage present. Together with the presence of the white layer the specimen from test *W2- 6* had the higher value for the *SGE*. Therefore in this case *W2-6* had higher *SGE*, surface discolouration and microstructural change. All factors supporting the initial classification that this sample had been subject to significant thermal damage as a result of the grinding process.

Sample			SGE	Comment
No.	Parameters			
W1-1	Q'_w	5	25	Low Q'_w (5) test with 213µm wheel - No visual burn - No Microstructure damage
	A	10		
	V_w	5		
	V_s	100		
W2-1	Q'_w	5	25	Low Q'_w (5) with smaller grit wheel - No visual burn - No Microstructure damage
	A	1		
	V_w	5		
	V_s	100		
W1-6	Q'_w	100	9.73	Medium Q'_w (100) - No visual burn - No Microstructure damage
	A	1		
	V_w	100		
	V_s	100		
W1-8	Q'_w	100	9.65	Medium Q'_w (100) with increased wheel speed - Lower SGE from previous test W1-6 - No visual burn - No Microstructure damage
	A	1		
	V_w	100		
	V_s	200		
W2-6	Q'_w	100	11.12	Medium Q'_w (100) with smaller grit grinding wheel - Higher SGE from previous test W1-8 - Severe visual burn - Microstructure damage
	A	1		
	V_w	100		
	V_s	100		
W2-8	Q'_w	100	10.91	Medium Q'_w (100) with increased wheel speed - Lower SGE from previous test W2-6 - No visual burn - No Microstructure damage
	A	1		
	V_w	100		
	V_s	200		
W1-12	Q'_w	375	8.61	High Q'_w (375) test - Medium level burn - No Microstructure damage
	A	5		
	V_w	75		
	V_s	200		
W2-12	Q'_w	375	8.76	High Q'_w (375) test but with smaller grit wheel now - High visual burn. - Higher SGE than previous test W1-12 - No Microstructure damage
	A	5		
	V_w	75		
	V_s	200		
W1-14	Q'_w	500	10.42	High Q'_w (500) test with low grinding wheel speed - Severe visual burn - Microstructure damage.
	A	5		
	V_w	100		
	V_s	100		
W1-15	Q'_w	500	8.96	High Q'_w (500) test with high wheel speed - Medium visual burn - No microstructure damage - Lower SGE than previous test W1-14
	A	5		
	V_w	100		
	V_s	200		

Table 4.1 – HEDG Sample and Microstructure Images

and Figure 4.9 respectively. Sample *W1-14* produced with the lower wheel speed clearly has a large white layer extending well below the surface, whereas for *W1-15* there is no detectable microstructural change. The *SGE* data supports these finding in that the higher value was that for the damaged component *W1-14*.

Q'_w ($mm^3/mm.s$)	a (mm)	V_w (mm/s)	V_s (m/s)	SGE (J/mm^3)
500	5.0	100	100	10.42

Figure 4.8 – Sample W1-14

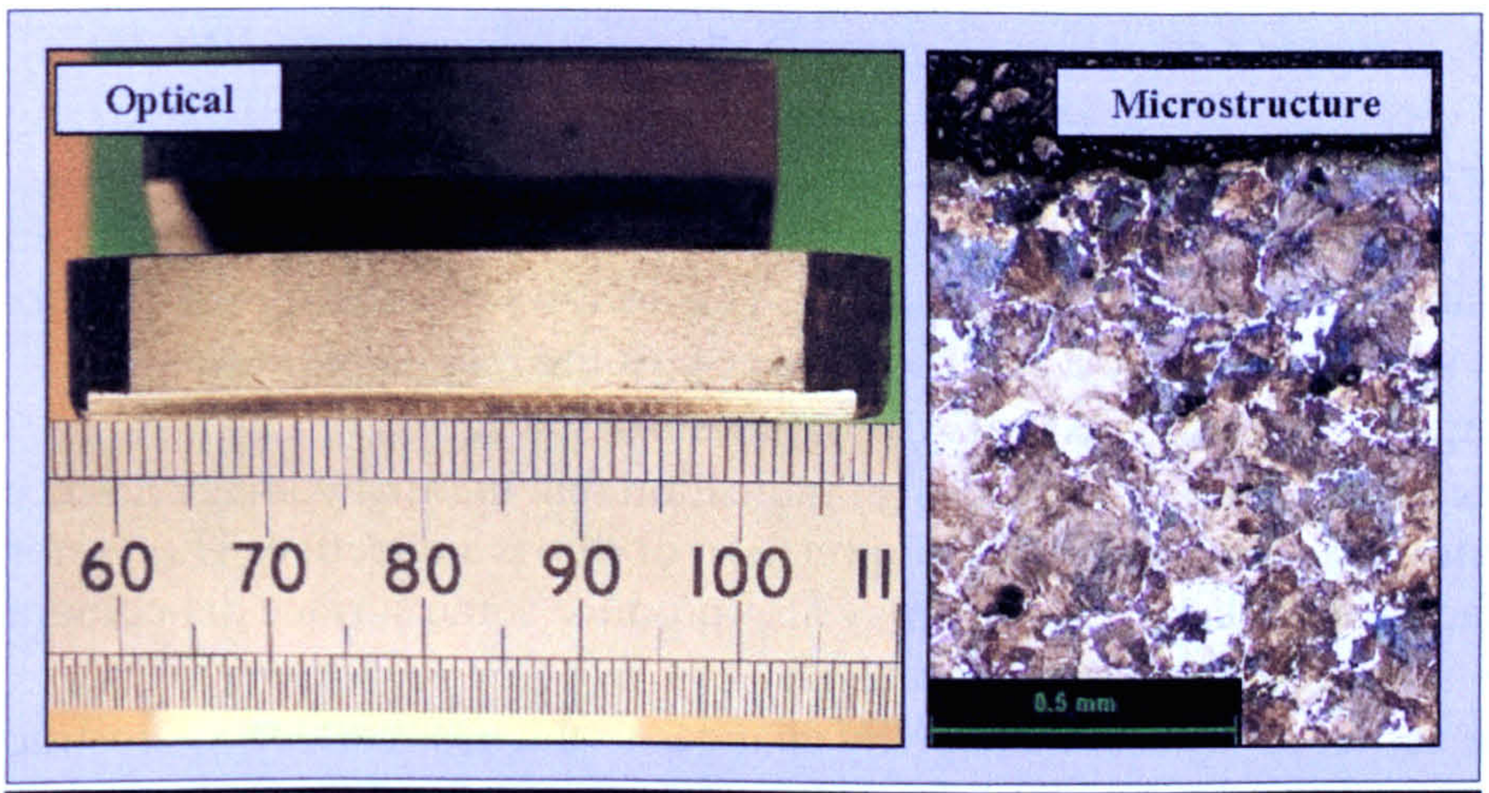

Q'_w ($mm^3/mm.s$)	a (mm)	V_w (mm/s)	V_s (m/s)	SGE (J/mm^3)
500	5.0	100	200	8.96

Figure 4.9 – Sample W1-15

To add additional evidence to the results and confirm the nature of the white layer seen in the microstructural specimens as a hardened layer, some micro-hardness profiles were carried out. The procedure for this procedure is fully described in *Chapter 3*. The two samples selected were W1-14 with white layer and W1-15 without. The micro-hardness results together with the associated microstructural images are shown in Figure 4.10. These clearly show that the former sample has a hardened layer for a depth of approximately $300\mu m$, whereas in the case of the latter there was no sign of near surface hardening.

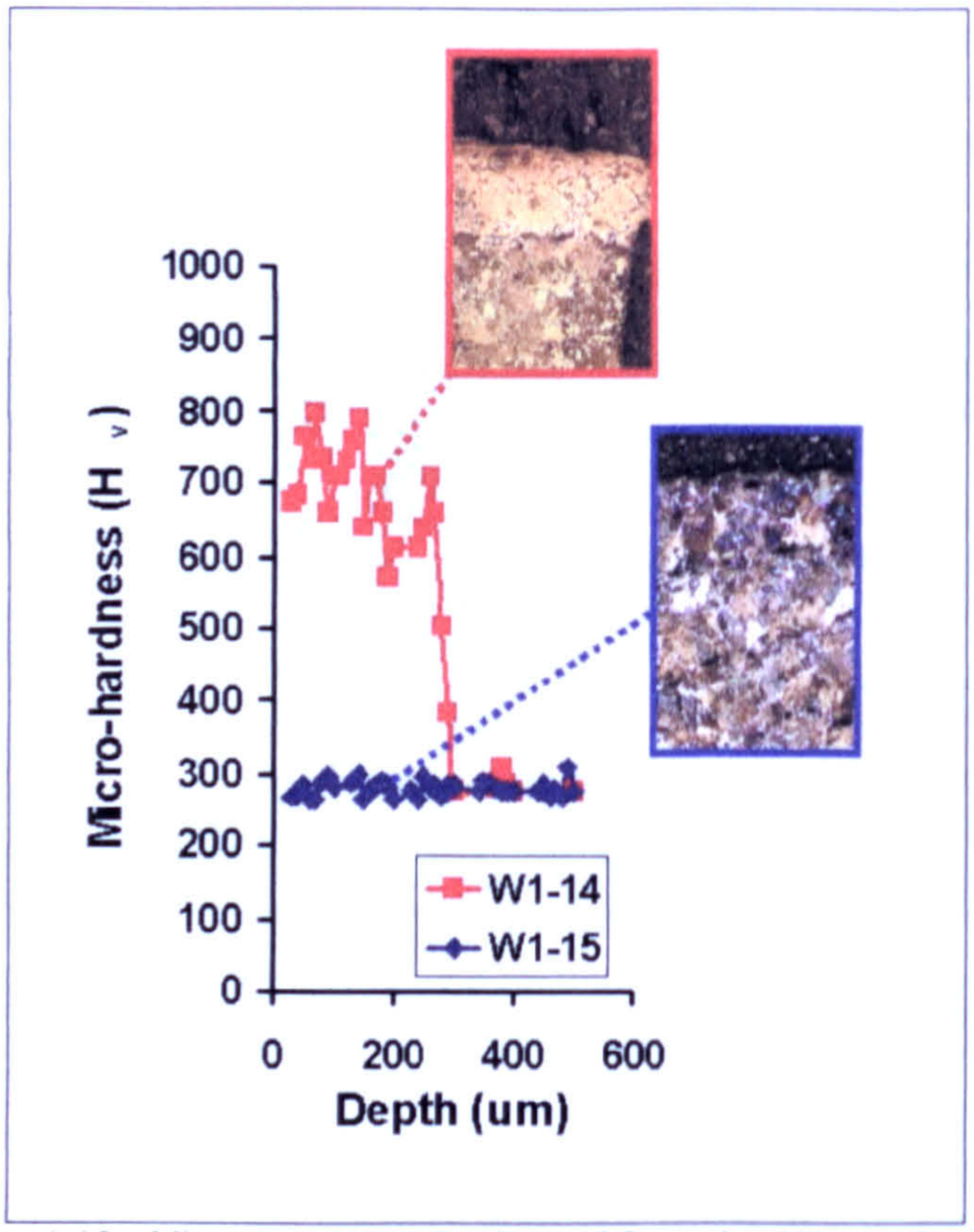

Figure 4.10 –Micro-hardness Profiles of Samples W1-14 &W1-15

In summary it can be concluded that these results clearly demonstrate:

- Higher grinding wheel speed reduces SGE and therefore the burn threshold boundary and microstructural damage. This follows the findings of Tawakoli in that higher wheel speeds are a significant aspect of the *HEDG* regime.
- The larger grit grinding wheel also reduces SGE
- Surface dis-colouration provides an indication that thermal damage has occurred to the component. However the interpretation of this is subjective. This factor coupled with fact that coolant oxidation may also produce some surface dis-colouration makes it an unrealistic tool for analysis.
- The detection of thermal damage by changes to the near surface microstructure of the component is far more reliable. However a component displaying white layer has been subject to a significant level of thermal damage. Ideally a method is needed to detect damage before this point is reached. Another factor to consider is that the analysis is both time consuming and destructive, neither lend themselves to a production orientated environment.
- The microhardness as with the microstructural technique provides reliable data but again is time consuming and destructive.
- Hence although these techniques can provide valuable information a faster non-destructive and less subjective method is required.

The next stage of the analysis was to measure the residual stress in the component created by the thermal effects of the grinding process. Two techniques were used, Barkhausen Noise (BN) Intensity and X-Ray Diffraction. The technique of primary

interests was that of BN as this is a proven fast and non-destructive approach. It is however a comparative measurement and so requires calibration. Descriptions of both techniques together with detail of the calibration process are given in *Chapter 3*. The work carried out with the BN instrument is described herein together with the results. Following this a few XRD measurements are presented in order to provide additional evidence and validate the BN results.

The burn threshold diagram previously shown in Figure 4.5 had defined regions for burnt and unburnt samples, however it proved difficult to place the threshold line reliably from the basic visual interpretation of the surfaces dis-colouration as has been seen so far. The transition occurs with the reduction in compressive stress finally resulting in tensile stress, this means that there is a transition region lying between the two defined regions, this is illustrated in Figure 4.11. In order to position the threshold line more effectively it is necessary to measure the level of residual stress of components over this region and classify them as burnt or unburnt or more accurately either thermally damaged or not.

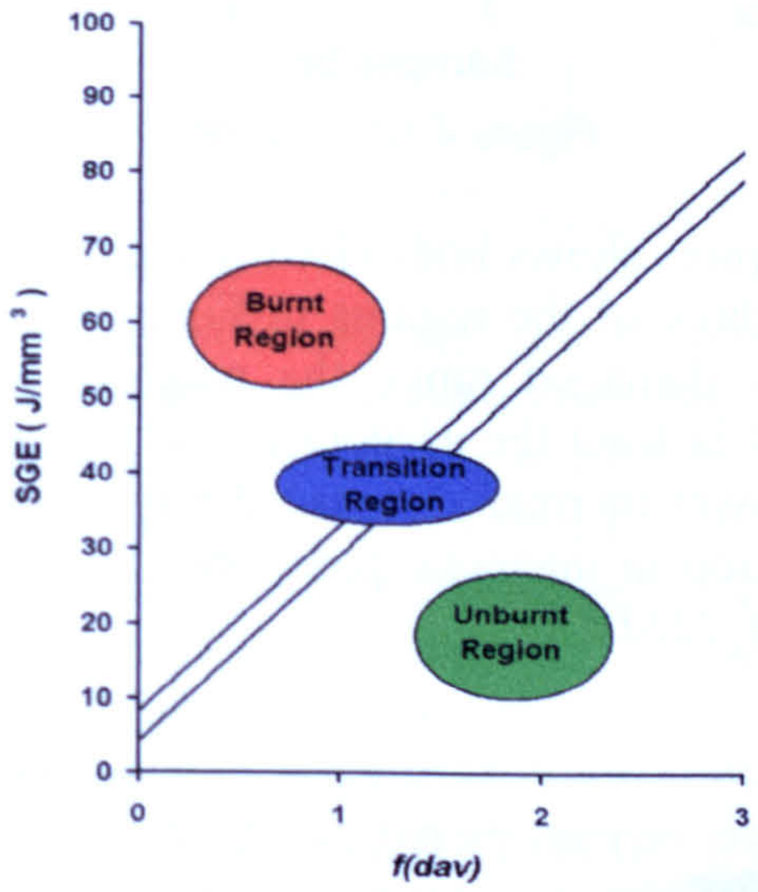

Figure 4.11 – Burn Threshold Diagram including BN regions

Surfaces from all three regions of the burn threshold chart were analysed with the BN instrumentation. It was found that those from below the threshold in the unburnt region had values of magnetic power of between *23MP* and *38MP*, whilst some of the surface at or near the threshold hence in the transition region had vales above that of *38MP*. This is clearly shown by the unburnt and marginal points in Figure 4.12. The magnitude of the BN signal rises with the reduction in compressive stress and any build up of tensile stress thus it follows that the unburnt surface are in fact compressive and of an acceptable quality. Whereas the increasing magnitude for the surface in the transition region indicates a reduction in the compressive stress, which at a predetermined level can be deemed unacceptable and therefore classed as thermally damaged. The last sets of surface were from the visually burnt region these are typified by the presence of rehardening in the form of white layer. The BN intensity is known to increase with the decrease in the compressive stress, however the opposite is true when there is an

increase in the hardness of a surface. Therefore in this case as rehardening has taken place the BN intensity has dropped, hence the samples from the burnt region lie below the *23MP* level.

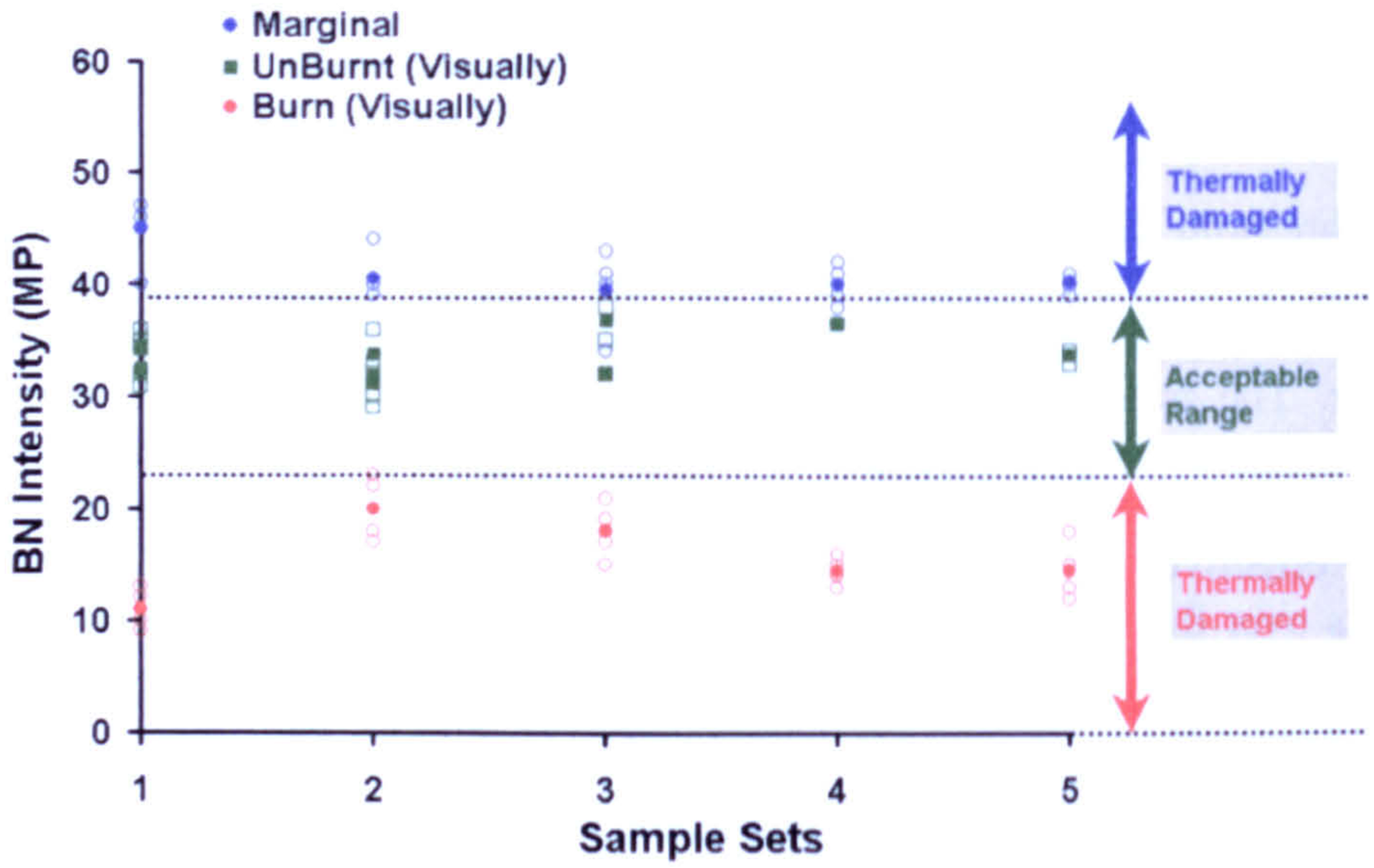

Figure 4.12 – BN Plot

The following series of figures shows both visual images and the BN surface trace for sample surfaces from all three of the regions in Figure 4.12. The first Figure 4.13 is from the upper thermally damaged range the magnetic power readings is *50MP*. Following that Figure 4.14 is from the acceptable and has a reading of *27MP*. Finally Figure 4.15 is from the lower thermally damaged range where rehardening has taken place and the associated drop in magnetic power can be seen midway along the trace where it drops to a value of *15MP*.

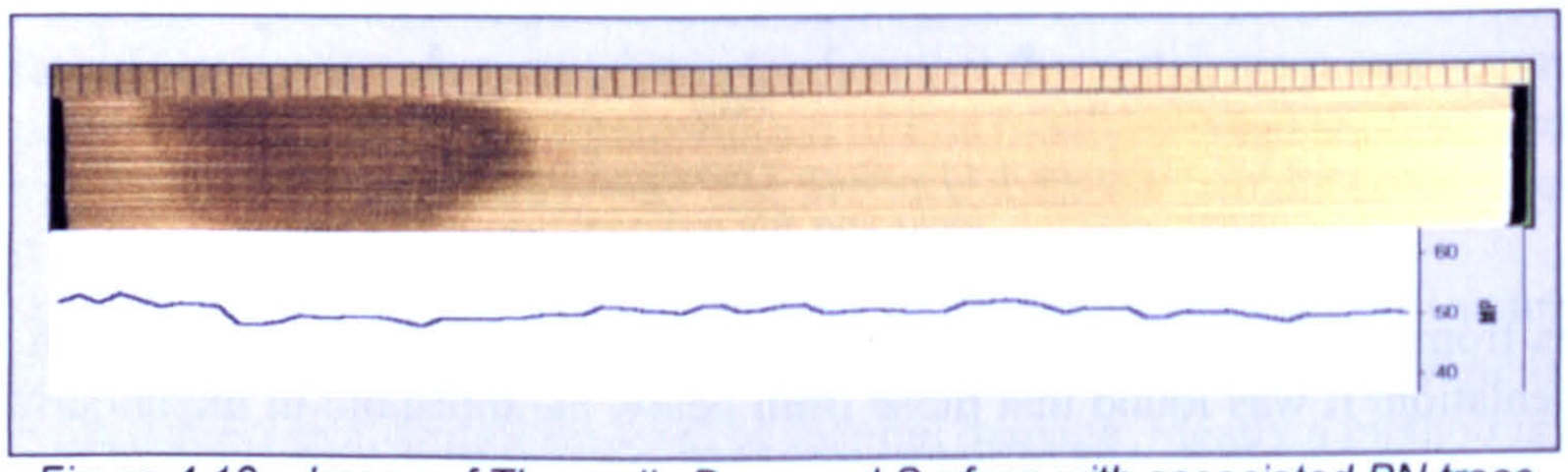

Figure 4.13 – Image of Thermally Damaged Surface with associated BN trace

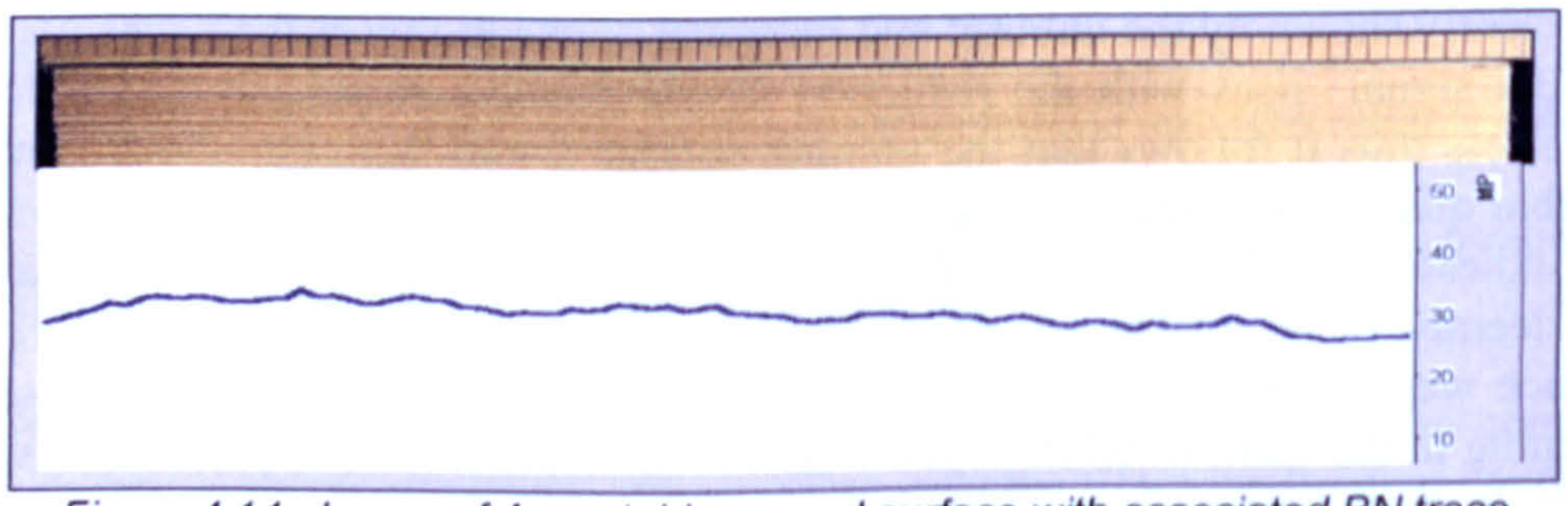

Figure 4.14 –Image of Acceptable ground surface with associated BN trace

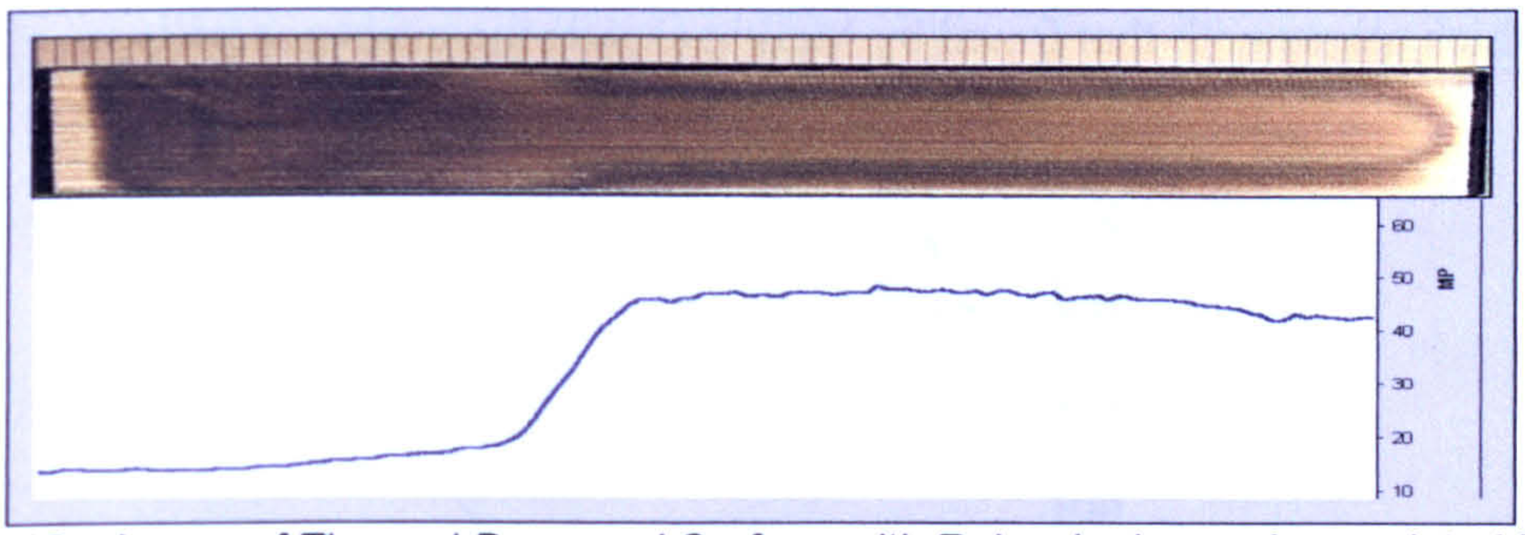

Figure 4.15 – Image of Thermal Damaged Surface with Rehardening and associated BN trace

XRD readings were carried out for surfaces from each of the three defined regions the results aligned with the findings from the BN intensity measurements. The data is presented in Table 4.2.

Surface Designation	*BN Intensity (MP)*	*XRD (MPa) [Uncertainty]*
Thermally Damaged	*50*	*184 [±22]*
Acceptable	*27*	*-120 [±35]*
Thermally Damaged	*15*	*106 [±8]*

Table 4.2 - XRD and BN Intensity Results for Burn Threshold Regions

In conclusion there are a number of issues that need to be considered when the use of BN intensity equipment is envisaged. There are sample size limitations, which meant in the case of the surface grinding here it was not possible to obtain readings on a large proportion of the samples due to the size of the sensor. It was possible to address these constraints for the later cylindrical grinding trials, hence it was possible to obtain wider result coverage on the later trials. Importantly it is possible to detect the gradual reduction in compressive stress caused by the onset of thermal damage, however once that damage becomes great enough to result in rehardening within the surface zone then the measurement trend is reversed. In this situation unless either periodic readings are taken to detect any gradual increase or a degree of interpretation is used, misleading results may arise as the magnitude of the readings drop back through the acceptable range. Taking these issues into account it was concluded that the system has the capability to detect the onset of thermal damage caused by grinding before the stages of visual dis-colouration and probable rehardening have occurred. This makes the method a valuable tool suitable for application within the production environment.

By application of this additional analysis data to the grinding results the burn threshold chart was revised and as can be seen in Figure 4.16 it was now possible to place a burn threshold line more reliably. Data points significantly above the threshold line were difficult to obtain as in this work mineral oil was used exclusively as the coolant and this resulted in several flash explosions within the machine enclosure when high temperature conditions were present. The precise combination of conditions within this region that result in these flash explosions was unclear at this stage in the grinding research and is the subject of further current research at Cranfield (IMRC project 22 – An integrated approach to High Efficiency Grinding Processes). The value of specific

grinding energy at which the boundary line crosses the vertical axis is in the region of 6 J/mm3 which aligns with that found by Malkin (1989) for steels generally.

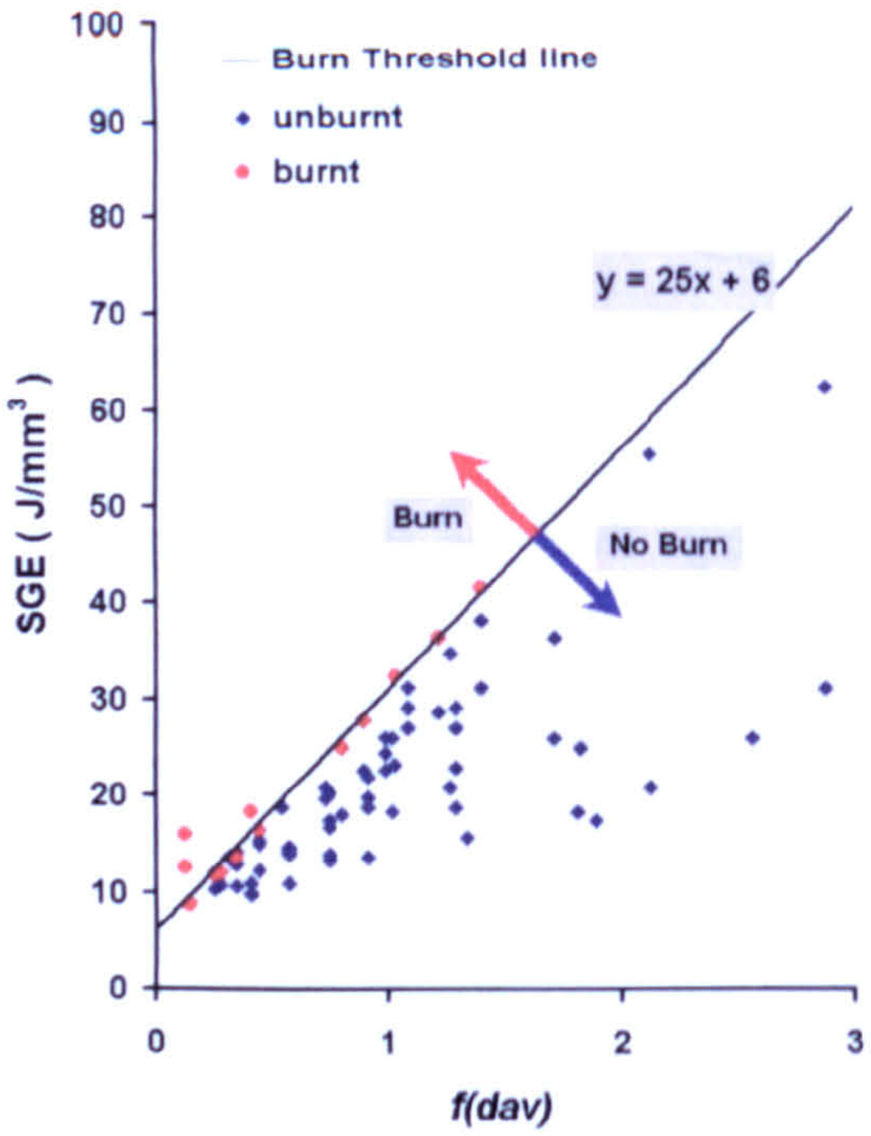

Figure 4.16 – Burn Threshold Diagram for Surface Grinding Trials

By combining Equation 2.14 and Equation 2.15 into the form given by Equation 4.1 then the components surface temperature for grinding conditions at the threshold line can be calculated. The second term of the function represents the gradient of the boundary line in the burn threshold chart.

$$\theta_m = \left(\frac{1.13\alpha^{1/2}}{k}\right)\cdot\left(\frac{u-u_0}{d_e^{1/4}\cdot a^{-3/4}\cdot v_w^{-1/2}}\right)$$

Equation 4.1– Jaeger's Temperature Equation (2)

Values for the material's thermal diffusivity and thermal conductivity *were* $1.295x10^{-5}$ Wm^2/J and *46.7 W/mK* respectively, whilst the burn threshold boundary gradient was *25* as shown in Figure 4.16. Hence θ_m was calculated to be *2170°C*, the high level of this predicted value can be explained by the fact that the model assumes that a large proportion of the chip forming energy in the region of *55%* is conducted as heat to the workpiece. This is in fact a far larger value than that expected for *HEDG* where Rowe (2001a) suggests that a higher proportion of the energy is removed by the chips thus reducing the input into the surface.

Now if the Specific Grinding Energy (*SGE*) is plotted against Q'_w the line exponentially decays to a base level of *6-10J/mm*^{3} for the higher material removal rates, as shown in Figure 4.17. This trend is similar to that reported by Stephenson (2002). It therefore follows that as the SGE can by reduced at the higher removal values and if as proposed

by Tawakoli (1993) more heat energy is removed by the chips, then HEDG should be possible without damage to the surface integrity of the ground component.

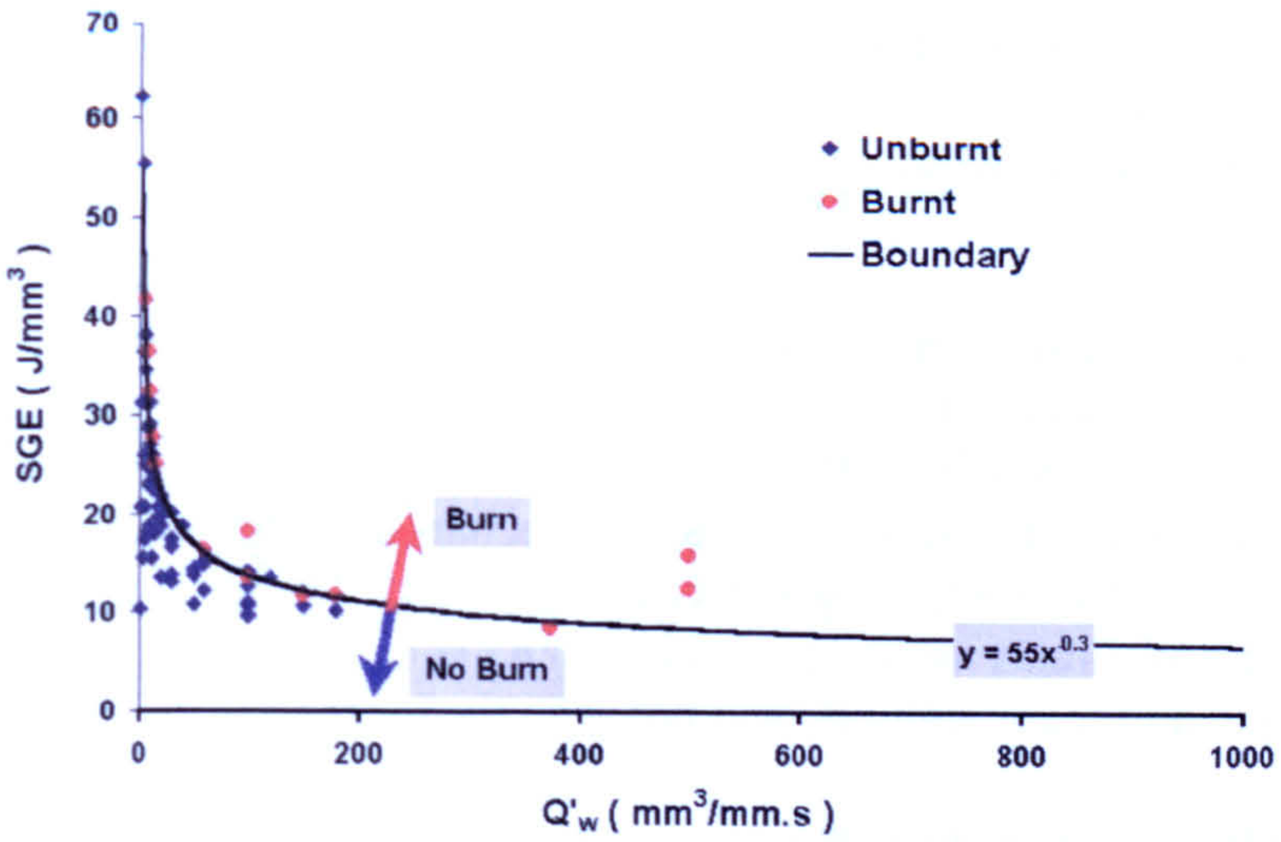

Figure 4.17 - SGE against Q'_w for W1 & W2 Grinding Trials

As discussed in *Chapter 2* a thermal model has been developed by Stephenson (2003) using the circular arc method and current energy partitioning theory. The model has been applied here to predict both contact and finished surface temperatures using the measured SGE values obtained from the grinding trials along with the grinding and material parameters.

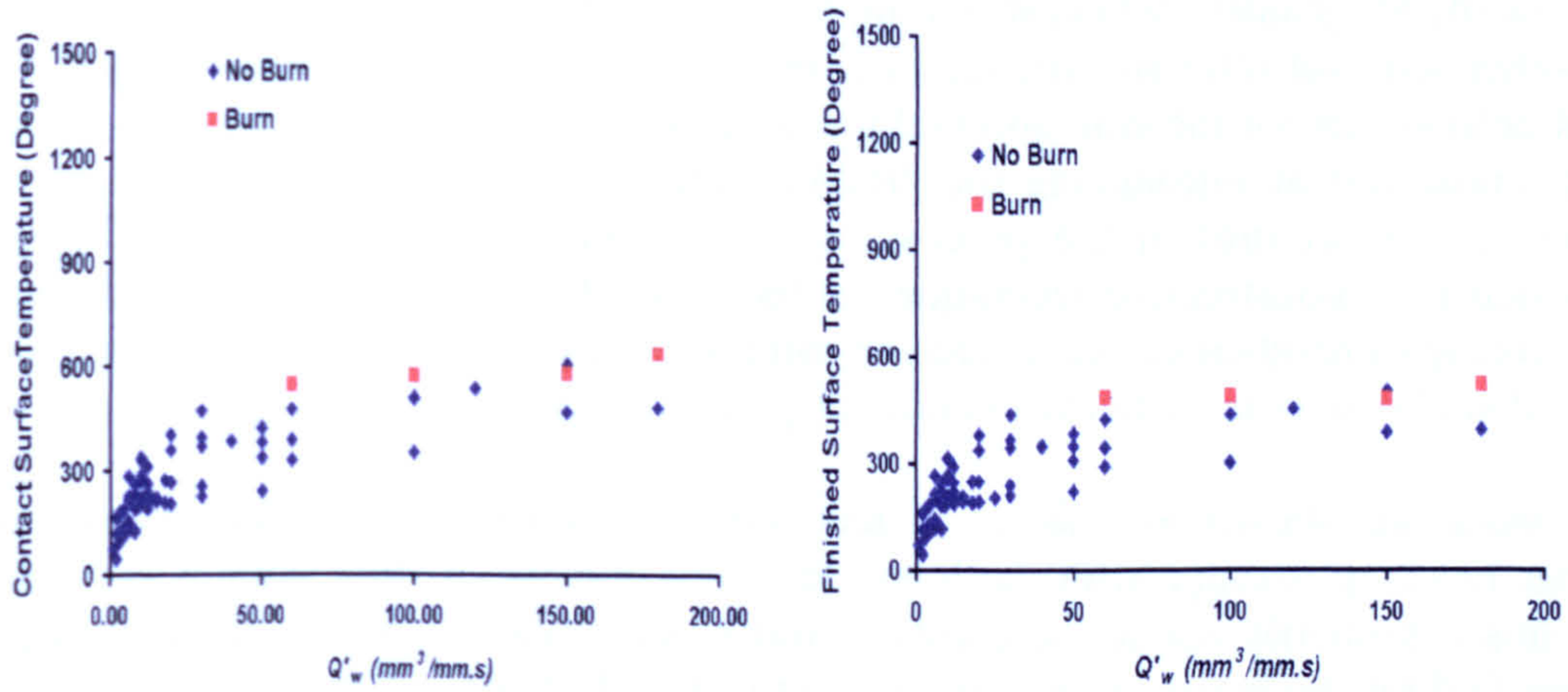

Figure 4.18 – Temperature Profiles using Thermal Modelling

The left-hand profile Figure 4.18 shows the predicted temperatures of the contact surface, the surfaces identified as burnt using the visual assessment technique are clearly above that of the unburnt samples. This provides a good degree of validation for the model as employed for this mode of grinding. The right-hand profile shown in Figure 4.18 is for the finished surface temperature and the temperatures are lower than those for the previous result. This means that although the temperature at the contact surface may exceed those acceptable, providing that the lower finished surface

temperature can be maintained below the critical level then any thermal damage to the component will be prevented.

This aligns with the findings of Tawakoli (1993), Rowe (2001c) and Stephenson (2002) who state that *HEDG* with its rapid rate of material removal coupled with a large chip size help reduce the percentage of heat produced from the grinding process entering the workpiece such that it prevents thermal damage.

At this point it is appropriate to summarize the results gained from the surface grinding *HEDG* regime trials to date. The higher grinding spindle speeds allow higher rates of material removal without thermal damage to the workpiece. These higher speeds require a greater spindle power however this is primarily as a consequence of coolant and spindle issues rather than the material removal mechanism. The requirement for higher power can be offset if the width of grind can be reduced. This means that the potential of these higher removal rates associated with *HEDG* is more appropriate for automotive crankshaft web pin and main features, and not with the journals.

There are a number of techniques that can be employed to analyse the condition of the surfaces produced, the first of these visual inspection has been shown to be of limited use as it is subjective even where no sparkout has occurred. For a potential application in cylindrical grinding where sparkout is difficult to eliminate and is often employed to improve surface finish, visual assessment is not an acceptable technique. The cross-sectional microstructural studies coupled with the micro-hardness analysis produced more reliable data as shown by the images and plots presented together with the SGE data. Both tools however are destructive, time and resource consuming which mean that they are only suitable for use in laboratory situations. These techniques illustrated again that the higher grinding wheel speed improved the performance of the process. Also that at higher removal rates the change in *SGE* which resulted in thermal damage was far smaller than that for the conventional lower removal rates. This last point is significant to the potential of introducing the *HEDG* regime into grinding operations as it may mean that the control of the process may prove more difficult. BN and XRD have provided a non-destructive technique for the detecting of thermal damage through the monitoring of residual stress. There are component size and shape limitations but these should not be an issue with the cylindrical grinding trials.

The work has shown the effects of reduced coolant levels, with the introduction of higher levels of damage with the lower levels of coolant. At this stage it is considered that this is primarily due to the ability to introduce coolant right into the grinding zone. These findings however raised the question of whether coolant reduction and increased material removal can be achieved in conjunction at this point. The initial thermal modelling using the Jaeger approach developed for conventional surface grinding has been shown to predict far higher temperatures than those found. The circular arc thermal model proposed by Jin (2002) has been shown to provide reasonable correlation to the grinding data and results. The grinding tests coupled with thermal analysis have therefore confirmed that it is possible to remove material with the *HEDG* regime in a surface mode without introducing thermal damage to a component of this material. The next stage was to undertake cylindrical mode grinding trials.

4.2 Cylindrical Grinding

The objective of these trials was to establish the Q'_w rates attainable in the cylindrical plunge grind mode and determine the existence of the *HEDG* regime. The work continued that carried out in the surface grinding trials using the same Edgetek machine tool. A spindle was added onto the rotary B-axis of the Edgetek, as shown on the left-hand image in Figure 3.6. Note that sample features were representative of the web and journal of a crankshaft. The component used, as representative of a crankshaft is shown in the right-hand image in Figure 3.6.

Thermal modelling was employed to increase understanding using the developments of the modelling carried out as part of current research activities at Cranfield University and as such the approach now covers both cylindrical peel and plunge modes. In conjunction temperature measurement and surface integrity assessment was carried out to validate the findings. As part of the development for coolant application both plain and modified segmented grinding wheels were used, see Figure 3.7 and Figure 3.8.

Table 3.4 shows the grinding parameters for this series of tests. Figure 4.19 shows the grinding power for both the web faces on the left side and journal on the right. With the web grinds the larger grit *427μm* wheel uses the least power and allows a Q'_w rate of $2300mm^3/mm.s$ to be achieved before reaching the power limit of the spindle. The *252μm* and *213μm* are closely matched in power terms. The former wheel is a dual grade made up of both *213* and *250μm* grit bands whilst the latter is a single grit wheel. The single grit wheels provide better consistency of active grit faces, but as a high proportion are active they become blunt around the same time. Whilst the dual grit wheels have a lower portion of active grit which progressively wear and allow new grit faces to come into action. Higher values for power are seen for the *213μm* and segmented *213μm* wheels running at *100m/s* (balance problem precluded running at *200m/s* due to vibration). Thus for the web feature the larger grit (*427μm*) wheel offered the best performance, lower power and higher Q'_w rates. The *252μm* dual grit wheel performed at similar levels to the single *213μm* grit but would be expected to show an advantage in the longer term as a result of its wear progression. The segmented wheels although offering better coolant application did not show any advantage with higher power and therefore probably higher levels of thermal energy being introduced into the component's surface.

For the journal features with the 427*μm*, 252*μm* and 213*μm* wheels running *at 200m/s* a Q'_w rate of $300mm^3/mm.s$ was achieved. The segmented 213*μm* wheel shows an advantage in the form of reduced power levels. No results are shown for the modified segmented wheel, initial work demonstrated that the through wheel coolant channels effectively placed coolant at the wheel periphery using far lower levels of coolant and power. However this resulted in a far greater level of coolant atomisation within the machine enclosure with which the extraction system was unable to cope with. This in turn resulted in a flash explosion followed by a fire during the early stages of testing. With the high probability of this reoccurring and further damaging the machine without additional development and production of new wheel coolant channels this direction of work was not continued at this stage.

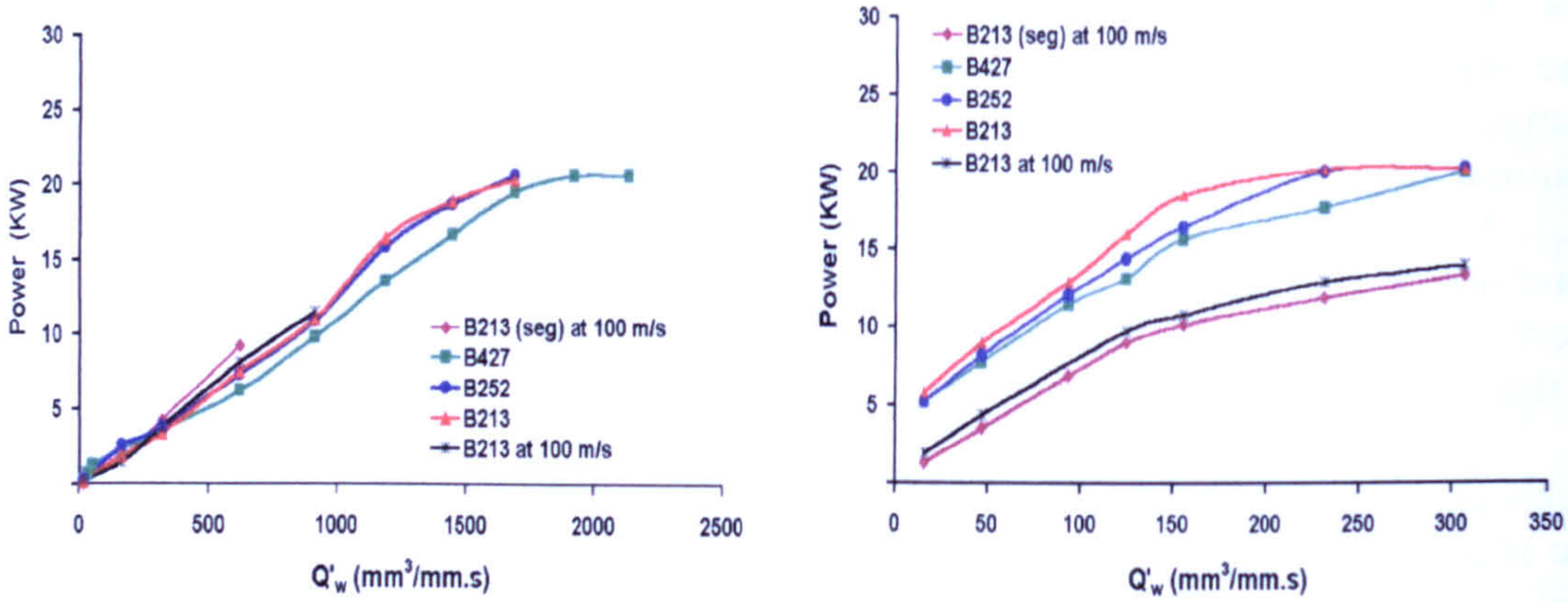

Figure 4.19 – Power v Q'_w for Web & Journal Grinds

Figure 4.20 shows the *SGE* versus Q'_w for the web and journal grinds. The results follow the trend observed previously in the surface grinding trials, the *SGE* leveling out at the *6* to *10 J/mm³* magnitude, and the larger grit wheels requiring lower energy levels. The point at which the spindle power becomes limited is shown by the dotted line and provides a realistic operating boundary for the Edgetek machine under these conditions. This translates to removal rates of *1100mm³/mm.s* for the web and *150mm³/mm.s* for the journal features, dependant on the width of grind.

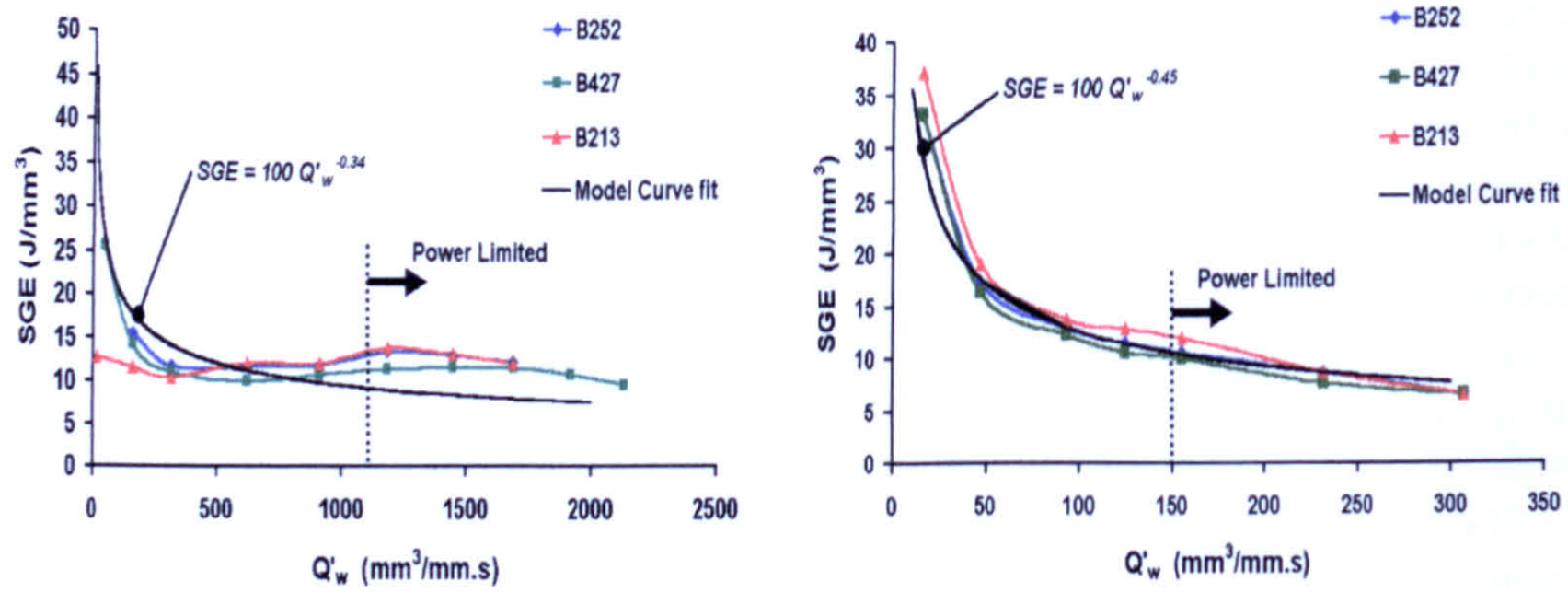

Figure 4.20 – SGE v Q'_w for Web & Journal Grinds

The Edgetek machine operates solely in a constant velocity mode, thus the material removal rate changes with the diameter. This effect was quiet small in the case of the journal features, however for the web features the effect was significant. To illustrate maximum Q'_w attained at the beginning of the web grind was the change in magnitude from the beginning in excess of *3500mm³/mm.s*. Because of this change in the web grinds interpretation of the results in relationship to Q'_w was more difficult. For the power and energy results presented the data from the midpoint of the grind was used for which the Q'_w rate was calculated. Subsequent residual stress readings and microstructural samples were taken at this point to ensure correlation. Finally in order to carry out the thermal modelling it was necessary to determine a relationship in the form of Equation 4.2 to represent the grinding performance.

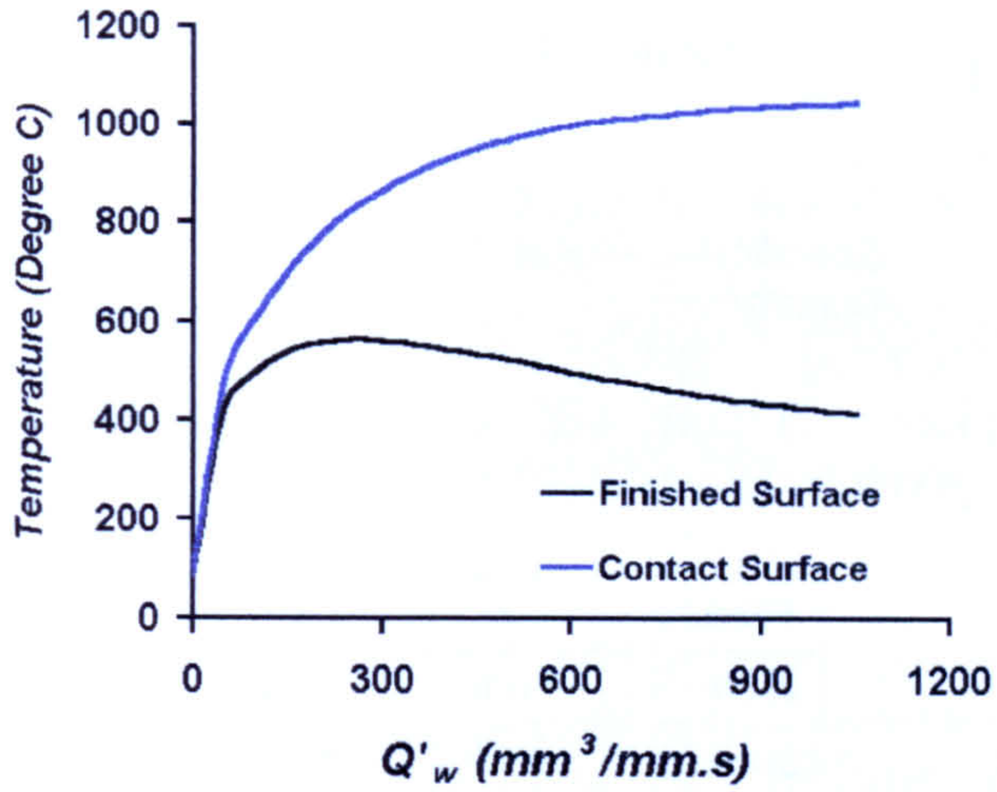

Figure 4.23 – Thermal Modelling Result for Web Grind

The thermal model has been verified using a novel temperature measurement developed for cylindrical grinding, by using a split testpiece as shown in Figure 3.9, the an inner surface is coated with a thin PVD coating of known melting point. Three coatings with a range of melt temperatures were used and the set ground under the same grinding conditions. Four sets of coatings were used to cover a range of grinding parameters ranging from a Q'_w of $200mm^3/mm.s$ through to $750mm^3/mm.s$

Post grind the testpieces were split to determine the melt depth of the PVD coating on each sample. Figure 4.24 through to Figure 4.27 shows the measured depths for each set of coatings and for the four Q'_w rates tested.

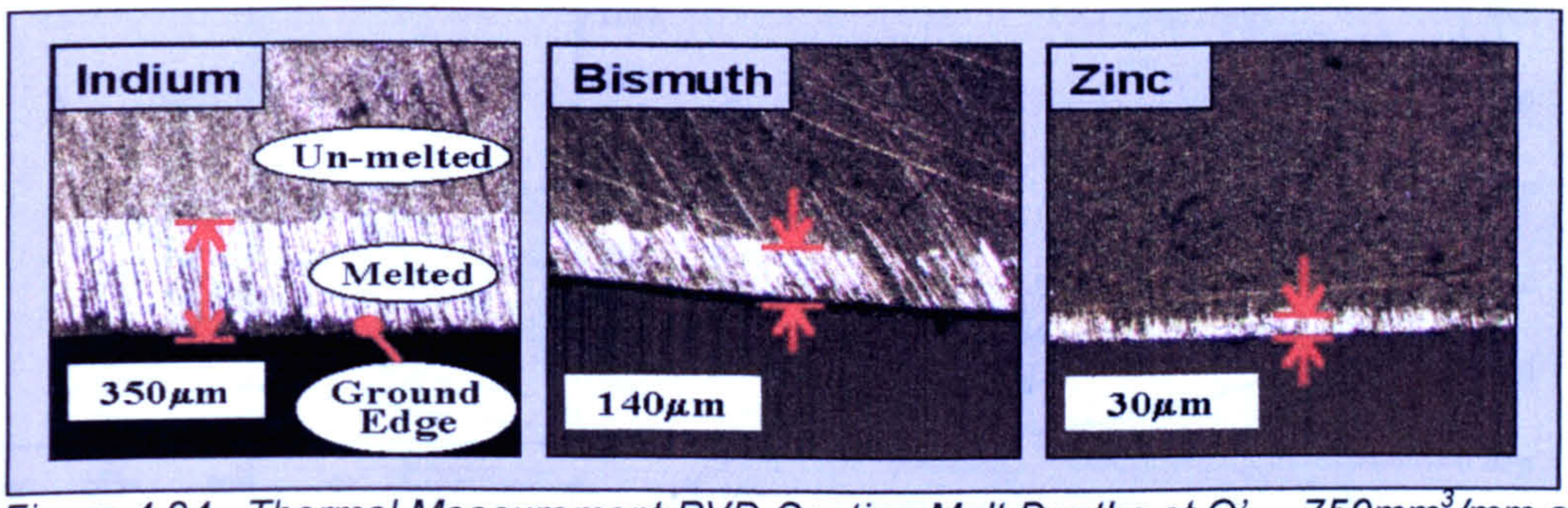

Figure 4.24 –Thermal Measurement PVD Coating Melt Depths at Q'_w - $750mm^3/mm.s$

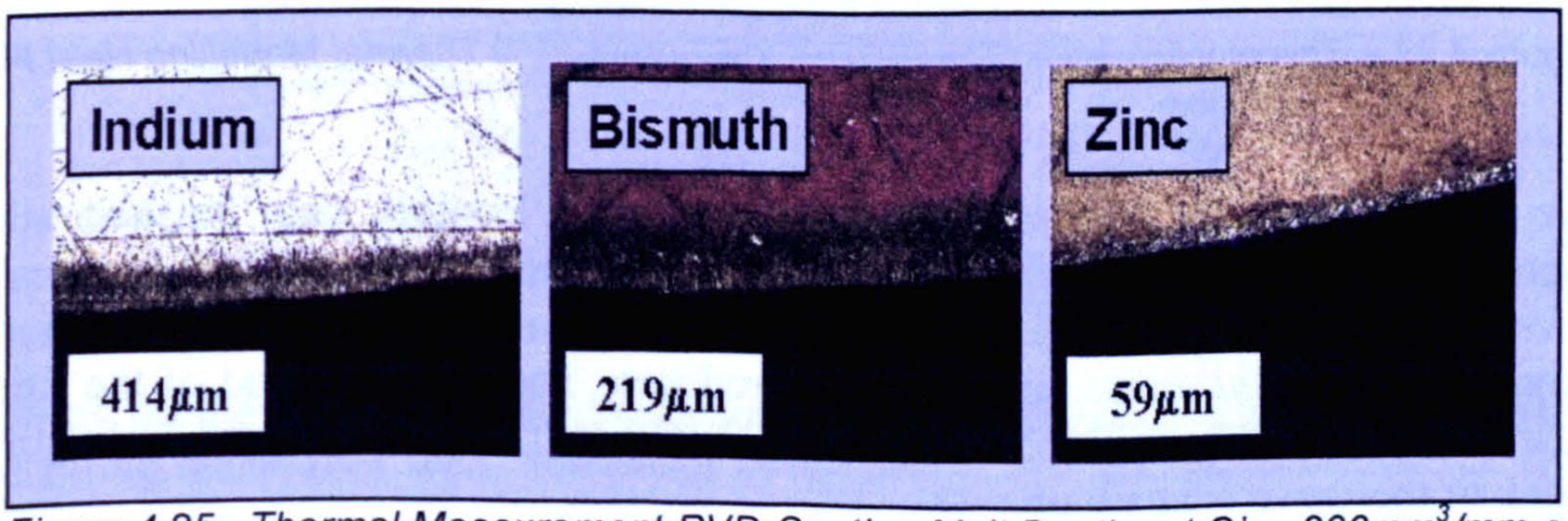

Figure 4.25 –Thermal Measurement PVD Coating Melt Depths at Q'_w - $200mm^3/mm.s$

$$u = A.(Q'_w)^{-t}$$

Equation 4.2– Thermal Modelling Power Relationship

Where:

u	-	*Specific Grinding Energy*	*(J/mm^3)*
Q'_w	-	*Specific Material Removal Rate*	*($mm^3/mm.s$)*
A & t	-	*Constants*	-

From the previous plots in Figure 4.20 values for the required parameters were established. These are given in Table 4.3.

Feature	*x*	*t*
Web	*100*	*0.34*
Journal	*100*	*0.45*

Table 4.3 – SGE Versus Q'w
Modelling Parameter Values

The thermal model (Stephenson, 2003) was applied using the relationship from Equation 4.2 for the web grinds. Figure 4.21 shows the partition ratios for the thermal energy distribution. Partitions for the wheel and fluid fall as Q'_w increases but are more than offset by an increase for the grinding chips. The final component for the workpiece peaks then falls with increasing Q'_w. Figure 4.22 illustrates the effect with regard to the heat flux, the overall level continues to rise but the amount reaching the workpiece surface peak then falls with Q'_w.

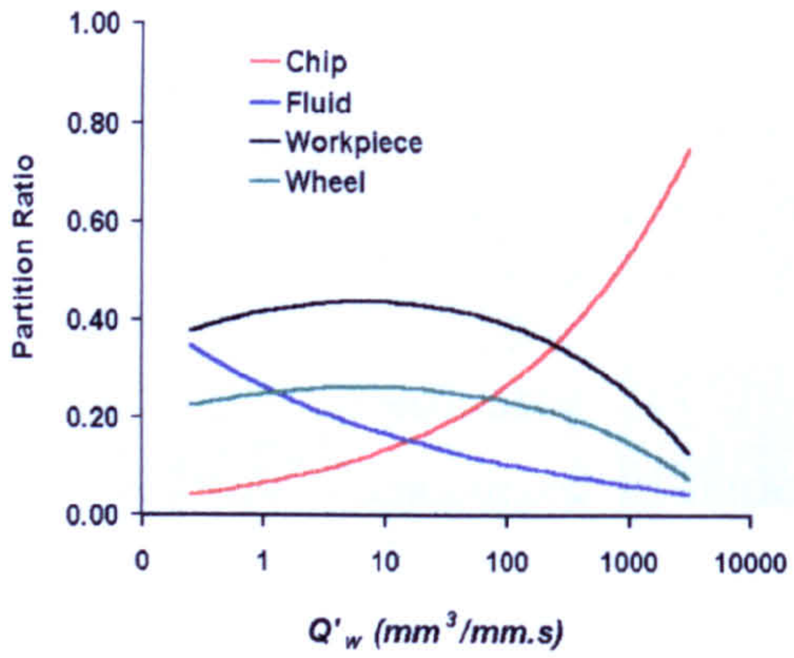

Figure 4.21 – Thermal Modelling Partition Ratios

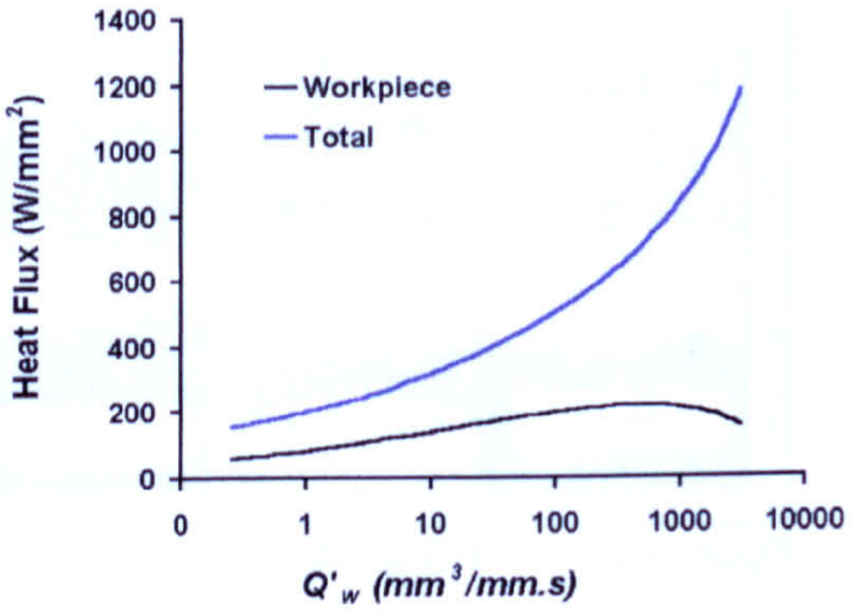

Figure 4.22 – Thermal Modelling Heat Flux

Figure 4.23 shows the model results for both the contact and finished surface temperatures. The contact surface temperature continues to rise with the increase in removal rate, whereas the finished surface temperature reaches a maximum at approximately $300mm^3/mm.s$, after which it reduces. The thermal trend of the finished surface matches that shown by Tawakoli (1993) for *HEDG* in a surface grinding mode, the peak of the curve is at a higher Q'_w.

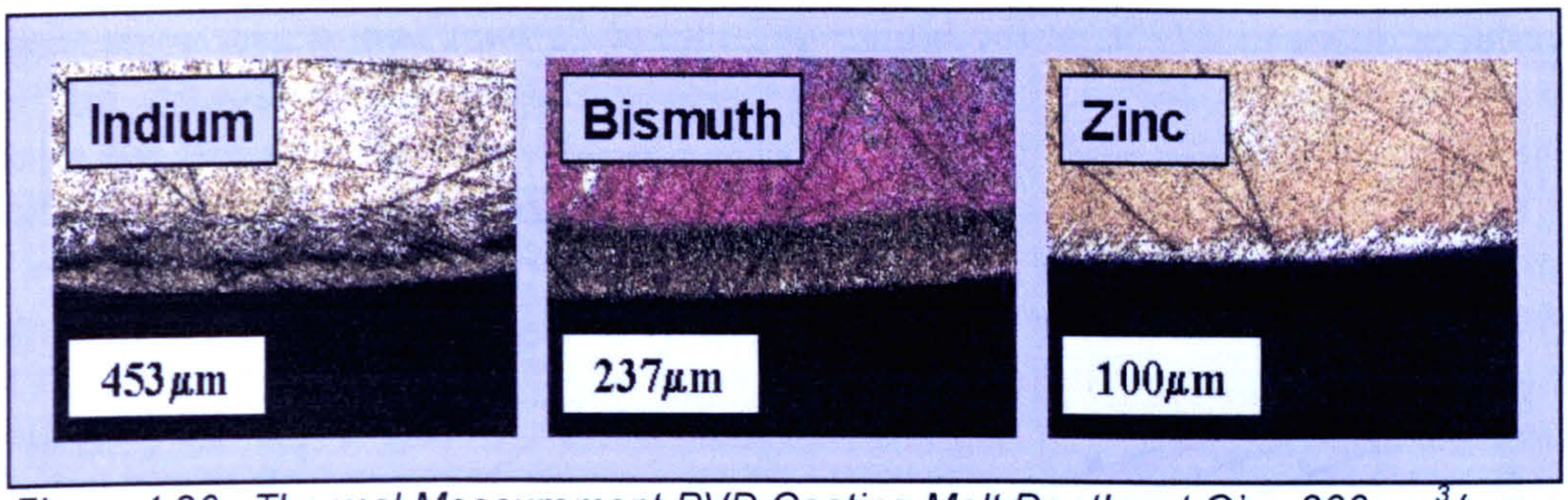

Figure 4.26 –Thermal Measurement PVD Coating Melt Depths at Q'_w - 300mm^3/mm.s

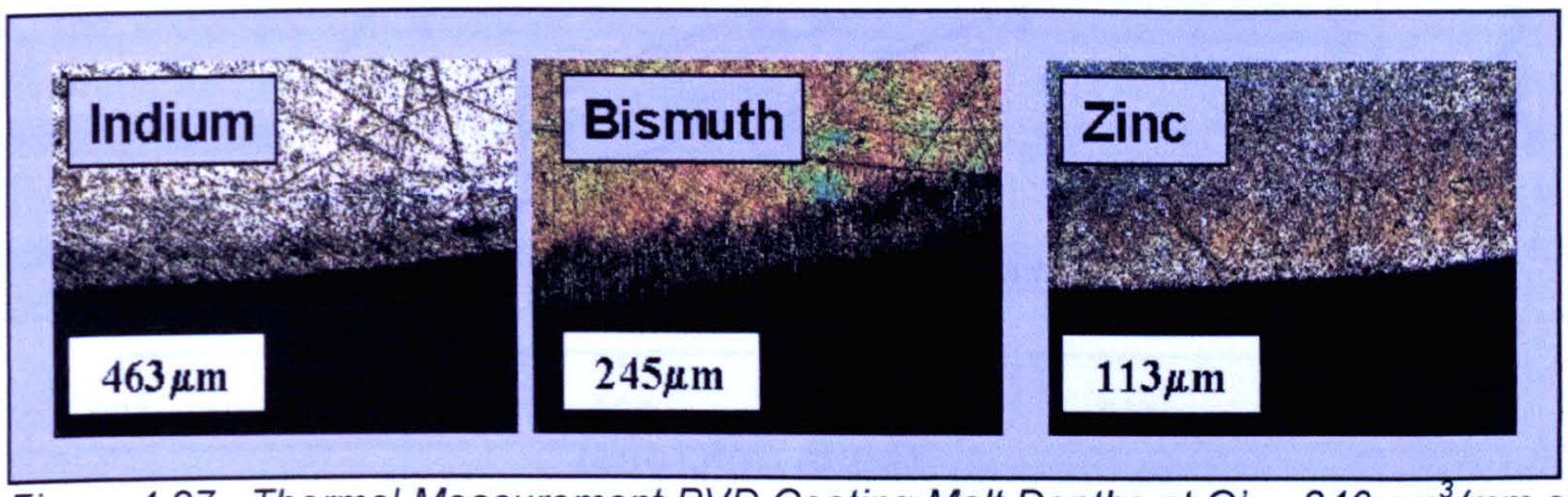

Figure 4.27 –Thermal Measurement PVD Coating Melt Depths at Q'_w - 340mm^3/mm.s

The measured depth data is shown in Figure 4.28 along with the spread of the readings. The maximum working depth (d_{max}) for the coatings is defined as derived from Equation 3.4.

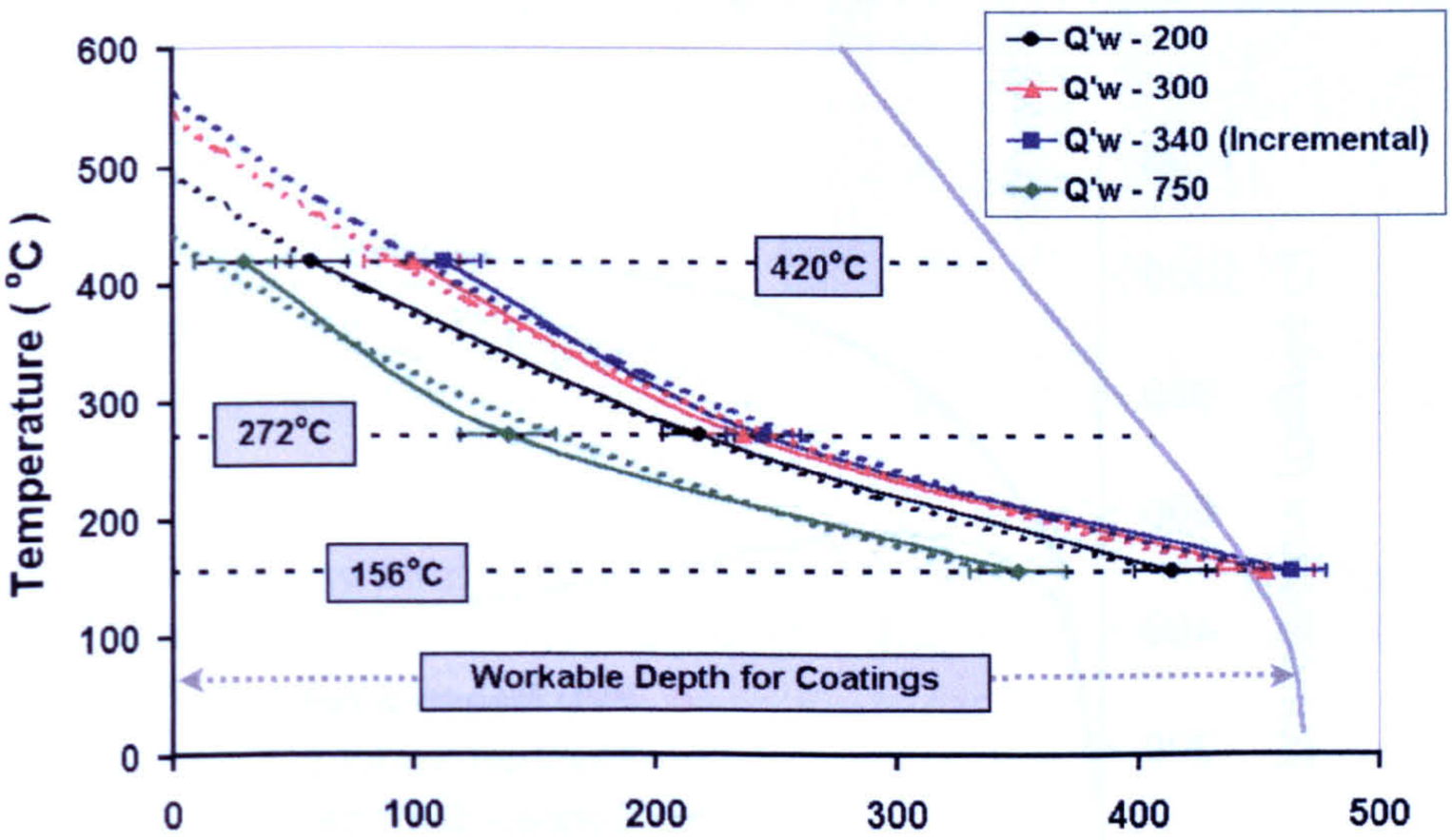

Figure 4.28 – Grind Temperature Measurement Profile

Following on the data was plotted on a log scale as shown in Figure 4.29. Exponential curve fitting techniques were employed to determine the intersection with the vertical axis, the value representing the finished surface temperature. The results follow that of the residual stress findings, the temperature increases from *496°C* at *200 mm^3/mm.s* to

$544\ ^{o}C$ and $563\ ^{o}C$ at $300mm^3/mm.s$ and $340mm^3/mm.s$ respectively. The temperature then reduces down to $442\ ^{o}C$ at the higher Q'_w rate of $750mm^3/mm.s$.

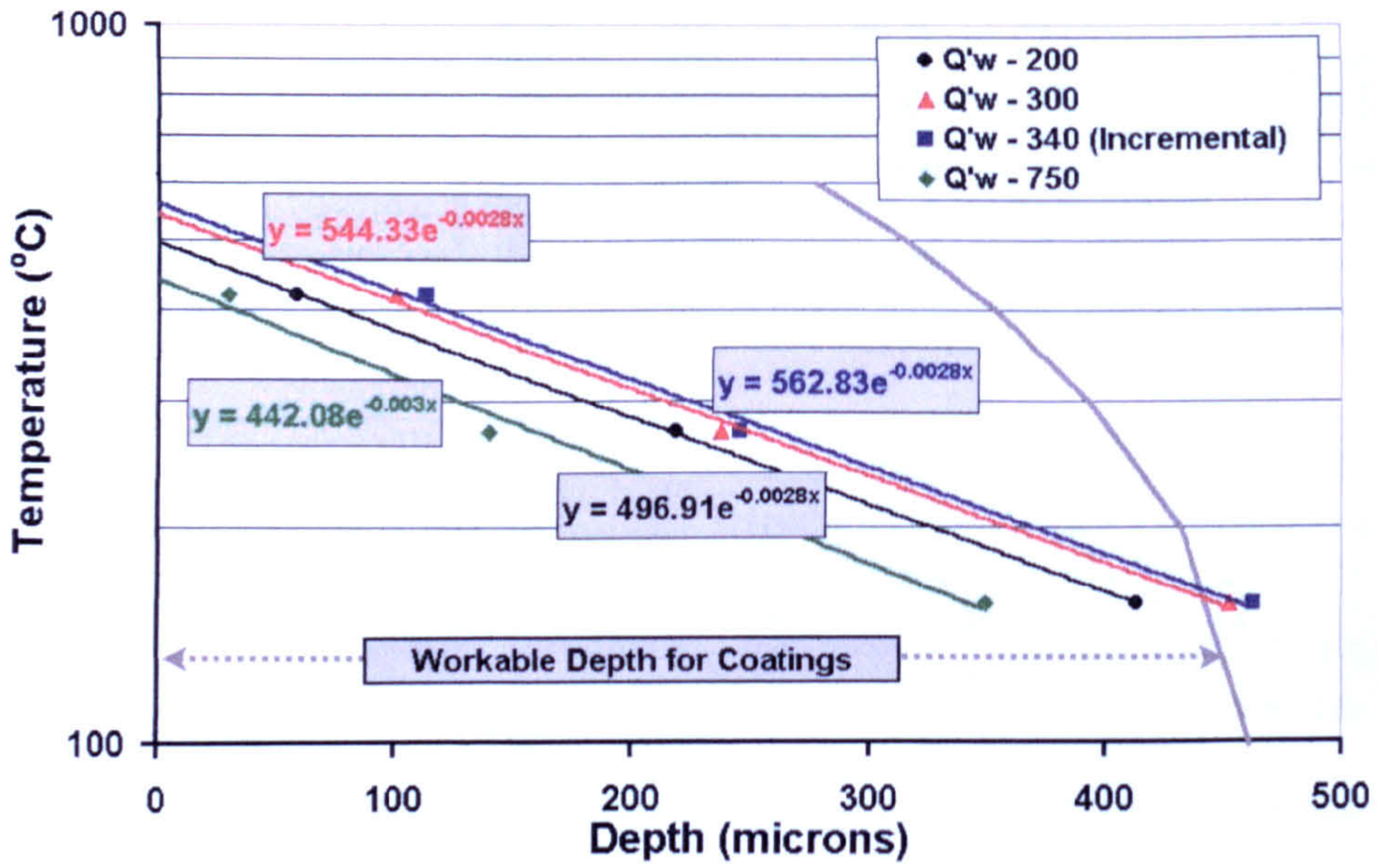

Figure 4.29 – Grind Temperature Measurement Log Profile

Figure 4.30 shows both the measured and modeled values for the finished surface and it can be seen that the measured data compares favourably. Thus it was concluded that the modelling was valid in the cylindrical plunge-grinding mode.

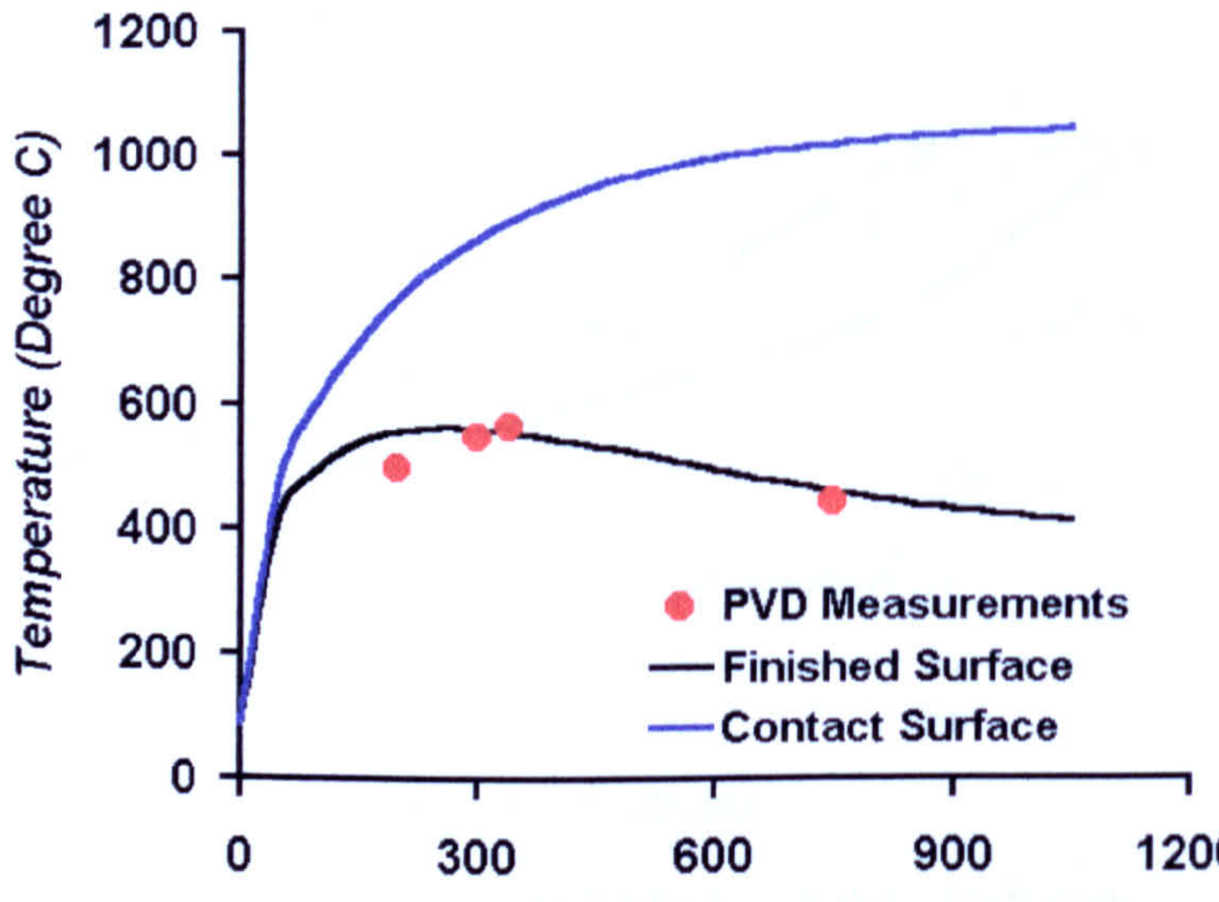

Figure 4.30 –Temperature Measurement & Modelling Comparison

The next stage was to carry out analysis of the surface integrity, for which both residual stress and microstructural measurements were made. The plot in Figure 4.31 shows readings for the web faces within the previously identified usable power range. The magnitude of readings is seen to grow from $200mm^3/mm.s$ up to around $350mm^3/mm.s$ after which point it begins to drop. This signifies that undesirable tensile stresses are being introduced as the removal rate climbs to the $350mm^3/mm.s$ level, once above this point the grinding returns to producing a near surface zone with a compressive stress condition. This curve follows the thermal modelling and measurement results thus validating those findings. Finally the surface integrity of a sample ground at a Q'_w of $750mm^3/mm.s$ was examined using microstructural analysis. Figure 4.32 shows the result, the cross-section together with high magnification images of the polished and etched areas are shown. The three areas corresponding to the sidewall bottom, corner, and bottom surface of the grind and it can be seen that there is no visible signs of significant thermal damage. This result supports the conclusion that the *HEDG* process prevents high levels of heat in the finish zone and so thermal damage can be avoided in the component's surface.

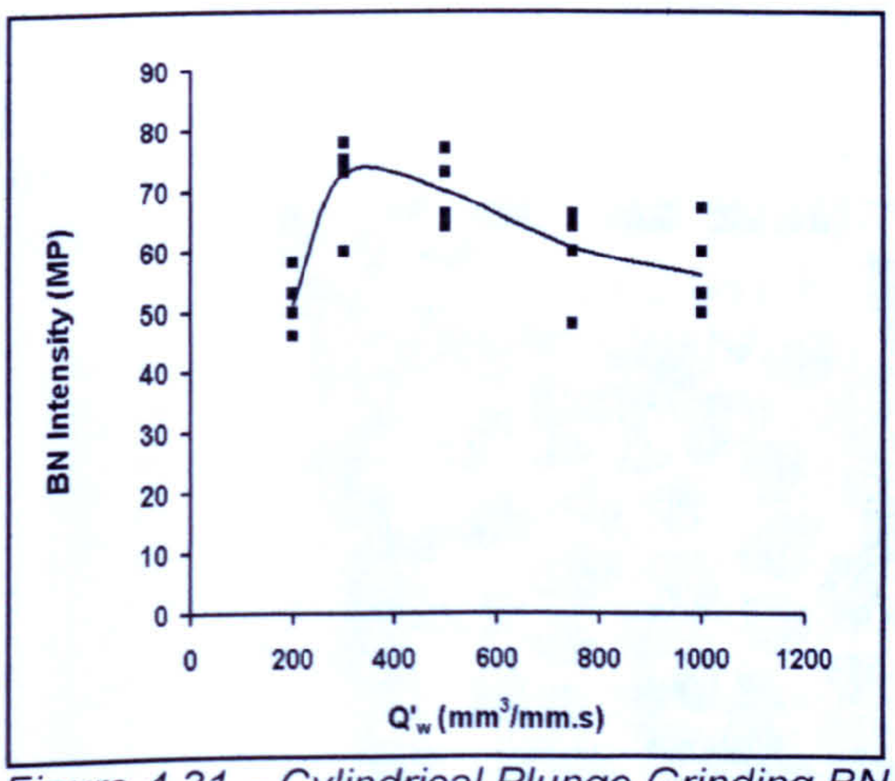

Figure 4.31 – Cylindrical Plunge Grinding BN Intensity Readings

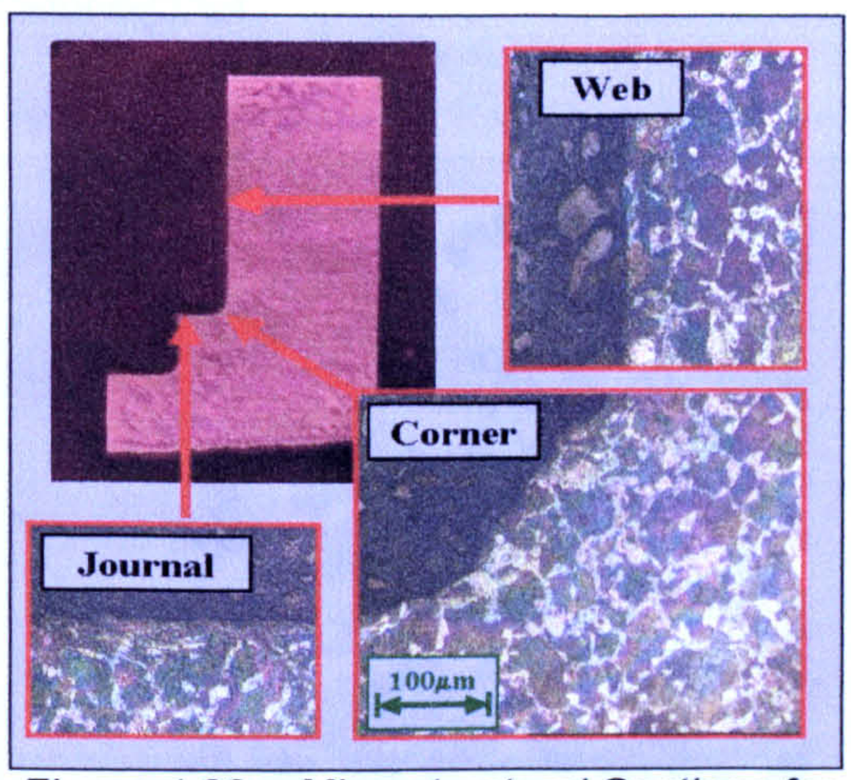

Figure 4.32 – Microstructural Sections for Sample Ground at $750mm^3/mm.s$

Finally if the BN intensity results are combined with those of the thermal modelling and measurement data, see Figure 4.32, it can be seen that there is reasonable correlation at the higher Q'_w levels of *HEDG*.

The final stage of these trials was to establish that the higher demands placed on the wheels by the *HEDG* process was not causing generalised grit failure. This was done by examining the wheel surfaces using basic optical techniques and making a visual assessment. Unused and used edges on each wheel were inspected, typical images are shown in Figure 4.34. There was no sign of any significant degree of either grit or bond wear and so it was concluded that the wheels selected were suitable for use in the *HEDG* regime.

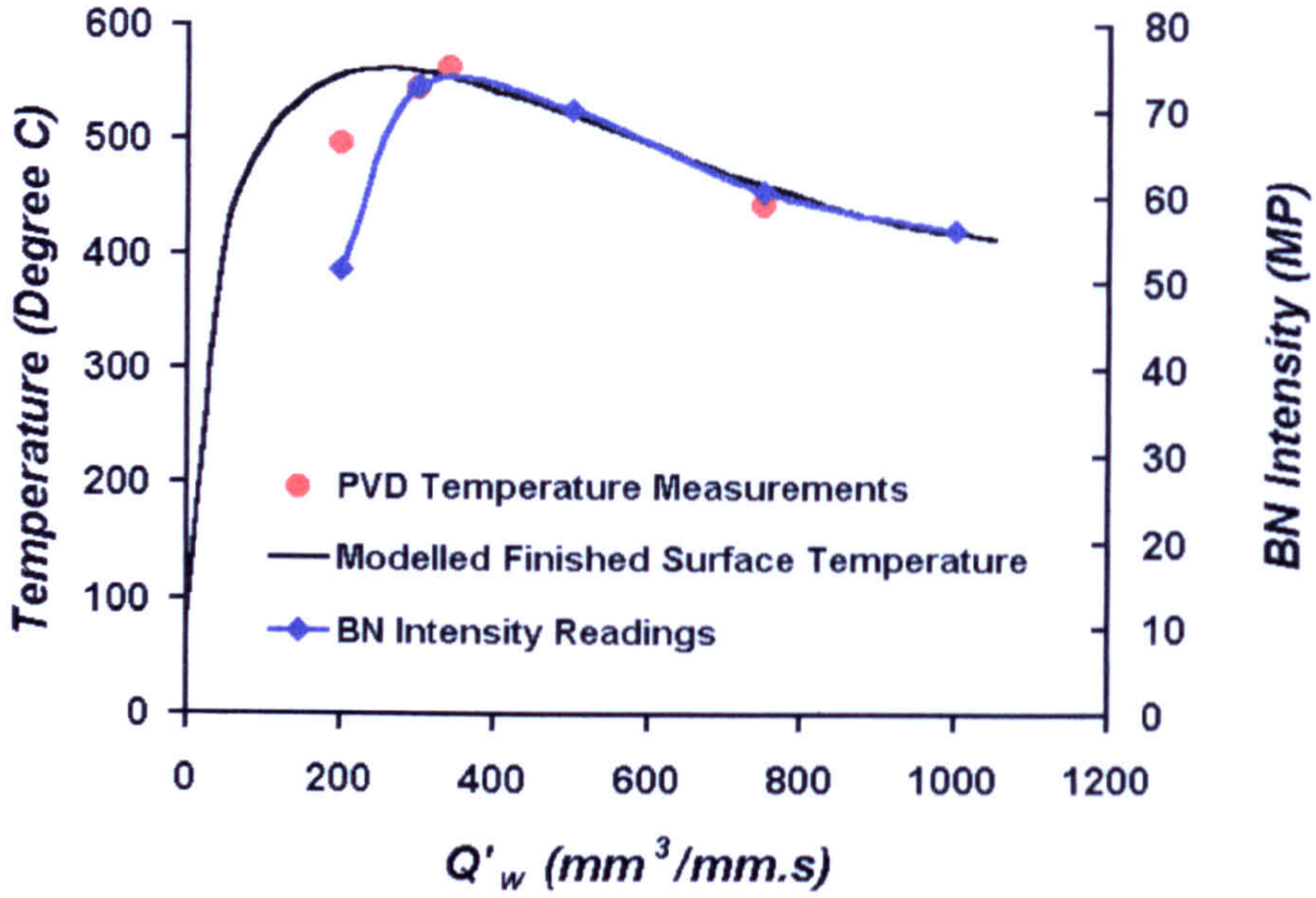

Figure 4.33 – Thermal modelling, Measurement and BN Intensity Results for Cylindrical Plunge Grinding

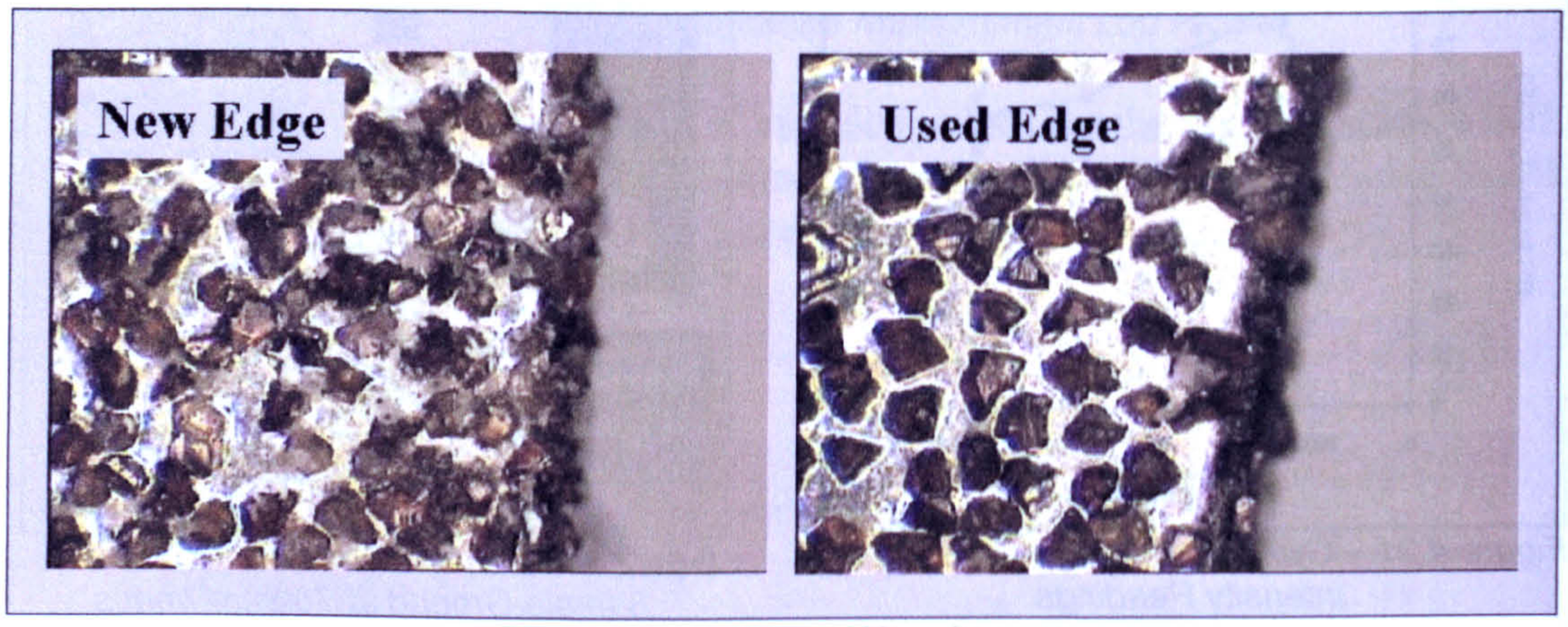

Figure 4.34 – Wheel Wear Images

4.3 Production Cylindrical Grinding

There were two stages to this part of the research, the primary aim was to establish the viability of *HEDG* as a process for the production of rough machined crankshafts. Full details of the grinding machine tool have been given in Chapter 3.

The initial portion of work covered a Q'_w range from *80* up to *2000mm³/mm.s* and tested a number of a number of different grinding wheels at cutting speeds from *120* to *180m/s*. This provided an opportunity to transfer the previous research findings to a production environment and so validate HEDG in that situation. A total of 100 crankshafts were ground primarily concentrating a material removal at this point analysis was carried out for spindle power, surface integrity in the form of residual stress and wheel performance. Finally thermal modelling was done

The second stage took the research the final step into the production of full form crankshaft components. There were two sections in this stage, the initial part involved the grinding of *50* components at Q'_w rates of $1000mm^3/mm.s$ for the web feature and $250mm^3/mm.s$ for the main and journals. Then a further 20 components at slightly reduced rates. All the rates used are given in Table 3.8. Power data was monitored and residual stress measurements carried out on a crankshaft from each batch.

The second part of the trial involved a batch grind of approximately 950 crankshafts at Q'_w rates of $250mm^3/mm.s$ for the web features and $200mm^3/mm.s$ for the main and journals diameters. At the conclusion of this batch shafts from the beginning and end were analysed for geometric conformity and surface integrity, this was carried out in conjunction with a major automotive manufacturer. The mean power trend was compiled from spindle power cycle data to establish process stability. Analysis of the grinding wheels were carried out by a major grinding abrasive manufacturer, the results from this provided realistic data for wheel wear and life. A typical wheel life for rough grinding varies between 1000-2000 components.

4.3.1 Initial HEDG Validation

The work was carried out with production crankshafts supplied by a major automotive manufacturer, a typical shaft is shown in Figure 4.35. Five grinding wheels were obtained four for use in the grinding trials and one to provide a benchmark 'as supplied'. The wheels as are listed in Table 4.4.

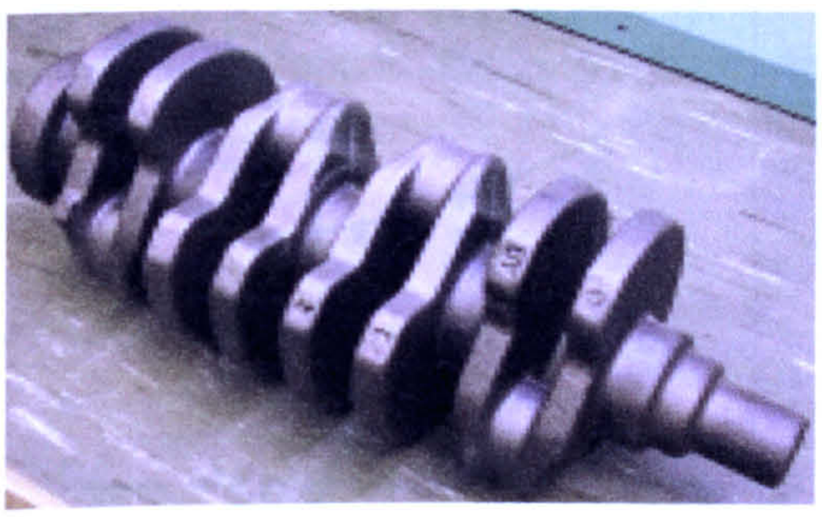

Figure 4.35 – Automotive Crankshaft & Grinding Wheels used for Trials

Serial No	Grit Size	Type
26000280 -1	B356	Normal
26000280 -2	B356	Normal
26000279	B252	Normal
26000278	B356	Segmented
26000277	B252	Segmented

Table 4.4 – Grinding Wheel Specifications

Initial tests investigated the performance of the four grinding wheels a normal and segmented $252\mu m$ and $356\mu m$ at three wheel speeds, *120m/s*, *150m/s* and *180m/s*. *180m/s* was the maximum wheel-head speed obtainable on this production machine. Work was primarily centred on the Web grinds as these offered the greatest potential for improvement in cycle time, having the longer grind path. The following results show the web grind data obtained for all the wheels at the three speeds. Figure 4.36 shows the $252\mu m$ wheel plots, with the normal on the left and segmented on the right. In the latter instance the wheel did not operate satisfactorily, this being illustrated by the wide scatter of results suggesting that it was not operating under stable conditions. The results obtained with the normal wheel show a similar trend to that seen with the previous cylindrical plunge grind trials carried out on the Edgetek machine. The higher speed grinds requiring greater energy at the lower Q'_w whilst at higher levels the energy converged to a level of $10J/mm^3$.

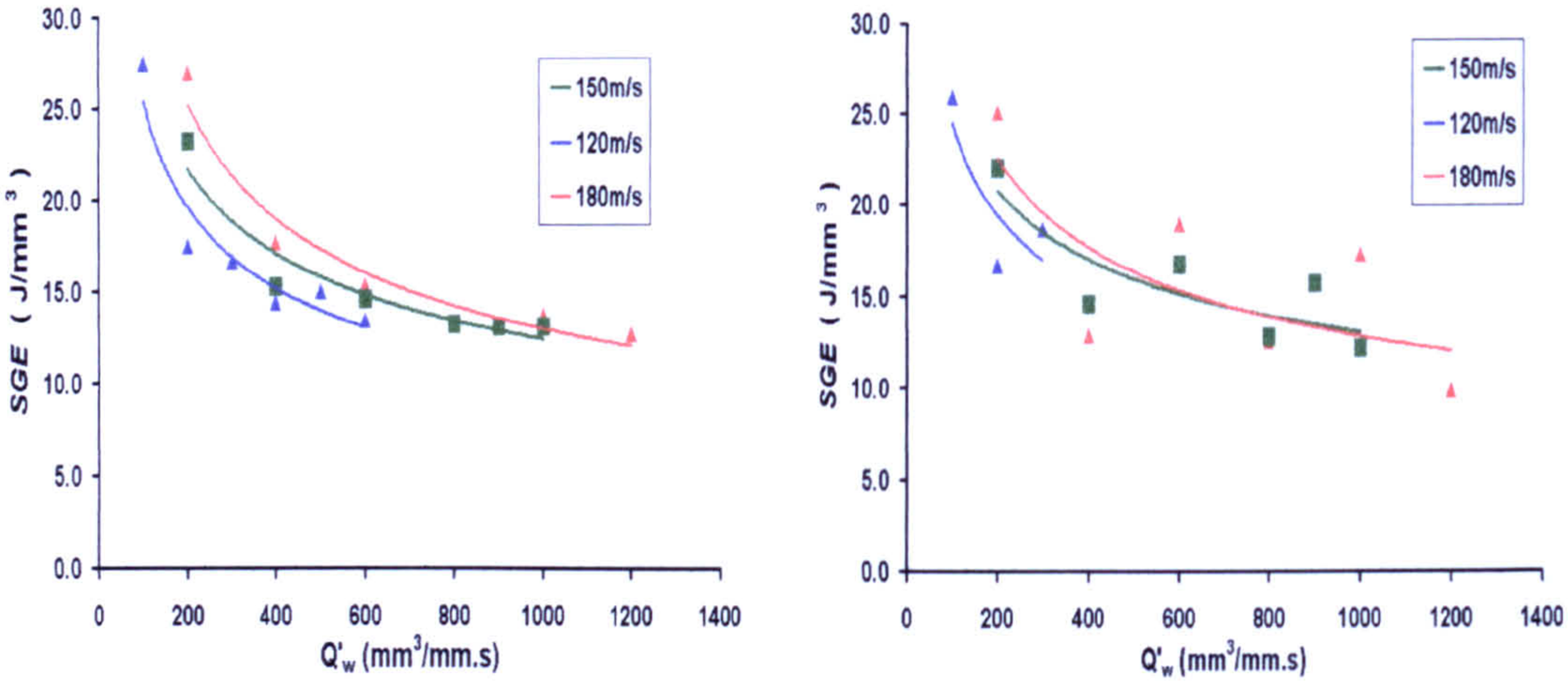

Figure 4.36 – SGE v Q'_w Plot for 252µm Normal & Segmented Wheels

Figure 4.37 shows the *356µm* wheel plots, with the normal on the left and segmented on the right. In this case both wheels showed a similar trend to that seen with the previous cylindrical plunge grind trials carried out on the Edgetek machine.

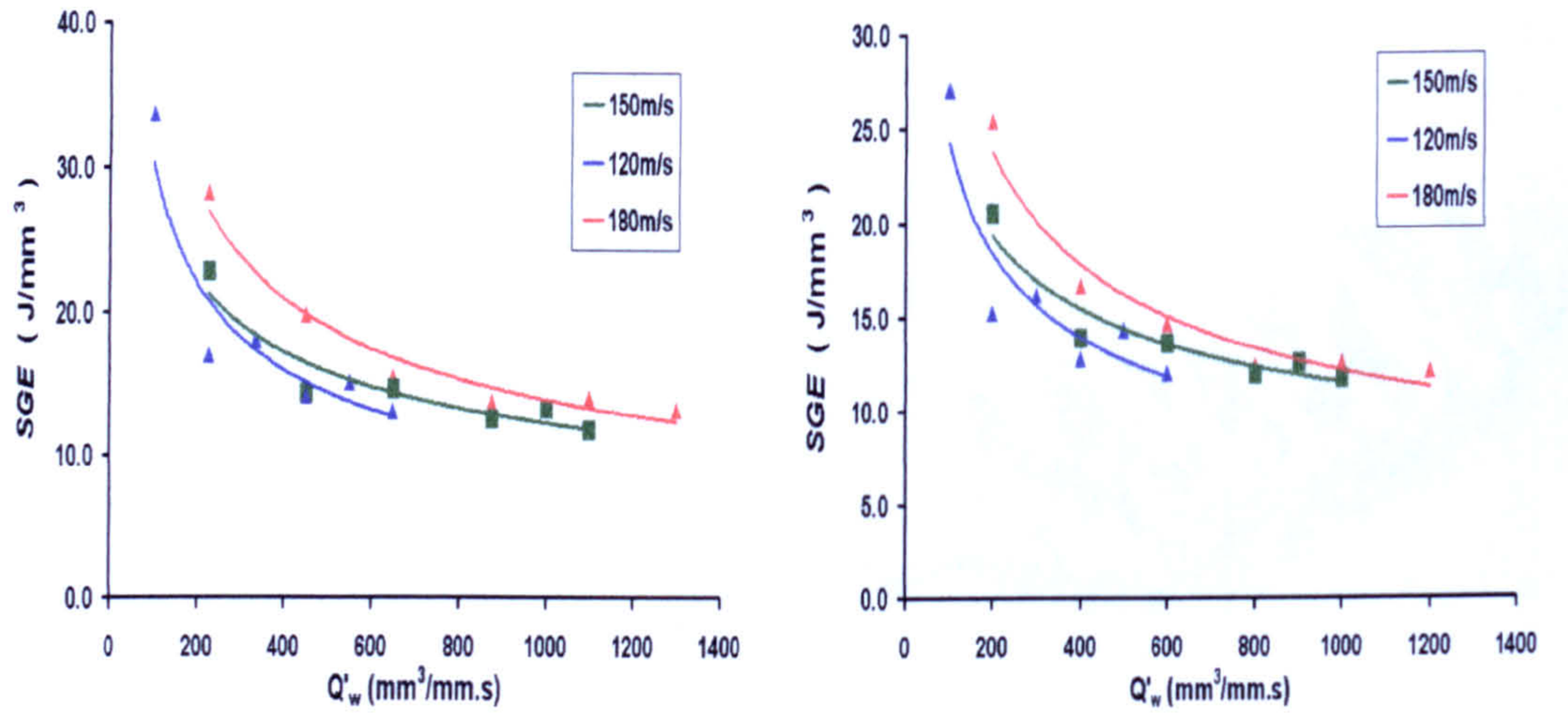

Figure 4.37 – SGE v Q'_w Plot for 356µm Normal & Segmented Wheels

With both wheel sizes the higher wheel speed allowed greater Q'_w rates to be achieved. Figure 4.38 shows the *SGE* versus Q'_w in the case of the higher wheel speed (*180m/s*) for all the grinding wheels tested. This shows that Q'_w rates of up to $2000mm^3/mm.s$ were attained on the Web grinds. A corresponding figure for the journals was a Q'_w of $250mm^3/mm.s$, in this case the limiting factor was one of total available spindle power. The segmented wheels offered a reduced energy consumption at the lower rates of Q'_w applicable to the journal features but not at the higher levels used on the web features. As was the case with the previous work the results can be represented by a power curve such as those shown. The values shown on the chart broadly follow those previously discussed and hence it was concluded that the thermal modelling conditions still remained valid in this production environment.

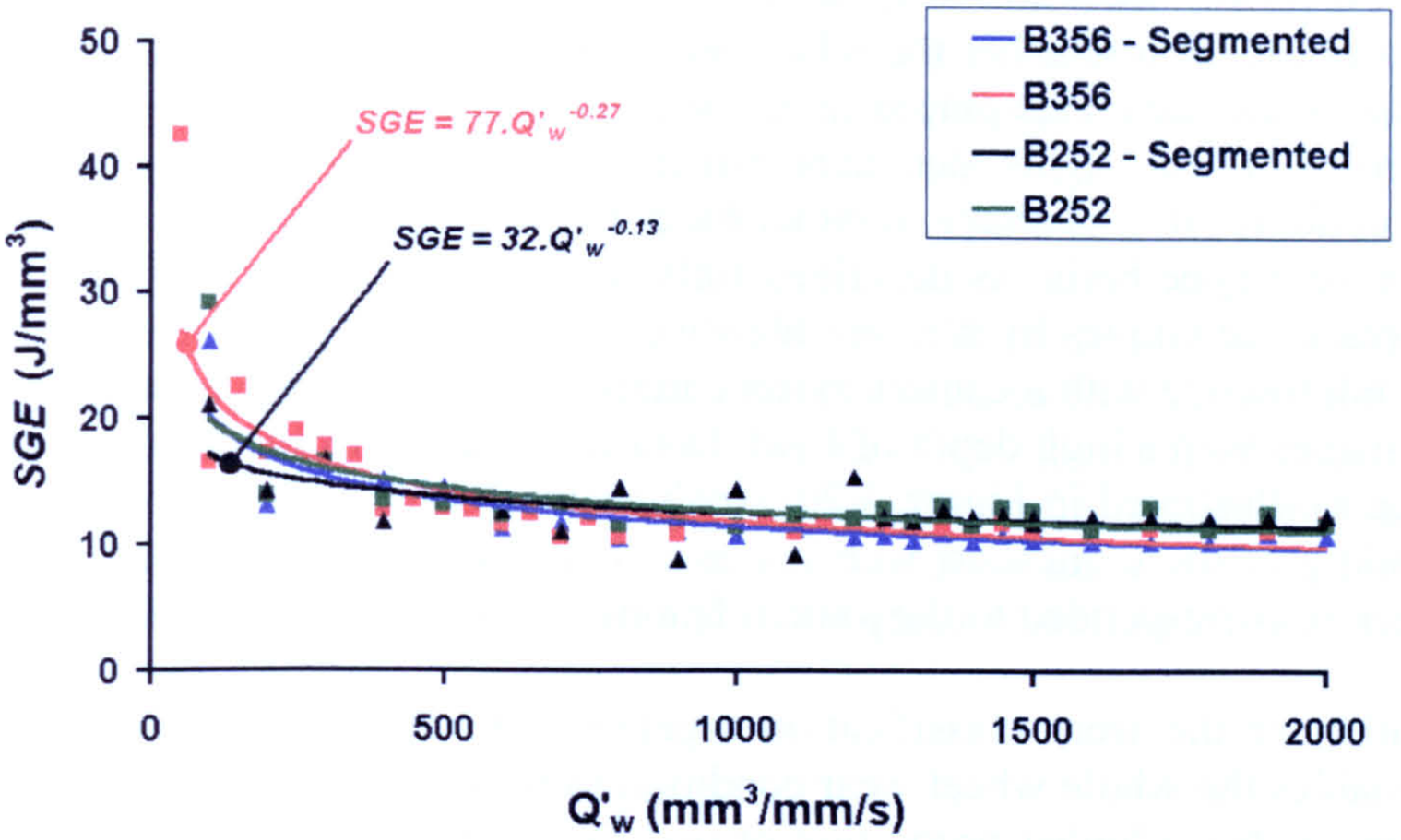

Figure 4.38 – SGE v Q'_w for all Wheels at 180m/s

As for the previous trials Barkhausen Noise intensity data was collected from the testpieces, in this case crankshafts in order to determine the residual stress state. Figure 4.39 shows the data form the web faces of the crankshafts. The trend is similar to that found previously with readings rising up to a Q'_w of approximately $350mm^3/mm.s$ then dropping off again. Therefore as before it was concluded that once a value of above $500mm^3/mm.s$ had been reached the residual stress state was one of compressive stress. This in turn demonstrated that the thermal energy at the finished surface of the component had not reached unacceptable levels.

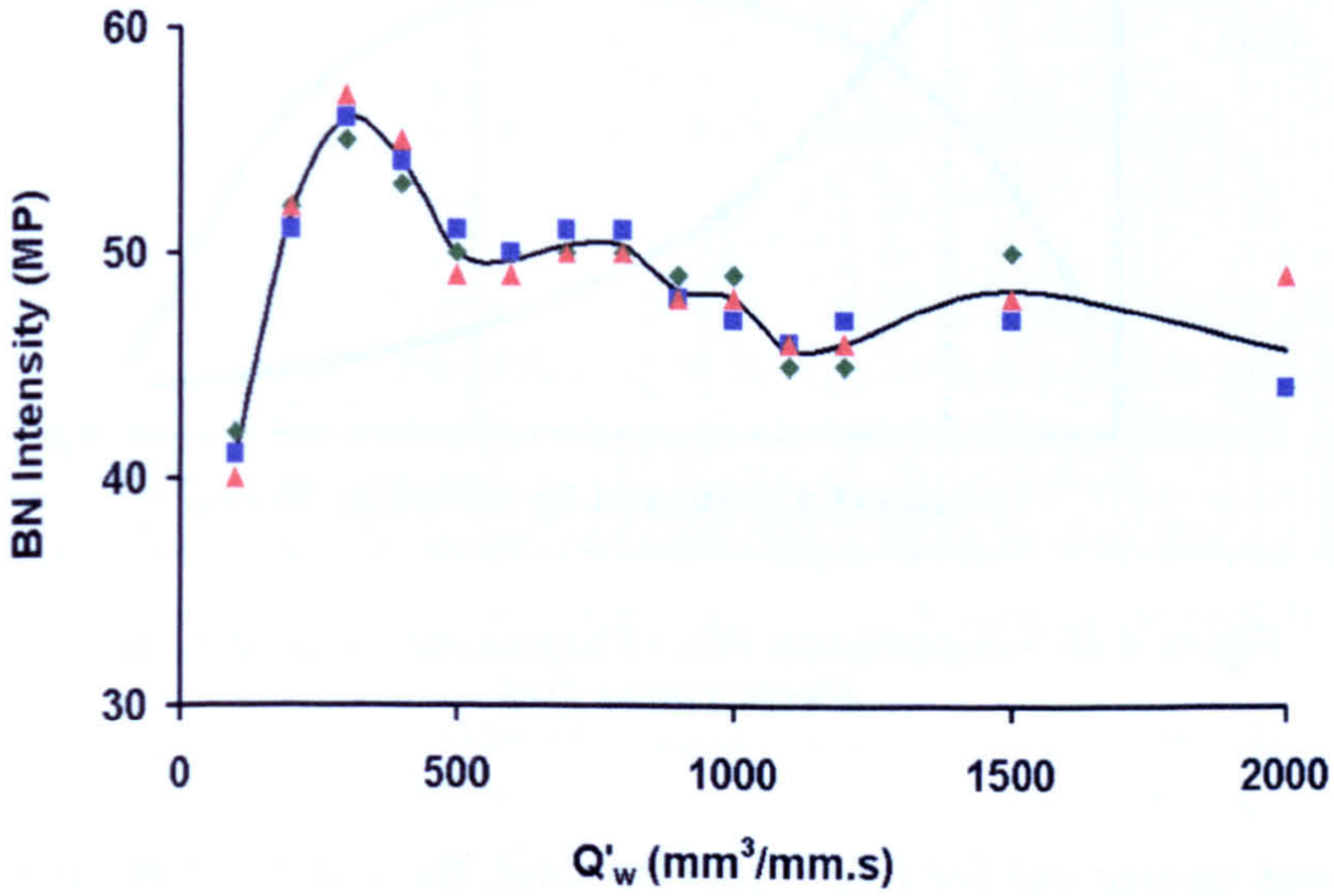

Figure 4.39 – Residual Stress Measurement on Web Face

The final part of the initial production validation was to examine the grinding wheels for any signs of damage or wear. Due to the relatively small number of crankshaft's ground, approximately 100 shafts, it was not possible at this stage to be able to establish realistic

figures for wheel life, this was done in the later trial. However the analysis was expected to establish whether there had been any significant deterioration in the wheels due to the higher demands placed on the wheels by the *HEDG* process in a production environment. These higher demands primarily in the form of higher thermal shock loading could result in damage to either the abrasive grit itself or the electroplated bond structure, or maybe both. As described fully in *Chapter 3* the analysis was carried out using optical techniques by a major abrasive manufacturer. The wheels were mounted under a microscope with a camera system attached, montage techniques were utilised to obtain images with a high depth of field. Data was collected from both the wheel centre and edge as illustrated in Figure 3.20. Analysis results from the wheel edges related to the grinding of the crankshaft web feature – high Q'_w long path grind – whereas the wheel centre corresponded to the journal feature – lower Q'_w short path.

Application of the wear classification together with the analysis of their respective levels enables the whole wheel wear condition to be determined see Figure 4.40. In this chart '*line A*' has a higher proportion of particles in the "New" category and a smaller proportion in the "Deep Hole" category, whereas '*line B*' has a higher proportion of microfractured and deep hole with a reduced level of new. It therefore follows that '*A*' is consistent with less wheel wear than '*B*'.

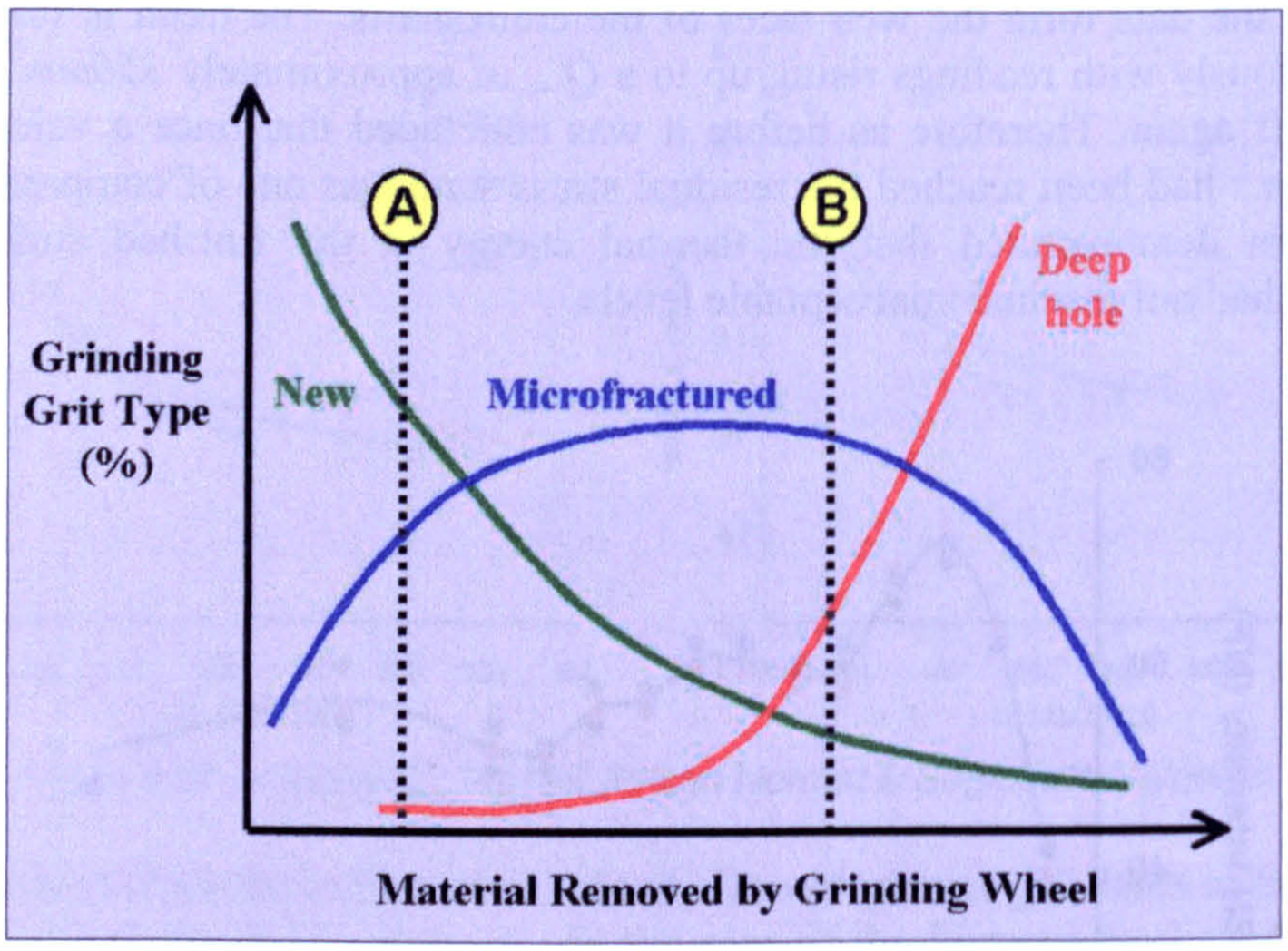

Figure 4.40 – Hypothetical Wear Progression for Single Layer Electroplated Tool

The analysis was carried out for five wheels in total, the four used in the trials and one '*as supplied*' wheel. The four used were a normal and segmented in both *356μm* and *252μm* grit sizes. These were designed *B356, B252, B356(seg)* and *B252(seg)* respectively. The '*as supplied*' wheel was a *356μm* designate *B356(new)* and provided a benchmark for comparison purposes. Results from the wheel edges are shown on the left in Figure 4.41 it can be seen that the remaining percentage of new grits for both the

normal and segmented wheels of both grit sizes were lower than that of the un-used wheel. The levels in the microfracture classification were broadly of a common level with the exception of the segmented wheel, which had a higher level. The result for the segmented wheels was significant since these wheels had been 'worked' far less than the conventional wheels, and so if performing similarly would have be expected to have had reduced levels of wear. The most significant results are those for the percentage of holes, as these are a result of either grit or bond failure. They showed that all the tested wheels had higher values than that of the un-used wheel as would be expected, also the smaller grit wheels were proportionally higher then the larger grit. The level of microfracture in the un-used wheel demonstrates the effect of truing operations carried out on the grinding wheel during manufacture in order to achieve the concentricity levels required for today's tight grinding tolerances required by automotive manufacturer's.

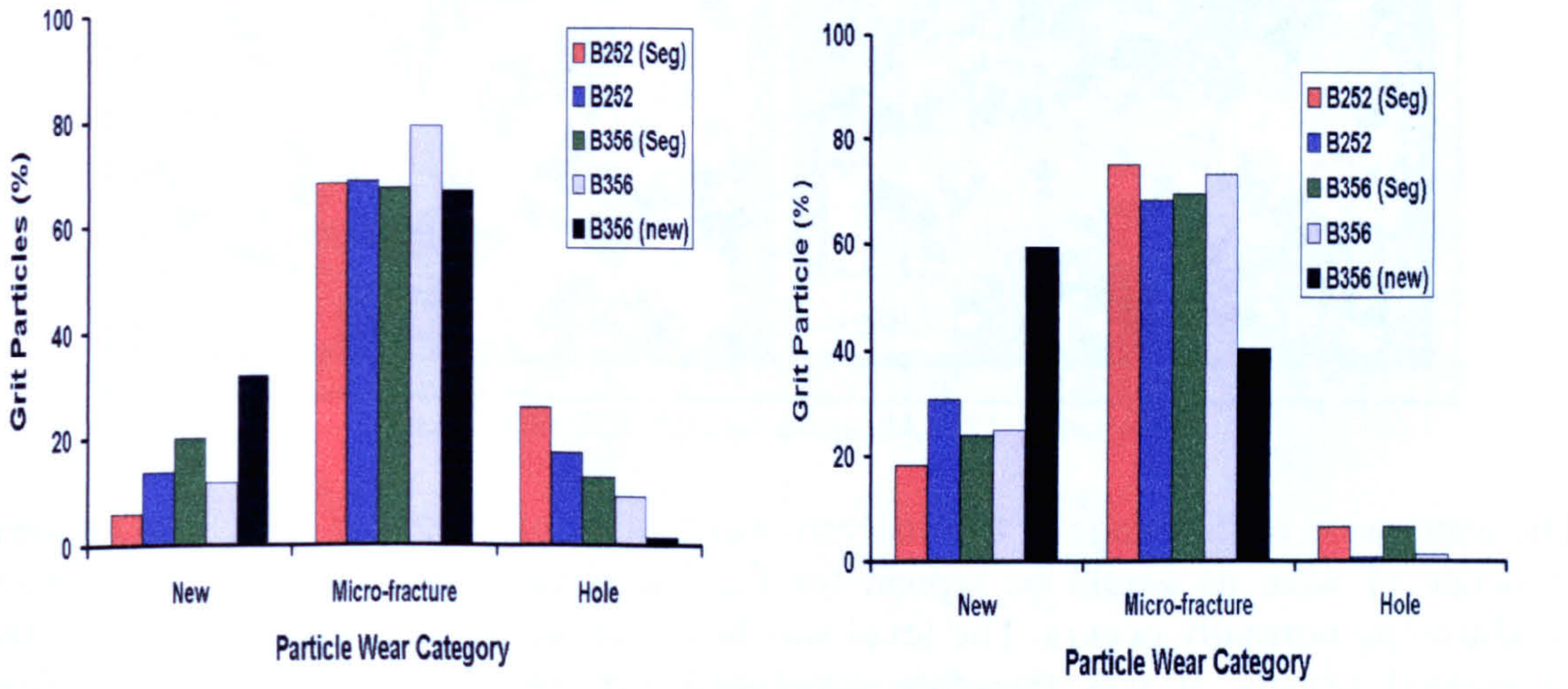

Figure 4.41 – Wheel Edge & Centre Grit Wear Analysis

Looking at the results for the centre of the wheels as shown on the right in Figure 4.41 it can be seen that the level of new grits is general higher and holes lower. This finding is in line with the lower number of trials carried out on the crankshaft journal feature where the full width of the wheel was utilised. The level of microfracture was in line with the results for the wheel edges and supports the assumption that this is a consequence of the wheel truing operation carried out during the wheel manufacture.

Figure 4.42 and Figure 4.43 are typical images used in the analysis. They show the grit at the centre and edge for the normal 252µm and 356µm wheels respectively and again help demonstrate that neither wheel had high levels of wear

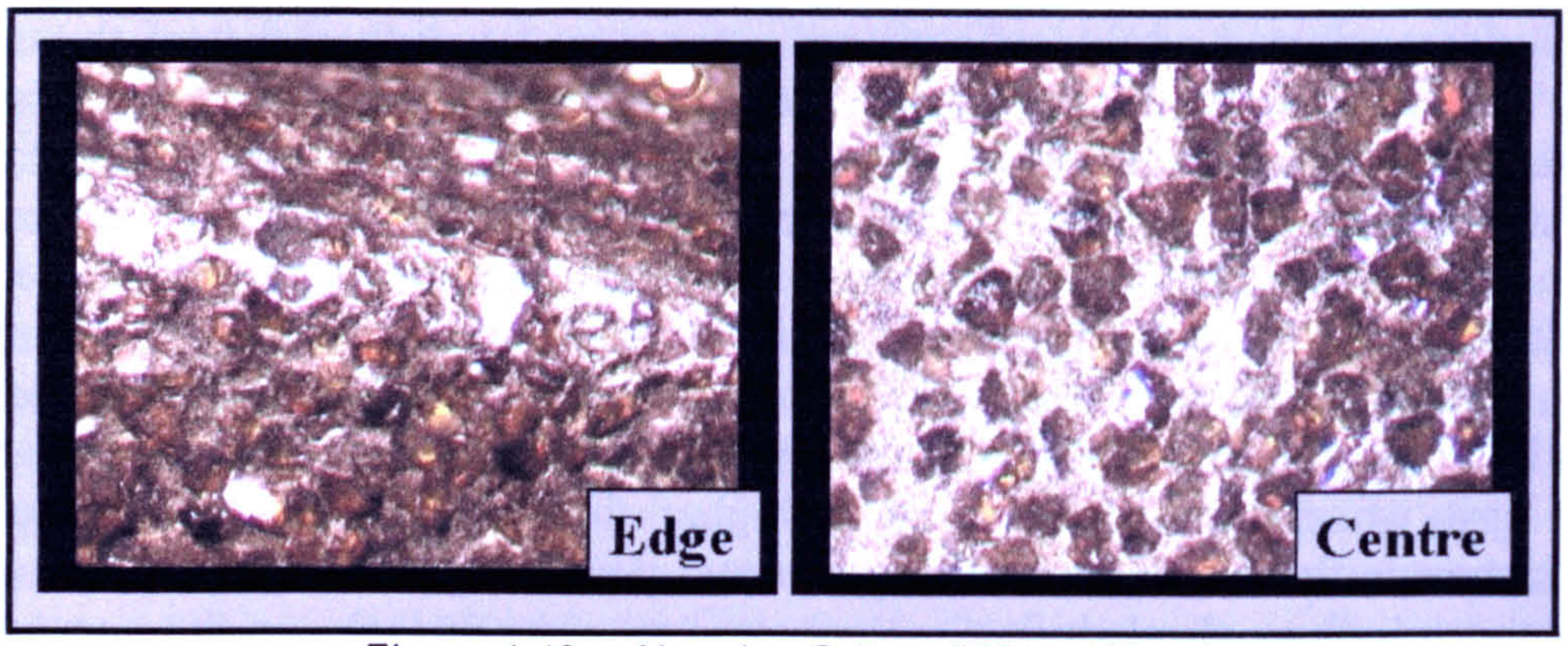

Figure 4.42 – Abrasive Grit on 252µm Wheel

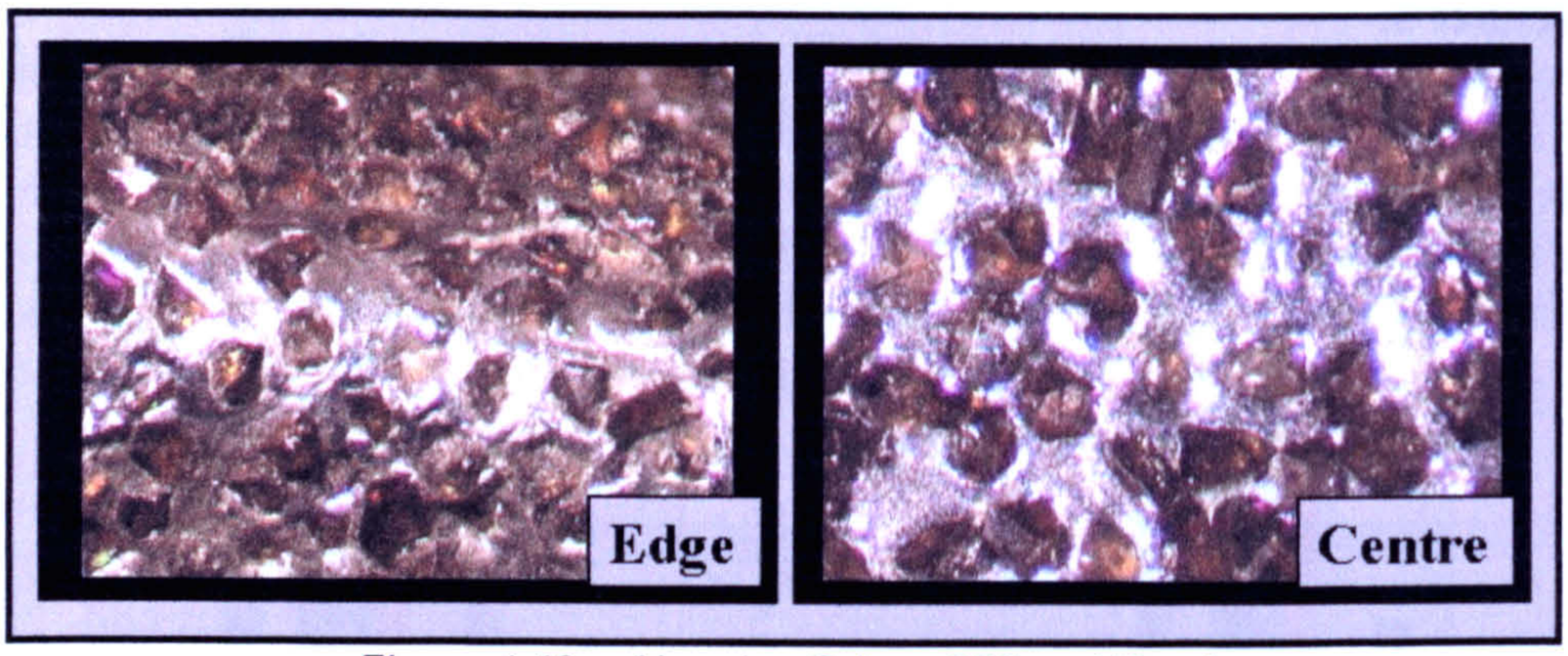

Figure 4.43 – Abrasive Grit on 356µm Wheel

The conclusion of this stage of the analysis was that all of the tested wheels had shown evidence of wear as would be typical for the initial stages of a wheel's life, where conditioning normally occurs. The level was however higher than that expected for the segmented wheels, it was therefore concluded that the increased level of coolant penetration had not overcome the effect of the higher grit loading over that of the conventional wheel. Overall the larger grit wheel showed less deterioration and so either because of their grit type or size offered better performance in the HEDG regime.

To consider the implication of the HEDG regime in regard to grinding time for the web grinds it is necessary to consider the increase in Q'_w with the grind path lengths. As stated the maximum Q'_w rate attained for the webs was $2000mm^3/mm.s$ the current standard used currently being $200mm^3/mm.s$. Table 4.5 shows the estimate grind times main (short grinds) and pin (long grinds) webs at both conventional and *HEDG* levels. This illustrates the potential that *HEDG* can offer when long narrow grind paths are required, any such advantage in regard to wider journal type grinds is far less.

Q'_w Rate ($mm^3/mm.s$)	Grind Time (sec)	
	Main Web	Pin Web
200 (conventional)	38	197
1000 (HEDG)	9	40
2000 (HEDG)	5	21

Table 4.5 – Estimated Grind Times for Webs with HEDG

In summary this stage of the research validated the findings from the previous cylindrical plunge grind work in a production environment on real components. The conclusion was that components can be ground at HEDG material removal rates without damage to the component or wheel grit failure as a result of the higher loading.

4.3.2 Extended HEDG Validation

The final stage of the *HEDG* research was the production of a full form crankshaft component. A photograph of the crankshaft both before and after grinding is shown in Figure 4.44, during the grinding operation a total of 1kg of material was removed from the shaft.

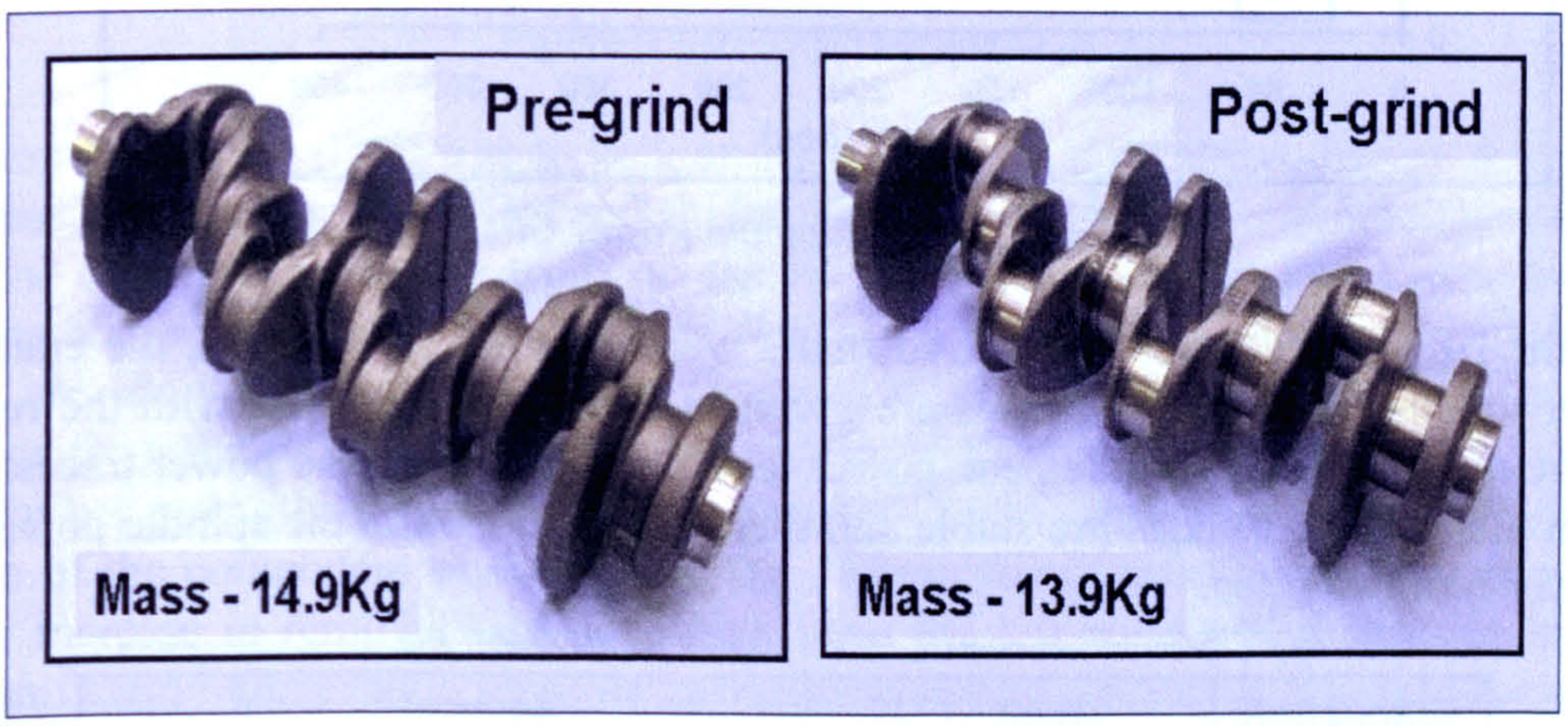

Figure 4.44 – Photograph of Crankshaft

The production of a full geometrical form meant there was a requirement to produce undercuts as previously discussed in *Chapter 3*. The undercut feature is illustrated in Figure 3.21, together with the required wheel form in Figure 3.22. Two new *252μm* wheels with this form were used for the trials.

The first step was involved the grinding of *50* components at Q'_w rates of $1000mm^3/mm.s$ for the web feature and $250mm^3/mm.s$ for the main and journals. Subsequently a further 20 were ground at the reduced rates. Figure 4.45 shows the complete spindle power trace for a full crankshaft grind, the left and right wheels are shown in the different colours. The exploded view shows the detail of the spindle power for grinding of a single web and diameter feature.

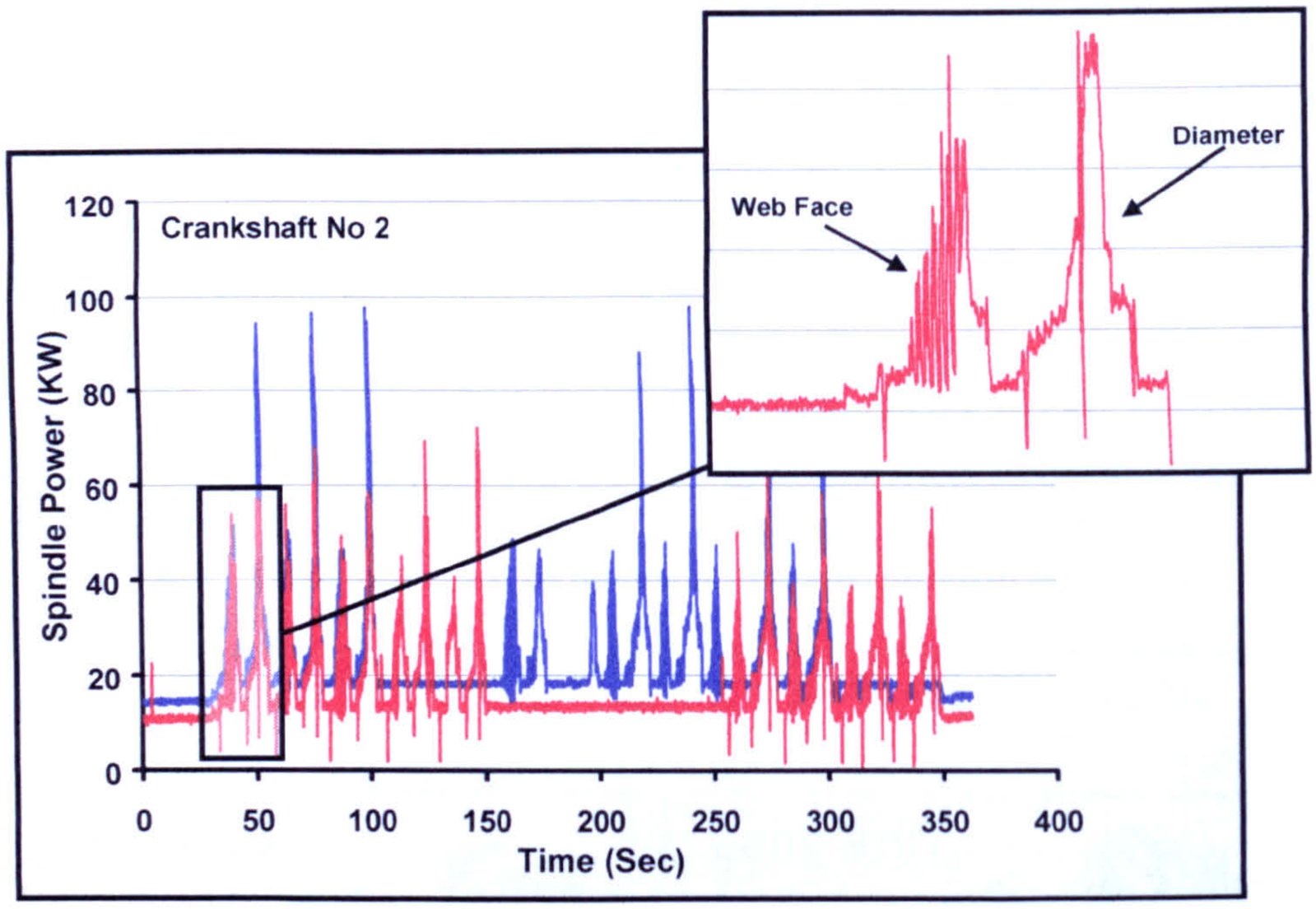

Figure 4.45 – Spindle Power Chart

From the batch of 70 crankshafts five shafts were selected for analysis, the crankshaft number together with the Q'_w rates are given in Table 4.6. Together with the removal rates are the right hand spindle peak power levels obtained from the power traces. It can be seen that the magnitudes are stable and there is a reduction in the spindle power with the lower removal rates.

Crankshaft No.	Web		Journal	
	Q'_w ($mm^3/mm.s$)	Power (kW)	Q'_w ($mm^3/mm.s$)	Power (kW)
2	1000	38	200	55
25	1000	38	200	55
43	1000	38	200	55
47	500	30	200	55
65	250	28	200	55

Table 4.6 - Removal Rates and Spindle Powers

Figure 4.46 shows the specific grinding energies for these grinding trials and their position in regard to the previous findings from the initial production tests. It can been seen that the results lie in the same region and can be described by a power curve similar to that previously. Therefore it follows that the thermal modelling conditions remain valid and support the conclusion that the *HEDG* process has been successfully implemented in production cylindrical plunge grinding.

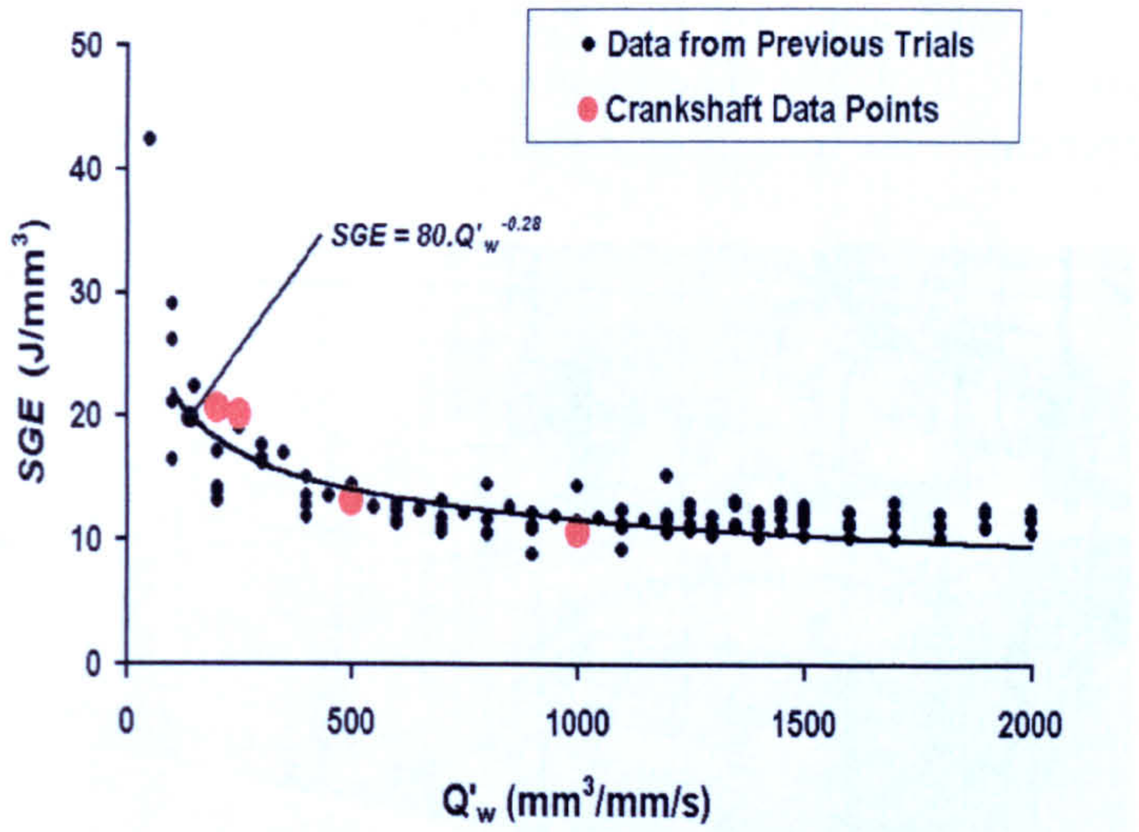

Figure 4.46 – SGE versus Q'_w

The next stage of analysis was to look at the state of residual stress. Figure 4.47 shows the measurements for the five crankshafts along with the previous readings obtained from the cylindrical grinding trials on the Edgetek machine. The latest measurements have been grouped into two categories. Those features produced with the right-hand wheel are shown in blue and those produced with the left-hand wheel in red. The readings from the right-hand wheel tend to align with the previous findings. This then adds further strength to the assumption that the thermal energy input to the finished surface of the component peaks around the $350mm^3/mm.s$ level and then reduces with further increase in removal rate. Readings from the left-hand wheel features however are significantly higher than those of the right-hand wheel ones. In this case the coolant application was found to have been sub-standard which would have resulted in a reduced cooling effect coupled with a reduced level of lubricity. Both these factors would explain the higher peak power levels seen for this wheel. In turn the higher power levels would have led to increased thermal energy input into the component leading to a reduction in compressive residual stress as witnessed in the measurements.

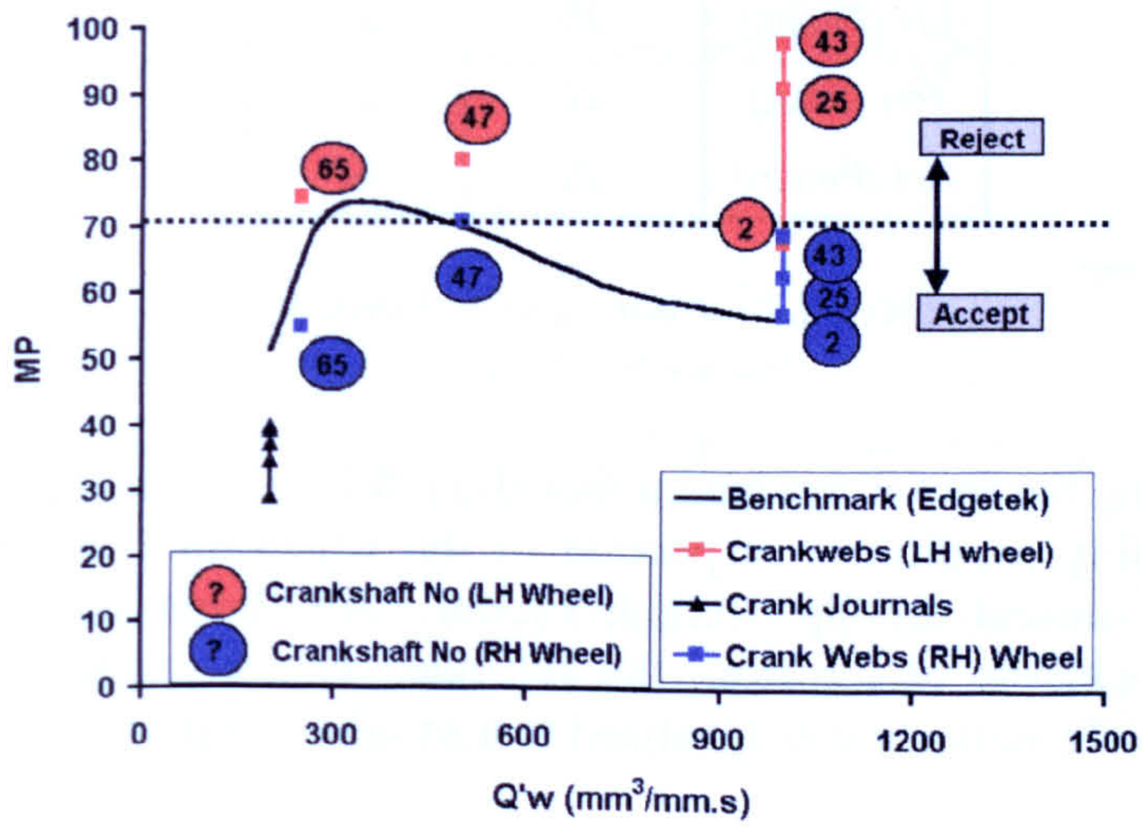

Figure 4.47 – BN Residual Stress Chart

The next section of this stage of the trial was the grinding of the 950 batch of crankshafts to look into tool life. The photograph in Figure 4.48 shows the completed shafts prior to shipment to the automotive manufacturer for assessment.

Figure 4.48 – Photograph of 950 Crankshaft Batch

The shafts were ground at a Q'_w rate of $250mm^3/mm.s$ on the web faces and $200mm^3/mm.s$ on the diameters. The spindle power curves for the complete grinding cycle were recorded through out the batch run, the spindle power peaked around 95kW on the wider features but remained within the limits of the 80kW high power spindle drive. Table 4.7 shows the peak power for both wheel spindles at the beginning and end of the batch run. It can be seen that there is little change in the power level of each spindle over the trial. The general power level for the left-hand unit was higher than that for the right-hand unit.

Wheel & Position in Batch	Spindle Power (kW)	
	Web	Journal
LH (Start)	34	95
LH (Finish)	35	97
RH (Start)	28	60
RH (Finish)	30	61

Table 4.7 – Peak Spindle Powers

Coolant issues during the initial run meant that the left-hand wheel had been subject to more adverse grinding conditions, inspection of the wheel after the run showed that there was damage around the lip section. Figure 4.49 shows both grinding wheel surfaces at the conclusion of the trial, the left-hand wheel image shows where the damage was found. The damage was localised to a small section of the wheel periphery.

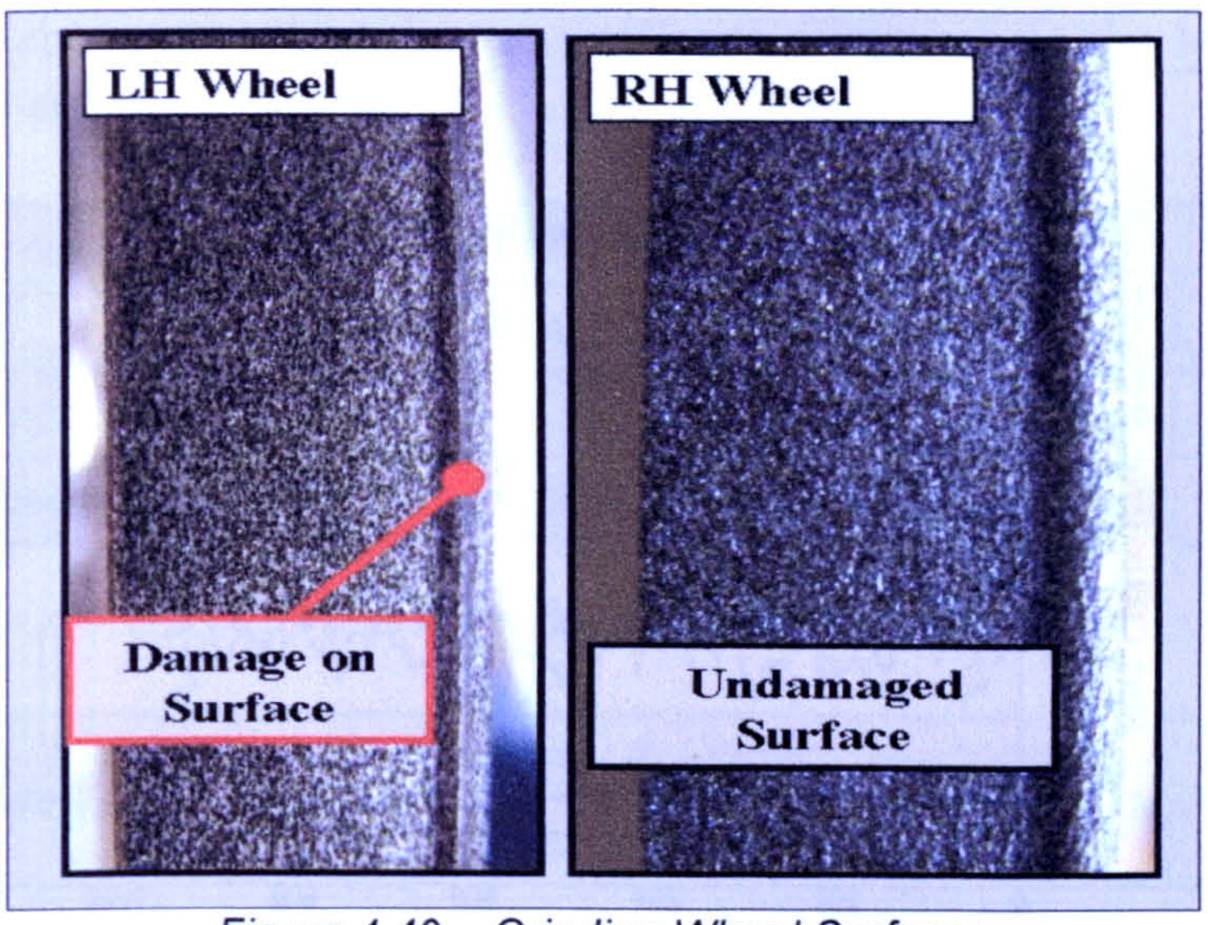

Figure 4.49 – Grinding Wheel Surfaces

In order to more accurately assess the spindle power trend over the complete test grind the machines log file viewer was used to analysis every 10th crankshaft grind for mean in-cycle and mean base level powers, namely the grinding and not grinding portions. The results for this analysis can be seen in Figure 4.50 and demonstrates that the overall power requirement did not increase over the duration of the trial therefore it was concluded that the process had remained stable

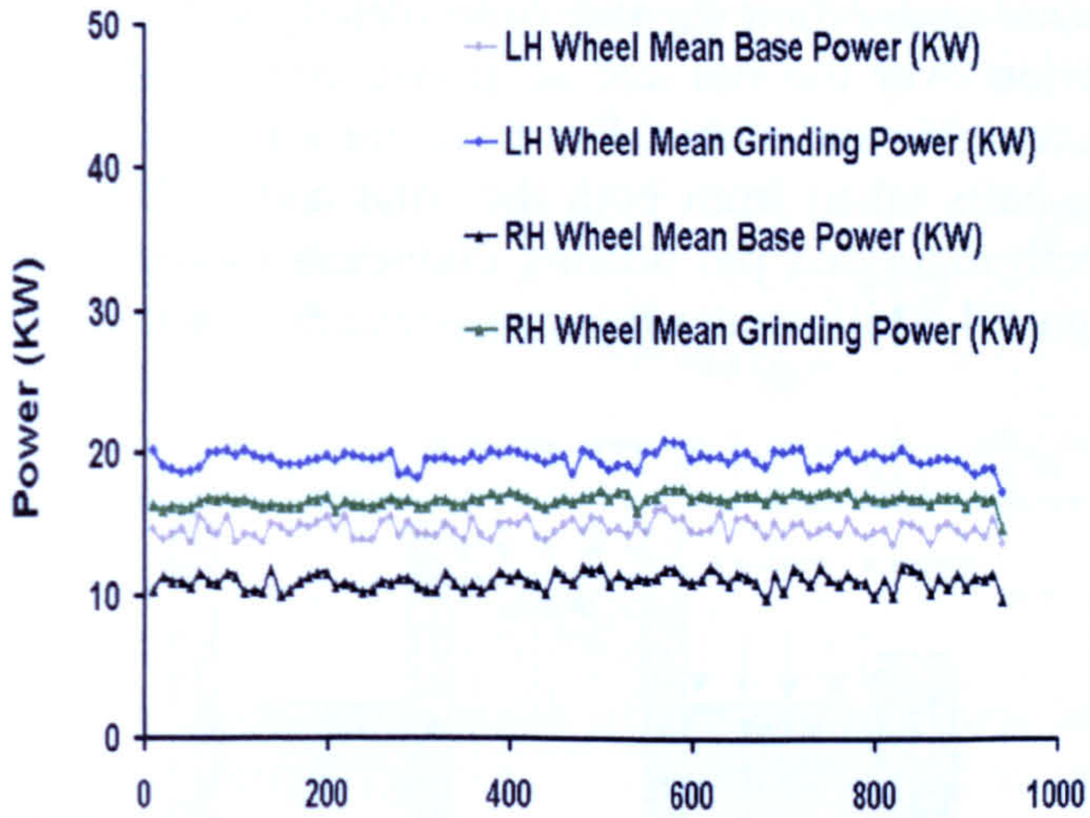

Figure 4.50 – Mean Spindle Grinding and Base Power Trend for Batch Grind

Figure 4.51 illustrates the grinding power trend (*i.e. overall power minus the base level*) for each wheel and shows that the power requirements for the two wheels were different. It was concluded that the initial coolant issues discussed caused this difference.

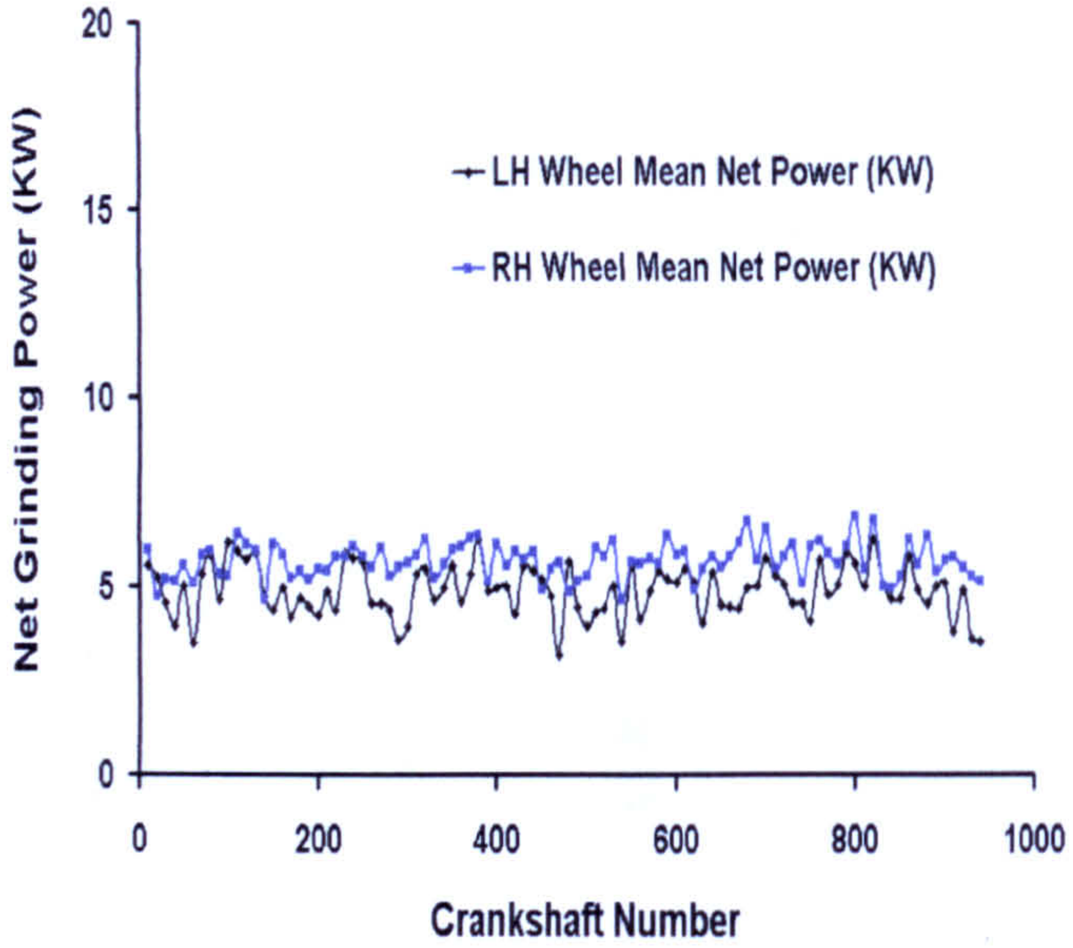

Figure 4.51 – Mean Net Spindle Power Trend for Batch Grind

The next stage of analysis consisted of both geometric and residual stress measurements, the latter being carried out by the automotive manufacturer. The geometric measurements were undertaken on 10 shafts selected from every 100 shafts throughout the batch, the geometric data for form and surface roughness demonstrated compliance to the requirements. Surface Roughness on the crankshaft diameters remained between $2\mu m$ and $2.3\mu m$ R_a and concentricity within $50\mu m$. There was no significant deterioration over the run and so it was concluded that in this aspect the process was both acceptable and stable. Residual stress were carried out with an XRD instrument on crankshafts taken from both the mid and end points of the batch run. Measurements on both main and pin bearing diameters including undercuts (grooves) were carried out. Figure 4.52 illustrates the measurement locations on the crankshaft.

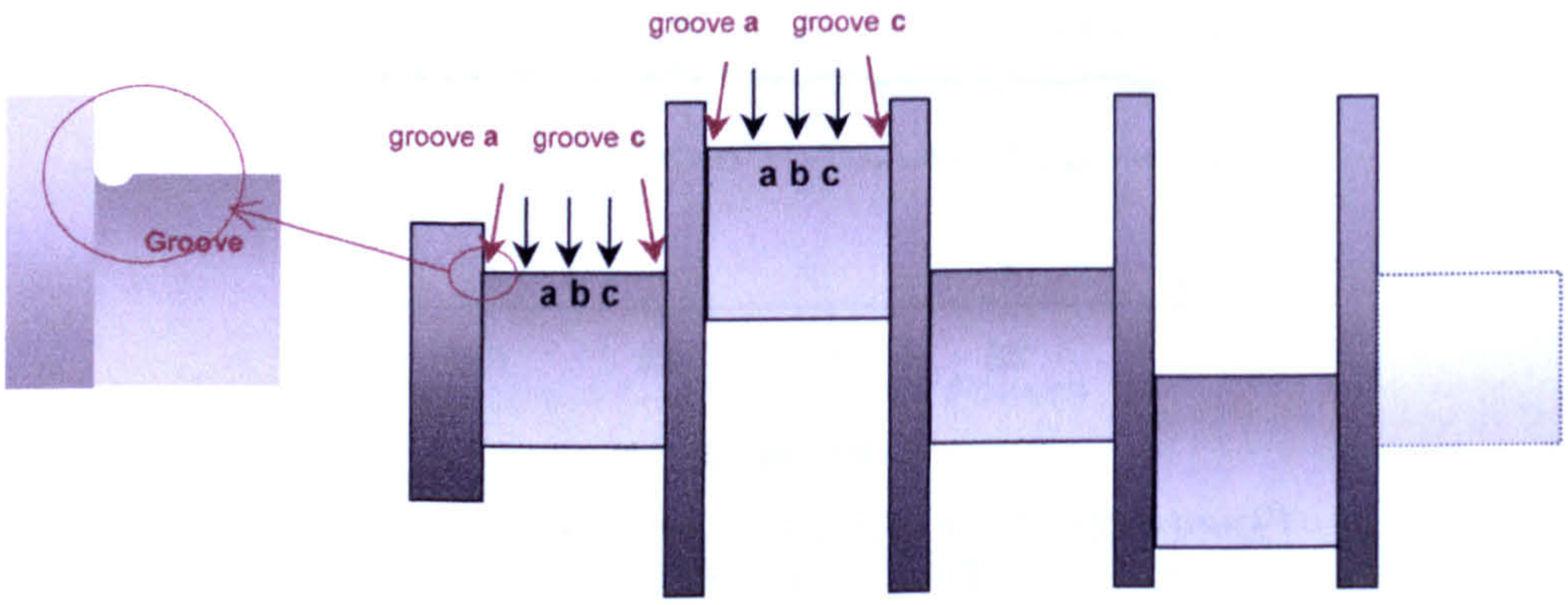

Figure 4.52 – Crankshaft Residual Stress Measurement Zones

Results for the analysis are shown in Table 4.8 and Table 4.9 for crankshafts 581 (mid-point) and 950 (end-point) respectively. These indicate slight compressive stresses for both the main and pin diameters, the same is true for the undercuts. Comparison of data

from the tables shows that there is no significant difference in the levels of residual stresses in either shaft.

Feature	Surface Residual Stresses (MPa)				
	Groove a	Zone a	Zone b	Zone c	Groove c
Pin Diameter	-102± 19	-153 ± 19	-95 ± 28	-194 ± 25	-116 ± 56
Main Diameter	-98± 16	-225 ± 24	-164 ± 18	-171 ± 16	-106 ± 25

Table 4.8 - Residual Stress Data for Crankshaft 581

Feature	Surface Residual Stresses (MPa)				
	Groove a	Zone a	Zone b	Zone c	Groove c
Pin Diameter	-103± 13	-	-146 ± 18	-	-97 ± 17
Main Diameter	-111± 15	-	-190 ± 16	-	-98 ± 13

Table 4.9 - Residual Stress Data for Crankshaft 950

It was observed that there was a slight reduction of compressive stresses within the 'zone b', although still at an acceptable level this was of interest. Further investigation of the profile across this area showed a small step in the order of 15µm in the central region as shown in Figure 4.53.

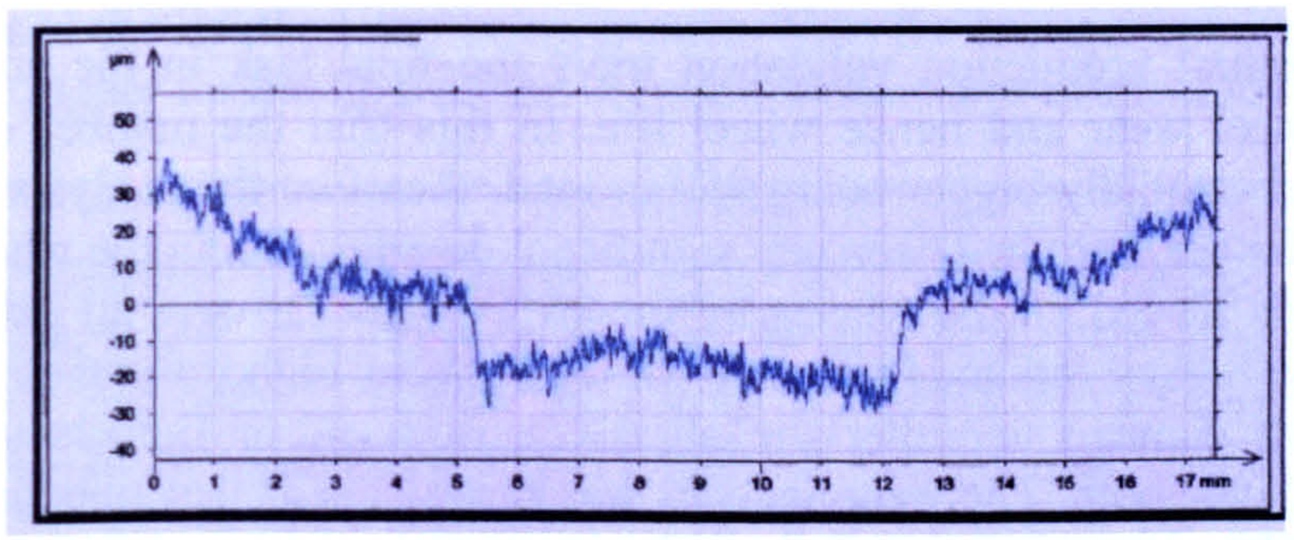

Figure 4.53 – Surface Profile Trace for Large Batch Production Trial

It was concluded that the step was a result of the overlap from the twin wheel grind cycle used in this case. Left and right-hand wheels are used to produce the required form on the two differing widths used for the main and pin diameters, the method is commonly referred to as double wheel and double plunge technology. Figure 4.54 illustrates the cycle and shows where the overlap region occurs. The diagram in Figure 4.55 shows how the wheels could hypothetically produce such a profile. The overlap region on the second grind operation would experience a reduced rate of material removal, that would in turn change the thermal energy partition to the components near surface region. In this case it is probable that that reduced rate of removal would result in a burnishing action and thus have a higher level of thermal input. The result of this increased thermal input would be a reduced compressive state as was observed.

However this effect did not result in an unacceptable change in the residual stress and so did not compromise the *HEDG* process.

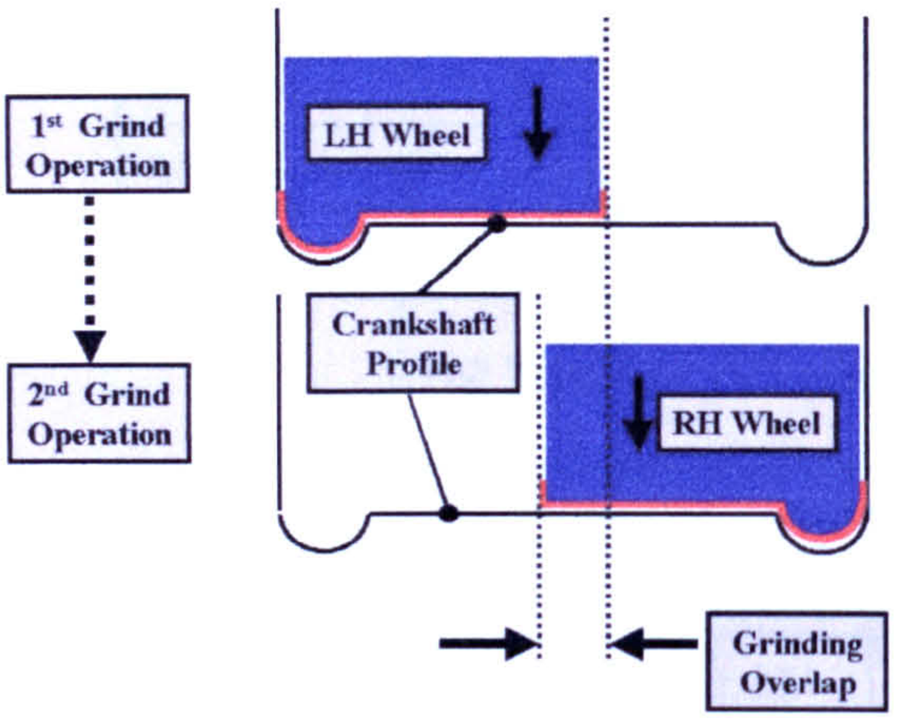

Figure 4.54 – Twin Wheel Grinding Cycle

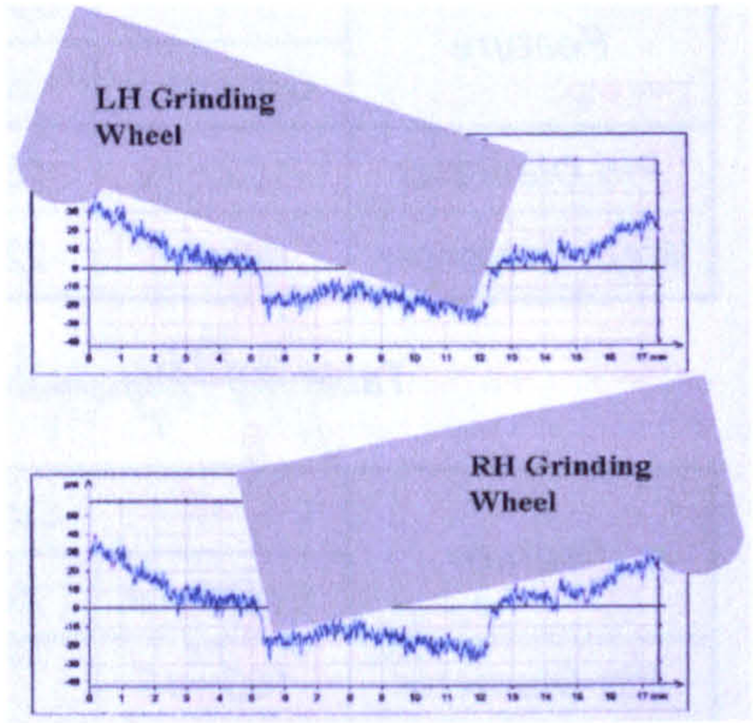

Figure 4.55 – Hypothesis for Step in Surface Roughness Trace

The conclusion of the stress measurements was that the measured state would be suitable for the remaining crankshaft production process chain. The residual compressive stresses on the pins would prevent any crack formation with subsequent machining operations, whilst with the grooves it would be advantageous for the subsequent rolling operation carried out on this feature.

As with the initial production validation trials the final task in the analysis was to investigate wheel wear and hence wheel life. In this trial the number of crankshafts ground was substantially bigger being 950 in total, therefore the analysis was expected to establish whether there had been any significant deterioration in the wheels due to the higher demands placed on the wheels by the *HEDG* process over an extended period. To recap these higher demands primarily in the form of higher thermal shock loading could result in damage to either the abrasive grit itself or the electroplated bond structure, or maybe both. The wear analysis was carried out as described in '*Chapter 3 - Experimental Procedures and Equipment'* with a *SEM* by the abrasive manufacturer Element Six..

The primary area of interest was the concentricity of the wheel periphery to the location bore. For the RH wheel concentricity figures were within normal tolerance levels of ±10μm, however for the LH wheel figures were far higher at +27μm to -19μm. The section of damage to the LH wheel aligned with that of the high section and therefore wheel analysis sections were taken at the high and low areas. Sections were taken from the periphery of the grinding wheels as illustrated by Figure 4.56 for SEM analysis. Two sections were taken from both the left and right hand wheels, these being allocated numbers *3 & 6*, and *7 & 10* respectively.

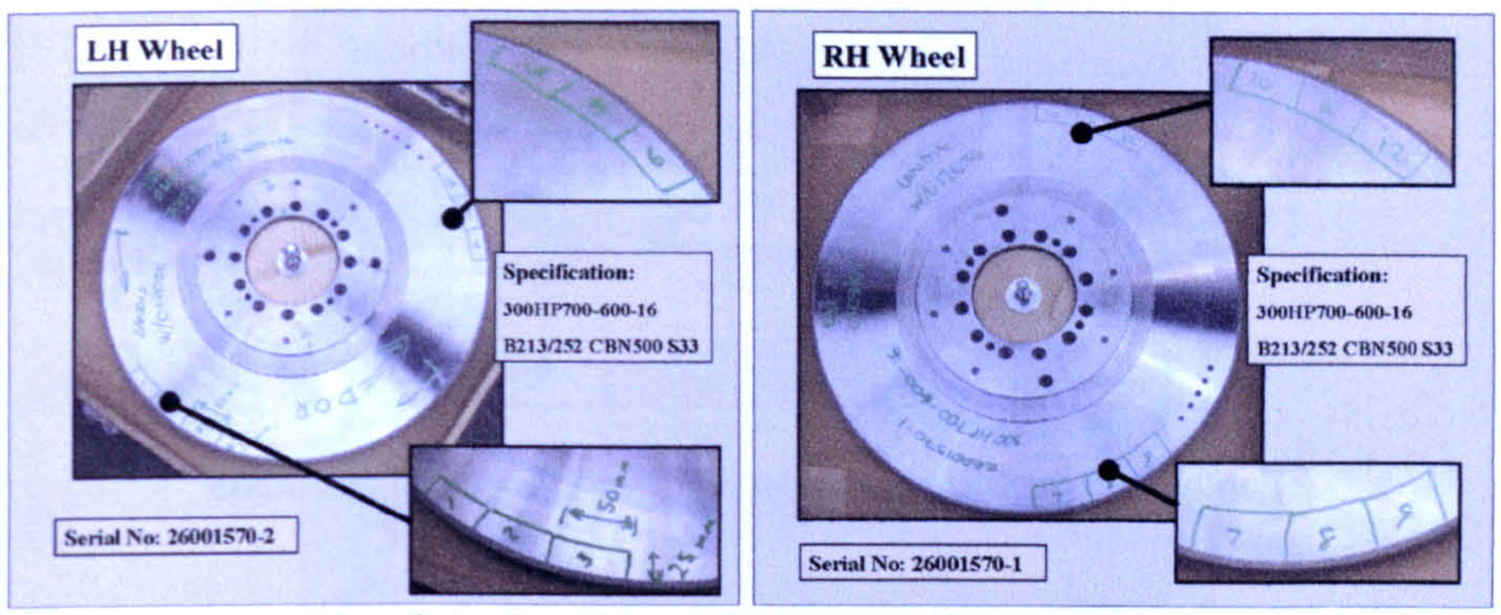

Figure 4.56 – Grinding Wheel Sectioning for Grit Wear Analysis

Each segment was divided into two areas for analysis, the middle and the lip as illustrated in Figure 3.23. The lip was the protruding edge of the wheel used to produce the undercut and fillet radius between the crankshaft diametrical and web face features and as such would normally be expected to be subject to far higher loading and wear.

The segments were approximately 50mm long (16mm wide) therefore at a magnification of x50 a maximum of 16 images SEM were recorded along the length of the segment. No edge was used in the analysis and any particle that did not lie 100% inside the image was disregarded. A typical example of two corresponding images from the middle on the left and edge on the right can be seen in Figure.4.57. The image of the middle shows some grit wear, whereas the one for the edge in this case for the left-hand wheel shows where bond failure has occurred. A consequence of the enhanced depth of field offered by this technique was that the surface areas imaged were different for that of the middle and the lip, the latter being greater. Thus the average count per image was expected to be higher for the lip than the corresponding image of the middle area.

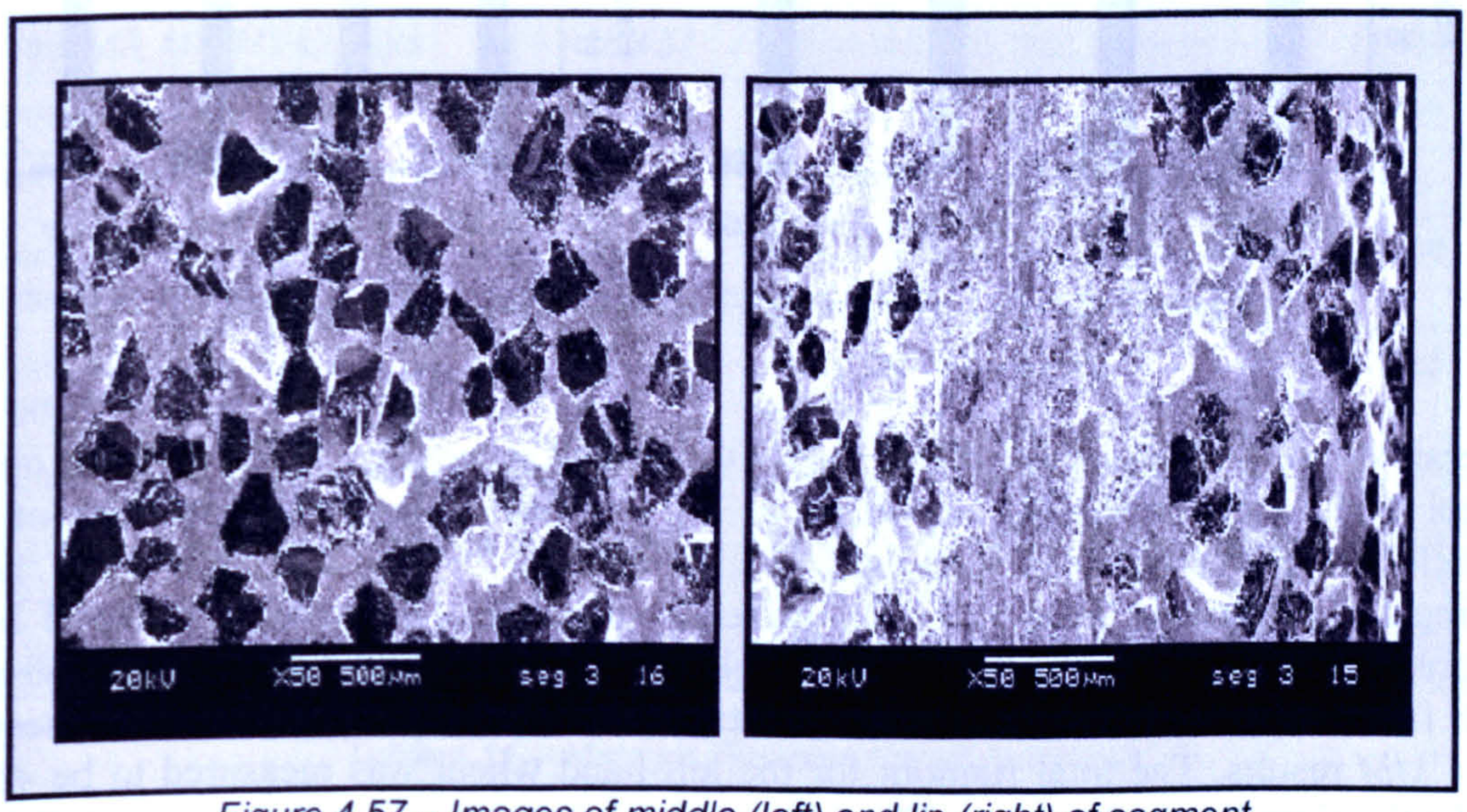

Figure.4.57 – Images of middle (left) and lip (right) of segment

Table.4.10 shows a summary of the average number of particles found on the different samples at the middle and lip positions. There were between 50 and 70 particles per image, the left-hand wheel being at the lower end particularly at the lip location.

Segment	LH Wheel		RH Wheel	
	3	6	7	10
Middle	59	58	70	69
Lip	52	60	60	67
Total	58	59	65	68

Table.4.10 - Summary of Average Number of Particles

Figure.4.58 shows the results, it is clear that most of the particles can be classified as 'working'. The number of 'new' particles remaining was relatively constant across the segments. Whilst the proportion of the particles that were classified as 'holes' also did not change much. Here a greater change had been expected in segment 3 where the bond failure had been observed. It was concluded that the bond smoothing had masked the number of 'holes' positions visible, as the average particle count seen in Table.4.10 had been lower. The frequency for 'worked' particles on the Left-hand wheel lip section was seen to be lower and as all other particle count levels were relatively similar this again lent support to the theory that there was a proportion of lost 'holes'.

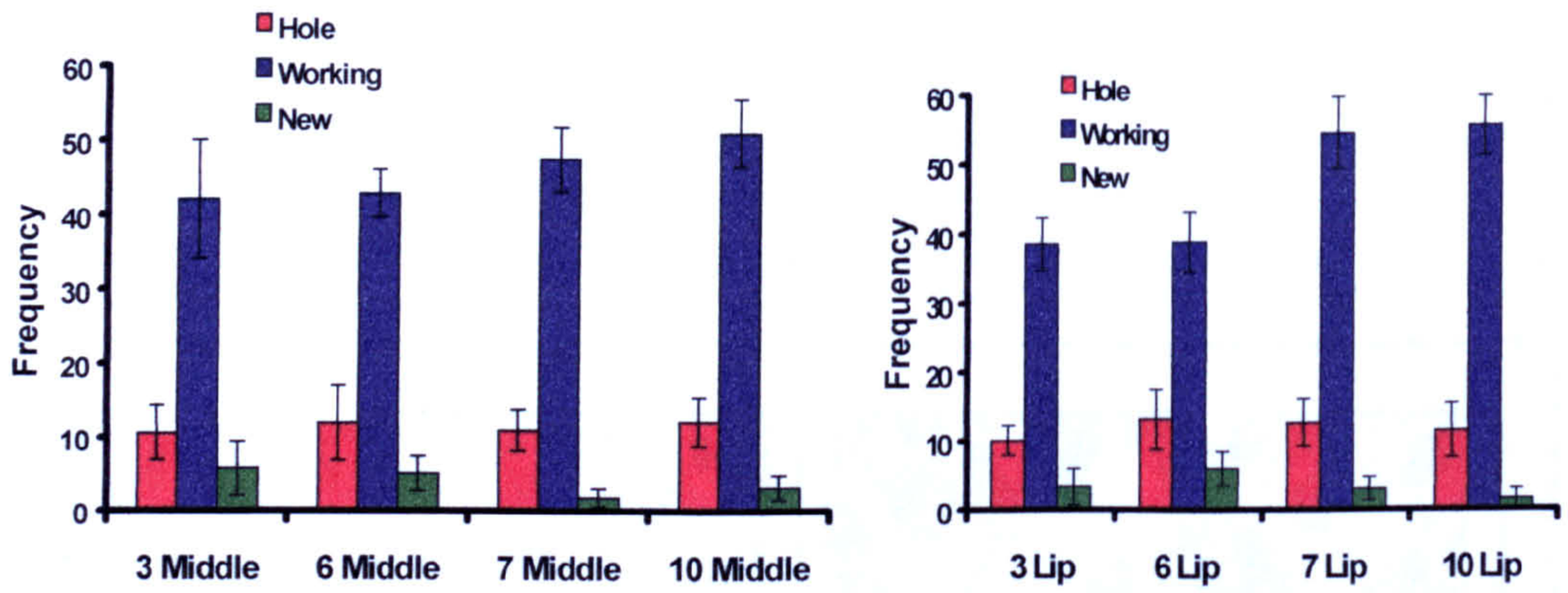

Figure.4.58 - Summary of the Particle Counts from Segments

Overall the wear results showed that only a very small percentage of the particles on the wheel surface could still be classified as 'new'. While on average 50-70% of the particles were classified as 'working', and between 22-30% of the particles as 'hole' having been removed from the bond material completely. Segment 3 suffered bond failure as seen by the presence of bond polishing in Figure 4.49. One likely cause of such failure was the level of wheel concentricity, evidence to support this was seen in the *CMM* results. The total runnout for the left-hand wheel was measured to be *46μm* whilst the right-hand wheel was *19μm*. Figure.4.59 shows the high point of the left-hand wheel runnout which was found to coincide with the failure area.

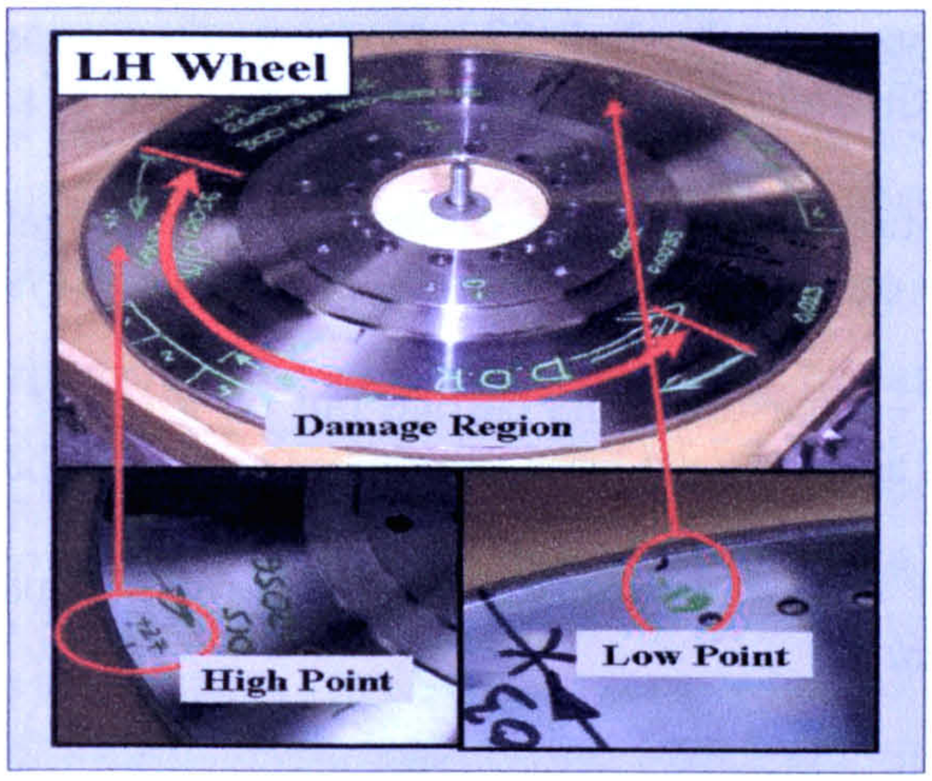

Figure.4.59 – LH Wheel showing Damaged Region

To help assess the wheel wear analysis it was necessary to look into the manufacturers projected wheel life. At Q'_w rates of $200mm^3/mm.s$ wheel life was expected to be in the order of $28,000,000mm^3/mm$, above this rate there was currently no available guide figures. Table.4.11 shows the constituent features and total volume per unit width for the crankshaft selected for these trials. The result from the figures indicate a projected wheel life of 606 and 655 components for the LH and RH wheel would be expected. The estimated number of crankshafts was significantly below the number of actual shafts ground in the trial.

LH Wheel	Volume (mm^3/mm)	RH Wheel	Volume (mm^3/mm)
Grind M5 Cheek	3,343		
Grind M3, M2, M1 Cheeks	15,457	Grind M5, M3, M2, Cheeks	15,457
Grind M4 Cheeks	3,082	Grind M4 Cheeks	3,082
		Grind M1 Diameter & Undercut	659
Grind M5, M3, M2, M1 Sidewalls & Undercuts	3,024	Grind M5, M3, M2, Sidewalls & Undercuts	2,268
Grind M4 Thrustwall & Undercut	2,826	Grind M4 Thrustwall & Undercut	2,826
Grind 4 x Crankpin Cheeks	13,371	Grind 4 x Crankpin Cheeks	13,371
Grind 4 x Crankpin Sidewalls & Undercuts	5,083	Grind 4 x Crankpin Sidewalls & Undercuts	5,083
Total Volume Removed	46,186		42,746

Table.4.11 – Material Removal from Crankshaft

The analysis of the grinding wheel condition is very positive, the right-hand wheel shows no sign of damage. Overall the power levels at the beginning and end of the batch are similar and surface roughness measurements remained within specification throughout. There were problems with the left-hand wheel, which resulted in some bond

failure occurring at approximately shaft 970. However these arose at a very early stage in the grinding - approximately shaft 10 - and were attributed to setup issues such as:

1) Coolant application to that wheel - Subsequent investigations have found some system failures on this side of the coolant delivery system during the initial batch.
2) Wheel runnout – Measurements carried out on a *CMM* indicated that the left-hand wheel had an increased level of runnout to that of the right-hand wheel.

In both cases however the wheel life exceeded that of the manufacturer's figure of *28,000,000mm^3/mm width.*

To fully quantify the improvement in the grinding cycle offered by the application of the *HEDG* regime detailed breakdowns of the total machine cycle time were carried out for both conventional and *HEDG* cycles. These cycle time breakdowns included all aspects of the machine cycle in addition to the grinding portion, such as load/unload, work-rest application, axes movements, crankshaft location. The removal rates used for conventional grinding were *200mm^3/mm.s* for web faces and *80mm^3/mm.s* for diameters. For *HEDG* the values were *1000mm^3/mm.s* for web faces and *200mm^3/mm.s* for diameters. The results of the cycle time calculations are given in Table.4.12 from which it can be seen that the total machine cycle decreases from *435.5* seconds down to *206* seconds a very significant improvement.

Grind Cycle		***Cycle Time (sec)***
HEDG		
Webs:	*200mm^3/mm.s*	*206*
Diameters:	*80mm^3/mm.s*	
Conventional Grind		
Webs:	*1000mm^3/mm.s*	*435.5*
Diameters:	*200mm^3/mm.s*	

Table.4.12 – Grind Cycle Times

The trials have shown that grinding crankshafts at the high removal rates of *HEDG* is feasible both in terms of wheel life and surface integrity. The next stage would be to carry out further extended trials in collaboration with a major automotive manufacturer.

5 Superfinish Regime Grinding Investigations

This Chapter describes the Superfinish Regime grinding investigations together with modelling of the surface finish. Detail of both the machine specifications and test set-ups are outlined in Chapter 3.

The surface grinding trials provided an effective platform to determine the wheel type, together with truing and dressing techniques required for these grinding investigations. Both resin and vitreous bond grinding wheels met the target surface finish specification of 0.1μm R_a. The vitreous wheel offered a more aggressive grind and therefore enabled higher removal rates to be achieved, whilst producing an improved surface quality. Thus the vitrified wheel provided a more viable option for production grinding demands, and was selected for the subsequent work. These trials then went on to produce benchmark performance data for the Superfinish Regime grinding mode. Surfaces were routinely produced with values below 0.2μm R_a in the conventional surface grind mode, and down to 0.011μm R_a in the modified grind mode. The latter surface value was indicative of the best possible surface achievable on the type of machine tool used.

Grinding Data from the surface grinding work was applied in the more complex cylindrical plunge-grinding mode. These tests initially provided surface finish data for the conventional straight plunge grind and following on from that data for the modified plunge grind using the sideways oscillation. In the conventional mode surface roughness values of less than 0.15μm R_a were obtained. A limited number of grind oscillation tests demonstrated an improvement in R_a values.

Benchmark trials on the *LT1* production machine tool utilised the current truing and dressing techniques together with a vitreous grinding wheel. Surface finish levels of around 0.18μm R_a were obtained. The final phase on the *LT1* production machine tool went on to show that surface finish levels of below 0.110μm R_a were achievable with the application of the improved dressing technique in a conventional standard plunge grind mode. Implementation of the modified grind path further enhanced the surface finish values, and the effect of the oscillation parameters was determined.

5.1 Surface Grinding

Surface Roughness values produced on the work-piece, when using different grinding wheel ranged between 0.11μm and 0.05μm R_a over the series of tests. Figure 5.1 shows the results for the surface finish versus feedrate. This illustrates the higher performance of the vitreous wheel set-up with surface roughness values of approximately 0.05μm R_a. Whereas the resin wheel values are in excess of 0.1μm R_a. The plot also shows that at the higher feedrates the quality of the surface finish deteriorates. In the case of the resin wheel this occurred at 100mm/s, and corresponded to an equivalent chip thickness (h_{eq}) of 0.016μm. With the higher operating wheel speed of the vitreous wheel the maximum h_{eq} value reached at the 125mm/s feedrate was 0.01μm, lower than that of the resin wheel.

The effect of the different grinding wheel speed can be seen in Figure 5.2. Two speeds for each wheel have been plotted 60m/s and 120m/s for the vitrified, and 42m/s and

63m/s for the resin. These correspond in the case of the vitrified wheel to an equivalent chip thickness of 0.04μm and 0.008μm at 120m/s and 60m/s for a 50mm/s feedrate, and 0.008μm and 0.017μm respectively for a 100mm/s feedrate. Similarly with the resin wheel the figures for equivalent chip thickness are 0.008μm and 0.012μm at 63m/s and 42m/s for a 50mm/s feedrate, and 0.016μm and 0.024μm for a 100mm/s feedrate.

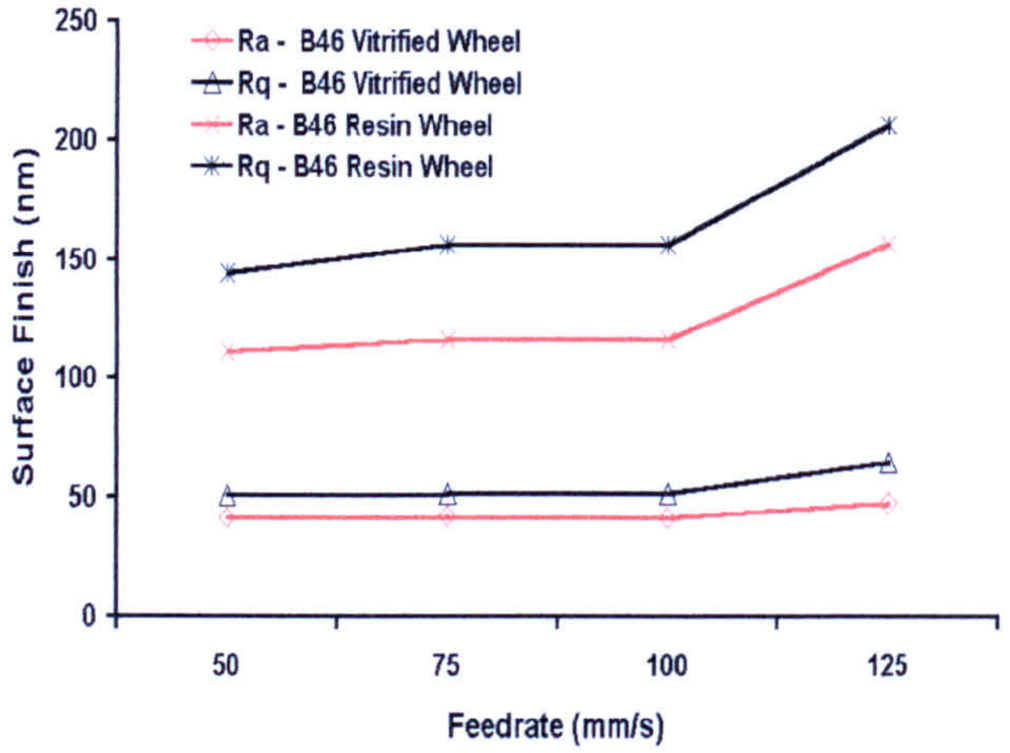

Figure 5.1 – Surface Finish against Feedrate for Surface Grinding

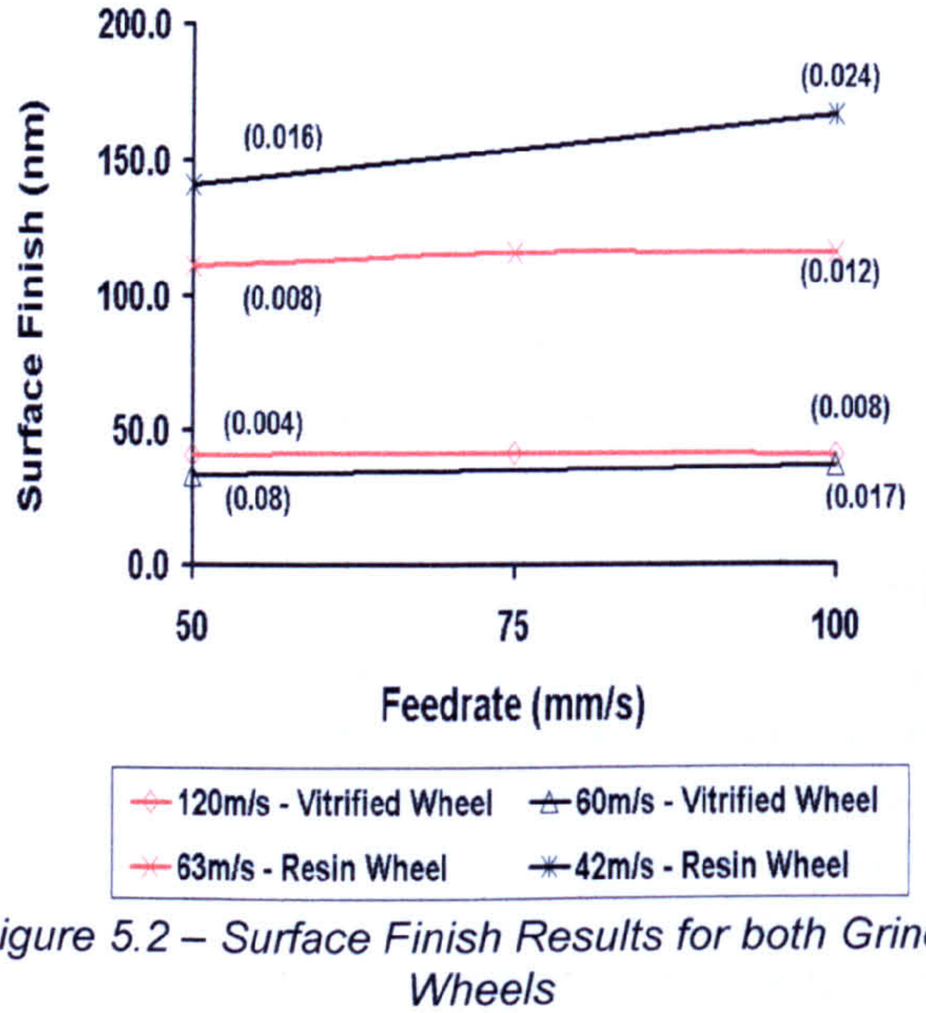

Figure 5.2 – Surface Finish Results for both Grinding Wheels

The h_{eq} figures are shown in brackets alongside the data points. The surface roughness for the vitrified wheel differs a small amount with grinding wheel speed, the lower speed producing a higher quality. Importantly the h_{eq} figure remains below the 0.016μm threshold seen in Figure 5.2 for all conditions. With the Resin wheel the effect is reversed with the higher grinding wheel speed producing an enhanced surface finish. The h_{eq} figure still remains below the 0.016μm level despite the lower wheel speed.

However at the lower of the two grinding wheel speeds the surface roughness is higher and deteriorates with an increase in feedrate. In this instance the h_{eq} figure exceeded the 0.016μm threshold.

The vitreous wheel produced consistent values over the whole test range at the higher quality finish. Whilst the resin wheel figures had a greater scatter and lower quality finish. The results are shown in Figure 5.3. It shows that the vitreous wheel coupled with the truing and dressing technique developed had a far more consistent performance and was superior to that of the Resin wheel. The bond structure for the vitreous wheel was both harder and more porous than that used for resin wheels. This in turn meant that the vitreous wheel had a more aggressive grinding nature and was therefore able to better withstand the grinding demands in this instance. Whereas the resin wheel was possibly subject either to breakdown, loading or a combination of the two. Other advantages of the more open bond structure is the ability to cope with a larger chip thickness and coolant retention, which enable a higher material removal rate and enhanced wheel life.

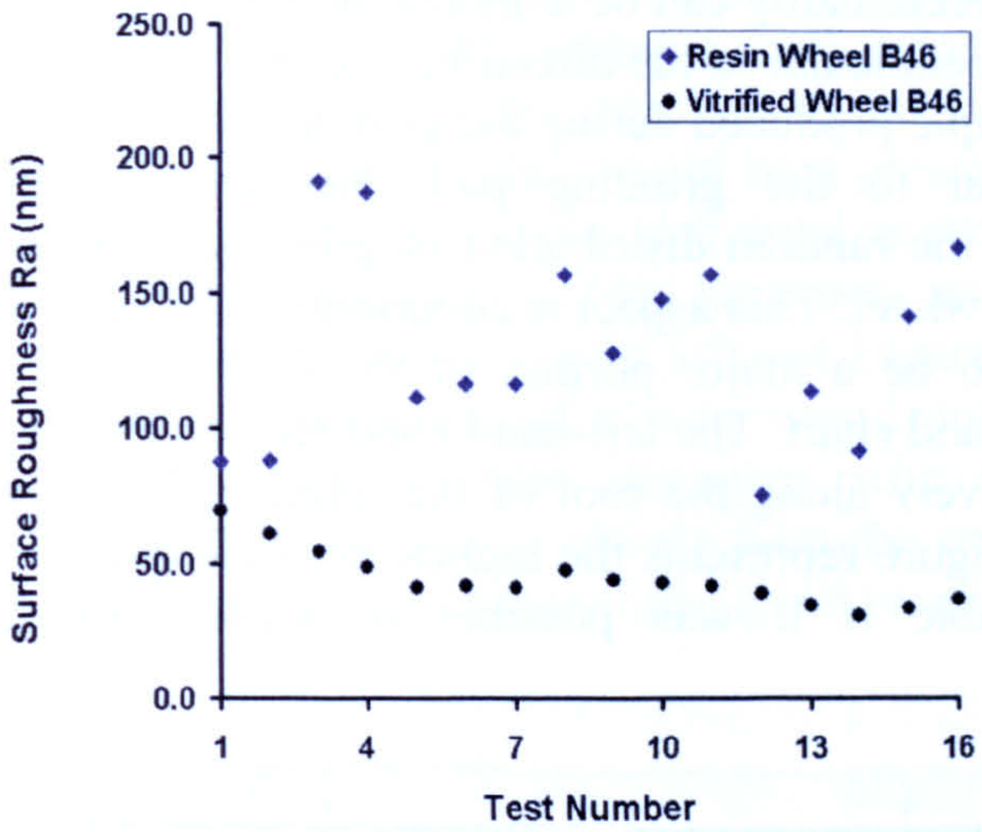

Figure 5.3 – Surface Finish Results for both Grinding Wheels

It has been demonstrated that the equivalent chip thickness h_{eq} has an impact on the grinding performance. Higher wheel speeds reduce h_{eq} and allow higher quality surface to be realised but need to remain within the boundaries of wheel balance.

At this stage measurement results were obtained for residual stress to ensure that the surface integrity remained stable. Figure 5.4 shows a representation of residual stress in terms of magnetic power (MP) obtained from the Barkhausen Noise (BN) instrument. As previously described in Chapter 3 the intensity of the Barkhausen noise signal is related to changes in residual stress, the instrument works as a comparator and the boundary between tensile and compressive stress in this case was set at a magnitude of 50. In the plot the figures all lie below the boundary level, hence it can be concluded that the grinding processes introduced desirable compressive stresses into the component surface. Therefore in this case there has been no thermal damage resulting from the grinding process.

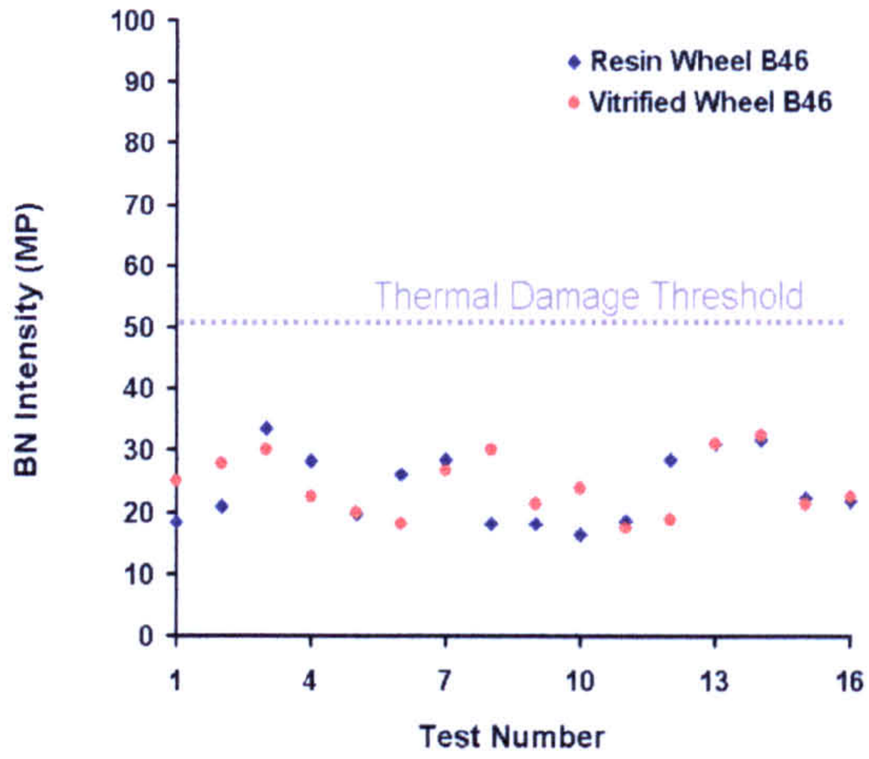

Figure 5.4 – Barkhausen Noise Readings for Surface Grind Trials

The effect of grinding directionality can be demonstrated by studying surface roughness profiles, parallel and perpendicular to the direction of grind. Figure 5.5 shows these two profiles for a typical sample produced during the grinding trials. The surface roughness data taken perpendicular to the grinding path includes the 'ploughed furrows' component produced by the random distribution of grinding grits throughout the bond structure of the grinding wheel. This aspect is commonly referred to as the grinding lay and can be assumed to be a major portion of the $0.087\mu m$ R_a surface roughness magnitude on the right-hand chart. The left-hand chart reinforces this in that the surface roughness figure, effectively along the root of the 'ploughed furrows' is far lower at $0.010\mu m$ R_a. The latter figure represents the highest possible quality surface roughness that would be achievable if it was possible to totally eliminate the grinding directionality.

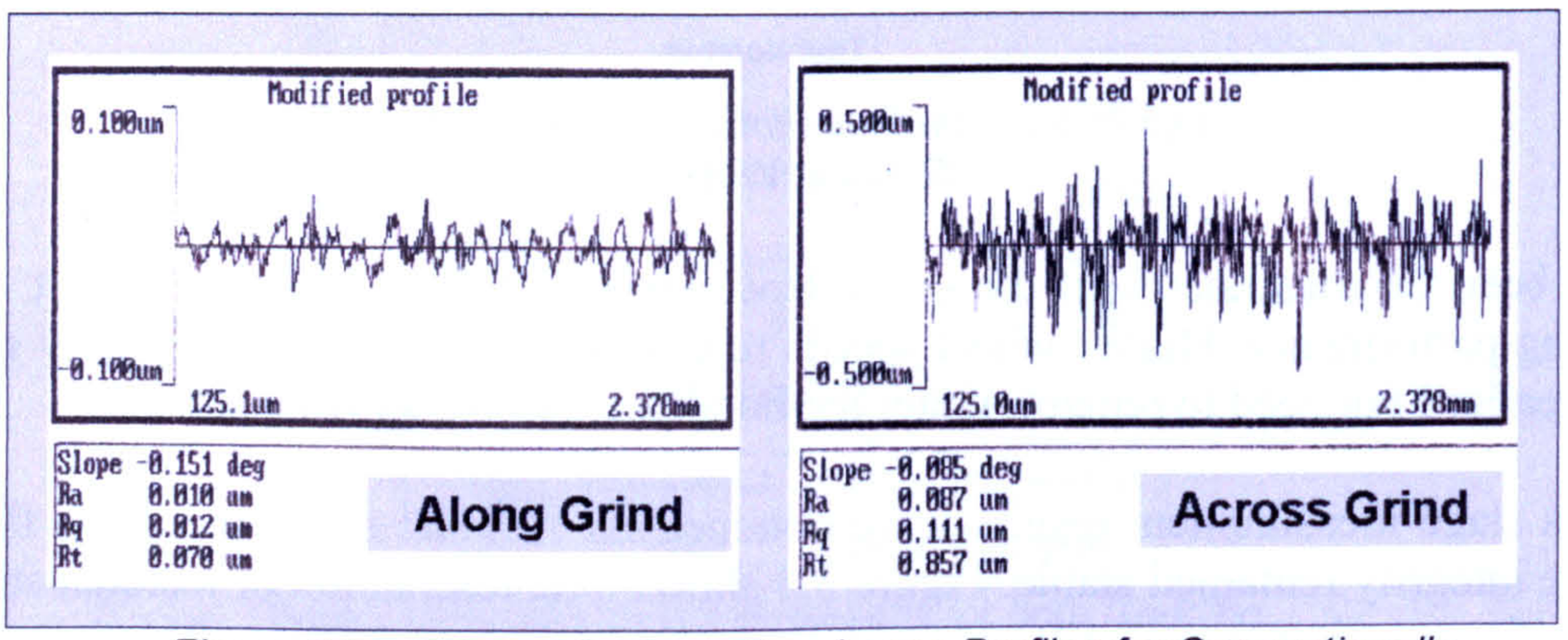

Figure 5.5 – Talysurf Surface Roughness Profiles for Conventionally Ground Sample

A more effective demonstration of the grinding lay is shown in Figure 5.6, a 3-dimensional surface profile measured using the Wyko white light interferometer. This measurement technique provides an overall surface roughness figure, in this case $0.072\mu m$ R_a for the same sample as in Figure 5.5.

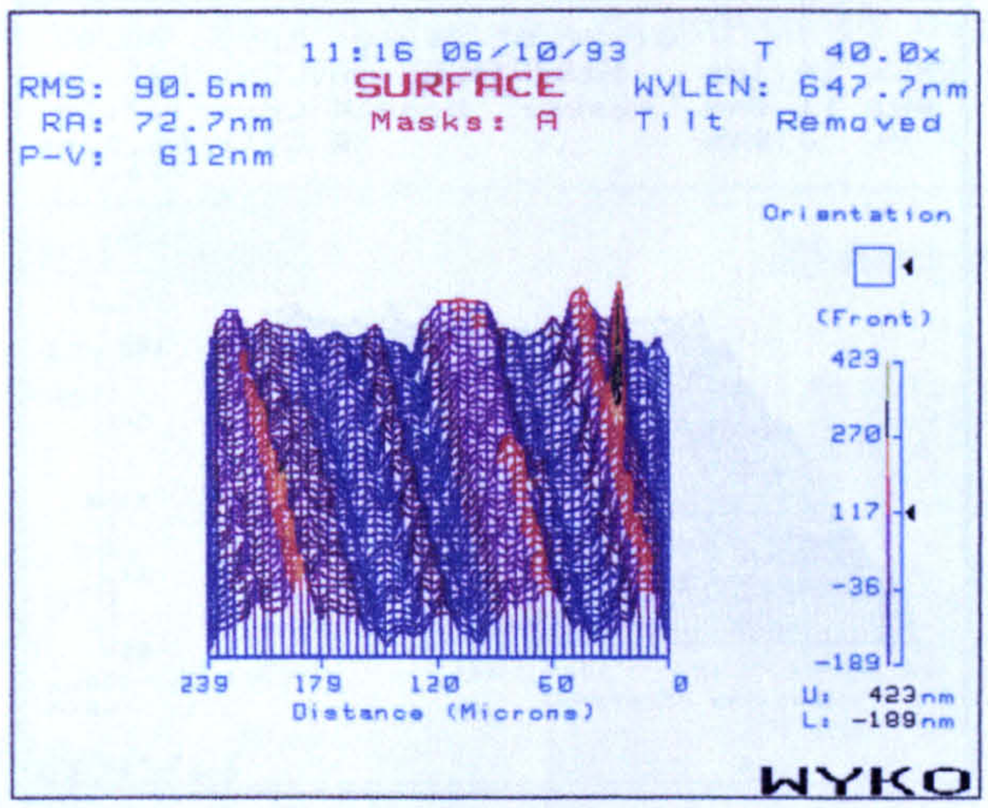

Figure 5.6 - Wyko Surface Profile of Conventionally Ground Sample

The final results for the surface grinding investigations consisted of the modified path ground sample, which in this case resembles a peel grind process. Therefore the magnitude of the surface roughness was expected to be in the region of the best achievable figure, namely *0.01μm* R_a. This would be a greater improvement than that expected by implementation of the oscillatory path grind as proposed for the cylindrical work. The results for both the profile surface roughness and 3-dimensional surface roughness measurements are shown in Figure 5.7 and Figure 5.8 respectively. These demonstrate that the grinding directionality was significantly reduced. An overall surface roughness of *0.011μm* R_a was measured with the Wyko white light interferometer for this surface, this aligns closely with the expected result. This is an order of magnitude better than for the conventional grind process used previously.

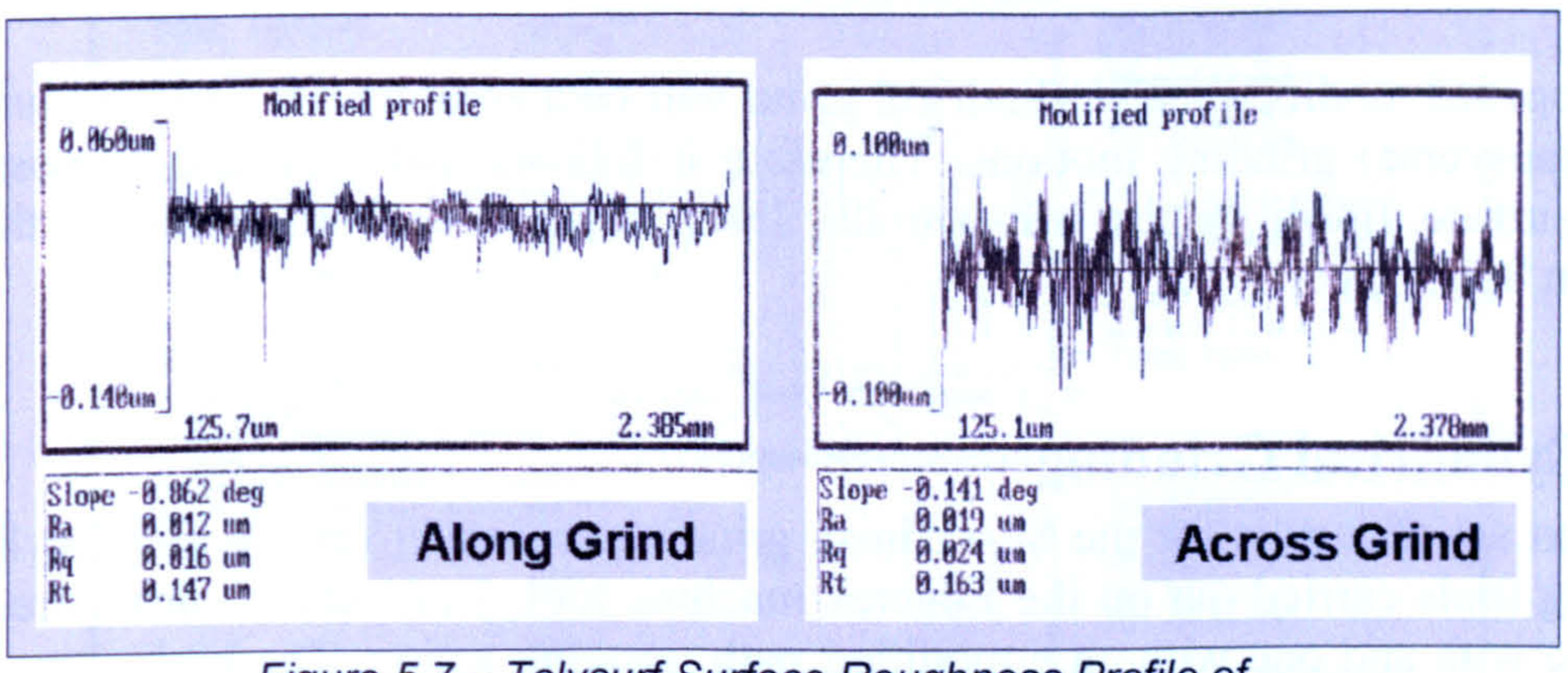

Figure 5.7 – Talysurf Surface Roughness Profile of Superfinish Sample

To reinforce the improvement achieved a visual representation of a conventional path and modified path components is shown in Figure 5.9. The image on the left is the conventional path component and the deterioration in the reflection, caused primarily by the effect of grinding lay is evident. Whereas on the right side the image for the grind test with the basic modified grind path is clearly of a higher quality.

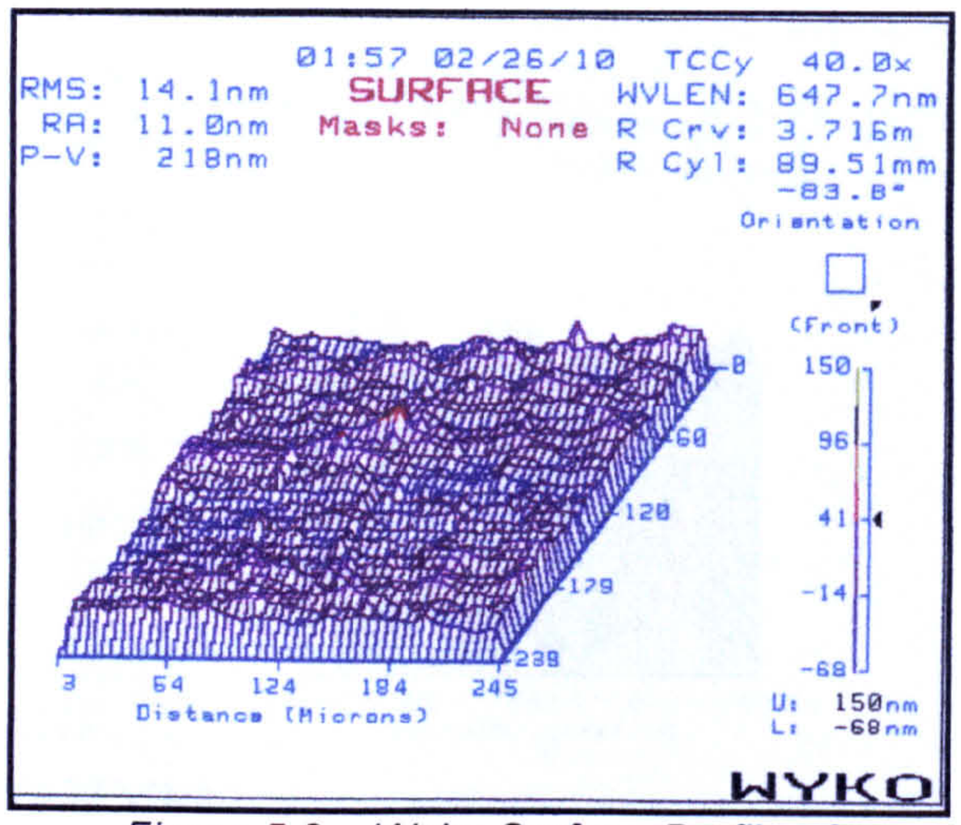

Figure 5.8 – Wyko Surface Profile of Superfinish Sample

Figure 5.9 – Photograph of Typical Finish & Superfinish Ground Samples

The proposed modified path cylindrical grind will be a combination of both plunge and peel (transverse) grinding motions. Therefore it follows that it should be possible to attain surface finish values between the levels achievable both types, in this case between 0.087μm and 0.011μm R_a.

5.2 Cylindrical Grinding

The next set of results for the Superfinish grinding regime cover the initial cylindrical grinding trials carried out on the Edgetek machine tool. Two sets of runs were carried out, one with and one without a modified path grinding action. The trials were limited by the capability of the machines standard CNC control system as outlined in section 3.2.2.3. Surface roughness data was obtained for both sets of samples with a Wyko RST interferrometric instrument. Results are shown for two samples, a conventionally ground testpiece (sample1), and a modified path grind testpiece (sample 9), see Figure 5.10 and Figure 5.11 respectively. The data in the plot contains both the 3-dimensional and profile roughness values, for the latter in both parallel and perpendicular orientations to the grinding lay. If initially the 3-dimensional plots are examined then in the case of sample 1 the surface roughness magnitudes are 0.115μm R_a and 0.147μm R_q. For sample 9 these values drop to 0.078μm R_a and 0.099μm R_q. Thus the result

demonstrate that the surface quality is indeed improved by using the modified path grind approach.

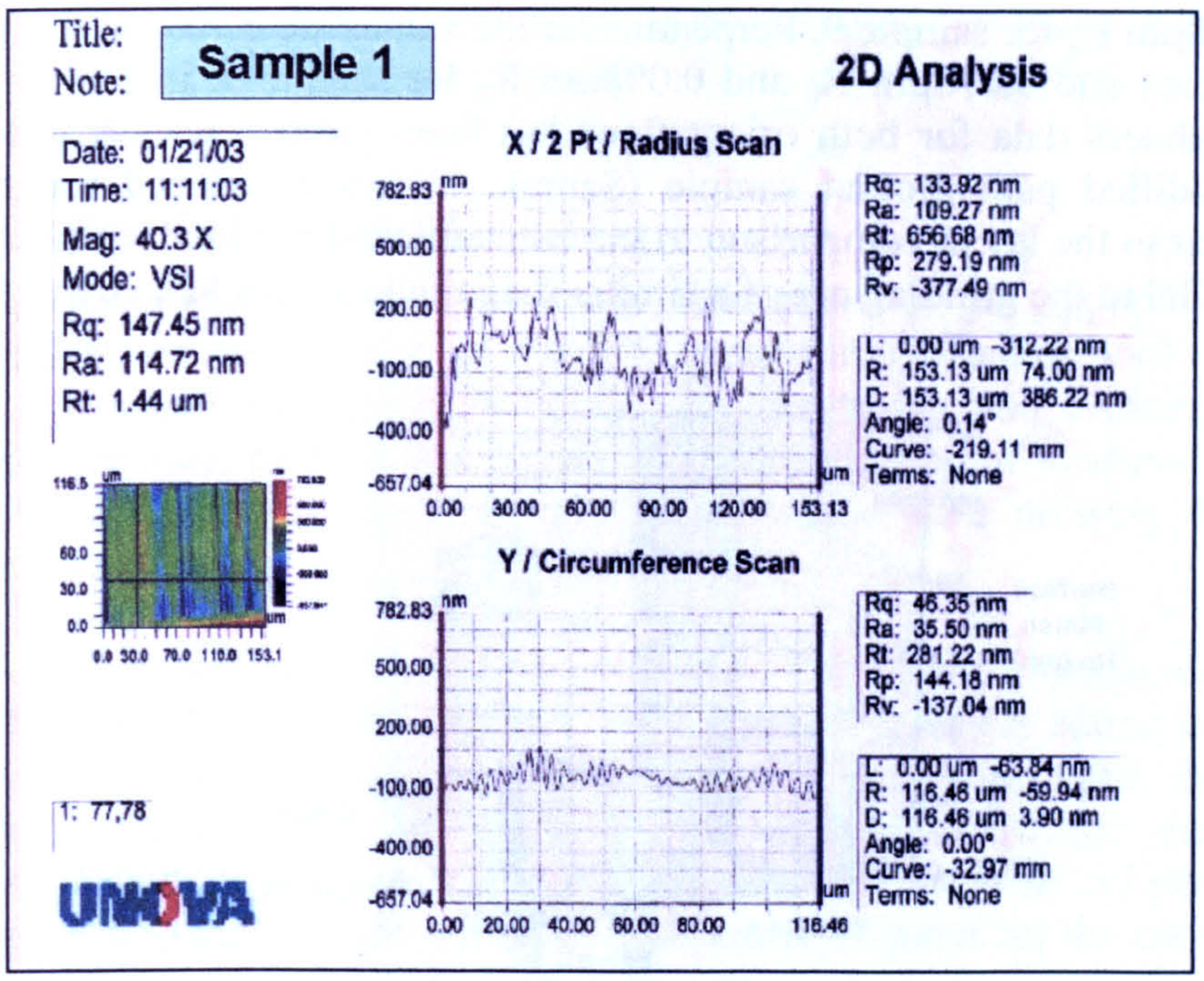

Figure 5.10 – Surface Roughness Plot for Conventional Cylindrically Plunge Ground Component

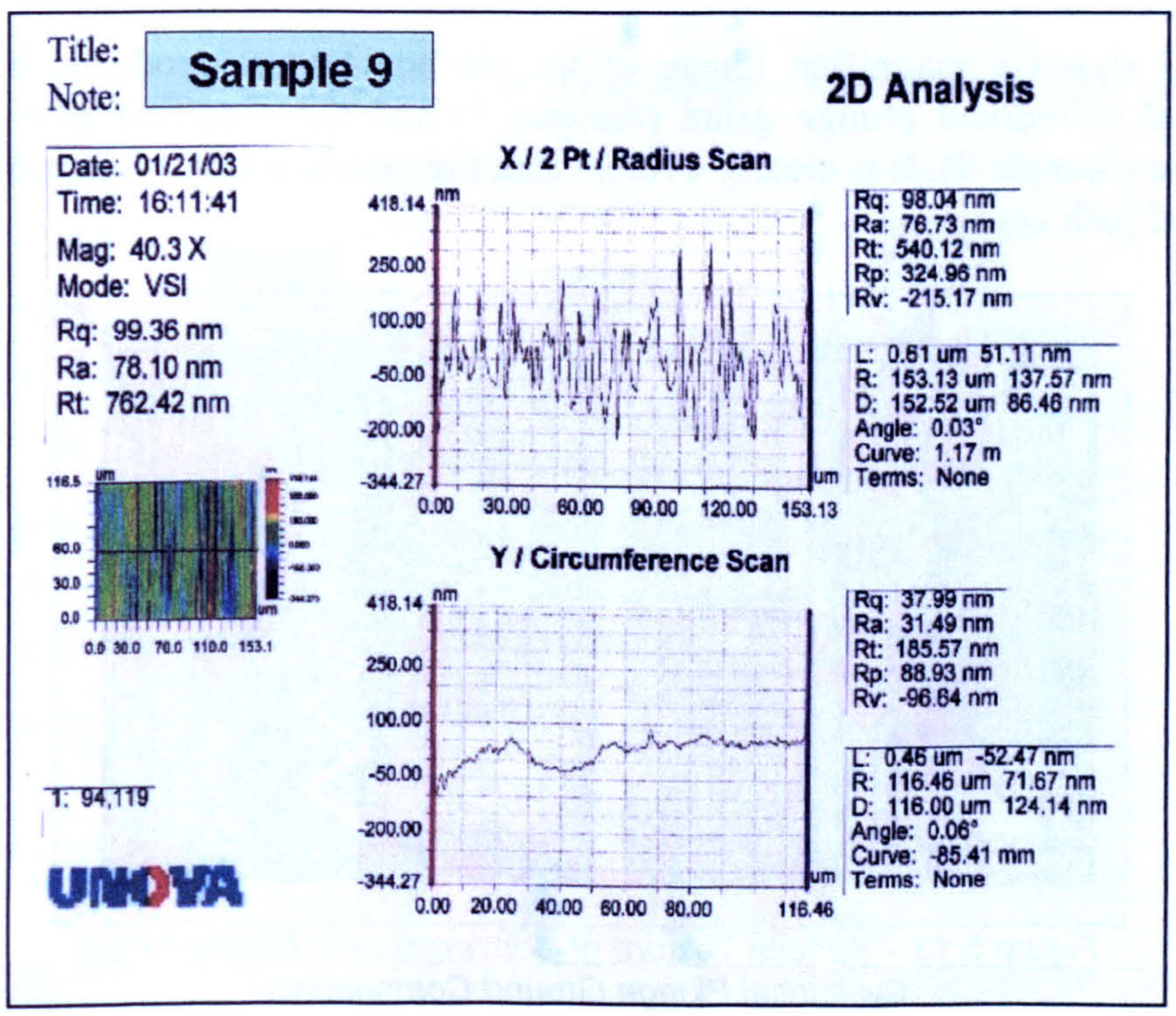

Figure 5.11 – Surface Roughness Plot for Modified Path Cylindrically Plunge Ground Component

If, the profile surface roughness data contained in Figure 5.10 and Figure 5.11 is examined then the effect parallel and perpendicular to the grinding lay can be seen. Parallel to the lay the values are 0.035µm R_a and 0.046µm R_q for sample1 and 0.031µm R_a and 0.038µm R_q for sample 9. Perpendicular the values are 0.109µm R_a and 0.134µm R_q for sample1 and 0.076µm R_a and 0.098µm R_q for sample 9. In Figure 5.12 the R_a surface roughness data for both orientations has been plotted, it clearly demonstrates that the modified path ground sample (Sample 9) has a reduced roughness value perpendicular to the lay in comparison to the conventionally ground sample (Sample 1). Values parallel to the grinding are of a similar magnitude as would be expected.

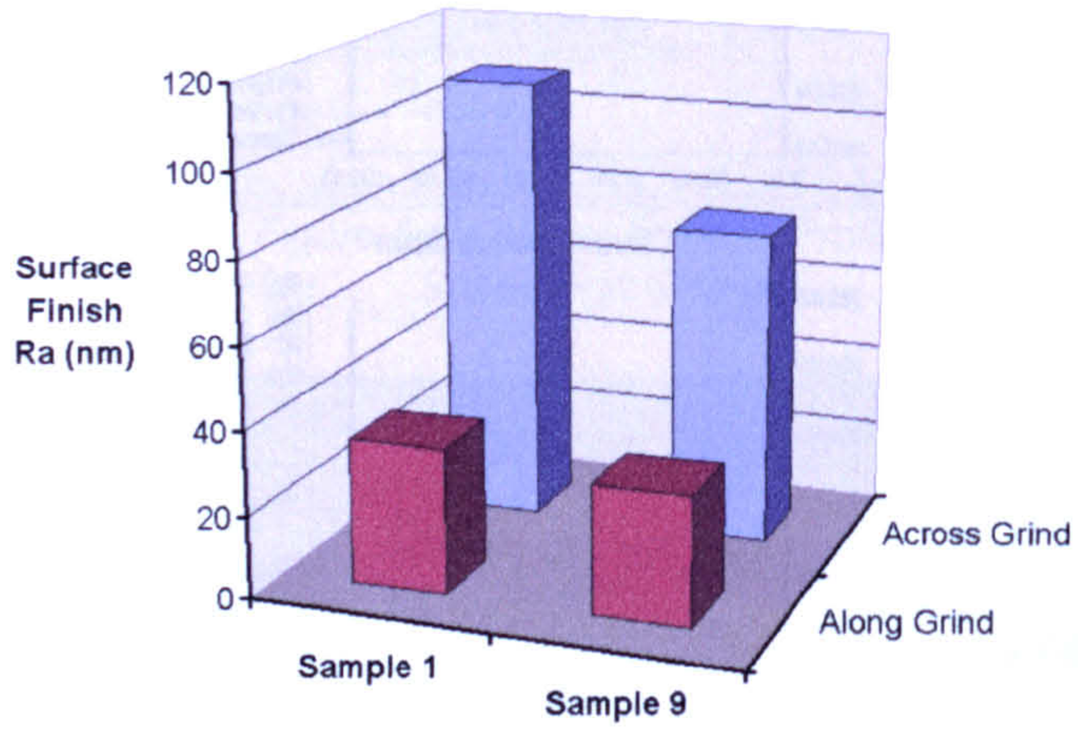

Figure 5.12 – Plot of Surface Roughness Data for Conventional and Modified Path Cylindrically Plunge Ground Components

Figure 5.13 shows a magnified image of the surface texture produced by both the conventional cylindrical plunge grind (Sample 1) and the modified path cylindrical plunge grind (Sample 9). It is clearly evident that the grinding lay is less pronounced in the modified path case.

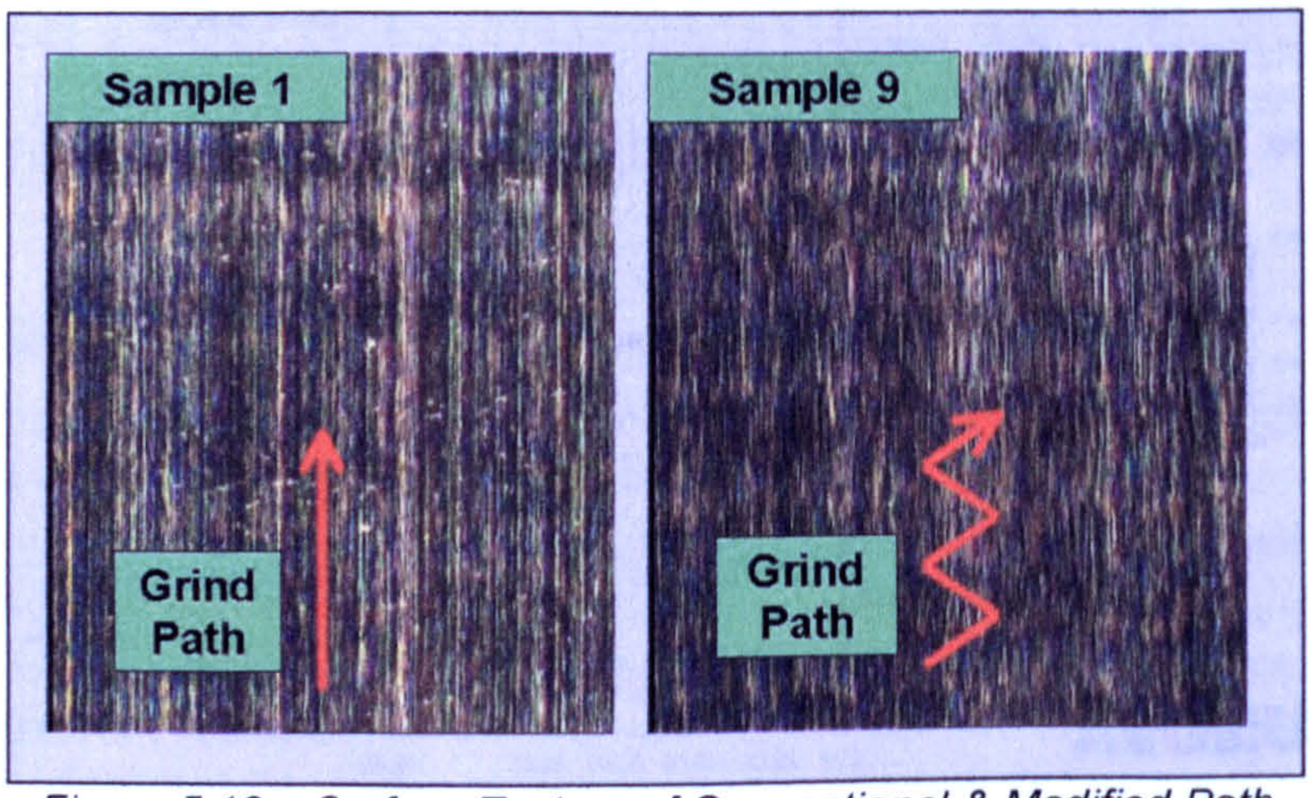

Figure 5.13 – Surface Texture of Conventional & Modified Path Cylindrical Plunge Ground Components

Again measurement results with the Barkhausen Noise (BN) instrument were obtained for residual stress to ensure that the surface integrity remained satisfactory. Figures remained below the boundary level, hence it was concluded that both the cylindrical

grinding processes, conventional and modified path did not introduce additional thermal damage which could result in undesirable tensile residual stress into the component.

Therefore it can be concluded that the effect of the grinding lay found in conventional grinding can be reduced by the implementation of a modified path grind.

5.3 Production Cylindrical Grinding

The results outlined in this section cover the final phase of the Superfinish grinding regime investigations carried out on the LT1 production machine tool. Results are presented for conventional plunge grinding with the truing and dressing technique utilised on the previous work, following that with the addition of modified grind path. These were compared with results from the benchmark trials utilising the standard truing and dressing.

The objective of the benchmark grinding trials was to provide comparison data for use throughout the superfinish grinding trials. Initially current wheel truing and dressing technology and a convention cylindrical plunge grind path were used. Subsequently modified path grinds were carried out at the rates selected for the following investigations. Figure 5.14 shows the results, for the conventional cylindrical plunge grind the surface finish was in the region of *0.105μm* R_a. Figures for the oscillatory tests ranged between 0.138*μm* and 0.142*μm* R_a.

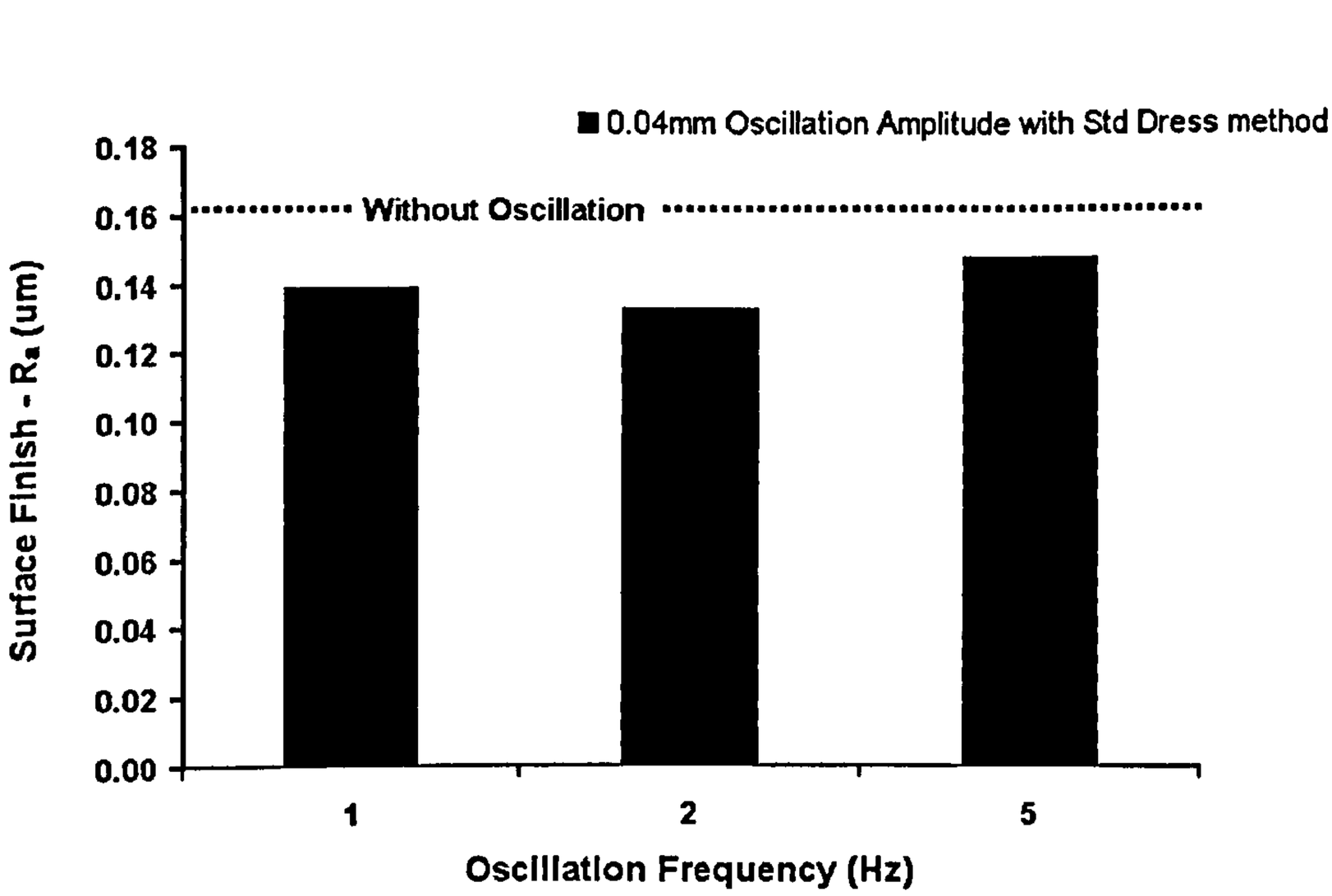

Figure 5.14 – Benchmark Grinding Data

In addition benchmark test data for the residual stress levels was recorded. The results can be seen in Figure 5.15. The results show that any induced thermal damage was below that of the threshold shown by the upper dotted line.

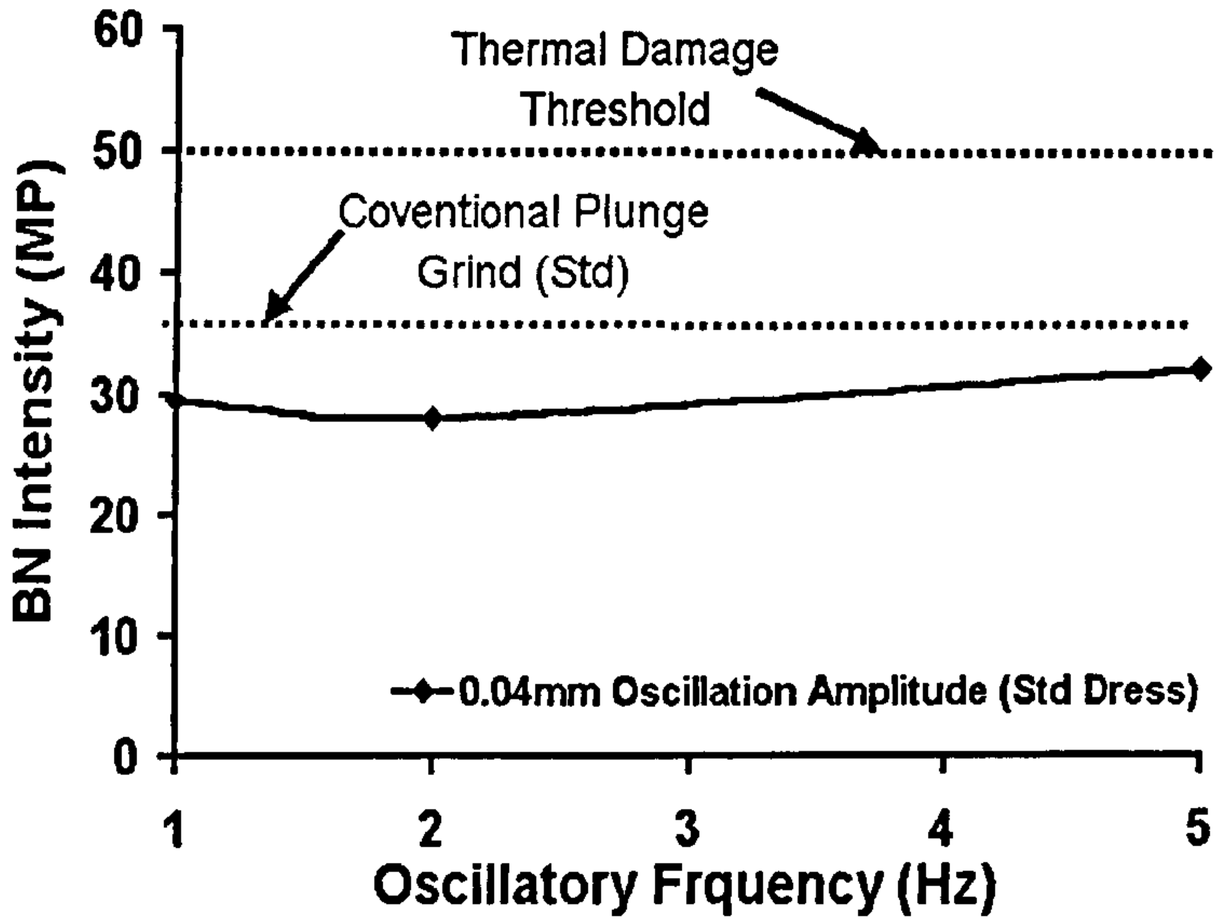

Figure 5.15 – Residual Stress Measurements for Benchmark Tests

Prior to carrying out the machine dresser modifications some measurements were carried out for both spindle stiffness and error motions to provide a comparison in the performance of both the existing and proposed truing spindles. The stiffness measurements demonstrated that the proposed Wendt unit offered an enhanced stiffness over that of the existing B&T unit, data is given in Table 5.1. For the radial orientation the stiffness increased from *37 N/μm* for the B&T to *58 N/μ*m for the Wendt unit and for the axial direction from *51 N/μm* to *108 N/μ*m respectively. The radial orientation being the most influential for the truing operation as applied to this work therefore provided a substantial improvement of 57%.

Orientation	***B&T Spindle***	***Wendt Spindle***
Radial	*37 N/μm*	*58 N/μm*
Axial	*51 N/μm*	*108 N/μm*

Table 5.1 - Table of Stiffness Data for Both Truing Spindles

Spindle error measurements also demonstrated an improved performance, the error motions can be seen in Figure 5.16. The synchronous errors were down from 1.39μm to 0.43μm for the Wendt spindle, the asynchronous errors reduced 0.488μm to 0.318μm.

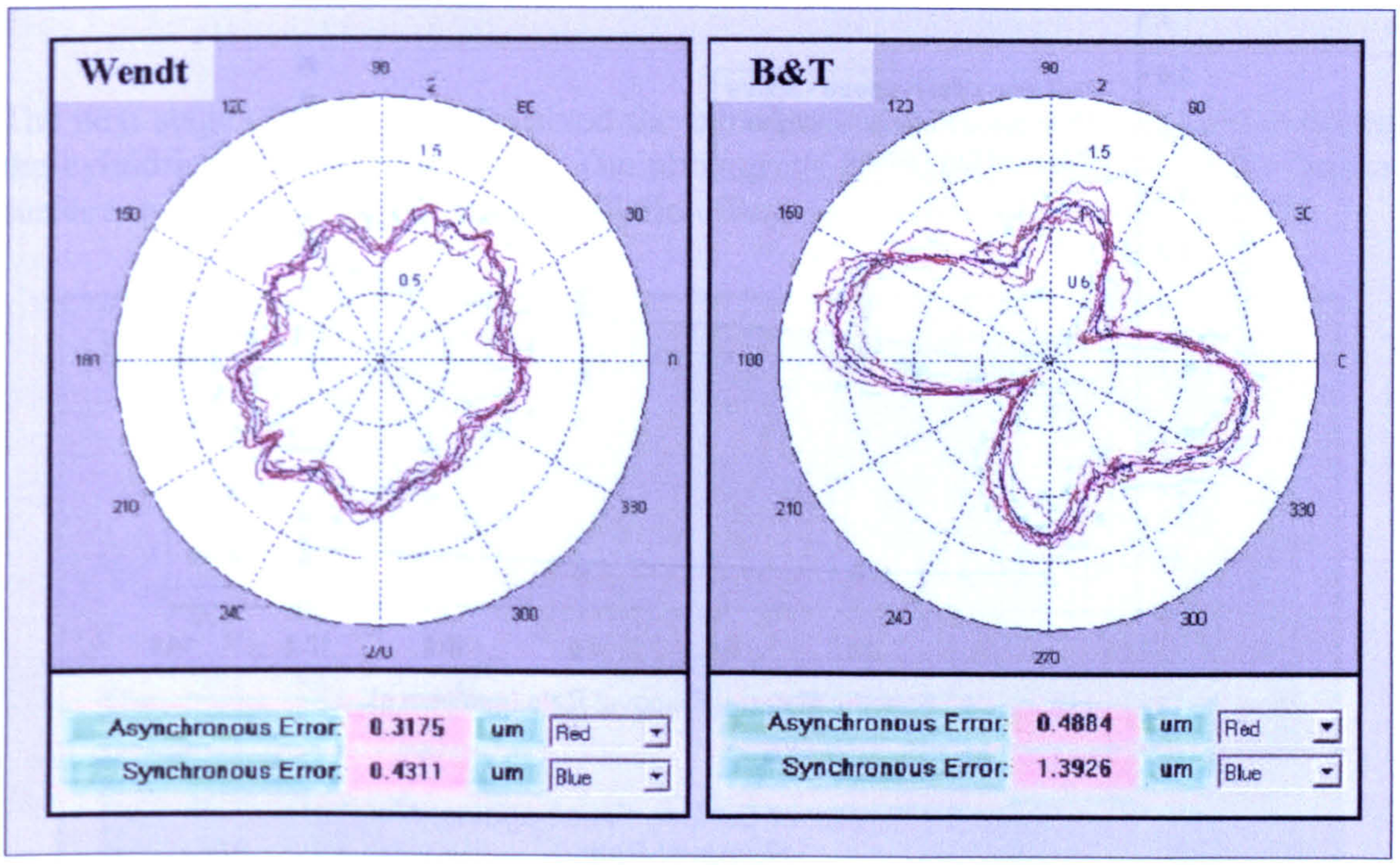

Figure 5.16 – LT1 Dresser Spindles (Error Motion Comparison)

Figure 5.17 below shows the surface roughness against material removal rate Q'_w ($mm^3/mm.s$) for the conventional cylindrical plunge grind mode tests with the improved truing and dressing techniques. Surface roughness readings were taken perpendicular to the grind path, values were consistently below the 0.15µm R_a level. The narrow spread of results for each test condition up to a Q'_w of $8mm^3/mm.s$ indicates that the process was operating in a stable manner, after this the spread increases thus indicating some instability is starting to occur. This increase was thought to be a result of grits separating from the bond structure as either a consequence of the grinding forces, wheel loading or a combination of these. These loose grits can then become trapped in the wheel / workpiece grinding zone where they can cause intermittent deep scratching of the surface. There was evidence of this occurring in the tests carried out at the Q'_w of $12mm^3/mm.s$ in the form of scratches, which were in the region of 3µm depth on the surface roughness traces taken. An example of this is seen in the results shown in Figure 5.18.

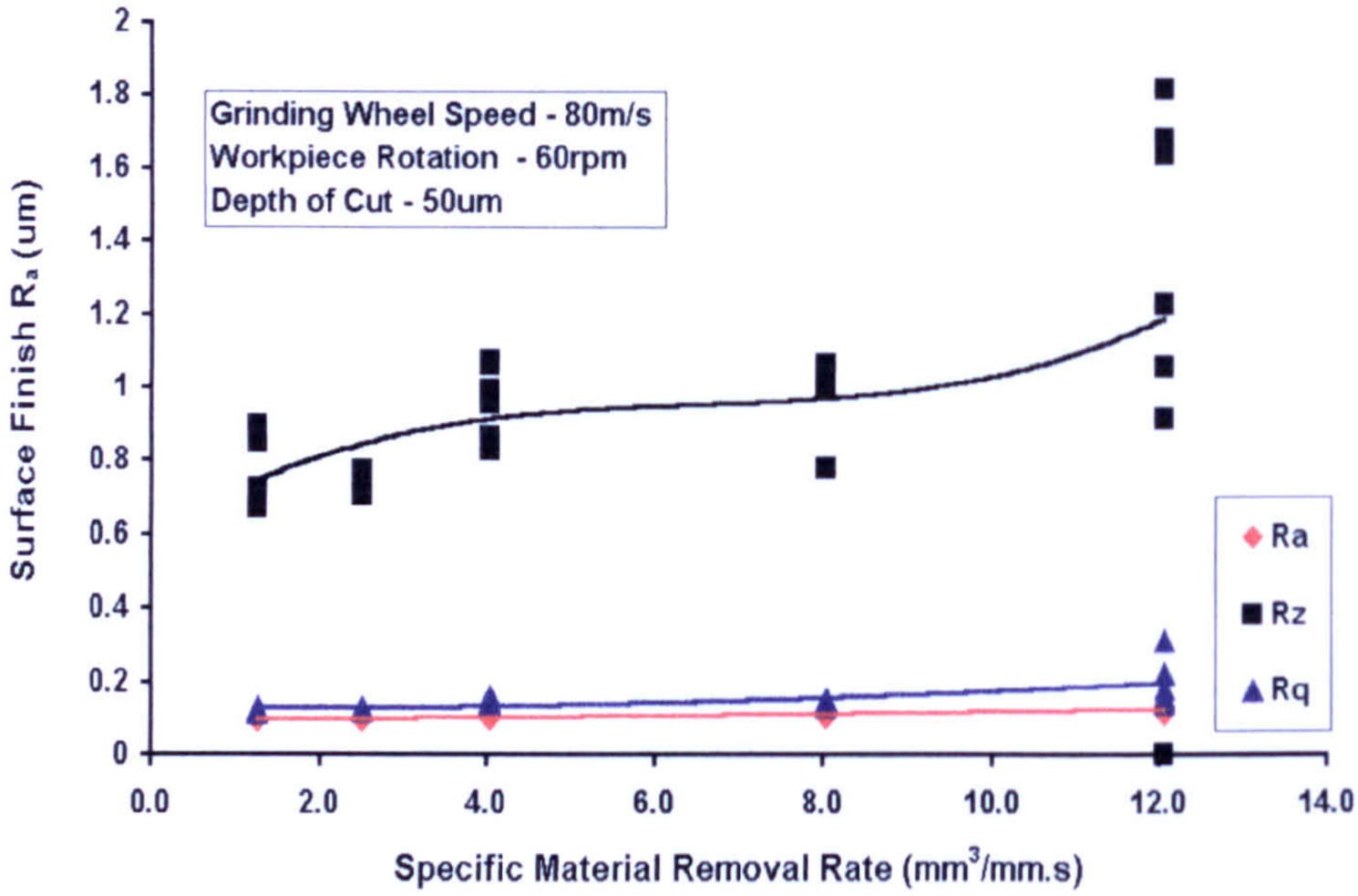

Figure 5.17 – Plot of Surface Finish against Material Removal Rate

The surface finish results were in general agreement with those carried out on the Edgetek machine tool in the earlier work and therefore it was concluded that the LT1 production machine tool was also capable of producing high quality surface finishes. As it was concluded that the machine was suitable to continue with the trials to validate an improvement in the surface quality of a component by the implementation of a modified grind path.

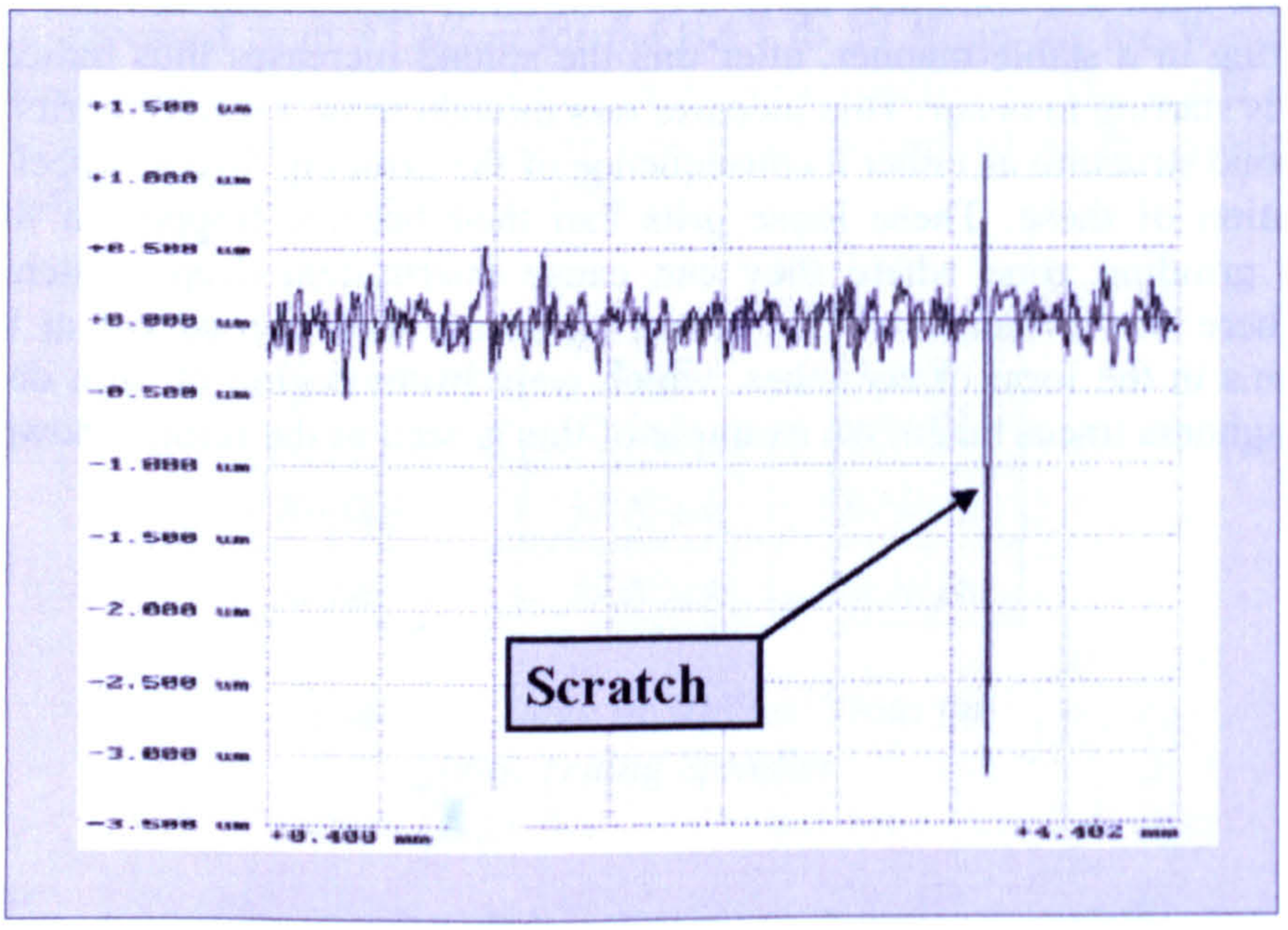

Figure 5.18 – Talysurf Trace illustrating Loose Grit Scratching of Surface

The next stage of these trials involved the introduction of the oscillatory motion during the cylindrical plunge grind mode. The photograph in Figure 5.19 shows some typical surfaces produced using the three oscillation frequencies (A–1Hz, B–2Hz, C–5Hz).

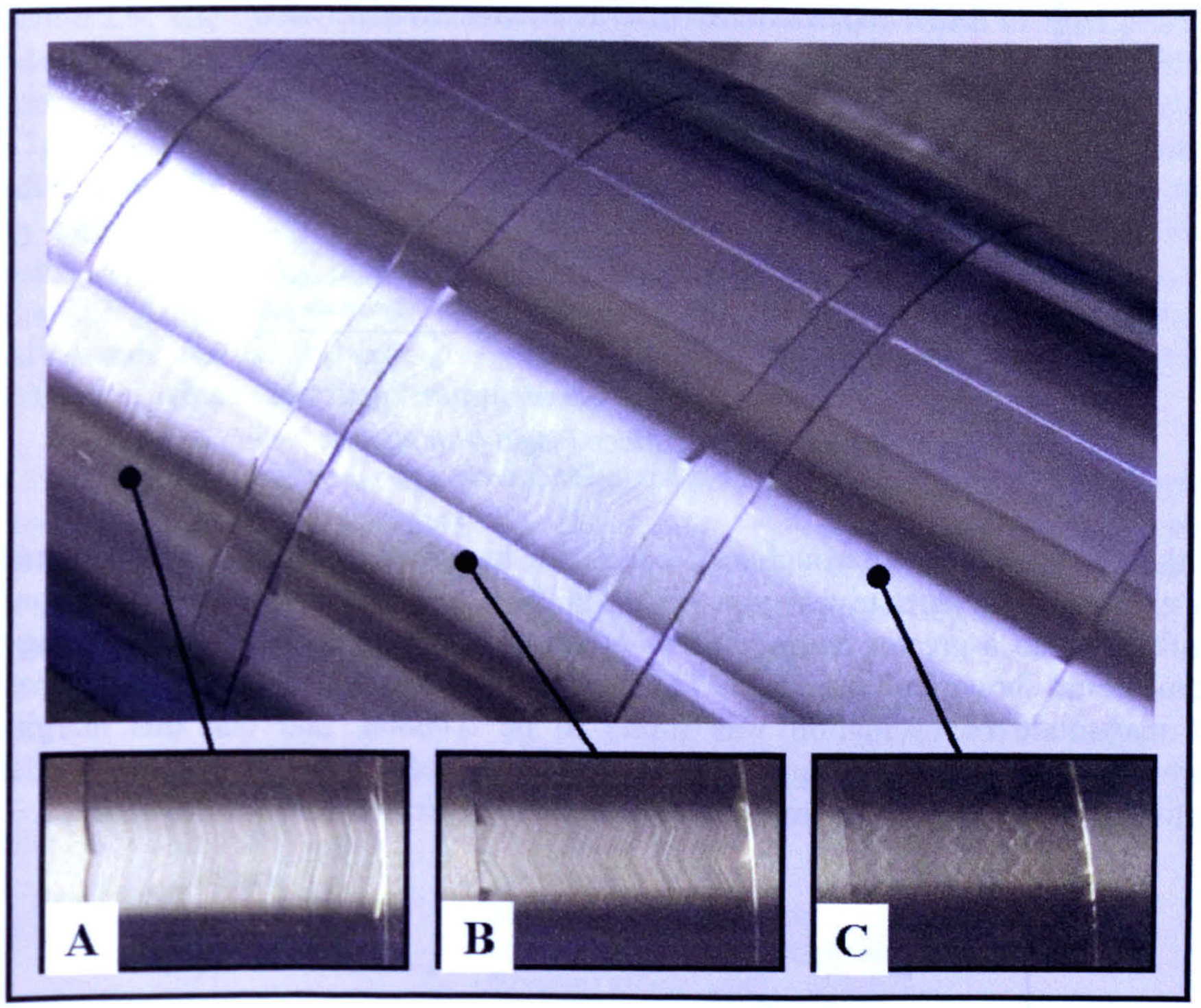

Figure 5.19 – Photograph of Oscillatory Ground Surfaces (A–1Hz, B–2Hz, C–5Hz)

In '*A*' the grinding lay was still predominately in the direction of the workpiece rotation. Whereas in 'B' and then 'C' this effect was reduced with the zigzag pattern commonly seen in honing and polishing operations becoming more evident. In Figure 5.20 the surface roughness data is shown against oscillation frequency. The oscillation frequencies were 1Hz, 2Hz,and 5Hz with amplitudes of 0.04mm, 0.25mm,and 0.5mm. Results show that the general level of surface roughness was reduced compared to that obtained for the conventional plunge grind test on the LT1. Hence it was concluded that the surface quality was improved with the implementation of a modified grind path. The general trend for the oscillatory results was for the lower amplitude test values to marginally improve with increasing frequency. Whilst the mid-range amplitude values remained broadly level and the higher amplitude increased roughness. It should be noted that in some instances the roughness value were down to $0.085\mu m$ R_a which is far

under that normally achieved on production finish grinding machines and is more typical of the region normally associated with post grind finishing processes.

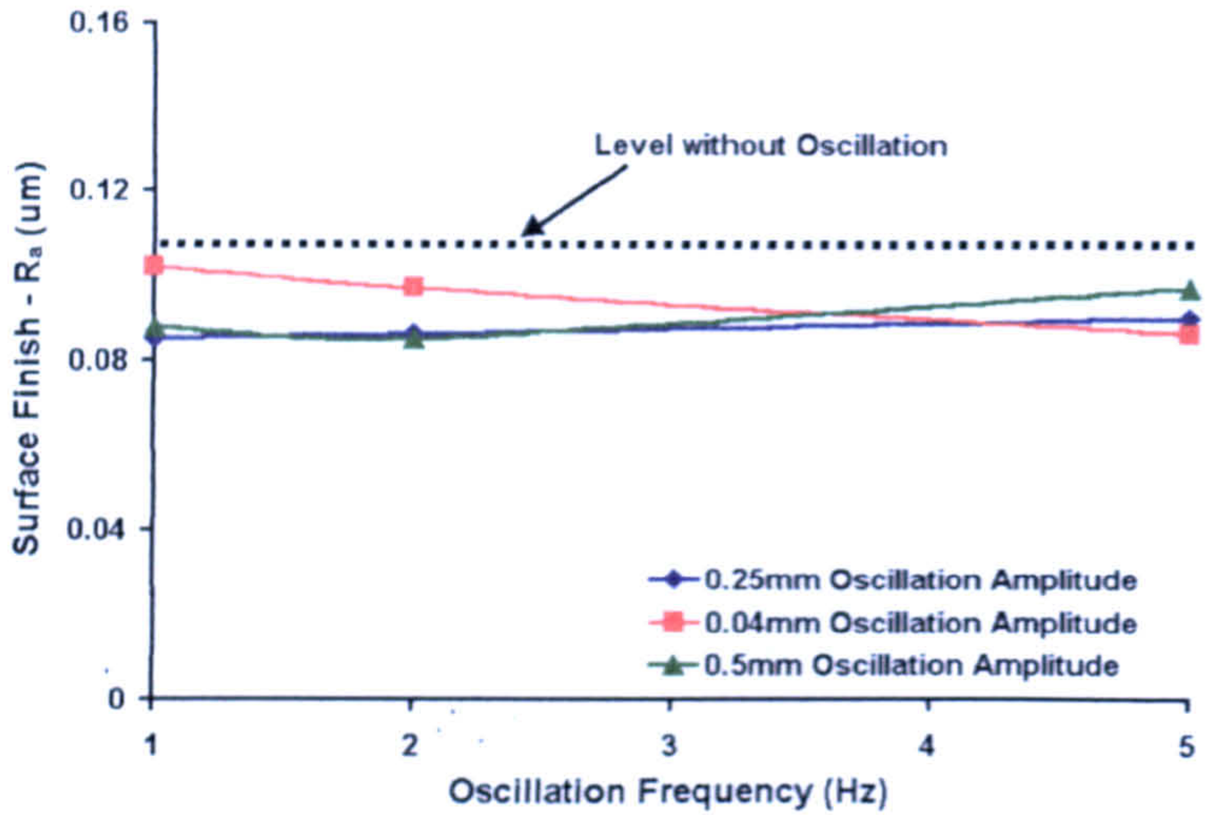

Figure 5.20 – Surface Finish (Ra) against Oscillation Frequency

Another average surface roughness parameter commonly used in the automotive industry is R_q. This term gives extra weight to the higher values (Dagnall, 1986) and so is influenced to a greater degree by the effect of grinding lay. The results using this parameter are shown in Figure 5.21. The plot confirms as for with results for R_a that the best magnitude of oscillation was found to be *0.08mm*, and that this marginally improved with frequency up to the tested value of *5Hz*. The larger oscillation amplitudes either showed no improvement or some deterioration with frequency.

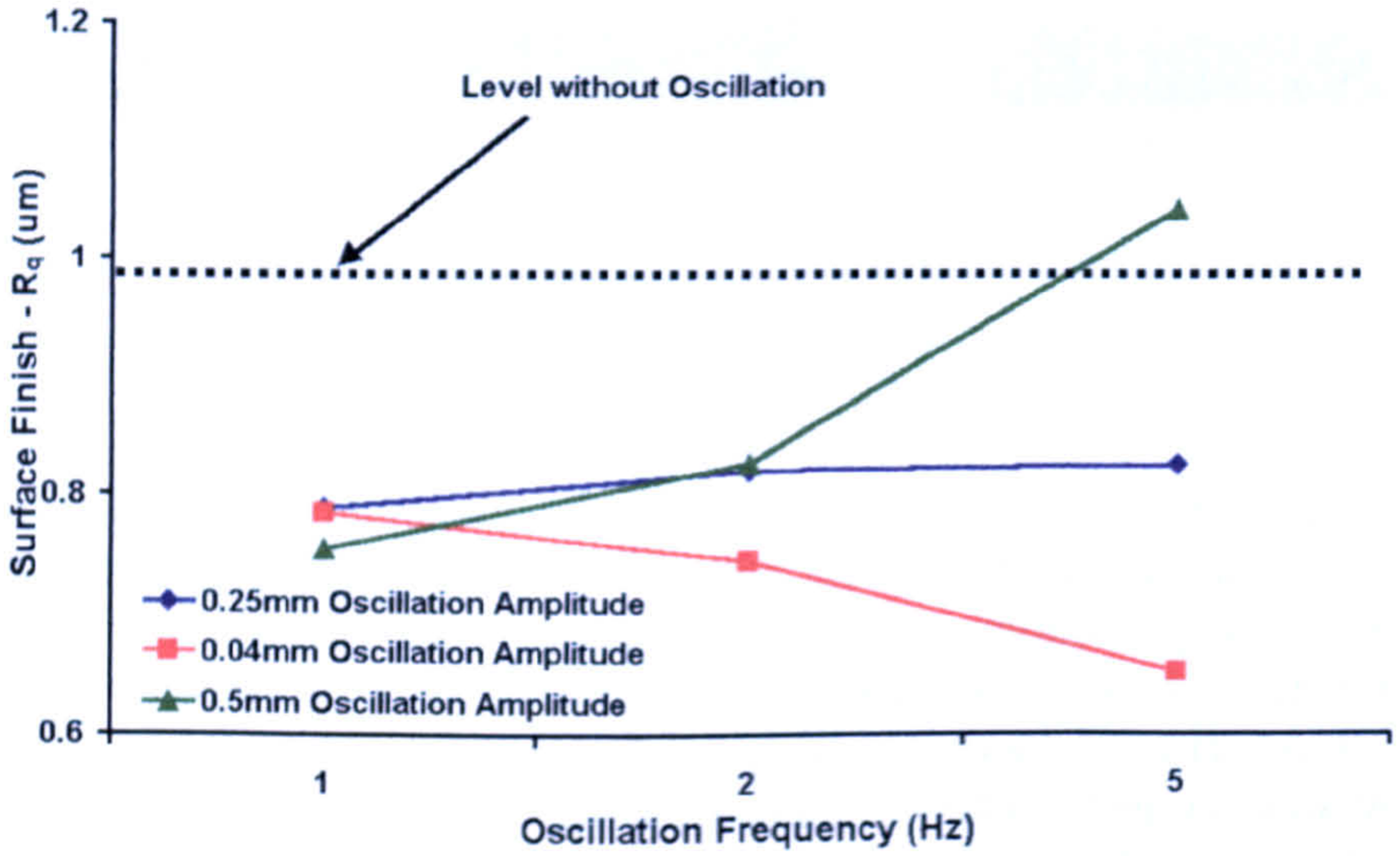

Figure 5.21 – Surface Finish (R_q) against Oscillation Frequency

Previous empirical roughness behavior investigations discussed by Malkin (1989) states that for conventional cylindrical plunge grinding the relationship given by Equation 2.8 holds. The investigations covered wheel grit sizes ranging from 450μm down to 107μm.

The corresponding range of y was found to be between 0.3 and 0.7, hence for grit sizes below this range a y value higher than 0.7 may be expected. For a grit size of 46μm and a *y* value of 0.73 the relationship predicts a value of 0.106μm R_a. This value aligns well to the measured value of 0.116μm R_a for the conventional plunge grind in Figure 5.20.

For transverse grinding which is akin to the sideways oscillation motion component implemented for the modified path grind, Malkin uses the relationship given by Equation 2.9. The relationship demonstrates that either a wider wheel or finer crossfeed should result in an improvement in the surface finish produced. For a wheel width of 20mm, a crossfeed of 0.5mm/s, and a z value of 1.2 the relationship predicts a value of 0.012μm R_a. This value aligns well with the experimental findings in the earlier surface grinding trials. In that case a value of 0.019μm R_a was obtained for the modified path (fully transverse) test, see trace on right in Figure 5.7. It was noted that at the higher crossfeed values a result of high oscillation magnitudes and frequency, the relationship produced high R_a values. These were higher than that for a straight plunge feed. As this clearly would not be the case it showed that there was a limitation in the level of crossfeed for which the relationship remained valid.

The surface finish results for the modified path trials shown in Figure 5.20 lie between the two values given by Equation 2.8 and Equation 2.9. This was to be expected as the modified path grind is a combination of transverse and conventional plunge paths and so is therefore a hybrid. The contribution from each path can be determined by the ratio of the two component velocities. Hence...

$$(R_a)_{MP} = \left(\left(\frac{s_p}{s_p + s_t}\right) \cdot d_g{}^{y}\right) + \left(\left(\frac{s_t}{s_p + s_t}\right) \cdot \left(\frac{b_s}{s_t}\right)^{-z}\right)$$

Equation 5.1 – Surface Finish for Modified Path Grinding

Where:

- d_g - *Grinding Wheel grit size*
- y - *constant dependant on grit size (0.73)*
- b_s - *Grinding Wheel width*
- s_t - *Crossfeed*
- s_p - *Peripheral Speed of Workpiece*
- z - *Constant (1.2)*

Equation 5.1 was used to model the modified path grinding process. Figure 5.22 shows the velocity ratios, surface finish components (plunge and transverse) and combined surface finish for the 0.25mm amplitude oscillation over the range of frequencies. As the oscillation frequency increases so does the transverse velocity (crossfeed) as it has further to travel. Hence as predicted by Equation 2.8 there would be a deterioration in the surface finish as illustrated by the green line. There is no transverse action in the plunge value as given by Equation 2.9 and so it remains constant, see blue line. With the increase in oscillation frequency the transverse velocity ratio increases as represented by the green dotted line. Whilst the plunge grind velocity ratio decreases, shown by the blue dotted line. The combination of these effects is shown by the red line and represents the modified grind path surface finish. This remains relatively constant with the frequency increase.

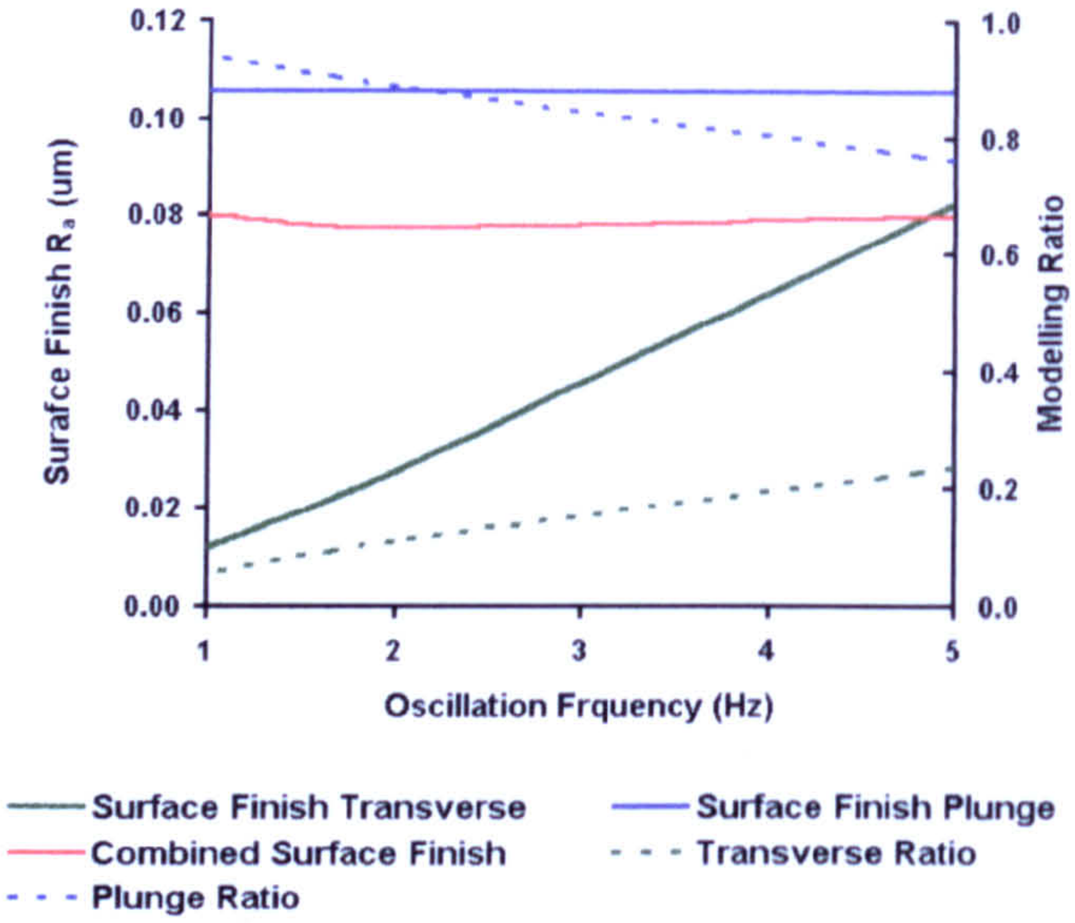

Figure 5.22 – Surface Finish Modelling Ratio's

In conclusion the modified path surface finish is governed by the combination of two factors:

1) The increase in the significance of the transverse surface finish component as the oscillation frequency increases
2) The deterioration in transverse surface finish as the oscillation frequency increases.

Figure 5.23 shows the model predictions for all three oscillation amplitudes used in the trials. It illustrates that whilst the lower two oscillation frequencies produced relatively constant surface finish predictions the larger values predicts a deterioration. These predictions were broadly in line with the experimental results shown in Figure 5.20.

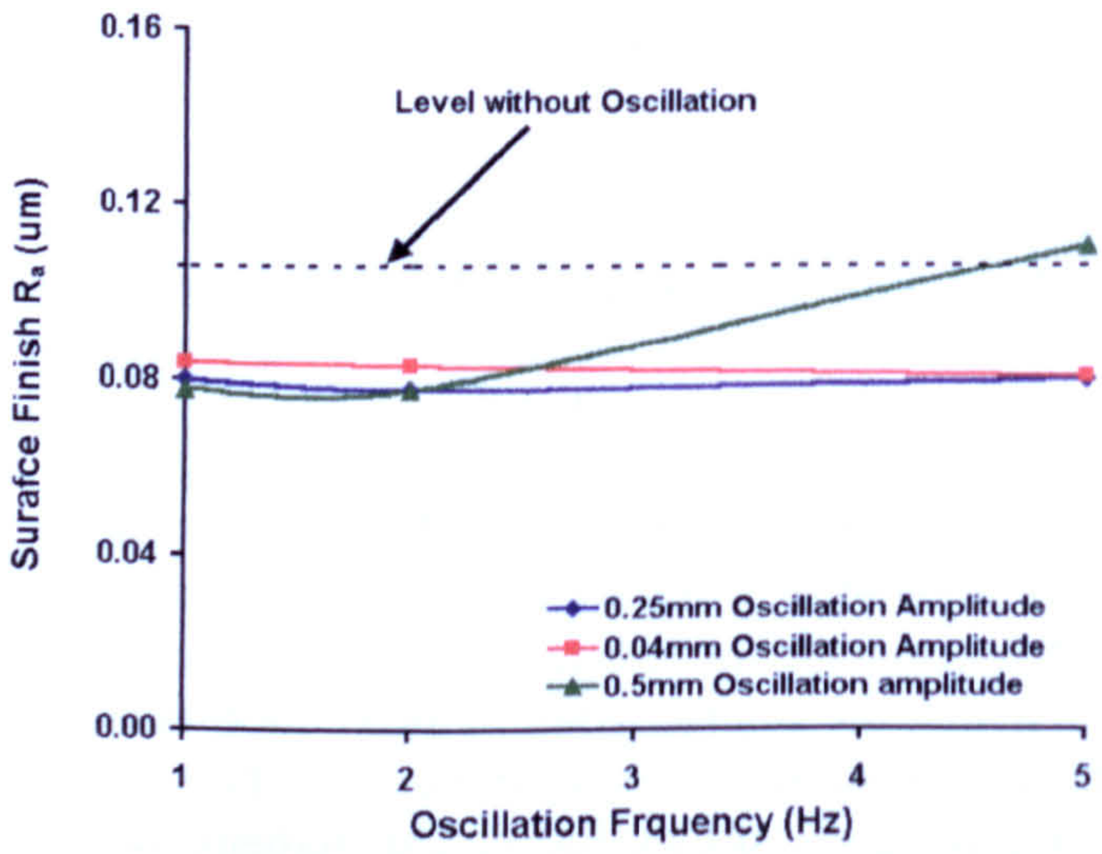

Figure 5.23 – Modelled Surface Finish (Ra) versus Oscillation Frequency

The next stage was to consider possible machine limitations imposed by the performance of the slideway axes and control system, namely:

- Generation and shape of oscillatory path motion
- Axis Bandwidth
- Machine Resonance

Machine data log files from the grinding trials were analysed which gave information for the axis position demand, actual position and error throughout the grinding cycle, these parameters were plotted against time. Figure 5.24 through to Figure 5.26 show the data for the 0.25mm oscillatory tests at 1,2 and 5Hz. The following error shown in the circled region and represented by the 'axes error' was seen to increase from a magnitude of 2μm at 1Hz, to 4μm at 2Hz and 8μm at 5Hz. Plots for the 0.5mm oscillatory tests are shown in Figure 5.27 and Figure 5.28, in this instance the 'axes errors' was 5μm at 2Hz and 10μm at 5Hz. Figure 5.29 shows the plot for the 0.04mm oscillation at 2Hz, this time the 'axes error' is less than 0.8μm. Therefore it was concluded that for the larger amplitudes of oscillation increasing frequency resulted in larger axes following errors. Hence these conditions would be more susceptible to vibration and resonates.

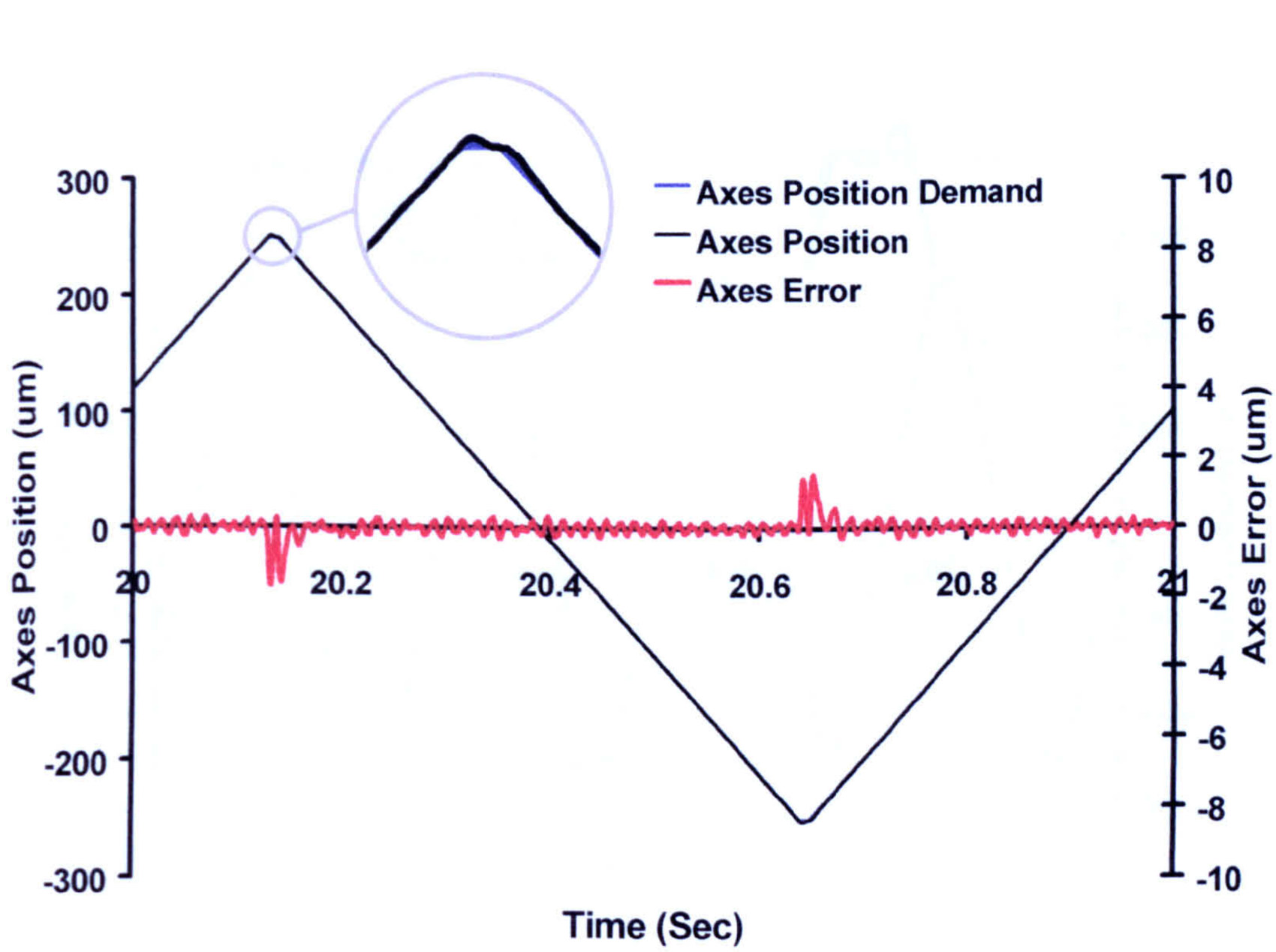

Figure 5.24 – Machine Performance for Oscillation of 0.25mm at 1Hz

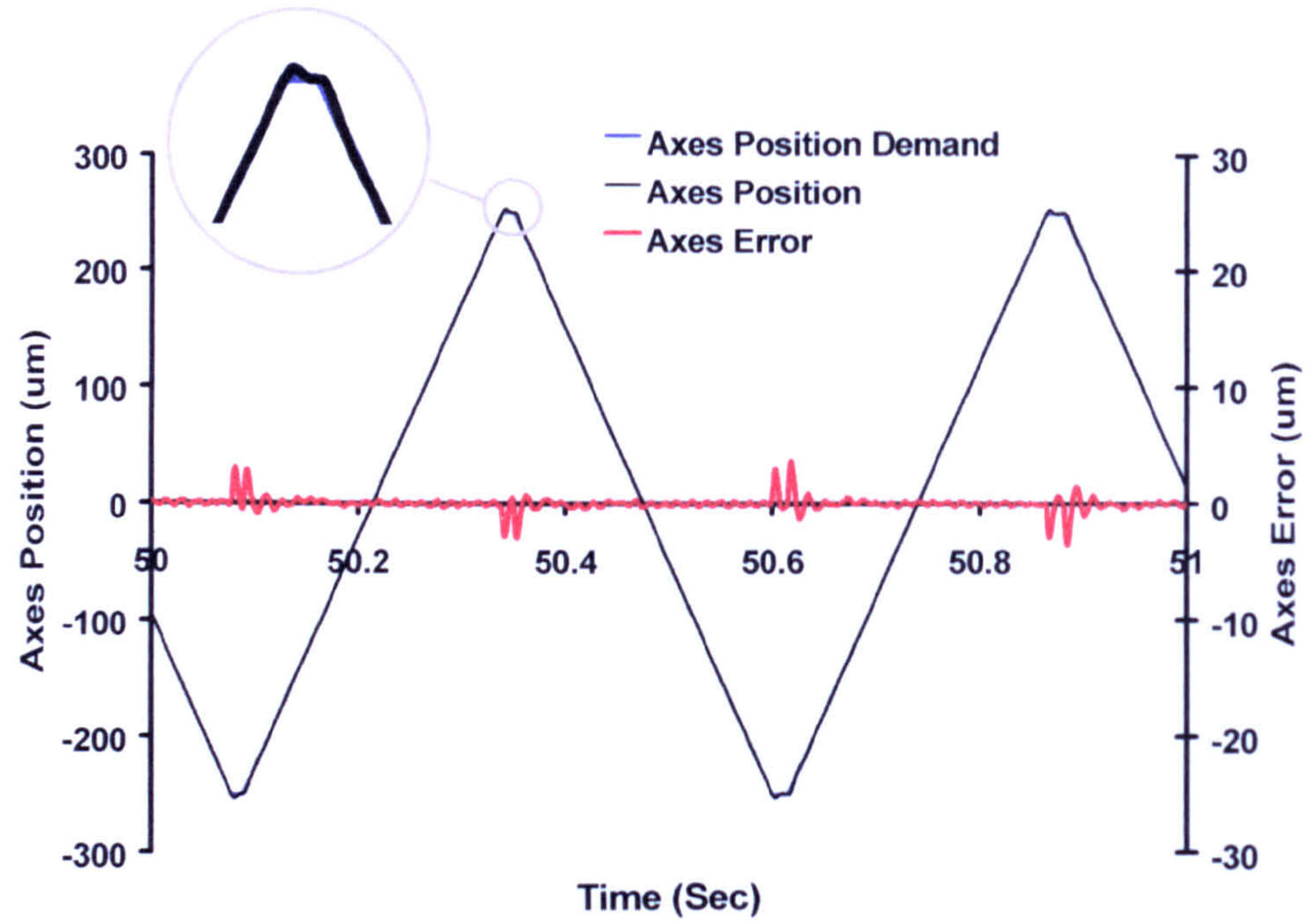

Figure 5.25 – Machine Performance for Oscillation of 0.25mm at 2Hz

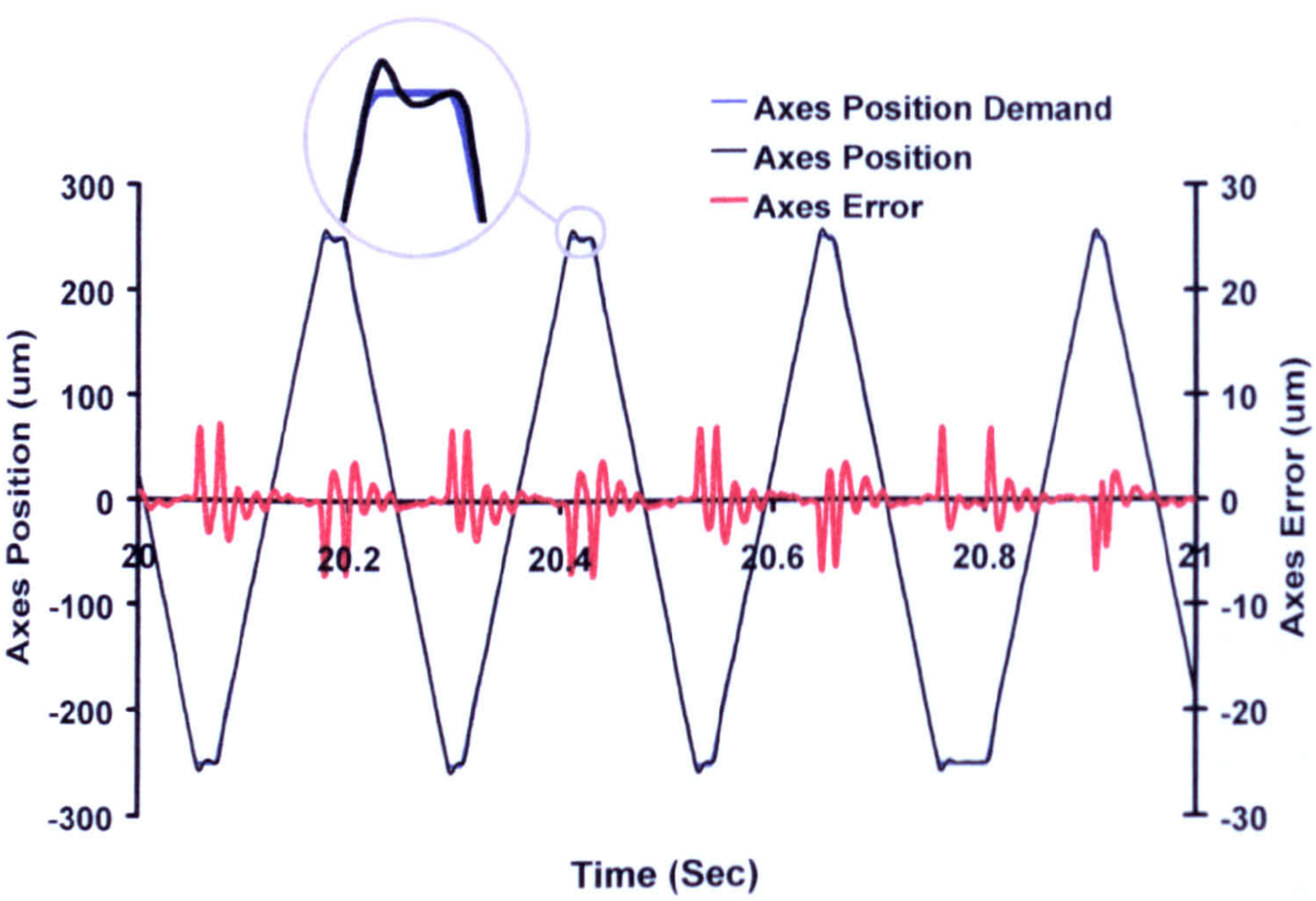

Figure 5.26 – Machine Performance for Oscillation of 0.25mm at 5Hz

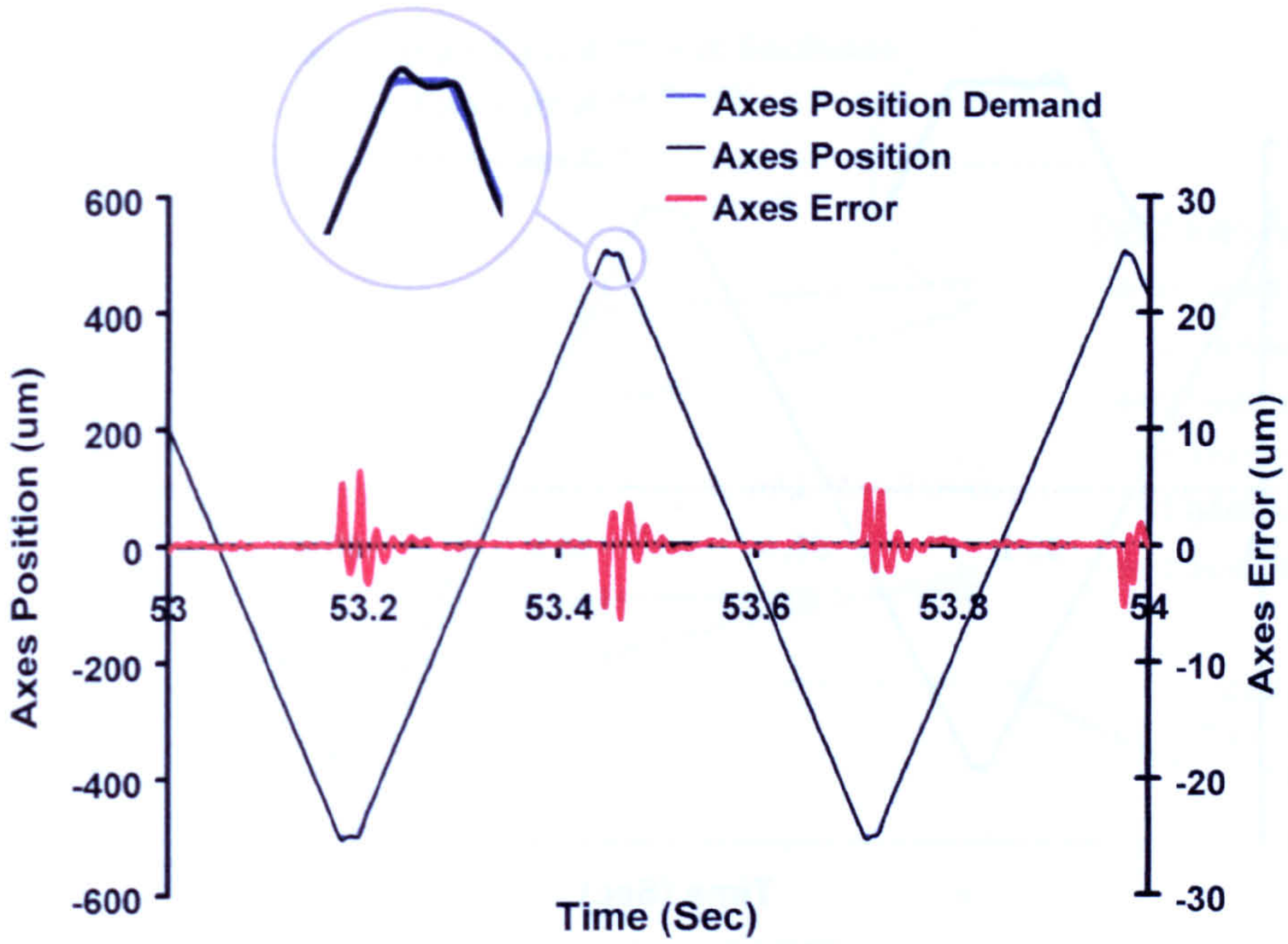

Figure 5.27 – Machine Performance for Oscillation of 0.5mm at 2Hz

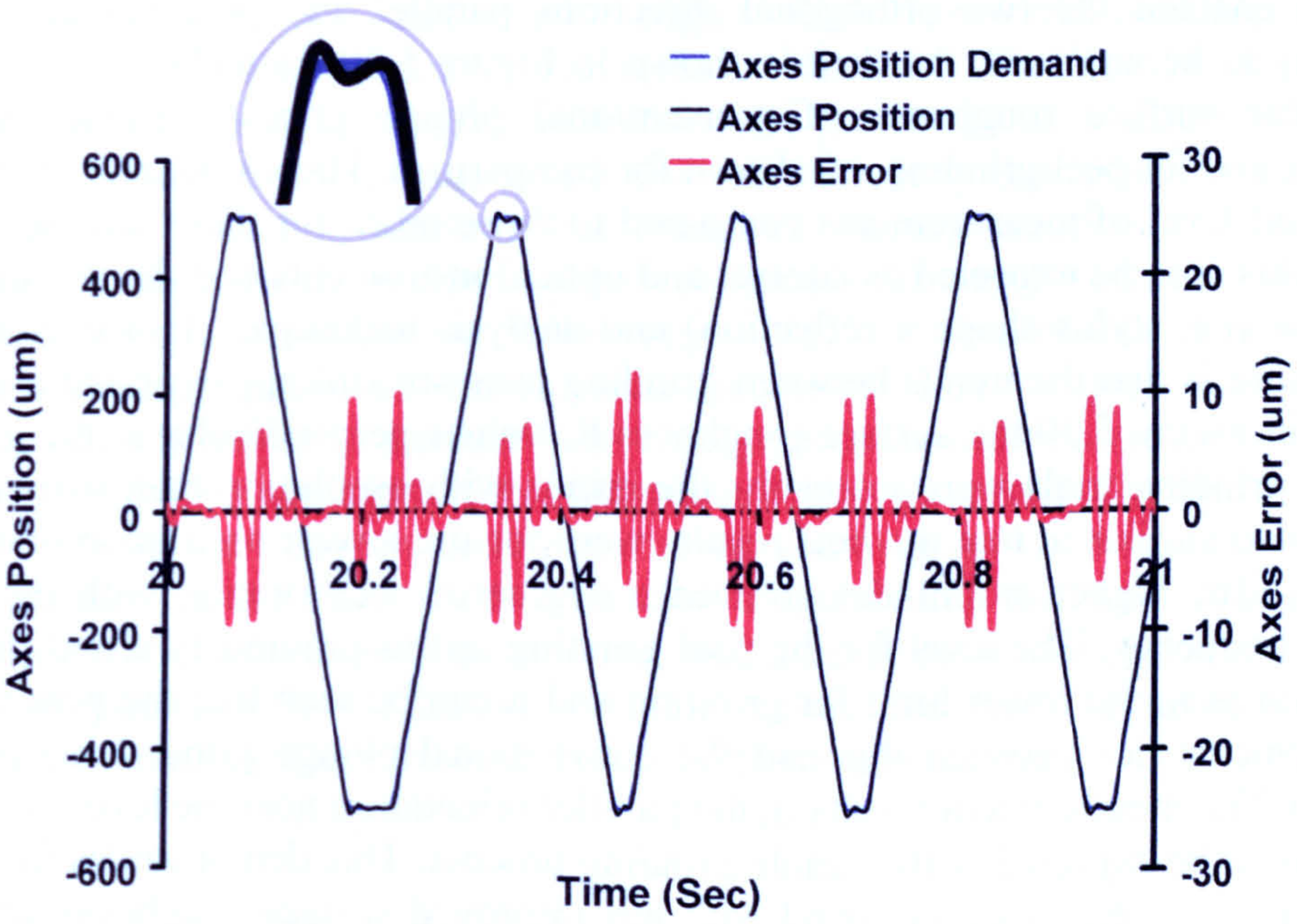

Figure 5.28 – Machine Performance for Oscillation of 0.5mm at 5Hz

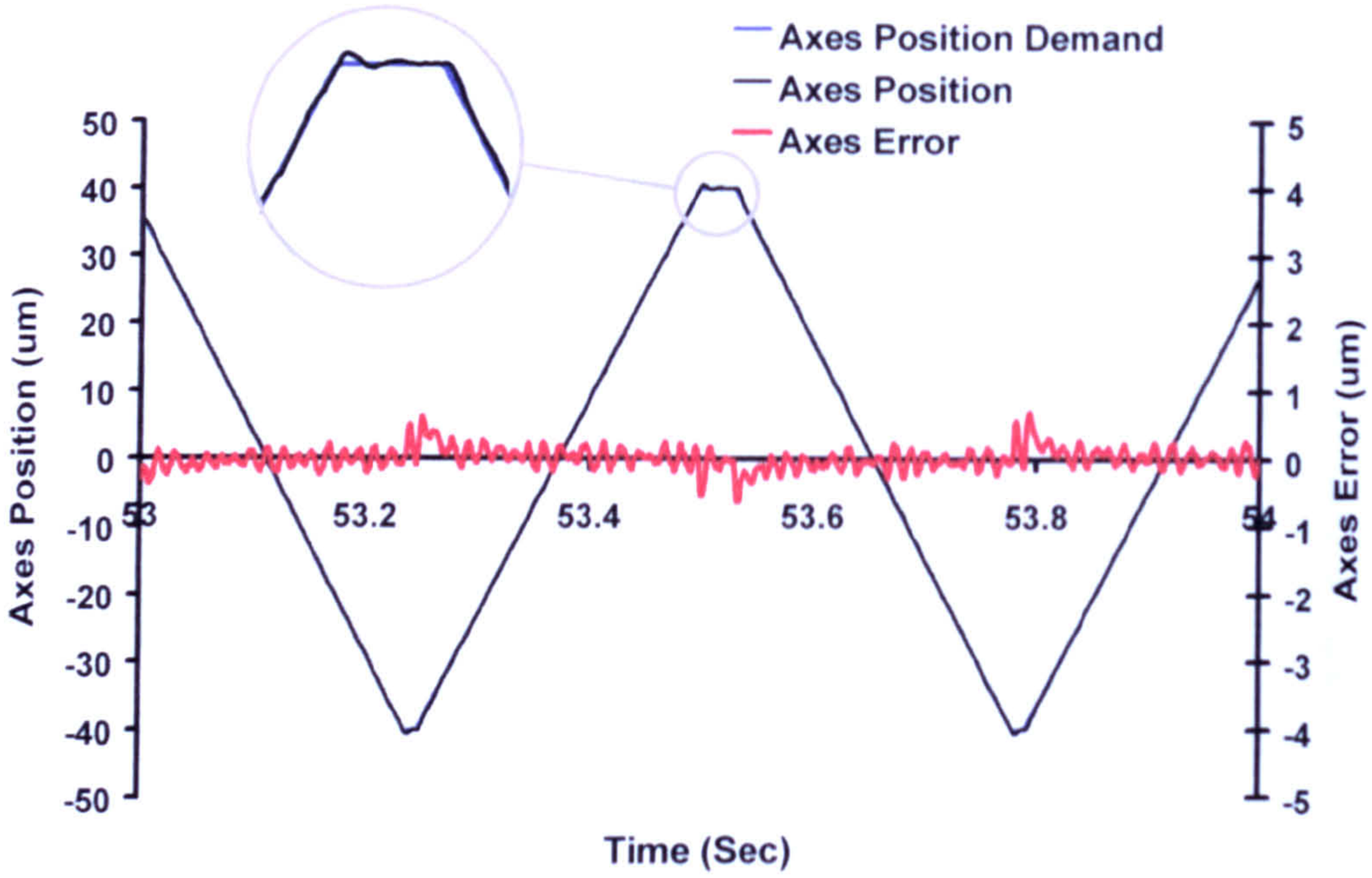

Figure 5.29 – Machine Performance for Oscillation of 0.04mm at 2Hz

As for the previous work, 3-dimenisional surface finish data was taken using the Wyko RST. This enabled the two orthogonal directions parallel and perpendicular to the grinding lay to be analysed, the data is shown in Figure 5.30. In addition data for the perpendicular surface roughness of conventional plunge grinding (hence without oscillation), and for peel grinding are shown for comparison. There was some difference in the overall level of measurements compared to those taken for these samples on the Talysurf. This is to be expected as contact and optical instruments both have a differing performance (i.e. stylus shape v reflection) and analysis techniques. However what is important here is that the trends between grinding tests are still apparent and are valid. As shown in Figure 5.30 the surface roughness R_a values perpendicular to the grinding lay for the grinding trials were lower for the grinds with oscillation than without. The trend was also similar in that the best results were for the lowest oscillation magnitude of 0.04mm. The higher amplitudes showed a degree of deterioration with increasing oscillation frequency. The level for the peel grinding test as previously stated provided an indication as to the lower limit for grinding and it can be seen that the general level of measurements lies between this and the conventional plunge grind value (without oscillation). The measurement results in the parallel orientation near the level of the peel grind as would be expected with a stable grinding process. This demonstrates firstly that implementation of the modified grind path has improved surface roughness level and secondly some potential for further enhancement exists.

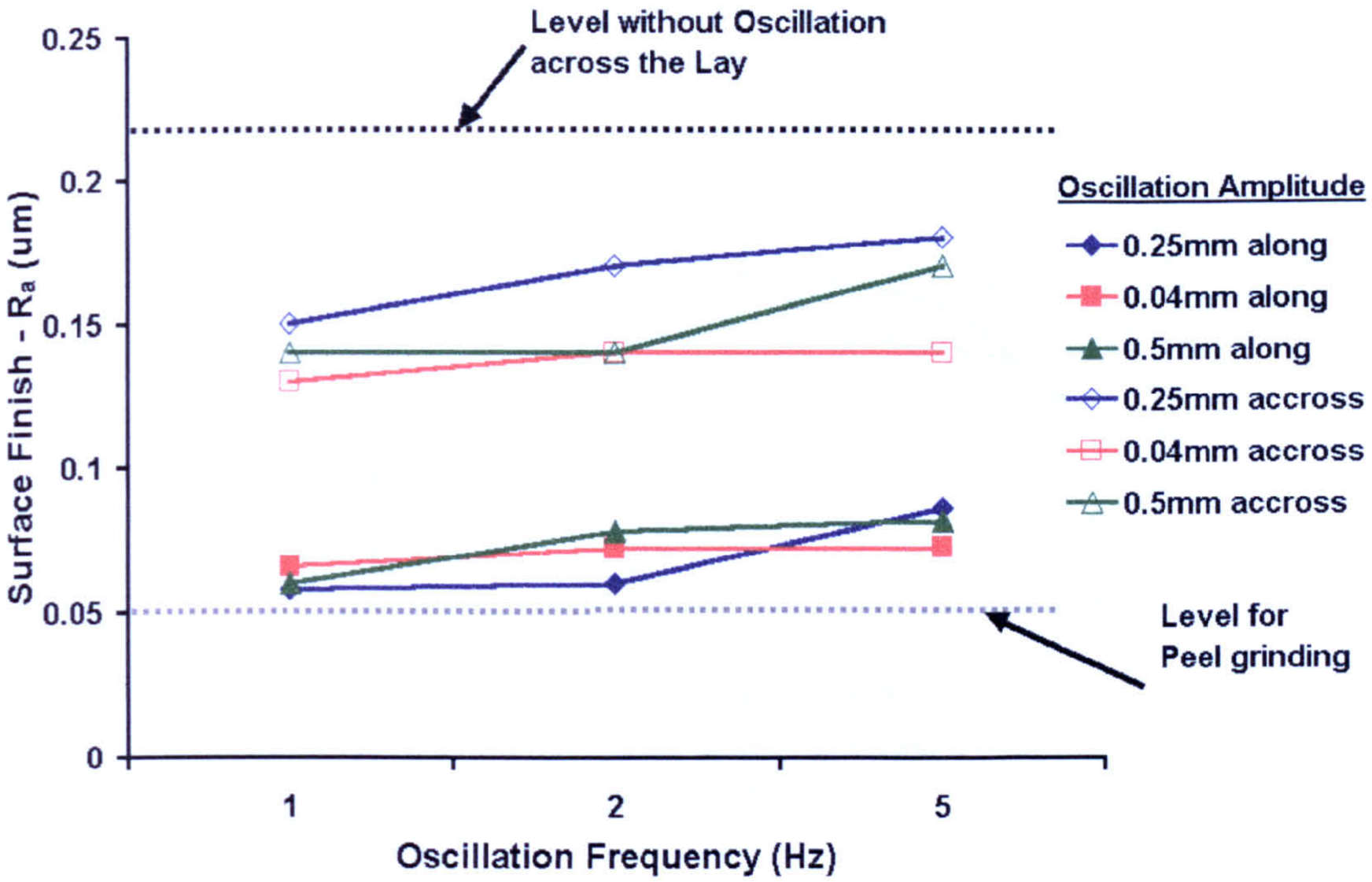

Figure 5.30 – Plot of Surface Finish (2D) against Oscillation Frequency

Following on from the surface roughness analysis, as with the previous stages of work the surface integrity was addressed. Figure 5.31 shows the measurement results obtained with the Barkhausen Noise residual stress equipment. The levels for the conventional plunge and peel grinds are shown by the dotted lines, the level of the latter is higher than that for the plunge grind. This was primarily due to an expected increase in the thermal load as a result of the increased rubbing component of this type of grinding. For the oscillatory grinding tests the level of residual stress increases with the increase in magnitude of the oscillation. Again this can be explained as a result of the increased rubbing action as the sideways motion is akin to peel grinding. As the frequency of oscillation is increased there is again an increase in the measured level of residual stress. One explanation for this could be the increased thermal loading as the removal rate for the sideways component of the grinding action increases. The increase is less obvious in the case of the 0.04mm oscillation test and would suggest from a induced stress consideration that the lower amplitude is the better option. All results are below the boundary level, hence it can be concluded that the grinding processes employed did not introduce thermal damage into the component.

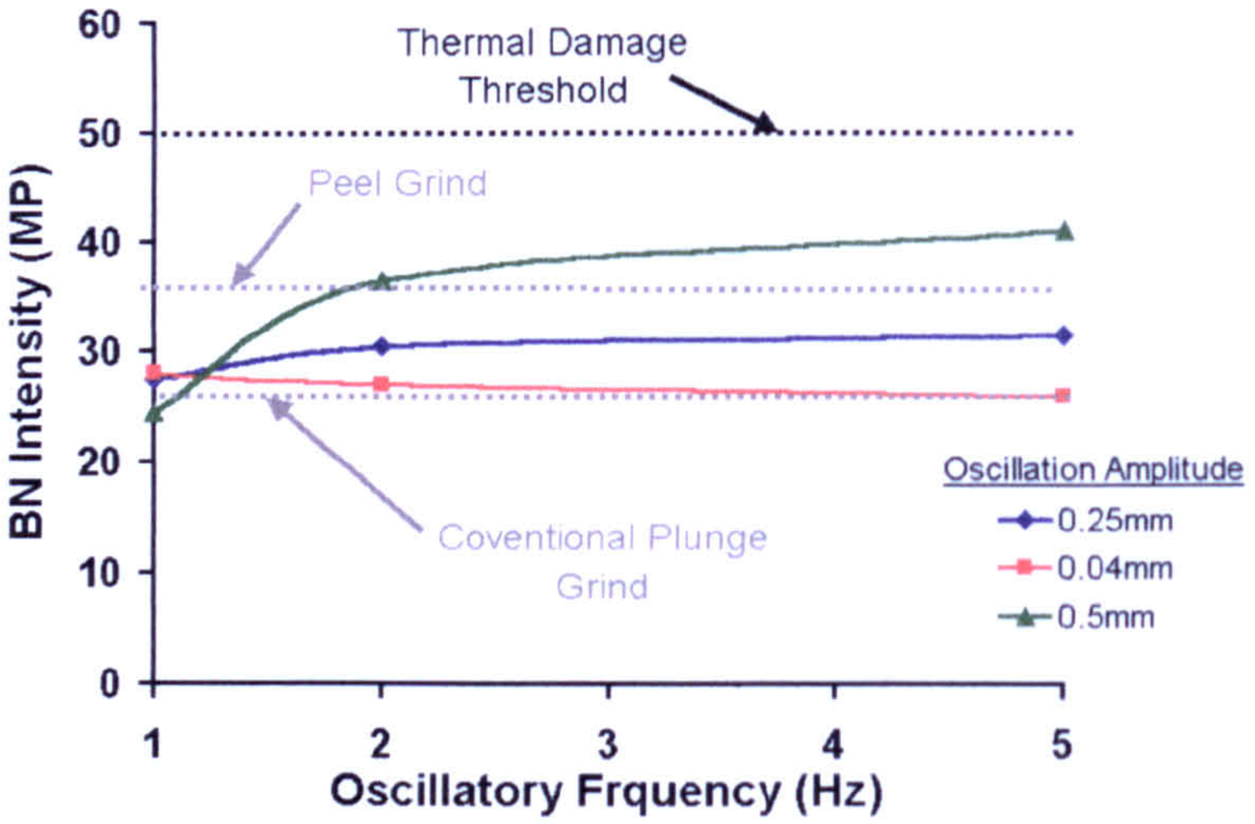

Figure 5.31 – Residual Stress Measurements for Oscillatory Grinding Trials

Figure 5.32 brings together the results discussed up to this point with those of the benchmark grinding tests carried out. The benchmark grinding tests used current wheel truing and dressing technology on the same wheel in a convention cylindrical plunge grind path. The two dotted lines show the surface roughness level achieved without any modification of the grind path. The upper black line used the current truing and dressing technique. The lower blue line used the enhanced system showing an improvement of 0.16μm to 0.1μm R_a. If now the modified grind path results are examined, then it can be seen that the general level for those utilising the improved truing and dressing techniques is better than those using the conventional approach. In this case the improvement is from 0.14μm to less than 0.1μm R_a.

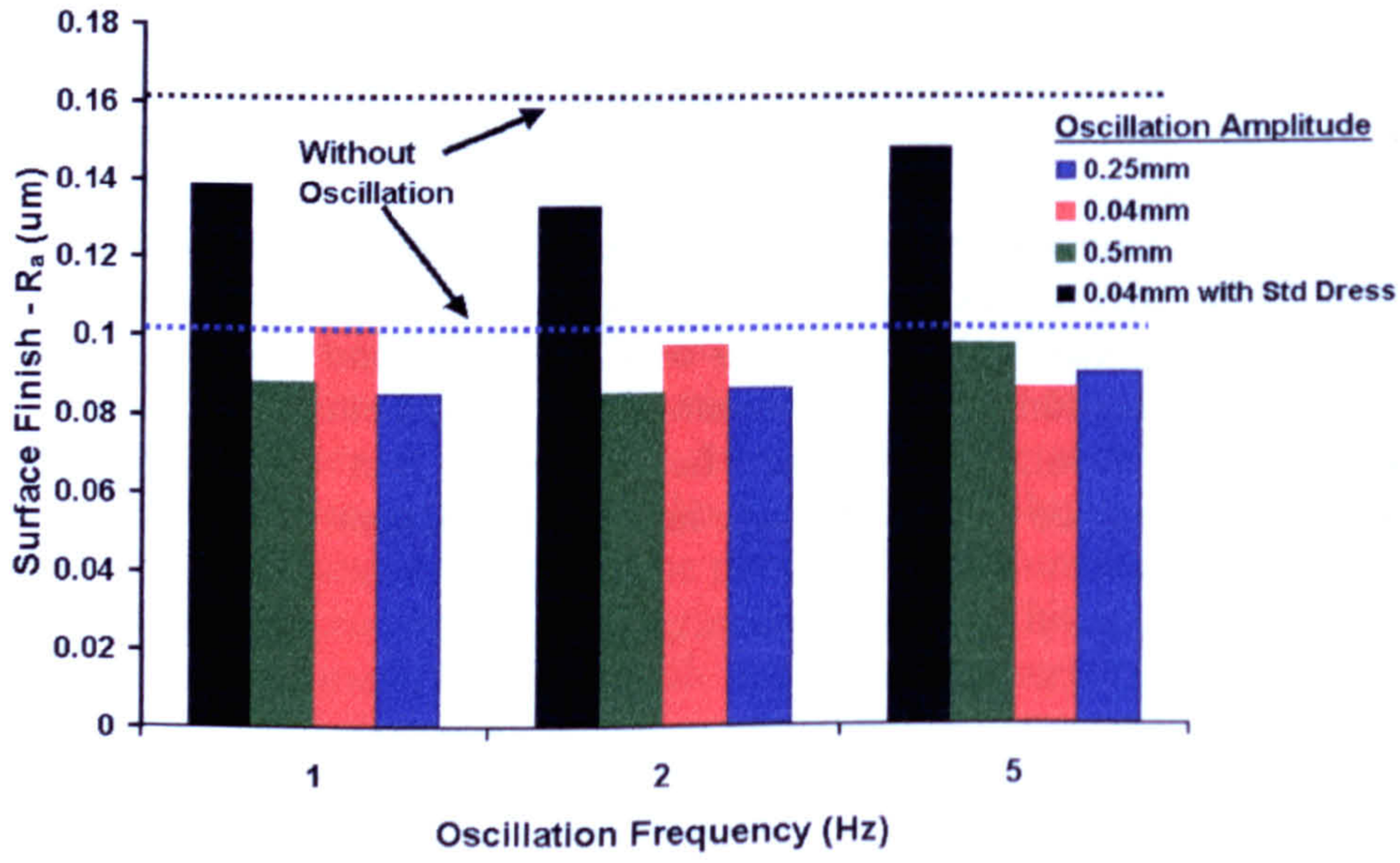

Figure 5.32 – Comparison of Surface Finish from Conventional and Modified Processes

The residual stress levels for the modified path grind were also compared with benchmark test data. The results can be seen in Figure 5.33, all tests maintained the induced thermal damage level below that of the threshold shown by the upper dotted line. With the conventional plunge grinding test residual stress was reduced by the implementation of the improved truing and dressing techniques, as can be seen by the two dotted lines in the figure. In line with this finding the oscillatory grind level was also reduced as illustrated by the two solid lines, the upper for the grind using conventional truing and dressing the lower with the improved arrangement.

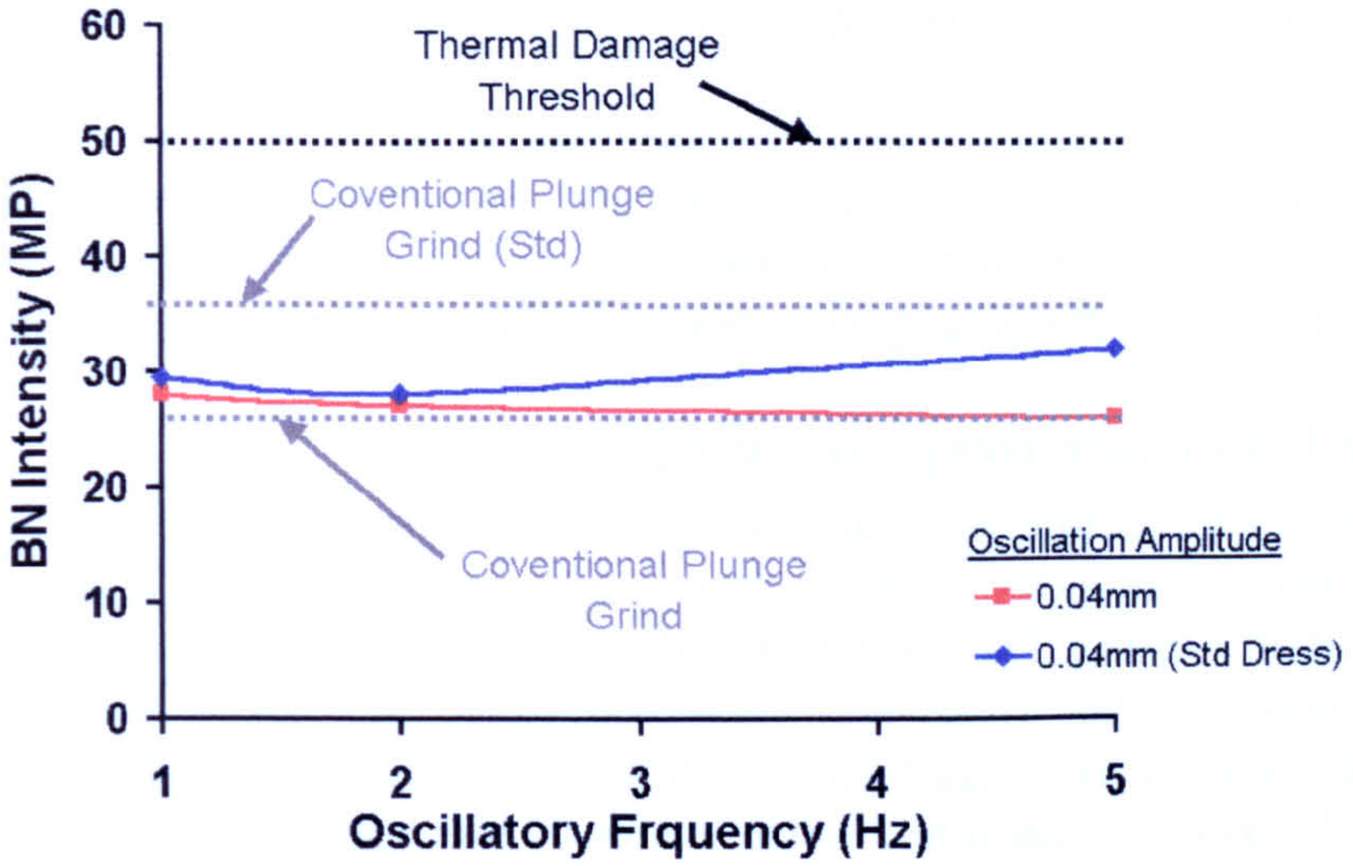

Figure 5.33 – Residual Stress Measurements for Oscillatory Grinding Trial Benchmark

The trials carried out on the LT1 demonstrate that the modified grind path approach improves the overall (3-dimensional) surface roughness and reduces the effect of grinding lay on a production based machine tool and in accordance with the results found from the Edgetek machine trials. The process does not induce unacceptable levels of thermal damage into the component. Lower oscillation magnitudes offer enhanced performance in regard to surface finish whilst subjecting the machine tool slide-ways to reduced levels of position error and hence possible vibration. The surface finish produced by the action of a modified path grind is governed by the combination of two factors:

1) The increase in the significance of the transverse surface finish component as the oscillation frequency increases
2) The deterioration is transverse surface finish as the oscillation frequency increases.

6 Discussion

The scope of the research was defined as follows...

> *The research will look at the grinding process and the effects this has on the component surface. Both 'High Efficiency Deep Grinding with its high stock removal, and Superfinish Grinding with micron level removal rates will be studied. The surface and subsurface investigation of components produced will enable characterisation and interrelationship analysis to be carried out. The aim is to increase the understanding and performance of the grinding process primarily through the study of the surface properties produced.*

Initially the research focused on *HEDG* and *Superfinish Grinding* and these are discussed separately, followed by a discussion regarding grinding applications, which includes the potential offered a by combination of the two grinding regimes.

6.1 High Efficiency Deep Grinding

Initially the HEDG regime was studied in a surface grinding mode where its existence has already been established in work reported by Tawakoli (1993), Rowe (2001a) and Stephenson et al (2002). The nature of surface grinding means that there is no further interaction between the wheel and workpiece after the wheel has passed over the surface. Therefore the evidence from the bulk material removal process remains and can be examined, whereas with many other modes of grinding some additional quantity of material is removed during the 'spark out' that occurs naturally, thus removing some of the grinding evidence from the surface. Hence surface grinding provided a good starting point for the analysis of the ground surface integrity, beginning with the traditional visual approach, then moving on to a metallurgical, and finally residual stress analysis. With a good understanding of the analysis tools the grinding investigations proceeded into the cylindrical plunge mode. Here no published work was found concerning the existence of the *HEDG* regime. However it was reasoned that the steep temperature gradients and high rates of material removal essential to the implementation of *HEDG* should be applicable in a cylindrical plunge mode. An important aspect in validating the existence of the *HEDG* regime in this mode was the ability to assess the thermal energy entering the workpiece. Initially thermal modelling developed by Stephenson & Jin (2003) and Rowe (2001a) was used to provide temperature profile estimations. A novel temperature measuring technique was then employed, using *PVD* coatings, based on earlier work in surface grinding by Kato (2000). These both provided a valuable insight into the thermal distribution for conventional grinding and how this compared with *HEDG*. An analysis of the residual stresses was undertaken in support of the thermal findings. The final phase in this part of the grinding research looked at the application of *HEDG* in a production environment, using a standard crankshaft grinding machine tool and an automotive crankshaft component. This allowed an industrial validation of the *HEDG* regime together with both the process stability and wheel wear assessment being made using the techniques developed during the earlier work.

6.1.1 Surface Grinding

The grinding trials covered a range of specific material removal rates (Q'_w), from $1mm^3/mm.s$ up to $1000mm^3/mm.s$. The range of removal rates covered that conventionally accepted as creep feed grinding and the *HEDG* regime. An assessment of surface integrity together with thermal modelling demonstrated the existence of the *HEDG* regime as described by Tawakoli (1993).

The power trend witnessed for different spindle speeds, shown in Figure 4.2, demonstrated that the higher wheel speeds required increased spindle power. Tawakoli (1993) proposed that these higher wheel speeds were a major requirement to the successful implementation of *HEDG*, as the reduced contact time helped to reduce the heat energy entering the workpiece. Higher wheel speed also reduces the chip size helping to prevent wheel loading, which is acknowledged as a cause of workpiece burn. The total spindle power comprises, powers to run the spindle, accelerate coolant to wheel speed, push coolant though the restriction of the grinding zone, and finally to remove material. All except the last are referred to as the base level or sparkout power. The results in Figure 4.3 demonstrated that although the higher spindle speeds required an increased base power (i.e. without material removal) the grinding component did not increase significantly with the increased wheel speed. Thus it was concluded that there was unlikely to be a significant increase in the thermal input to the component's surface, a fact supported by surface integrity tests carried out on samples ground at both wheel speeds which showed no evidence of thermal damage. The large power requirements for the higher wheel speed mean that there are significant gains to be made in any reduction of the base level component. One way this could be achieved would be by improved coolant efficiency. Webster (1995) states that the application of laminar flow nozzles offer better directionality, reducing the quantity of fluid, and by matching the fluid velocity to the peripheral wheel speed significantly reduce the braking effect on the wheel.

With regard to the grinding wheel grit size it was found that at the lower Q'_w of $100mm^3/mm.s$ that there was no significant advantage with the larger grit size wheel. However at the higher Q'_w rates above $200mm^3/mm.s$ the larger grit wheel enabled a higher removal rate to be attained without the occurrence of workpiece burn, see Figure 4.4. The increased chip space of the larger grit size wheel would have been significant in increasing the burn threshold level.

The relationship for Specific Grinding Energy (*SGE*) versus Q'_w was shown to decay exponentially to a base level of $6\text{-}10J/mm^3$ at the higher material removal rates, see Figure 4.17. This trend follows that reported by Stephenson et al (2002) for *HEDG* on low alloy steels where a power function (Equation 4.2) was used to describe the relationship. Table 6.1 shows values for the equation constants from Stephenson's work and from the surface grinding trials discussed here. The constants show good correlation, which confirms the validity of the experimental techniques used in this work. With this *SGE* trend, and if as proposed by Tawakoli (1993) more heat energy is removed by the chips, then *HEDG* should be possible without damage to the surface integrity of the ground component.

Surface Grind		Stephenson (2003)	
A	55	A	70
t	0.3	t	0.25-0.4

Table 6.1 – Values of A and t for SGE v Q'_w Trends

Burn threshold charts (Malkin, 1989 pg 148) based on Jaegers sliding heat source link *SGE* with process parameters (Section 2.2.4.2), a threshold line being placed along the boundary separating thermally damaged and undamaged ground surfaces. Process parameters are grouped by the function $f(d_e^{1/4}, a^{-3/4}, v_w^{-1/2})$, derived from the Jaeger thermal model. A range of process conditions are required to provide a good spread of tests across the chart, with samples grouped in both categories, namely thermally damaged and undamaged. Commonly visual assessment is used to identify thermally damaged samples. As illustrated in Figure 4.5, the placement of the boundary line can be subjective, in this case due to the data points signifying burnt components, being grouped mainly at the lower end of the chart.

Classification solely by visual means was found to be a crude and subjective approach open to interpretation, and the use of additional surface integrity assessment techniques were therefore required. The techniques looked at the microstructure and microhardness in the near surface region. For the metallurgical assessment, a limited number of interesting samples were selected, and the results are contained in Table 4.1. Beginning with two samples ground at a low Q'_w of $5mm^3/mm.s$, with the different wheel grit sizes $213\mu m$ and $151\mu m$, neither had any visible surface discolouration. The *SGE* level was also similar for each sample, suggesting that there was no thermal damage. Microstructural analysis supported this with no evidence of structural changes at the near-surface region. Two further samples were ground with the $213\mu m$ grit wheel at a higher Q'_w of $100mm^3/mm.s$, with wheel speeds of *100m/s* and *200m/s*. As before there was neither surface discolouration nor changes in the microstructure of either specimen. The *SGE* level was again of a similar level, which supports the assumption made that with the increased spindle power requirement (associated with the higher wheel speed), resulted in no increase in thermal energy reaching the component's surface. Another set of samples ground at the same Q'_w with the smaller $151\mu m$ grit wheel, indicated higher levels of *SGE*. The sample produced with a lower wheel speed had some visual surface discolouration, and there was evidence of microstructural damage in the form of a white layer at the surface region, see Figure 4.6. However the sample ground with the higher wheel speed had neither surface discolouration nor microstructural damage. The *SGE* was lower in this case, which in turn means that there was lower energy input into the grind region, which correlates with the microstructural damage findings. With equivalent Q'_w values and differing wheel speeds, the lower wheel speed results in a larger chip size than that for the higher speed, thus in all probability the smaller grit wheel had reached the limiting chip size at this Q'_w. It was therefore concluded that grit sizes below $213\mu m$ would not be suitable for reaching the target Q'_w of $1000mm^3/mm.s$.

For samples ground at a Q'_w of $375mm^3/mm.s$ and a wheel speed of *200m/s* with the $213\mu m$ and $151\mu m$ grit wheels respectively, the *SGE* values were extremely close, suggesting a similar thermal condition for both samples. Visually both had evidence of

surface discolouration, but neither sample showed any sign of microstructural change. Finally for two samples ground with the larger grit wheel at a Q'_w of $500mm^3/mm.s$, and wheel speeds of *100m/s* and *200m/s,* both had surface discolouration. The discolouration was greater for the sample using the lower wheel speed, and there was clearly microstructural damage with a white layer extending well below the surface, shown in Figure 4.8. At the higher wheel speed there was no detectable microstructural change and the *SGE* was lower. With lower wheel speeds the contact time increases and hence a larger partition of the thermal grinding energy enters the workpiece surface, as is seen with creep feed grinding. Thus it was concluded that the increased wheel speed, with the shorter contact time, reduced the thermal energy being transferred into the surface. A microhardness analysis was conducted on these samples. The microhardness profiles, shown in Figure 4.10 indicate that the damaged surface had a hardened layer for a depth of approximately $300\mu m$, whereas in the case of the higher wheel speed there was no sign of near surface hardening. Thus the results from the microhardness analysis support those from the microstructural analysis.

Together, the visual and metallurgical analysis techniques used up to this point show that surface discolouration can provide an indication that thermal damage is present in the ground surface. However the interpretation is subjective, and coupled with the fact that coolant oxidation may also produce some surface discolouration, this makes it an unrealistic tool for analysis. Detection of thermal damage by a change in the microstructure or microhardness in the surface region is far more reliable, but a surface displaying these changes has been subject to a significant level of thermal damage. Ideally a non-destructive method is needed to detect the onset of thermal damage at an earlier stage, making it suitable for application in a production environment.

To address these issues the surface integrity assessment was carried out by the measurement of residual stress. Two techniques for the measurement of residual stress were studied, Barkhausen Noise *(BN)* intensity and X-Ray Diffraction *(XRD)*. When high thermal gradients are created across the near surface region by the grinding action this reduces levels of compressive stress until, if gradients and temperatures are great enough, the surface is left in a state of tensile stress. Still greater thermal shock causes localised rehardening in the near surface region typified by the present of a white layer. Therefore the detection of changes in residual stress levels provide an earlier indication of thermal damage than the metallurgical techniques considered so far. With this enhanced sensitivity to thermal damage the ground surfaces can be broadly classified into three groups namely, unburnt, transitional and burnt. Figure 4.11 illustrates how these regions would appear on a burn threshold chart. *XRD* is the most commonly accepted approach for the determination of residual stress as it provides absolute values. However the equipment is quiet specialised and its use has implications in regard to health and safety when used outside an enclosed area, because of the exposure risk to x-rays. Another consideration is that to avoid x-ray reflections, which can lead to errors in results, it is often necessary to remove the sample area from the component. These constraints mean that the approach is more suited to research environments as opposed to industrial applications. Whereas *BN* intensity provides a far more industrial friendly approach, at much lower capital cost, with no health and safety issues. Measurements can be made directly from the component surface without any preparation, provided a appropriate sensor head is selected, see Figure 3.41. The output is given in terms of

magnetic power *(MP)* and the readings are comparative therefore calibration is required, using known burnt and unburnt samples, before the method can be used successfully, see Figure 3.42. The *BN* intensity output is sensitive to both residual stress and hardness at the surface zone, the relationship between these two properties versus output in *MP* is illustrated in Figure 2.17. The progression from a desirable compressive state to one approaching that of tensile produces an increase in readings, the boundary in this case is set at *38MP*. Whilst an increase in the hardness has the opposite effect, reducing the level of readings to below *23MP* in this instance. As previously discussed these changes occur sequentially not simultaneously, meaning that the output should first rise before falling again as thermal damage levels continue to increase. It is therefore necessary to periodically monitor surfaces to ensure detection of the initial reduction in compressive stress, otherwise misleading conclusions may result if hardening had begun to take place. With the BN intensity instrument it was possible to analysis the ground surfaces and categorize them accordingly, as shown by Figure 4.12. Those from the unburnt region had readings in the mid-level between *23MP* and *38MP*, whilst surfaces in or near the transition region had values above this level. XRD measurements for samples in each of the two regions indicated a compressive stress of *–120MPa* and a tensile stress of *+184MPa* respectively. Thus the technique was clearly able to identify the build up in residual stress resulting from thermal energy reaching the surface at a much earlier stage than the previous methods used. *BN* intensity readings from the visually burnt region fell into the lower region, below *23MP*. These surfaces are typified by the presence of rehardening in the form of white layer. As the *BN* intensity is known to decrease with an increase in the microhardness this correlated with the previous metallurgical findings for this region of the burn threshold chart, see Figure 4.8. *XRD* results taken from the region of lower *BN* intensity readings indicated high tensile values, thus supporting the findings.

Therefore, it was concluded that with *BN* intensity instrumentation it is possible to detect the gradual reduction in compressive stress caused by the onset of thermal damage. Allied to the enhanced sensitivity of this approach is the nondestructive nature of this method and its suitability for production environments for the assessment of surface integrity.

Returning to the burn threshold chart the additional analysis data from the residual stress measurements allow the boundary line to be reliably established, as illustrated in Figure 4.16. The gradient of the boundary line together with the material properties produces an estimate of *2170°C* for the burn threshold temperature. It was clear that the material examined had not reached this level. The high estimate is a result of Jaeger's model assuming that a large proportion of the chip forming energy, in the region of *55%,* is conducted as heat into the workpiece. This is in fact a far larger value than that expected for *HEDG* conditions where Rowe (2001a) suggests that a higher proportion of the energy is removed by the chips, thus reducing the heat input into the surface. The thermal model described by Stephenson et al (2003) uses a current energy partitioning theory for *HEDG*. The model predicts both contact and finished surface temperatures using the measured *SGE* values from the grinding trials together with the grinding parameters and material data. Results from the modelling, see Figure 4.18, showed that temperatures for surfaces previously classified as burnt, using visual assessment, were above those of the unburnt samples, thus confirming the validity of the model for the

HEDG regime. The finished surface temperatures were lower than those of the contact surface, this correlates with Rowe's (2001b) findings for creep feed grinding where he found a steep temperature gradient across the contact length leading to lower finished surface temperatures. Therefore, although the contact surface may exceed the critical temperature, the finished surface temperature can be maintained at a lower level. This finding is an important fact in the support of the *HEDG* regime as proposed by Tawakoli (1993).

6.1.2 Cylindrical Grinding

Trials with Q'_w removal rates of up to $3000mm^3/mm.s$ established the existence of *HEDG* in the cylindrical plunge grind mode on the Edgetek grinding machine. Surface integrity analysis together with both thermal modelling and temperature measurement, determined the trend for the thermal energy entering the finished surface in relation to the material removal rate.

The grinding power trends for sample features representative of a crankshaft web and journal are shown in Figure 4.19. For the web feature the larger grit wheels offered the best performance at the higher Q'_w requiring lower powers. The dual grit wheel provided a comparable performance to that of the single grit size wheels, so with their larger grit size distribution, and all other conditions similar, this would be expected to improve the grit wear progression and thus wheel life. Therefore this makes the dual grit wheel a good candidate for high removal grinding. The plain and modified segmented wheels, illustrated in Figure 3.7 and Figure 3.8 did not improve performance. The plain segmented wheel required higher power resulting in an increased thermal energy input into the surface. The modified segmented wheels caused high levels of coolant atomization, which in turn lead to potentially explosive conditions within the machine enclosure. For the journal features the larger grit wheels once more offered the best approach, however in this case the segmented wheels showed an advantage with a reduced power requirement.

The *SGE* versus Q'_w trend shown in Figure 4.20 follows that seen previously for the surface grinding investigations, with the *SGE* leveling out at around *6* to $10\ J/mm^3$ at the higher removal rates. The relationship can be defined by Equation 4.2, together with the constants given in Table 4.3, and the results broadly align with the data published by Stephenson (2003) shown in Table 6.1. The *SGE* versus Q'_w power relationship was used, together with grinding parameters, as inputs to the thermal model (Stephenson, 2003). Temperature measurements were carried out with a novel technique using PVD coating (Section 2.2.4.1 & 3.2.1.2), and residual stress readings made with BN intensity instrumentation (Section 3.3.4.2) to determine levels of thermal damage. The results for these are shown in Figure 4.23 to 4.35 respectively, and are summarized here in Figure 6.34.

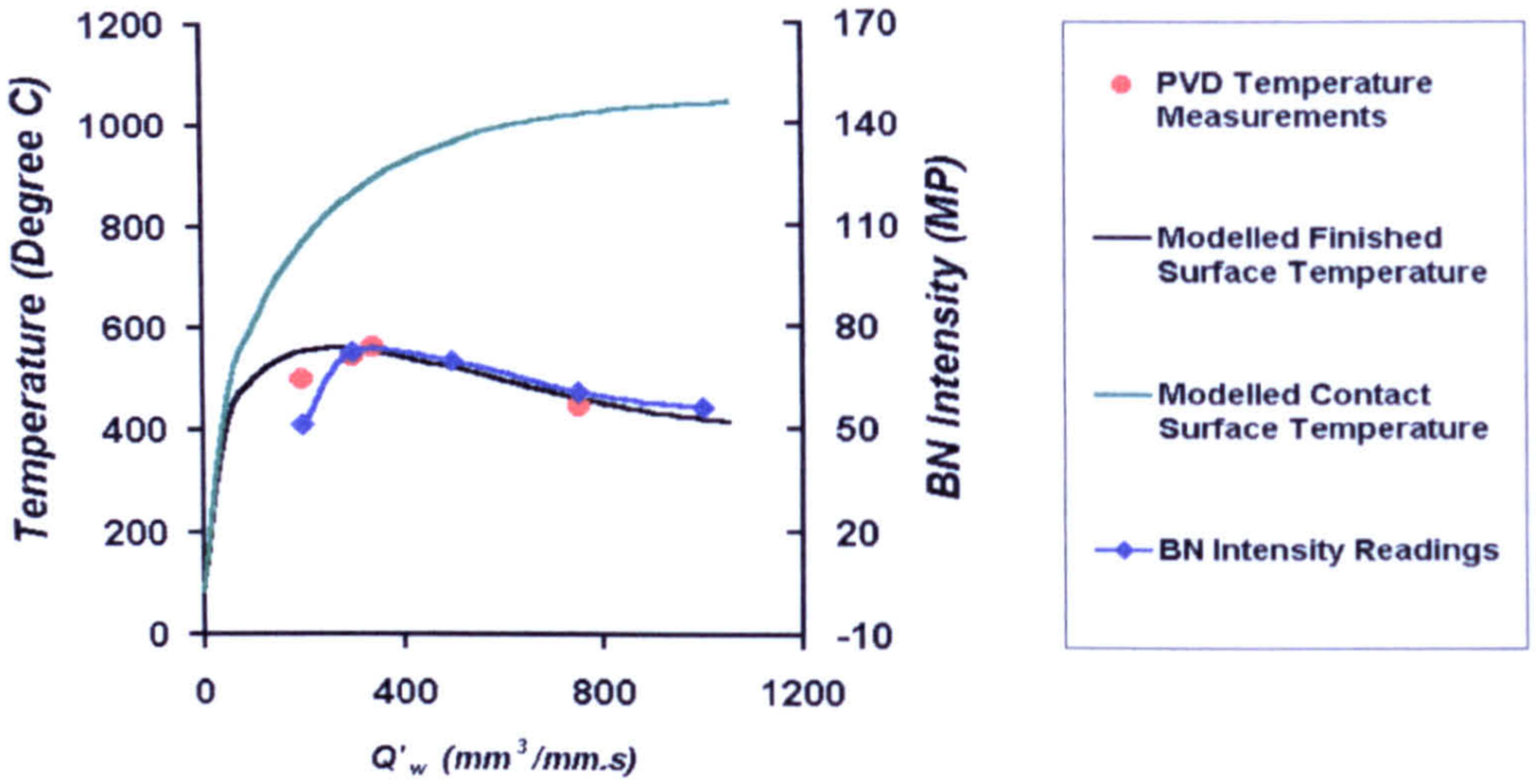

Figure 6.34 – Combined Thermal Results for Edgetek Cylindrical Grinding Trials

Although the contact surface temperature continues to increase, the finish temperature peaks at approximately $300mm^3/mm.s$ and then falls. Data from the temperature measurement using the PVD coatings aligns with the finished surface temperature from the model. The temperature increases from 496^oC at $200\ mm^3/mm.s$, to $544\ ^oC$ and $563\ ^oC$ at $300mm^3/mm.s$ and $340mm^3/mm.s$ respectively, then reduces down to $442\ ^oC$ at $750mm^3/mm.s$. Thus it can be concluded that the thermal model originally developed for surface and peel grinding is valid for cylindrical plunge grinding. The Barkhausen Noise intensity readings, representative of the residual stress, increased from $200mm^3/mm.s$ up to around $350mm^3/mm.s$, then progressively dropped to previous levels. The trend showed that the peak deterioration of compressive stress occurred at approximately $350mm^3/mm.s$, thus it was concluded that grinding at either above $450mm^3/mm.s$ or below $250mm^3/mm.s$ would result in acceptable stress levels. Microstructural analysis was carried out on a sample ground above the peak, at a Q'_w of $750mm^3/mm.s$, and showed no evidence of thermal damage confirming the residual stress analysis findings.

This thermal trend shown in Figure 6.34 for the finished surface is similar to that found by Tawakoli (1993) for surface grinding, and therefore confirms that the *HEDG* regime can be applied in cylindrical plunge grinding. Although in this mode of grinding with the chosen material, the *HEDG* peak occurs at a higher Q'_w than for that published for surface grinding.

The thermal model can provide a valuable insight into what is happening at the grinding zone. With higher material removal rates the grinding power continues to rise and the thermal model shows a corresponding increase in the total heat flux at the grinding zone, see Figure 4.22. Importantly for the successful application of the *HEDG* regime, and as demonstrated already, the heat flux entering the workpiece surface rises to a peak at approximately $350mm^3/mm.s$ and then begins to fall. The model provides information on changes in the heat flux distribution, see Figure 4.21. At the lower removal rates, commonly associated with creep feed grinding, the partition ratios for the fluid along

with the workpiece are high. The ratio to the wheel follows closely, whereas the ratio to the grinding chips is low. Thus substantial amounts of heat flux are known to enter the workpiece, fluid and wheel. Therefore at the lower removal rates both the fluid and wheel are important in respect to their ability to remove heat, which explains why *CBN* abrasive grit with its high conductivity has improved creep feed grinding performance. It also explains why modern vitreous *CBN* wheels, with high porosity that carry more fluid into the grinding zone, offer benefits. As the removal material rate increases the balance changes, with far less heat removed by the wheel and fluid. Importantly the heat removed by the grinding chips increases dramatically reaching levels of over *60%* at *1000mm^3/mm.s*, the overall effect being that the heat entering the workpiece drops at these higher removal levels. The reduction in the ability of the fluid to remove heat results from fluid film boil out in the grinding zone, therefore in all probability the only contribution being made by the fluid at this point would be one of lubricity.

The use of PVD coatings to determine surface grinding temperatures was first carried out by Kato (2000). The technique uses a thin (*0.2μm*) *PVD* coating sandwiched internally through the cross-section of the workpiece, see Figure 3.9. This enables the temperature at a measured depth from the ground surface to be determined accurately. By using a variety of coatings with a range of differing melting temperatures, such as indium bismuth and zinc, a thermal profile across the sample can be established. The technique offers a number of advantages over other approaches such as thermocouples, photoelectric cells and infrared sensors. There are no electrical connections, data logging or filtering requirements, and the presence of coolant at the grinding zone does not affect the performance. With the added complication of cylindrical plunge grinding the PVD technique offers a simple reliable approach. Hence the technique was developed as described in section 3.2.1.2 as part of the research, and provided the ability to attain the thermal profile approximately *400μm* down into the workpiece surface. Kato (2000) states that the coatings maximum working depth (d_{max}) was determined by the workpiece velocity and the materials thermal diffusivity, see Equation 2.12. Converting this relationship for cylindrical grinding produces the relationship given in Equation 3.4

The working depth is normally calculated to be a set figure, irrespective of the variations in the materials thermal diffusivity with temperature. For this work the variation was included in calculations, thus reliably establishing the boundaries of the technique. Figure 4.28 shows how the working depth decreases with rising material temperature for the selected material

The work carried out here has established a thermal measurement technique which is particularly suited to industrial application. Samples can be prepared in advance and utilised simply in the industrial environment without either machine modifications or complicated additional systems such as data loggers and filters. Interpretation of results is straightforward, simply by measurement of the melt depths followed by the plotting of data points.

6.1.3 Industrial Trials

The initial tests investigated the material removal process on crankshafts without the constraint of meeting a full geometric form specification. The *SGE* and residual stress versus Q'_w profiles were compared with that of the preceding cylindrical grinding trials on the Edgetek machine. The tests covered a Q'_w range from *80* up to *2000mm³/mm.s* with a number of different grinding wheels at cutting speeds from *120* up to *180m/s*. Further tests moved on to the grinding of full geometric form crankshafts, when once again the *SGE* and residual stress were monitored. At this stage geometric form measurements were made to ensure that the process had the capability to meet full production requirements.

As with the previous findings the results showed that with both wheel grit sizes (*252μm & 356μm*) the higher wheel speed allowed greater Q'_w rates to be achieved, in this instance up to *2000mm³/mm.s*. The higher wheel speed reduces the chip size which means that increased infeed velocities can be used, which once again increase chip size, before the grit chip space limit is reached. The dual grit (*252μm*) wheel performed at similar levels to the other wheel, illustrated by Figure 4.38, thus this option also offered potential, in that with a larger grit size distribution it would be expected to have better grit wear progression and thus wheel life.

The constants for the *SGE* versus Q'_w trend are given in Table 6.2, for the higher wheel speed (*180m/s*). Results for the segmented wheels aligned with those from the surface grinding trials, offering a reduced energy consumption at the lower Q'_w values applicable for the journal features, but not at higher Q'_w levels as would be used on the web features. This is illustrated by the lower values seen with the *SGE* versus Q'_w trend for the *252μm* segmented wheel. The *SGE* versus Q'_w trend for the *356μm* wheel is again approximately the same as shown in Table 6.1, thus the thermal energy conditions remained broadly similar to the previous cylindrical results, suggesting that *HEDG* conditions were continuing to be met.

356μm Wheel		***252μm (Seg) Wheel***	
A	*77*	*A*	*32*
t	*0.27*	*t*	*0.13*

Table 6.2 – Values of A and t for Cylindrical SGE v Q'w Trend (for a wheel speed of 180m/s)

Assessment of the surface integrity using the Barkhausen Noise intensity confirmed that the residual stress profile remained the same, building up to a peak at around *350mm³/mm.s* then dropping off again. Figure 4.39 illustrates the trend for the crankshaft components. With the results in agreement with the previous cylindrical findings it was concluded that the thermal conditions had remained consistent for the production environment and that *HEDG* was therefore a viable process. The results were an important step in demonstrating the move from bar stock components ground in a representative process, to full production forged components with full size grinding wheels (*Ø600mm*).

The progression to the grinding of full geometrical form crankshafts provided the opportunity to assess the effects of the higher grinding forces, associated with *HEDG,* on the form accuracy and finish of the components. It was necessary to remove *1kg* of material from the crankshaft and produce undercuts by using formed grinding wheels, which placed additional demands on the process. The *SGE* values for a number of selected removal rates *(250, 500, 1000mm^3/mm.s)* closely matched that of the previous results for the crankshafts, see Figure 4.46. Residual stress measurements provided some interesting findings when compared against the previous trend. Levels for features ground with the right-hand wheel corresponded with previous ones. However readings from the features ground with the left-hand wheel were significantly higher, which highlighted the combined effects of both poor wheel runnout and insufficient coolant. The latter, being caused by a coolant valve failure which reduced the coolant flowrate. The wheel runout led to localised wear on the high load area of the wheel surface, as discussed later. The coolant issue was likely to have had a greater impact, with reduced heat energy removal coupled with reduced lubricity, the latter resulting in higher ploughing and sliding energies. Both effects would lead to a higher proportion of the grinding heat energy reaching the workpiece surface, in turn leading to the reduction in compressive residual stress. With these implications understood, it could be concluded that the results remained consistent, so it follows that the thermal modelling conditions remained valid and support the finding that *HEDG* can be successfully implemented for production cylindrical plunge grinding of full form components.

Finally a batch of *950* crankshafts were ground to determine power trends, residual stress, geometrical stability and tool life, concentrating primarily on the journal features. These, with their increased width, provided the greatest challenges in terms of wheel and workpiece forces. Grinding power and geometric form remained stable over the batch. Surface Roughness on the diameters remained between *2μm* and *2.3μm* R_a with concentricity under *50μm*. Residual stress analysis carried out using *XRD* indicated slight compressive stresses for both the main and pin diameters, with the same for the undercuts (Table 4.8 & Table 4.9). As there was no significant deterioration in the measured variables over the run, this demonstrated that the process was acceptable and stable. The fact that the power and residual stress remained stable meant that the heat flux entering the workpiece had not changed throughout the run. Thus it could be concluded that the overall distribution was unlikely to have changed.

Interestingly, although still of an acceptable level, there was a slight reduction of compressive stress in the central zone of the diameter. This was as a result of the grinding overlap between the two wheels, the first wheel removing the bulk material with the second providing a finish grind or burnishing action in this region. A low removal rate would have led to an increased *SGE*. This in turn, as shown by the thermal model, would result in a higher proportion of the heat energy going into the workpiece and hence a reduction in compressive stress.

The thermal modelling can be used in two ways. First as a predictive tool to provide a valuable insight into the *HEDG* process and the effects on surface integrity with regard to thermal energy distribution. Secondly as a tool to monitor the *HEDG* process, used in conjunction with the monitored spindle power, it provides a means to identify possible process variations that will result in thermal damage to the workpiece surface.

Variations such as wheel wear and coolant efficiency result in changes to the power requirements and hence heat energy. Taken one stage further the model could be used to monitor and then control the grinding process once integrated into the machine tool's *CNC* control system.

6.1.4 Grinding Wheel Wear

A comprehensive wheel analysis was carried out to identify whether any possible breakdown occurred in the electroplated *CBN* grinding wheels when exposed to the high demands placed on them by the *HEDG* regime. In order to assess the wheel condition it was necessary to investigate the abrasive grit breakdown, which was done by classifying the grits. In this case three groups as outlined in section 2.1.2.1 were selected namely, new, microfractured and deep hole. The relative percentage present for each type demonstrated the condition of the wheel as depicted in Figure 2.11.

Optical microscopy and *SEM* techniques were selected to quantify the grit distribution. The optical method required multiple *CCD* images focused sequentially for each wheel position, which were then merged using computer software. This approach provided an acceptable depth of field for flat wheel surfaces such as those from the initial stages of the cylindrical work. With the provision of a suitable wheel fixture arrangement it was possible to examine the surfaces of large diameter grinding wheels (i.e. Ø600mm) with the wheels still intact. Thus this technique had the potential to allow the wheel condition to be assessed at a number of stages throughout the wheel life, or scheduled test run. The *SEM* technique provided a far greater depth of field than the optical approach, using a single image. The advantage here was that the analysis of non-flat wheel sections was now possible; therefore the profiled wheels used in the final production trials could be assessed effectively. A drawback was the size constraint of the vacuum chamber of the SEM, housing the sample for analysis, meant that it was necessary to section all but the smallest wheels. Therefore when applied with standard production wheels the technique was destructive and did not allow staged examinations.

Wheels from the initial cylindrical production trials had a flat surface and so were examined using the optical approach. With material removal rates well into the *HEDG* regime (up to *2000mm^3/mm.s)*, and a test grind of *100* crankshafts, the objective was to determine if any significant grit deterioration had occurred. The analysis found that there had been no significant abrasive grit deterioration and that the wheels showed little evidence of wear. This was demonstrated by the ratios present of each grit classification (i.e. new, microfractured or deep hole) which was broadly in line with position '*A*' in Figure 4.40, typical of the initial stages of wheel wear, during which conditioning normally occurs. The segmented wheels did exhibit greater signs of wear at the regions associated with the web grinding (i.e. edge), illustrated in Figure 4.41. This suggested that although there was increased coolant penetration into the grinding zone through the 'segment gaps', this did not overcome the effects of the higher grit loading resulting from the reduced number of active grits. With the regions associated with the journal grinds (i.e. centre) there was no such indication of increased wear, see Figure 4.41. Therefore in this instance any improved coolant penetration had offset the higher loading. Considered in conjunction with the finding for the grinding power, this would suggest that segmented wheels could offer an advantage for the journal but not

the web features. Overall the larger grit wheels showed less deterioration, and so, either because of the grit type or size, could potentially offer better wear performance in the *HEDG* regime. A much extended trial would be required to reliably establish an indication of wheel life, and any difference for the two wheels tested here. For example, the different grit size distributions (i.e. *252μm* is a dual grit), mean that the rates of wear progression would be expected to differ, making comparisons at early stage difficult. The level of microfracture seen in the 'as new' wheel demonstrated that a truing operation had been carried out during the manufacturing process, most probably to achieve the required concentricity specified by automotive manufacturer's. It was therefore important to take this into account, as a starting point, in any wear assessment.

Wheels from the final production trials had a raised protrusion on the periphery in order to generate an undercut in the crankshaft profile. As a result the optical method was no longer suitable and so the *SEM* technique was used to examine the wheels. In this case a total of 1000 shafts were ground providing a far better opportunity to assess wheel life. Overall the wear results showed that only a very small percentage of the particles on the wheels remained as 'new'. While 50-70% of the particles were classified as 'working', and between 22-30% of the particles as 'holes' having been removed from the bond material completely. Grit ratios were therefore in line with position '*B*', in Figure 4.40, indicating that significant portion of the total wheel wear had occurred. A section of the left-hand wheel suffered bond failure at approximately shaft 970. This was attributed to problems at a early stage in the grinding, illustrated by the residual stress readings seen in Figure 4.40, these were identified as:

- Coolant Application - Investigations found system failures in the coolant delivery system to that wheel.
- Wheel Runout – *CMM* data indicated that the wheel had a high level of runout.

Manufacturers' projected wheel life are given in terms of 'volume of material removed per unit width'. When grinding at a Q'_w of $200mm^3/mm.s$ the wheel life expectancy declared by the manufacturers was $28{,}000{,}000mm^3/mm$; for higher Q'_w rates there was no guide figures provided. Figures for the material removed from a crankshaft by the left and right-hand wheels are given in Table.4.11. Using these, a projected wheel life of *606* shafts for the *LH*, and *655* for the *RH* wheel, would be expected. These figures lay significantly below the *1000* crankshafts ground in the trial without wheel failure. As a result of this work material removal figures are beginning to routinely exceed the $200mm^3/mm.s$ on web features and are approaching this figure for journal features. As a result far greater data on wheel life will become available. It is not unexpected to see the manufacturer's figures to be on the conservative side, but from the findings here it would be reasonable to expect an increase in manufacturers' wheel life figures at the high removal rates over the next few years.

With the stable power figures seen over the duration of the extended industrial trial it is reasonable to assume that the observed grit wear had not significantly changed the grinding conditions and hence importantly the heat flux distributions. With further increases in the grit wear there will come a point where the *SGE* will increase. The model, through its sensitivity to small changes in *SGE* at the higher removal rates,

indicates that such changes will have a significant effect on the heat flux and so potential thermal damage at the components surface. Thus although *HEDG* has benefits there is a trade off in that small changes in say grit wear can have significant effects on the process. Whereas at lower rates such affects that cause small changes in the *SGE* would not be so significant. Another consideration is that with the material here it has been demonstrated that levels of grit wear are reasonable, however for some materials used, in say, the aerospace industry wear figure would be far greater which would affect the viability of the *HEDG* as a production process.

The thermal model also shows that with the high material removal processes, such as *HEDG*, the heat flux removed by the wheel falls dramatically when compared to that of the low removal processes, such as creep feed grinding. This means the use of *CBN* grit because of its enhanced thermal conductivity is no longer such an important consideration. Hence any advantage offered by *CBN* in the *HEDG* regime is probably more to do with its increased knoop hardness, *4700kg/mm²* against *2100kg/mm²* for Al_2O_3, and better thermal stability. Unfortunately details of the *CBN* abrasive grit types and how these varied with grit size was not available for the wheels used in this research. Details of different grit types was discussed earlier in section 2.1.2.1, one important issue in regard to *HEDG* being the level of resistance to thermal loading. With *HEDG* there are steep thermal gradients involved, and therefore there is a need for some investigations into the performance of different grit types when used in the *HEDG* regime.

6.2 Superfinish Grinding

The approach for the *Superfinish Grinding* was similar to that of the *HEDG* work, beginning with surface grinding trials and moving onto cylindrical plunge grinding trials. The most important aspect of surface integrity with regard to grinding performance was the surface texture, made up of the surface roughness and grinding directionality. Secondary was the residual stress, to ascertain whether thermal energy conditions at the workpiece surface remained within acceptable limits.

6.2.1 Surface Grinding

Initial trials using newly applied wheel technology, see section 3.2.2.2, demonstrated that surface roughness values of *0.1μm* R_a were achievable with current high stiffness production machine tools, albeit with the addition of improved truing/dressing systems. The surfaces were characterized by an undesirable directional profile, which is typical of that produced by conventional grinding, and which is commonly referred to as the grinding lay. Early trials using a basic modified grinding path demonstrated that surface roughness values of down to *0.01μm* R_a were attainable, with significantly reduced directionality. Figure 5.5 through to Figure 5.9 illustrate the changes in terms of both surface profiles and visual appearance. BN intensity readings indicated that the residual stress remained at acceptable compressive levels.

These initial findings using the Edgetek machine confirmed that both the improved wheel technology and the implementation of a modified grind path would improve the surface quality when using a standard production machine tool. With the vitrified grinding wheel, the use of crush dressing with a peripheral wheel mounted on a high

stiffness dressing spindle meant that a more consistent wheel surface was produced. The higher stiffness of structures and spindles used on today's production machine tools also enable a stable grinding condition to be maintained, without the flexure seen on previous machines. The combination of these resulted in the improved surface roughness capability witnessed. Usually with surface grinding, the abrasive grit and axis motion vectors are in a common plane, but with the modified path grinding action this is no longer the case. The separation of the vector paths lead to a reduction in the grinding directionality produced, and hence an improvement in the surface quality seen.

6.2.2 Cylindrical Grinding

Basic cylindrical plunge grinding trials demonstrated that the approach used in the surface grinding work was transferable. In a similar way to the surface grinding mode, the modified path alters the relationship of the motion vectors. With the conventional cylindrical plunge grind mode, the grit, infeed axis and workpiece motion vectors all lie in a common plane (Figure 2.4). In the modified grind approach a side to side oscillation is introduced which results in the grit and workpiece motion vectors no longer being common, as can be seen by combining the motion paths shown in Figure 6.35. The amplitude and frequency of the oscillation control the degree to which the separation occurs. At this early stage of development the application of the oscillatory motion capability was restricted, so testing was limited. Surface roughness results from the trials on the Edgetek machine confirmed that the roughness measured across the grinding lay reduced with the implementation of the modified path motion. Both the surface roughness results and visual images in Figure 5.12 and Figure 5.13 illustrate this.

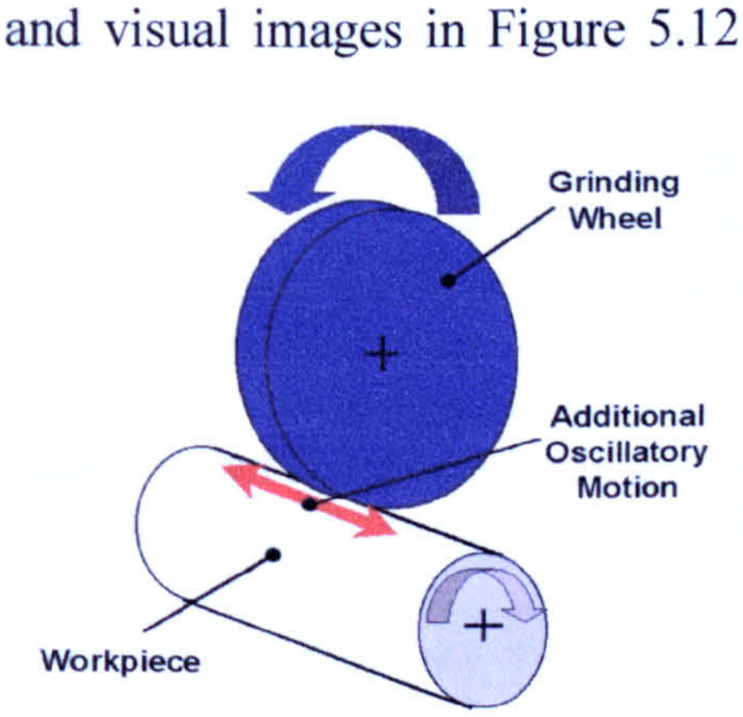

Figure 6.35 – Motion Paths for Modified Path Grinding

Enhancement of the *Landis Lund LT1* machine tool's CNC capability was carried out by the introduction of a triangular waveform generator, such that an oscillatory motion was introduced during the final stages of the finishing infeed cycle and for any sparkout dwell. The changes increased the capability and therefore allowed the effect of oscillation frequency and amplitude to be investigated in greater depth. Grinding trials using the existing dressing technology (i.e. single point rotary dresser on a conventional dresser spindle), without the modified path, gave a benchmark $3D$ surface roughness figure of $0.16\mu m$ R_a. Subsequent tests introducing the modified path demonstrated improvements to the surface quality, see Figure 5.14, with some values below $0.14\mu m$ R_a. BN intensity readings demonstrated that the residual stress became more compressive with the oscillatory grinds. With the newly applied wheel technology the

benchmark *3D* surface roughness (i.e. no modified path) improved to *0.1μm* R_a, a significant improvement, which remained consistent up to *8mm³/mm.s*. At higher rates the spread of results increased significantly indicating that some degree of wheel breakdown had occurred, see Figure 5.17.

A model to predict surface roughness was developed for modified path grinding using a combination of empirical functions for conventional plunge and transverse cylindrical grinding modes previously described by Malkin (1989). These were combined using velocity ratios, and the resulting function is shown in Equation 5.1.

Subsequent trials showed a good degree of correlation with the model at mid and high oscillation magnitudes, whereas for the lower magnitude there was some difference in the trends. Data for the experimental trials and modelling are shown in Figure 5.20 and Figure 5.23 respectively. The difference in the lower magnitude was possibly a consequence of the oscillation magnitude approaching the grit size of the wheel. This was taken as an indication of the lower limitation of the process. The modelling indicated that for the higher magnitudes and frequencies of oscillation, the surface roughness approaches the level that would be achieved without oscillation. This was considered to be a result of the increasing influence of the crossfeed velocity component, where higher crossfeed velocities in the transverse mode result in a lower quality surface roughness. Overall the experimental results demonstrated that the modified path approach improved the surface quality to below *0.1μm* R_a.

Figure 5.32 provides a summary of the experimental results, including those from the initial benchmark tests. The latter used current wheel truing and dressing technology with the *46μm* grit wheel in a conventional cylindrical plunge grind mode. The two dotted lines show the surface roughness levels achieved without a modification to the grind path. The upper line used the current truing and dressing technique, the lower line used the enhanced system. These show an improvement from *0.16μm* to *0.1μm* R_a. With the modified grind path it can be seen that the general level for those utilising the improved truing and dressing techniques is better than that of the conventional approach. In this instance the improvement is from *0.14μm* to less than *0.1μm* R_a.

The performance of the machine tool axes ultimately limited the range of frequencies and magnitudes possible. Performance could be further improved by using a sine wave profile, embedding the motion function into the *CNC* executive and increasing the axis servo bandwidth.

To fully conclude the surface integrity assessment it was necessary to assess residual stress levels. The measurements for the transverse peel grind showed higher levels than that for the conventional plunge grind, and it was concluded that this was a result of an increased thermal load caused by the rubbing and burnishing action associated with the transverse grinding. With the oscillatory grinding the *BN* intensity readings increased with both, greater amplitude and frequency of oscillation. As, in both instances, the transverse component increased this was to be expected. However, all the modified path readings fell below the boundary level, and so it was concluded that the modified grinding process together with the improved dresser techniques did not introduce

unacceptable changes in compressive stress, and therefore thermal damage into the component.

The surface finish model provides an insight into the *Superfinish Grinding* process, which can be used to further enhance performance. Figure 6.36 shows the predicted surface finishes for three different amplitude over the oscillation frequency range of 1 to 10Hz. The results demonstrate that the *0.4mm* oscillation offers good performance at around *4 Hz*, with higher frequencies the surface finish deteriorates as a result of increasing crossfeed velocity (i.e. High magnitude and frequency).

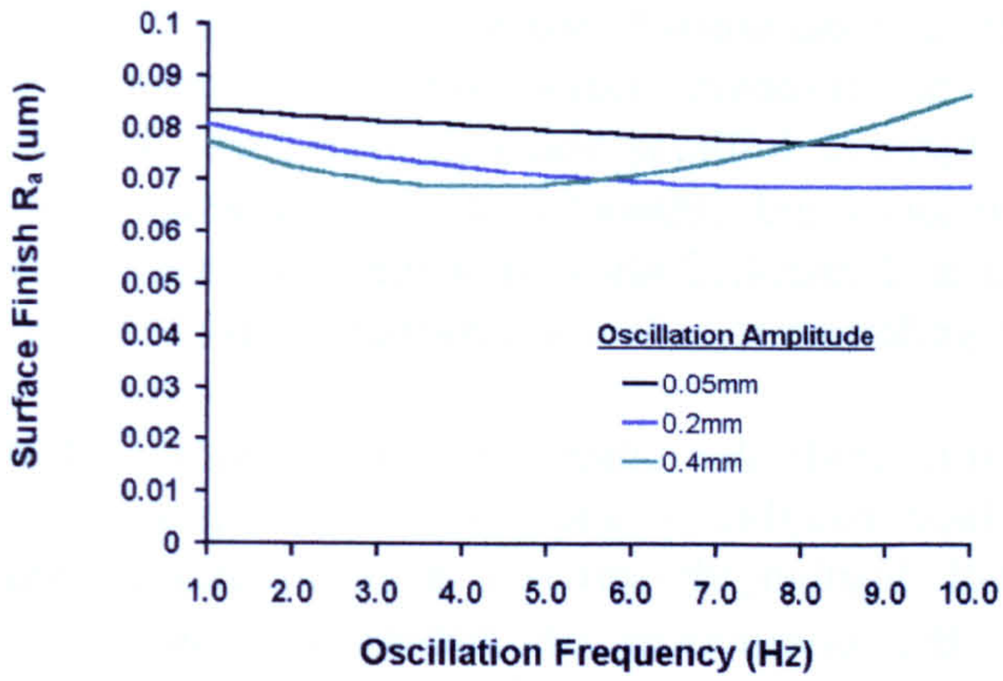

Figure 6.36 – Surface Modelling Results

Because the model uses empirical data its use is limited to very specific applications. Once changes are made in regard to wheel size or type, dressing conditions, or machine characteristics then it would become necessary to update the empirical data.

6.3 Grinding Application

To understand the implication of the *HEDG* regime, with regard to the grind cycle time for the web features, it is necessary to look at the increase in Q'_w together with the grind path lengths. The maximum Q'_w rate attained for the webs was $2000mm^3/mm.s$ whereas the standard removal rate in current use is $200mm^3/mm.s$. Table 4.5 showed the estimated grind times for the main webs (short grinds) and pin webs (long grinds) for both the conventional and *HEDG* conditions. Reductions of 87% for the main webs and 90% for the pin web illustrates the potential that *HEDG* can offer when long narrow grind paths are required. Although any such advantage, with regard to the wider journal type grinds, where the achievable increase in Q'_w rates are lower is far less. Attention must be paid to the application of these high removal rates to the grinding of some features in cylindrical plunge grinding. A balance needs to be maintained with regard to grind path length and workpiece rotational speed, the latter can often be a limiting factor. As the grind path length decreases, and the axis velocities increase, a situation is reached were the infeed motion is complete before a single workpiece rotation has occurred. In this case the Q'_w will vary through the workpiece rotation changing thermal and grinding loading. Therefore in some cases the cycle time is limited, not by the infeed but by the rotational speed of the workpiece. Thus once the infeed time falls

below the period for a single workpiece rotation there is no advantage to further increases in feedrate of the infeed.

In today's market automotive manufacturers purchase machinery on the basis of cost to produce 'x' number of components per shift. Thus reductions in cycle time translate into a reduced number of machines required, and hence lower purchase prices. It is therefore clear that reducing cycle time without modification to the machinery offers a potential advantage. To fully quantify the improvement in the crankshaft grinding cycle time, offered by the application of the *HEDG* regime, detailed breakdowns of the total machine cycle time were carried out for both conventional and *HEDG* cycles. These cycle time breakdowns included all aspects of the machine cycle, in addition to the grinding portion, such as load/unload, work-rest application, axes movements, and workpiece location. The removal rates used for conventional grinding were $200mm^3/mm.s$ for web faces and $80mm^3/mm.s$ for diameters. In *HEDG* the values were $1000mm^3/mm.s$ for web faces and $200mm^3/mm.s$ for diameters. The results of the cycle time calculations given in Table.4.12 show that the total machine cycle time decreases from over 7 minutes to under 3.5 minutes, a significant improvement.

The *Superfinish Grinding* trials demonstrated that the modified grind path approach improves the *3D* surface roughness and reduces the grinding directionality on a production machine tool. Further, the process does not induce unacceptable levels of thermal damage into the component. A model was developed to increase the understanding of process parameters and offers a valuable tool for further optimisation of the *Superfinishing Grinding* process. The surface texture produced by the action of a modified path grind is governed by the combination of factors with the increase in oscillation frequency. These are:

- An increase in the significance of the transverse velocity
- Deterioration in the transverse surface finish component
- Reduction in the significance of the plunge velocity ratio

Although this procedure increases the finish grind cycle time it removes the requirement for further machining processes such as polishing/honing and the associated transfer time. Removal rates for conventional finish grind camshaft machines are given in Table 6.3 using a $151\mu m$ grit vitreous wheel. Typically a surface roughness of $0.2\mu m R_a$ would be achieved, with the surface texture exhibiting grinding directionality and therefore requiring further operations.

Cycle	Feedrate (mm/rev)	Q'_w ($mm^3/mm.s$)
Start	0.2	18.7
Finish pass 1	0.007	0.7
Finish pass 2	0.005	0.5
Finish pass 3	0.002	0.2

Table 6.3 – Conventional Camshaft Grinding Rates

The *Superfinish Grinding* process, achieved removal rates of up to $8mm^3/mm.s$ using a $46\mu m$ grit wheel, with a surface roughness of under $0.1\mu m R_a$, which exhibited reduced grinding directionality. Although the initial material removal rate is less than that of the current values, with the improved surface quality there are substantive reductions offered by the reduced handling and post processing times. This coupled with the reduced floor area and increased machine flexibility offers a viable option with significant advantages.

The work carried out has demonstrated that the capability of a standard automotive crankshaft/camshaft production machine could be increased both in roughing and finishing operational modes. It has been shown that high Q'_w rates in the *HEDG* regime are possible in cylindrical plunge grind mode grinding without thermal damage to the work-piece. *Superfinish Grinding* can also be achieved. This radically increases the machine's performance and versatility at both ends of the material removal scale, Figure 1.3 illustrates how *HEDG* and *Superfinish Grinding* could be applied in the production chain for automotive crankshafts. The result would be to improve the competitiveness of grinding with current conventional processes.

Implications are that standard production machinery currently in use within the automotive industry, in combination with superabrasives, can be extended to provide:

- More efficient grinding regimes that compete with conventional cutting processes in terms of stock removal rate
- Reduced process chains through the elimination of several process stages
- Reduced manufacturing costs as a result of higher production rates and lower capital investment
- Higher precision through more effective grinding cycles and fewer work-piece set-ups
- Improved surface integrity and therefore better component performance and reliability

The importance of surface integrity together with techniques for its assessment have been demonstrated and documented as a result of this research. In terms of the thermal energy seen by the component's finished surface, the application of the BN intensity is an effective tool to monitor the residual stress state, in both rough and finish grinding. It provides a means to detect the onset of thermal damage at a far earlier stage than the other techniques, in a similar fashion to *XRD*. However as the *BN* intensity approach is nondestructive and suitable as an in-process tool, it offers a more effective lower cost implementation to that of *XRD* analysis. The *3D* approach to surface roughness assessment readily identifies grinding directionality and the associated software tools allow the level to be measured and hence controlled by the grinding process.

7 Conclusions & Recommendations for Future Work

The work on grinding within the High Efficiency Deep Grinding *(HEDG)* regime has demonstrated that specific material removal rates as high as $1500mm^3/mm.s$ can be achieved without thermal damage to the workpiece. At the other extreme, the superfinishing results indicate that high quality bearing surfaces in the order of $0.1\mu m\ R_a$ can be produced using the same production grinding machine. The ability to assess surface integrity has been an important factor in enabling these developments.

The main conclusions of the work are:

- Assessment of thermal damage using visual burn identification is both limited and subjective. Whereas metallurgical methods offer a more reliable assessment, these are time consuming and destructive. Neither approach is suitable for implementation in a production environment.
- Thermal damage can be monitored through changes to the residual stress in the near surface region. Residual stress can be measured with X-Ray Diffraction *(XRD)* and Barkhausen Noise *(BN)* intensity instrumentation. *XRD* provides an absolute measurement but is a destructive technique, whereas *BN* intensity provides comparative readings, and is nondestructive and relatively quick, making it suitable for application in a production environment. Changes in the residual stress occur at a much earlier stage than the metallurgical indicators and therefore provide a more sensitive approach to monitoring thermal damage.
- A novel thermal measurement technique using low melting point PVD coatings has been adapted for cylindrical plunge grinding.
- The *SGE* versus Q'_w relationship for *HEDG* grinding can be described by a power function using 'linear' and 'power' constants. For the steel material in this work the linear constant was found to lie in the range of *32* to *100*, and the power exponent *–0.12* to –0.45. Variation was attributed to a combination of process conditions, such as wheel grit size, diameter and condition, and coolant efficiency.
- It has been demonstrated that the concept of *HEDG* was valid for cylindrical plunge grinding using the selected steel material. The thermal trend for increasing material removal rate is similar to that shown by Tawakoli (1993), for surface grinding. The thermal trend rises up to a peak in the region of *300 – 350* $mm^3/mm.s$ after which it falls.
- The thermal modelling approach described by Stephenson & Jin (2003), for surface grinding, was shown to be valid for cylindrical plunge grinding, correlating well with both thermal measurement and residual stress data.
- There was no catastrophic abrasive grit or wheel failure as a result of the higher loads associated with the *HEDG* regime at Q'_w in excess of $2000mm^3/mm.s$.
- Surface integrity and thermal modelling work has both increased the understanding of the grinding process and provided a tool for further optimisation.
- The implementation of a modified path in finish grinding referred to here as *Superfinish Grinding*, offers improvements in both surface roughness with values below $0.1\mu m\ R_a$ and grinding directionality.

- A surface finish model has been developed for *Superfinish Grinding* using a combination of empirical relationships, linked by velocity ratios.

The implication of the results is that the performance level of standard production machinery currently in use within the automotive industry in combination with superabrasives can be extended to provide:

- more efficient grinding regimes that compete with conventional cutting processes in terms of stock removal rate
- reduced process chains through the elimination of several process stages
- reduced manufacturing costs as a result of higher production rates and lower capital investment
- higher precision through more effective grinding cycles and fewer workpiece set-ups
- improved surface integrity and therefore better component performance and reliability

Although the work centred on the application of grinding automotive crankshafts, there are many other potential applications.

There are a number of recommendations for further work, namely:

1) The steel material utilised for these investigations had a high thermal diffusivity, which increased its suitability for *HEDG*. The full impact of the materials thermal diffusivity in relation to *HEDG* needs to be understood for the range of materials used in the automotive industry.
2) The introduction of laminar flow nozzles coupled with the use of a wheel scrubber represented the 'state of the art' in current coolant application. However without further design and optimisation the quantity and pressure of coolant used in *HEDG* meant that a significant proportion of the total spindle power was used in accelerating and pushing the coolant through the wheel/workpiece gap. Thus this remains an important area that requires further investigations in this application. The release of additional spindle power would in itself allow higher Q'_w to be attained before machine power limitations were reached.
3) The implementation of modified-segmented wheels with internal coolant channels offers enhanced coolant application for other grinding applications. The limited work within the scope of the work meant that there was limited time for testing, and it was not successful in proving applicability at this stage. More investigations are required to address the increased atomization of the coolant as it exits the wheel face and to determine whether the approach could offer further benefits.
4) The thermal modelling showed good overall correlation with measurements of temperature and residual stress. There was some difference at lower Q'_w levels before fluid film boiling is likely to occur, thus more work needs to be done in this area.
5) Current thermal modelling in conjunction with the defined power relationships between SGE and Q'w should allow the use of the models as a process design tool. Whilst, by monitoring the spindle power in real time the temperature of the finished surface could be monitored.

6) There are a number of different abrasive grit types, which have become available over the last few years that enhance thermal shock resistance. There needs to be additional work carried out to investigate the performance of these whilst operating in the *HEDG* regime.
7) The modified grind path trials demonstrated that it provided enhanced finishes with reduced grinding directionality. A further stage needs to be carried out with wheel grit sizes currently in use for finish grinding (*151μm*) in order to determine possible levels of improvement.

References

Bailey M, & Juchem H,' The advantages of CBN grinding: Low cutting forces and improved workpiece integrity', Industrial Diamond Review 3/98 Pg. 83-89, 1998.

Booker K, 'Manual of British Standards in Engineering Metrology', © British Standards Institute 1984 ISBN 0-09-151931

Borland D.W, 'Residual Stress Measurement – Methods, Limitations & Significance', Surface Engineering Pg. 114-121 March 1994

Brinksmeier E, Cammett J.T, König W, Leskovar P, Peters J, Tönshoff H.K, 'Residual Stresses – Measurement and Causes in Machining Processes', Annals of the CIRP Vol 31/2 1982

Brinksmeier, E. Minke, E. 'High-Performance Surface Grindng – The Influence of Coolant on the Abrasive Process', Annals of the CIRP Vol. 42/1 1993. Pg367-370.

Brinksmeier, Tönshoff H.K, Czenkusch C, 'Modelling and Optimization of Grinding Processes', Journal of Intelligent Manufacturing Vol 9 1998, pg.303-314

Brinksmeier E, Heinzel C, Wittmann M, 'Friction, Cooling, and Lubrication in Grinding', Annals of the CIRP Keynote STC G 48/2 1999 pg.581-598

Brinksmeier E, Heinzel C, Wittmann M, 'Visualisation of Coolant Flow in Shoe Nozzles and their Effect on the Residual Grinding Stresses', Production Engineering Vol VII/1 2000 pg.9-12

Chen X, Rowe W.B, 'Modelling Surface Roughness Improvement in Grinding', Proc Instn Mech Engrs Vol 213 Part B Pg. 93-96, 1999

Coyle R.A, 'The Measurement of Residual Stress', Non-Destructive Testing Vol 21 No.1 Jan/Feb 1984

Crooks C.S, Parker D.D, 'The Importance of Crankshaft Surface Texture to Bearing System Reliability', International Congress & Exposition Detroit Michigan, February 26-29 1996 Paper 960983

Cullity B.D, 'Elements of X-Ray Diffraction', Addison Wesley Publishing Company Inc, London ©1967 ISBN 0-201-01174-3

Dagnall H, 'Exploring surface texture', Published Rank Taylor Hobson Ltd 1986 2nd Edition ISBN 0 901 920 07

DeVries W.R, Colwell L.V, 'The Surface Topography of Journals', Annals of the CIRP Vol 31/1 1982

Ebberll S, Woolley N.H, Tridimas Y.D, Allanson D.R, Rowe W.B 'The Effects of Cutting Fluid Application Methods on the Grinding Process', International Journal of Machine Tools & Manufacture 40 (2000) pg.209-223

Field M, Kahles J, 'Review of Surface Integrity of Machined Components', Annals of the CIRP 20/2 1971 pg. 153-163

Field M, Kahles J, Cammett J.T 'A Review of Measuring Methods for Surface Integrity', Annals of the CIRP 21/2 1972 pg. 219-238

Fix R.M, 'Automated Control of Camshaft Grinding Process by Barkhausen Noise', Materials Evaluation Vol 48 No.7 1990 pg.904-908

Fix R.M, 'Applications of Barkhausen Noise analysis (BNA), a Review of Three Cases Having Industrial Significance', Abrasives December/January 2000 pg.30-41

Gibbons A, 'Applications of Viper Grinding Technology', Advances in Grinding Technology, IGT Annual Seminar, 6th April 2005.

Guo C, Malkin S, 'Analytical and Experimental Investigation of Burnout in Creep-Feed Grinding' Annals of the CIRP Vol 43/1 1994 pg.283-286

Guo C. Wu Y, Varghese V, Malkin S, 'Temperatures and Energy Partition for Grinding with Vitrified CBN Wheels', Annals of the CIRP Vol 48/1 1999 pg.247-250

Harris P, 'At the Cutting Edge – Abrasives & their Markets' Industrial Minerals, January 2000 pg. 19-24

Hayden S, ' Superabrasives – a hard act to follow', Engineering Technology, March 2003, pg. 40-44

Higgins R.A, 'Engineering Metallurgy 1.Applied Physical Metallurgy', Hodder & Stoughton Fourth Edition ISBN 0 340 17673 3, 1973

Hillmann R, 'Combined NDT Testing of Camshafts', 1st International Conference on Barkhausen Noise and Micromagnetic Testing September 1-2 1998

Howes T, 'Assessment of the Cooling and Lubricative Properties of Grinding Fluids' Annals of the CIRP Vol 39/1 1990 pg.313-316

Howes T.D , Tönshoff H.K, Heuer W, 'Environment Aspects of Grinding Fluids', Annals of the CIRP Vol 40/2 1991 pg.623-630

Inasaki, I. Tönshoff, H.K. Howes, T.D, 'Abrasive Machining in the Future', Annals of the CIRP Vol. 42/2 1993 pg.723-732

Jin T, 'Burn Threshold of High-Carbon Steel in High Efficiency Deep Grinding', Proc Instn Mech Engrs 2002 Vol 216 Part B: J Engineering Manufacture pg.357-364

Jin T, Stephenson D.J, 'Three Dimensional Finite Element Simulation of Transient Heat Transfer in High Efficiency Deep Grinding', Annals of the CIRP Vol 53/1 2004 pg259-262

Johnstone I, 'A Critical Study of High Efficiency Deep Grinding', PhD Thesis, School of Industrial & Manufacturing Science, Cranfield University, July 2002

Kato T, Fujii H, 'Temperature Measurement of Workpiece in Surface Grinding by PVD Film Method', Journal of Manufacturing Science and Engineering, May 2000 Vol 122 pg.297-303

Kato T, Hiroshi F, 'Temperature Measurement of Workpieces in Conventional Surface Grinding', Journal of Manufacturing Science and Engineering, November 1997, Vol 119 pg.689-694

Klocke F, Baus A, Beck T, 'Coolant Induced Forces in CBN High Speed Grinding with Shoe Nozzles', Annals of the CIRP Vol 49/1 2000 pg.241-244

Kuang-Hua Fuh, Jen-Sheuan Huang, 'Thermal analysis of Creep-Feed Grinding', Jouranl of Materials Processing Technology 43 1994 pg.109-124

Loladze T.N, Batiashvili B.I, Butskhrikidze D.S, Mamulashvili G.L, Grdezlishvili L, Markevich J.I, 'Lowtemperature Precision Grinding and Outlook of its Development', Annals of the CIRP Vol 31/1 1982, pg.205-210

Lucca D.A, Brinksmeier E, Goch G, 'Progress in Assessing Surface and Subsurface Integrity' Annals of the CIRP Vol 47/2 1998, pg.669-693

Maksoud T.M.A, Dean C, 'Theoretical and Experimental Investigation into the Effect of Lateral Oscillation in Cylindrical Plunge Grinding', Proceedings of Third International Grinding Conference 4th-6th October 1988 Fontana Wisconsin, Society of Mechanical Engineers MR88-601-1-17

Malkin S, 'Thermal Aspects of Grinding Part 1 – Energy Partition', Journal of Engineering for Industry November 1974 pg.1177-1183

Malkin S, 'Grinding Technology – Theory and Applications of Machining with Abrasives', © Society of Manufacturing Engineers 1989, ISBN 0-87263-480-9

Marinescu I .D, 'Belt Superfinishing of M50', Abrasives Magazine October/November 1997 pg.16-24

Merchant M.E, 'Delphi-Type Forecast of the Future of Production Engineering', Annals of the CIRP Vol. 19-20 1971 pg.213-225

Moorthy V, Shaw B.A, Evans J.T, 'Evaluation of Tempering Induced Changes in the Hardness Profile of Case-Carburised EN36 Steel using Magnetic Barkhausen Noise Analysis', NDT&E International 36 2003 pg.43-49

Morgan M.N, Rowe W.B, Black S.C.E & Allanson D.R, ' Effective thermal properties of grinding wheels and grains', Proc Instn Mech Engrs Vol 212 Part B 1998 Pg. 661-669

Rowe W.B, Black S.C.E, Mills B, Qi H.S, Morgan M.N, ' Experimental Investigation of Heat Transfer in Grinding', annals of the CIRP Vol 44/1 1995 pg.329-332

Rowe W.B, Black S.C.E, Mills B, 'Temperature Control in CBN Grinding', International Journal of Advanced Manufacturing Technology 1996 12 pg.387-392. **(1996a)**

Rowe W.B, 'A Simplified Approach to Control of Thermal Damage in Grinding', Annals of the CIRP Vol. 45/1 1996 pg.299-302. **(1996b)**

Rowe W.B, 'Grinding Temperatures and Energy Partitioning', Proc R. Soc. Lond A 1997 453 pg1083-1104

Rowe W.B, Chen X, 'Application and Performance of CBN Wheels', Abrasives Oct/Nov 2000 pg. 36-41

Rowe W.B, 'Temperature Case Studies in Grinding including an Inclined Heat Source Model', Proc Instn Mech Engrs Vol 215 Part B pg.473-491 2001. **(2001a)**

Rowe W.B, Jin T, 'Temperature in High Efficiency Deep Grinding (HEDG)', Annals of the CIRP Vol 50/1 2001 pg.205-208. **(2001b)**

Rowe W.B, 'Thermal Analysis of High Efficiency Deep Grinding', International Journal of Machine Tools & Manufacture 41 2001 Pg.1-19. **(2001c)**

Rowe W.B, 'Energy and Temperature Analysis in Grinding' Laser Metrology and Machine Performance – Lamdamap 2003 p3-23 ISBN 1-85312-990-9

Shaw B.A, 'Detection of Grinding Damage in Hardened Steels', 1st International Conference on Barkhausen Noise and Micromagnetic Testing September 1-2 1998

Shaw M.C, Vyas A, 'Heat –Affected zones in Grinding Steel', Annals of the CIRP Vol 43/1 1994 pg.279-282

Shaw M.C, 'Principles of Abrasive Processing', Oxford Science Publications, ©1996, ISBN 0-19-859021-0

Shi Z, Malkin S, 'An Investigation of Grinding with Electroplated CBN Wheels', Annals of the CIRP Vol 52/1 2003 Pg.267-270

Shore P, 'Machining of Optical Surfaces in Brittle Material using an Ultra-Precision Machine Tool' PhD Thesis, School of Industrial & Manufacturing Science, Cranfield University, 1995

Smith N.P, Ashfold M.N.R, Smith D.J, Pearce T.R.A, 'Manufacture and Performance of Diamond-coated Thermocouples', Diamond & Related Materials No.8 pg.956-960 1999.

Snoeys R, Maris M, Peters J, 'Thermally Induced Damage in Grinding', Annals of the CIRP Vol 27/2 1978 pg.571-581

Stephenson D.J, Laine E, Johnstone I, Baldwin A, Corbett J, 'Burn Threshold Studies for Superabrasive Grinding Using Electroplated CBN Wheels', Proc 4th International Machining & Grinding Conference USA 7-9 May 2001, SME Technical Paper MR01-219

Stephenson D.J, Jin T, Corbett J, 'High Efficiency Deep Grinding of a Low Alloy Steel with Plated CBN Wheels', Annals of the CIRP, Vol. 51/1, 2002, 241-244

Stephenson D.J, Jin T, 'Physical Basics in Grinding', 1st European Conference on Grinding, 6-7 November 2003 Pg. 13-1 → 13-21

Suto T, Waida T, Noguchi H, Inoue H, 'Wheel Design for Grinding', Industrial Diamond Review 1990 Vol 50 No. 538 Pg.133-136 1990

Tawakoli T, 'High Efficiency Deep Grinding' © Mechanical Engineering Publications Ltd London 1993, ISBN 0-85298-820-6.

Tönshoff H.K, Peters J, Inasaki I, Paul T, 'Modelling and Simulation of Grinding Processes' Annals of the CIRP Vol 41/2 1992 pg.677-688

Webster J.A, Cui C, Mindek Jr, 'Grinding Fluid Application System Design', Annals of the CIRP Vol 44/1 1995 pg.333-338

Webster J.A, Heinzel C, Wittmann M, Thoens K, 'Assessment of Grinding Fluid Effectiveness in Continuous-Dress Creep Feed Grinding', Annals of the CIRP Vol. 51/1 2002 pg.235-240

Webster J.A Tricard M, 'Innovations in Abrasive Products for Precision Grinding', Annals of the CIRP Vol 53/2 2004 pg.597-617

Werner G, Tawakoli T, 'Deep Grinding Narrow Slots with CBN Wheels', Industrial Diamond Review 1988 3/88 Pg.285-288

Whitehouse D.J, ' Handbook of Surface Metrology', © Inst of Physics 1994, ISBN 0-7503-0039-6

Wickman D, 'Superfinishing with Water-Based Coolant', Abrasives Magazine February/March 2001 pg.22-24

Wojtas A.S, Suominen L, Shaw B.A, Evans J.T, 'Detection of Thermal Damage in Steel Components after Grinding using the Magnetic Barkhausen Noise Method', NDT September 1998, Vol 3 No.9

Yokogawa M, Yokogawa K, ' Improving Grinding Performance of CBN Wheels by Dual Fluid Supply Method', Int J Japan Soc Prec Eng Vol 27 No1 March 1993 pg.11-16,

Yossifon S, Rubenstein C, 'The Surface Roughness produced when steel is ground by alumina wheels', Annals of the CIRP 31 (1) pg. 225-228 1982

Zheng H.W, Gao H, 'A General Thermal Model for Grinding with Slotted or Segmented Wheel', Annals of CIRP Vol 43/1/1994

Appendix – Associated Collaborative Projects

Development Of Innovative Manufacturing Technologies For Reducing the Process Chain - UltraFlex

The *Brite-Euram* project '*UltraFlex*' has a sizeable *HEDG* and ultra precision grinding content, the work on this is scheduled to begin in January 2001. Landis Lund and the *School of Industrial and Manufacturing Science* at Cranfield University are collaborators in this programme of work. The aim of the project is to develop innovative manufacturing technologies for reduction of the process chain in the automotive industry. The objective is to minimise the number of process steps – ideally one single machining stage that includes both rough and finish grinding producing an optical quality surface. Components will be both crank and CVT gear shafts. The HEDG investigations on the crankshaft are due for completion in the latter part of 2002.

The chart below outlines all sections of the project together with the collaborators. The contribution relating to HEDG is highlighted and relates to the machining of the component before hardening.

Chart of Ultraflex Project Tasks and Collaborators

- **Dry and MQL Machining of High Alloy Steel before Hardening**
  - ⇨ Dry Turn-Milling
  - ⇨ Laser Integrated Machining
  - ⇨ High Efficiently Deep Grinding
  - ⇨ Laser or Induction Hardening
- **Ultra Precision Machining of High Alloy Steel after Hardening**
  - ⇨ Ultra High Speed Mono Wheel MQL Grinding
  - ⇨ Dry Hard Turning in Combination with Hard Roller Burnishing
  - ⇨ Laser Assisted Turning
  - ⇨ Ultra Precision Machining
  - ⇨ Laser Micro-Machining
- **Industrial Application: Process Chain Validation on Real Components**

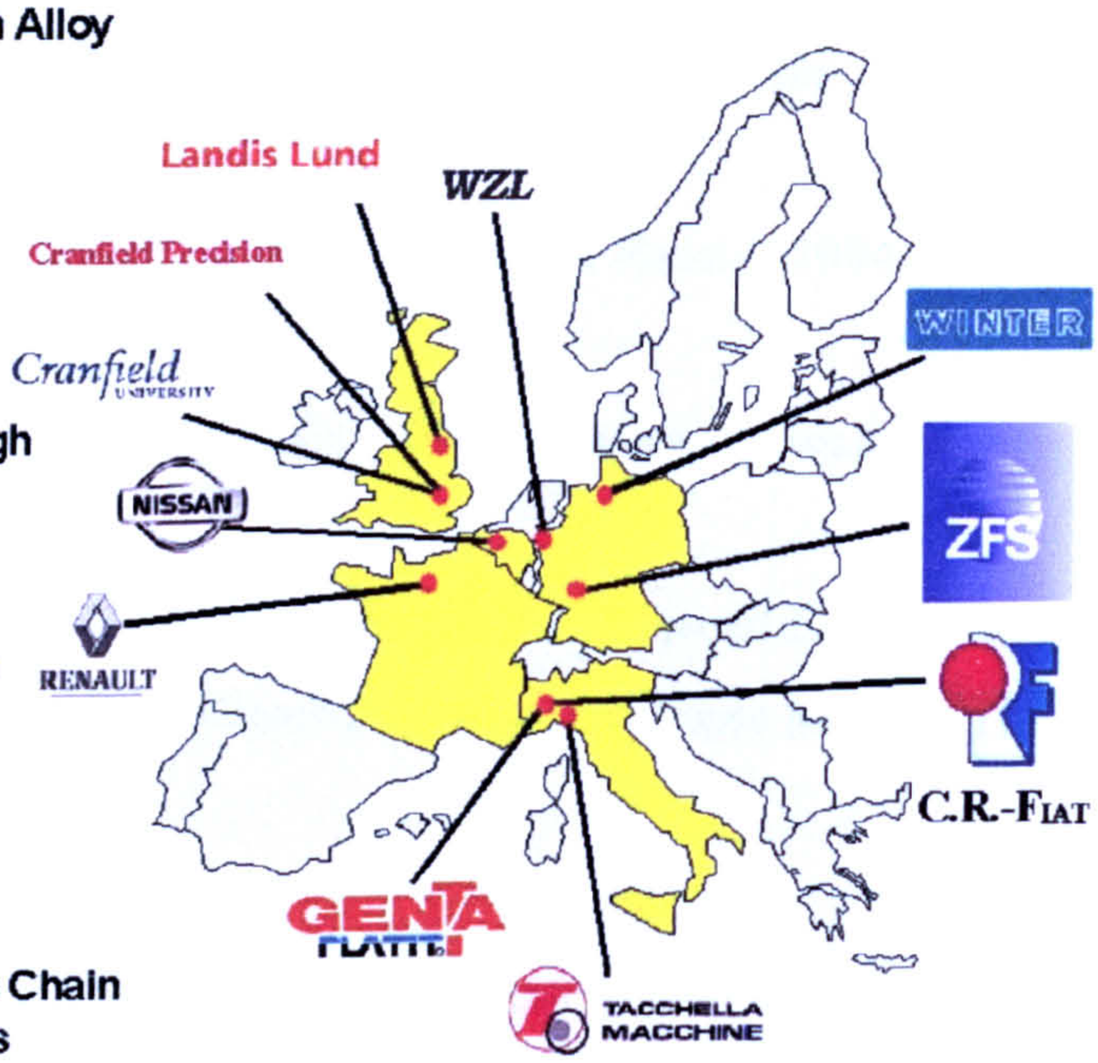

Thermal Limitations to Metal Removal by Grinding (High Efficiency Deep Grinding)

This is a collaborative program between Cranfield University, Liverpool John Moores University and a number of industry partners of which LL are one. A full list of participants is given below.

The research objective is to study grinding zone temperatures and coolant efficiency in order to optimize material removal rates whilst reducing surface and sub-surface damage. The project began in April 2002 with completion planned for June 2005.

List of project participants:

Cranfield University
Liverpool John Moores University
Landis Lund / Cranfield Precision
Element Six (formally DeBeers Industrial Diamond Division (UK) Ltd)
Renold
Saint Gobain Abrasives
Stresstech – AST
Castrol Industrial
Weston EU